

Redox Potential and Metabolic Stability:
Development of High Throughput Assays for
Early Compound Profiling

Inauguraldissertation

zur
Erlangung der Würde eines Doktors der Philosophie
vorgelegt der
Philosophisch-Naturwissenschaftlichen Fakultät
der Universität Basel

von

Anabel Felix

aus

Bad Säckingen, Deutschland

Basel, 2009

Genehmigt von der Philosophisch-Naturwissenschaftlichen Fakultät, Universität Basel

Auf Antrag von

1. Referent: Prof. Dr. M. Hamburger, Institut für Pharmazeutische Biologie,
Universität Basel

2. Referent: Prof. Dr. G. Gescheidt, Institut für Physikalische Chemie, TU Graz

Externer Experte: Dr. M. Kansy, F. Hoffmann-La Roche, Basel

Basel, den 22. Mai 2008

Prof. Dr. H.-P. Hauri
Dekan

To the ones I love 😊...

Acknowledgements

The studies in this thesis were carried out at F. Hoffmann-La Roche Ltd. Basel/Switzerland and supported by the department of Pharmaceutical Biology, Faculty of Philosophy and Sciences, Basel/Switzerland.

I would like to thank everybody who was somehow involved in the realization of my PhD-thesis.

First I would like to thank Prof. Matthias Hamburger and Dr. Manfred Kansy for the opportunity to realize this interesting PhD-thesis. Their excellent advice and their encouraging and demanding character inspired me to achieve the determined aims and turned my work into an exciting challenge with successful results.

I would also like to extend my grateful thanks to Dr. Holger Fischer, whose great knowledge and experience in Physical Chemistry and Computational Sciences helped me to achieve successful results.

His readiness for help and discussions were motivating me. He has also proof read my manuscripts and provided valuable feedback.

Thanks a lot to F. Hoffmann-La Roche, in particular to Prof. Klaus Mueller and Dr. Torsten Hoffmann whose generous financial support enabled a successful and good collaboration. The modern infrastructure and manpower provided, facilitated a lot research in my PhD-thesis.

I appreciate a lot the great effort of Prof. Georg Gescheidt, whose excellent scientific support contributed a lot to the successful realization of my PhD-thesis. He has also introduced me into the interesting field of electrochemistry. I am particularly grateful to Georg as he has agreed to be the co-referee in my PhD exam.

Thanks a lot to my colleagues of the Lab "**Molecular Properties and Structure Properties Correlations**" in Discovery Chemistry, F. Hoffmann-La Roche Björn Wagner, Stefanie Bendels, Frank Senner, Virginie Micallef, Isabelle Parrilla und Gregori Gerebtzoff. Their loyal attitudes as well as the practical support helped me to feel comfortable and become part of the group.

Especially great thanks to Björn, who was always there, whenever I need a helping hand in the lab environment. Also great thanks to Stefanie, who has always provided me support whenever possible. It was great fun to plan and organize together our group events which were always of great success.

Thanks too to Virginie. I have enjoyed a lot to speak in French to her and sometimes have coffee with her, but also thanks to Frank, Gregori and Isabelle who have heartily welcomed me.

I would like to extend my grateful thanks to the colleagues of the "**Applied Analytics Methods Departments**", section "**Molecular Structure Research**". Iris Ruf and Sigggi Stolz have helped me a lot with their readiness to repeat several experiments of my PhD-thesis in their highly sophisticated lab environment. In agreement and collaboration with their group leader Dr. Heribert Dollt, they have provided valuable support in the interpretation of MS-data, but this collaboration would not have been possible without the agreement of Dr. Stephan Mueller und Dr. Michael Hennig.

Thanks to the colleagues of the department "**Technical Sciences**", Section "**Discovery DMPK**". Franz Schuler and his team have contributed to these successful results of my PhD-thesis by their willingness to re-measure some of my compounds being essential for the PhD-thesis. I have also enjoyed the interesting scientific discussions with Franz.

Thanks a lot to the people of Discovery Chemistry at F. Hoffmann-La Roche especially Doris, Jasmine, Nicoletta and Pia, but also Daniel, Gerold, Axel, Matthias, Rosa, Klaus, Alex, Rene, Philipp, Sandra, Rainer, Lilli, Maggie, Patricia and all the others who I have not mentioned explicitly. Special thanks to Daniel, my office colleague for our special teatimes and the good time in our office.

Thanks a lot to the desktop IT-Support: Peter, Andre, Heinz, Jan, Silvano and all the other team members. I appreciated your quick help and helping hand in any cases of computer problems. Additionally I have enjoyed all the good moments with them.....☺

I wish to extend my thank you to all the colleagues and friends of the other departments at F. Hoffmann-La Roche as Peter, Mickael, Andre, Silvano, Thomi, Rene, Silvia, Silke, Susanne, Christine and Michael.

☺ All of you made my PhD-study years at Roche unforgettable! ☺

Thank as lot to my colleagues of the group of "Pharmaceutical Biology" at University of Basel. Unfortunately, I did not have the chance to get to know them better, but I have always enjoyed a lot our annual dinner events. I am especially grateful to Manuela, who has provided help and encouragement whenever needed.

Thank you too to Iwo Gatlik from Gatlik Ltd. for the interesting collaboration.

Special thanks to my proof readers: Maggie Holme and Nigel Bold. I appreciate a lot your contribution to my PhD-thesis. You have done a great job!

Thanks to some special people, who have supported me a lot during my PhD years; my parents Prof. Michael and Hildegard Felix, my brothers Sebastian and Fabian and my dear friends, Franzi, Alise, Phil, Nigel and Gloria. Last but not least, thanks to my darling Kay.

I wish to express my gratitude to all the people I have not explicitly mentioned here.... Without you, the thesis would not be! Thank you very much for these unforgettable years. Merci Beaucoup, Danke schön, Muchas Gracias!

Summary

In recent decades, the pharmaceutical drug discovery and development process has been hampered by identifying efficacious and safe drugs. Among absorption problems, interference with ion channels (hERG), extensive hepatic metabolism leading to inadequate metabolic profiles of discovery compounds, has been cited as one of the most common problems associated with failures in early drug discovery and development.

Inadequate metabolic profiles of discovery compounds, namely low metabolic stability, an increased risk of CYP450 dependent inhibition and a number of clinically significant drug-drug interactions are largely due to oxidative degradation (phase-I metabolism). This degradation is usually enzymatically catalyzed by the most important members of the mono-oxygenases, the CYP450 superfamily.

The most important and common member of the CYP450 superfamily, CYP3A4, is responsible for the metabolic degradation of over 60% of known drugs [1, 2]. Additionally, the relatively large active cavity site of CYP3A4, resulting in a large diversity of possible substrates, makes this isoform especially important in the evaluation of metabolic and safety profiles of drugs and metabolites. Furthermore, the large cavity site allows the optimal orientation of the drug molecule resulting in a successful attack of the chemically most liable positions of CYP3A4 substrates.

Unlike for other CYP450 isoforms, structure-property relationships for CYP3A4 have so far not been feasible as various functions and mechanisms of components of the CYP3A4 active site are still not identified.

Besides the electronic orientation of liable structural moieties within the cavity site is an additional factor influencing the CYP3A4 induced catalysis. Therefore improved knowledge of the ionization potentials could be an important factor in a better understanding of CYP450 catalysis. The ionization potential of a compound can be described as the compound's redox potential. Guengerich and Lewis, for example, have proven the correlation between ionization- and redox potentials [1, 3, 4].

In the current study we could show that the redox potentials of discovery compounds are an important factor to be considered in the description of rat or human clearance and thus with the metabolic stability.

Standard early metabolic stability determinations are biological based mainly focusing on the degradation of drug by microsomal or hepatic cell preparations.

Usually these assays only deliver information on the rate of metabolism by the determination of the drug disappearance.

Without doubt, there is a need for a better understanding of metabolic processes. A larger focus on structural aspects of drugs candidates could probably improve understanding of metabolic degradation processes and structure-effect relationships.

Two novel approaches for early metabolic stability profiling of drug candidates have been developed and investigated in the current PhD-thesis.

The first approach is based on redox chemistry. Ideally, the optimal redoxchemical indicator should exhibit reversible two-electron transfer behaviour to best simulate the two-electron transfer process occurring in the CYP450 catalytic cycle.

After intensive investigations, *p*-chloranil has been identified as a suitable component for a redoxchemical based assay which meets the required criteria of reversible two-electron transfer behaviour.

The second approach is electrochemical based. Several research groups have already worked on electrochemical approaches and tried to establish EC/LC/MS as screening/profiling tool for metabolic stability. Quite a few disadvantages, e.g. non-physiological experimental conditions and low throughput have prevented EC/LC/MS from routine use so far.

An external collaboration with Gatlik (Gatlik Ltd., Basel/CH) gave rise to the **Electroactive Pharmaceutical Screening System (EPSS)**, a novel HT-cyclic voltammetric screening/profiling system which allows electrochemical determinations under more physiological conditions in the 96-well format.

For the first time, a larger quantity of compounds can be measured per day. Obtained oxidation potentials well correlate with the microsomal rat clearance so that EPSS can be regarded as an attractive screening/profiling method compound ranking/selection based on the found relationship between redox potential and metabolic stability.

The aim of the PhD-thesis was the development of fast and easy profiling systems, allowing improvement of the understanding of metabolic processes at the structural/compound level. Thus, compounds/compound classes with high probability to be metabolically instable with focus on phase-I metabolism processes can be identified.

Based on the previously reported hypothesis and the obtained results of the PhD study, we therefore propose EPSS as a promising and attractive screening or profiling tool for early metabolic stability determinations in early drug discovery, as first information on the compound's metabolic stability can be easily obtained without the use of biological materials.

Table of Contents

Acknowledgements	4
Summary	6
Table of Contents	8
Chapter 1: Introduction	12
1.1 The Fate of a Drug Administered Orally in the Human Body [5]	12
1.2 Role of Early ADME Studies in Drug Discovery & Development	13
1.3 Metabolic Stability: Definitions and Key Concepts	15
1.3.1 Definitions	15
1.3.2 Intrinsic Clearance and Metabolic Stability	15
1.3.3 Mathematical Concepts	17
1.4 Assessment of Drug Metabolism <i>In Vitro</i> and <i>In Silico</i>	18
1.5 Biotransformation and Drug Metabolism	20
1.5.1 Liver and Drug Metabolism.....	20
1.5.2 Lipophilicity and Metabolism.....	20
1.5.3 Phase-I and Phase-II Metabolic Reactions	22
1.6 Structure of CYP3A4	27
1.7 Aim of the PhD-Thesis	30
Chapter 2: Description and Comparison of Classical Cyclic Voltammetry with High-Throughput Cyclic Voltammetry for the Determination of Redox Potentials	33
2.1 Introduction	33
2.1.1 Background on Electrochemistry	33
2.1.2 Experimental Aspects of Cyclic Voltammetry	33
2.2 Experimental Section	38
2.2.1 Drugs and Chemicals	38
2.2.1.1 Preparation of Sodium Dihydrogen Phosphate Buffer (PB) [50]	38
2.2.2 Cyclic Voltammetry	38
2.2.3 Data Analysis	40
2.3 Results	40
2.4 Discussion	42
2.4.1 Classical Cyclic Voltammetry	42
2.4.2 HT-Cyclic Voltammetry: EPSS	42
2.4.3 Solvent-Related Issues.....	43
2.4.4 Internal Standards.....	43
2.4.5 Further Approaches in Electrochemistry.....	44
2.5 Conclusions and Perspectives	45
Chapter 3: Redoxchemical Approach for the Prediction of Metabolic Stability	47
3.1 Introduction	47
3.2 Experimental Section	49
3.2.1 Drugs and Chemicals	49
3.2.1.1 Preparation of Sodium Dihydrogen Phosphate Buffer	49
3.2.1.2 Preparation of <i>p</i> -Chloranil Solution.....	49
3.2.2 Methods	49
3.2.2.1 Cyclic Voltammetry	49
3.2.2.2 UV-Spectroscopy	49

3.2.2.3 LC/MS Equipment: Agilent 1100 Series and 6140.....	50
3.2.2.4 LC/MS Method: Agilent 1100 Series and 6140.....	50
3.2.2.5 MS-Parameters for Agilent 1100 and 6140 Series.....	50
3.2.3 Final conditions for the sample preparation.....	51
3.2.4 Assay Optimisation.....	52
3.2.5 Data Analysis.....	52
3.3 Results and Discussions.....	53
3.3.1 Selection of p-Chloranil.....	53
3.3.2 Stability of p-Chloranil.....	56
3.3.2.1 Light Influence.....	56
3.3.2.2 pH-Related Influences.....	57
3.3.2.3 Physical Stability of p-Chloranil.....	59
3.3.3 Compound Selection Procedure.....	60
3.3.4 Assay Set-Up.....	61
3.3.5 Assay Validation: Reproducibility, Robustness.....	63
3.3.6 Reaction Products of p-Chloranil and MS.....	65
3.4 Conclusions and Perspectives.....	69
Chapter 4: Prediction of Metabolic Stability by Redoxchemical and Electrochemical Approaches.....	71
4.1 Introduction.....	71
4.1.1 Biotransformation and CYP450.....	72
4.1.2 CYP450 Catalysis.....	72
4.1.3 Aim of the Study.....	73
4.2 Experimental Section.....	75
4.2.1 Selection Procedure of Datasets.....	75
4.2.2 Collection of Structural, Metabolic and Electrochemical Information from Literature.....	75
4.2.2.1 Descriptors for In Silico Prediction.....	77
4.2.3 Methods.....	77
4.2.4 Data Analysis.....	77
4.3 Results and Discussions.....	78
4.3.1 Literature Search Results.....	78
4.3.2 Redoxchemical Results.....	78
4.3.3 Electrochemical Results.....	83
4.3.4 Mass Spectrometric Confirmation of Successful Electrochemical Conversion.....	84
4.3.5 Statistical Determinations using PLS-Analysis.....	86
4.3.6 Comparison of Classical and Novel Determination/Prediction of Metabolic Stability.....	89
4.4 Conclusions and Perspectives.....	90
Chapter 5: Final Considerations and Perspectives.....	92
6. References.....	94
7. Abbreviations.....	106
8. Glossary.....	108
Figure Index.....	110
APPENDIX.....	114
Results from p-Chloranil studies [96] [97].....	115
Table A: Structure-Activity Relationships of literature data related to their E _{ox}	132
Table B: Fragment-Table [69, 84, 119-192].....	133
Table C: Colour Compound List.....	151
Table D: List.....	155
Table E: Data of Fig. 17, Chapter 4.....	168

Table F: Data of Fig. 3 and 4, Chapter 4.....	169
Table G: Cyclic Voltammograms of compounds used in Fig. 9, Chapter 4.....	170
Curriculum Vitae	180

Theoretical Part

Chapter 1: Introduction

1.1 The Fate of a Drug Administered Orally in the Human Body [5]

Drug action is the result of numerous and complex processes in the body. Typically, there is a chain of events which can be divided into three consecutive stages termed as: **pharmaceutical**, **pharmacokinetic** and **pharmacodynamic** phases.

The fate of a drug in the human body and the most important processes occurring after oral application are depicted in Fig.1.

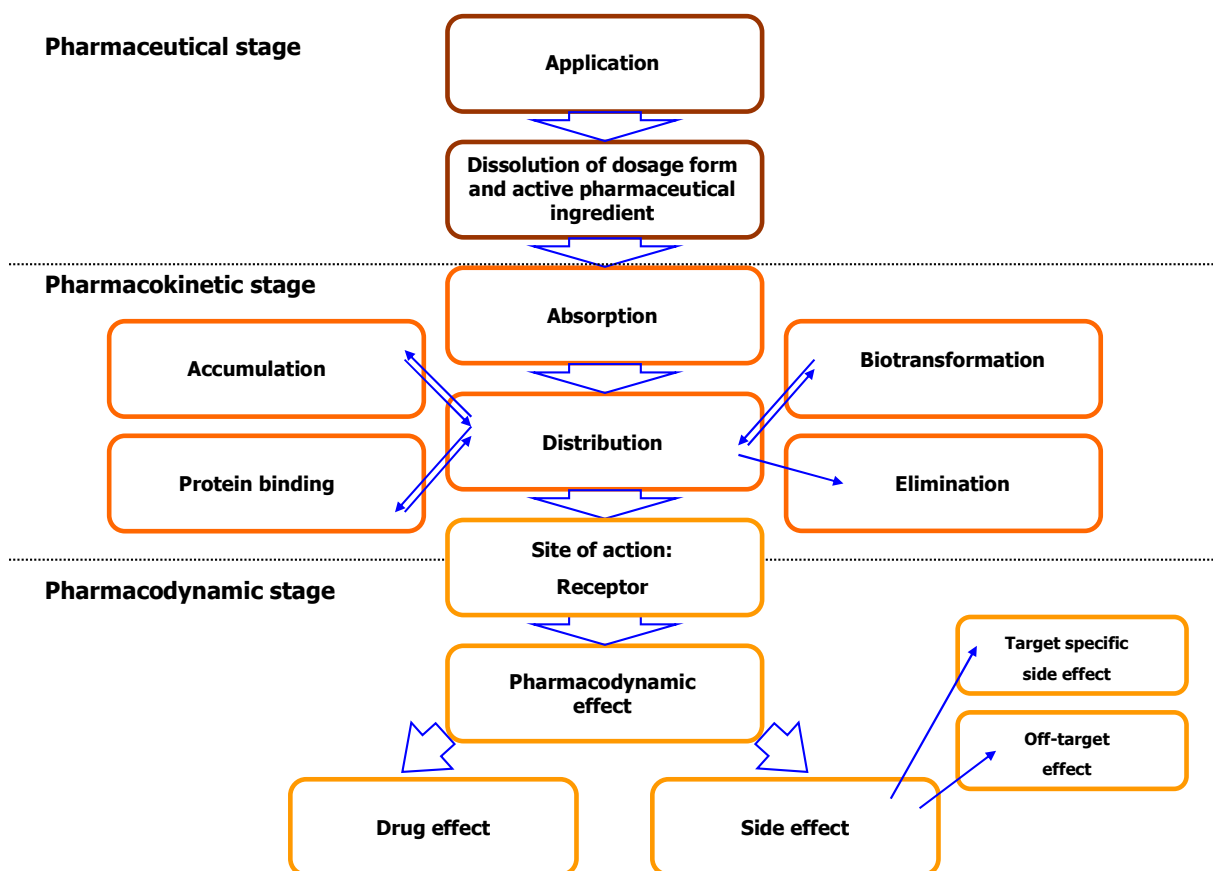


Fig.1 Adapted from Mutschler, a schematic overview on the fate of a drug after oral application [5]

Investigations at the pharmaceutical stage concern the application of a solid oral dose. The pharmacokinetic stage mainly deals with Absorption, Distribution, Metabolism and Elimination (**ADME-processes**), and thus with the determination of complex pharmacokinetic (**PK**) parameters. At the pharmacodynamic stage, drug-receptor interactions are described which should typically result in the desired effect at the *in vivo* level.

In particular, the pharmacokinetic stage can be regarded as the most complex of the previously described three stages.

The uptake of an applied drug by the organism is evaluated via studies of its absorption behaviour. Detailed studies of tissue and distribution partitioning are essential in describing distribution behaviour which influence, in combination with protein binding, biotransformation and elimination processes.

Elimination is defined as the process which decreases the concentration of a **xenobiotic** in the organism. Xenobiotics are chemical substances that are foreign to the biological system. They include naturally occurring compounds, drugs, environmental agents, carcinogens, insecticides and etc. [5] so the body's natural objective is to rapidly remove xenobiotics. This fact provides the basis of the elucidation of biotransformation and metabolic pathways of discovery compounds.

The optimisation and the decision-making processes are supported by numerous of *in vitro* and *in vivo* assays for the described complex phases.

The results of the *in vitro* metabolic assays provide the basis for the establishment of further pharmacokinetic parameters of the drug at the pre-clinical stage e.g. the maximal concentration (C_{max}), *in vitro* half life ($t_{1/2}$) and area under the curve (**AUC**).

1.2 Role of Early ADME Studies in Drug Discovery & Development

In the past, especially in the 1980s & 90s of the last century, ADMET studies typically took place at the later stages of pre-clinical drug development [5-9]. This in turn led to an unacceptably high failure rate of discovery compounds due to PK/ADME problems.

Numerous review articles were published about the major reasons for the failure of discovery compounds in 1991 as shown in Fig.2 [8, 9]. At that time, poor pharmacokinetic parameters combined with toxicity issues were the most common reasons for failures [5, 7, 9].

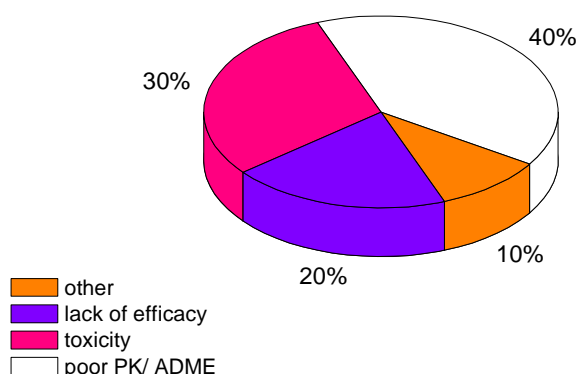


Fig.2 Typical reasons for failures in 1991 [9]

Numerous approaches for the early assessment or prediction of drug metabolism of discovery compounds have been proposed and introduced over the past few years by

pharmaceutical companies with the goal of facilitating the development of new drug molecules with an overall suitable profile [4].

The importance of ADME in the fate of a drug (**Fig.1**) provides the rationale for studying ADME related parameters in the early phases of the discovery process.

The drug discovery and development process currently involves several steps, from target identification and screening, lead generation and optimisation, pre-clinical and clinical studies to final registration of a drug and finally the market introduction (**Fig.2**)[8].

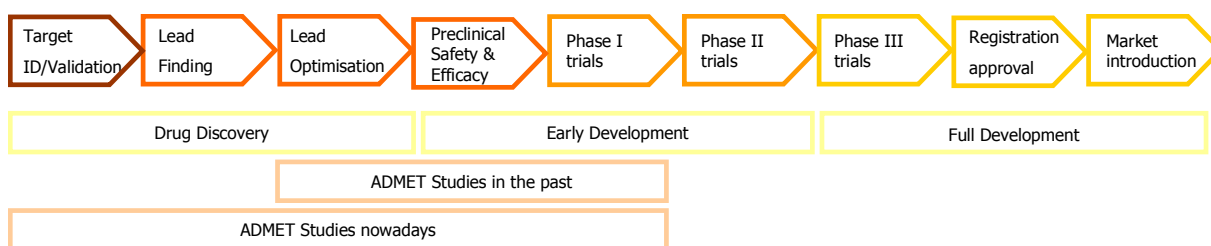


Fig.3 The drug discovery and drug development process [10]

Early optimisation of **ADME(T)** (**A**bsorption, **D**istribution, **M**etabolism, **E**limination and lately **T**oxicology) related parameters are therefore an essential part of the pre-clinical lead optimisation (**LO**) phase. The implementation of ADMET profiling and optimisation at the early discovery and development phase has to be seen as an attempt to overcome major weaknesses of the drug development processes. The biggest advantage of ADMET profiling is its time- and cost effectiveness [9, 11].

The ultimate goal of early ADMET related optimisation processes is the selection of clinical candidates with favourable pharmacokinetic parameters and safety profiles.

Following experiences in the early 90s with the unsuccessful development of new drug molecules, the pharmaceutical industry kept their main focus on the optimisation and metabolic profiles of discovery compounds [7, 9].

These days, toxicology related problems and efficacy are the reasons for most drug failures whereas pharmacokinetic related attritions can be reduced [12, 13].

Currently, ADMET studies especially studies on the metabolism of discovery compounds, are assessed in parallel with LO to avoid failure in late drug discovery. Not only metabolic stability determinations, but also CYP450 dependent inhibition and the investigations of significant drug-drug interactions are included in early metabolic profiling of discovery compounds.

Metabolic stability studies are part of the early ADMET related optimisation processes performed in the pre-clinical discovery [9]. The importance of metabolic stability studies has been illustrated by a rapidly increasing number of research papers and review articles published over the last decade [6, 9, 12, 14, 15]. In the following chapters, more key concepts and definitions of metabolic stability are provided.

1.3 Metabolic Stability: Definitions and Key Concepts

1.3.1 Definitions

Metabolic stability is a term widely used in the description of the rate and extent of metabolism of a compound [12]. A molecule which is rapidly and extensively metabolized is defined as a compound with a low degree of metabolic stability [11].

In vitro half life ($t_{1/2}$) and the **intrinsic clearance** (CL_{int}) are the primary pharmacokinetic parameters used in the description of metabolic stability.

Secondary pharmacokinetic parameters such as the **hepatic clearance** (CL_H), **bioavailability** and **in vivo half-life** ($t_{1/2}$) can be calculated on the basis of the primary pharmacokinetic values [12].

Clearance is a pharmacokinetic term used for the description of drug elimination from the body without identification of the mechanism or the process. It is a key parameter in pharmacokinetics and therefore explained in more detail.

The definition of clearance is the volume of fluid of a drug which is irreversibly cleared [$CL = (\text{ml}/\text{min}/\text{kg})$] [16].

The systemic clearance CL_{total} is the main measure. For most drugs, the systemic clearance is a combination of hepatic clearance and renal clearance as shown in *equation 1* [2, 14, 16]:

$$CL_{total} = CL_{hepatic} + CL_{renal} \quad (1)$$

Alternatively, the total clearance (*equation 2*) may be defined as the rate of drug elimination divided by the plasma drug concentration [16]:

$$CL_{total} = \frac{\text{elimination rate}}{\text{plasma concentration}} \quad (2)$$

1.3.2 Intrinsic Clearance and Metabolic Stability

Intrinsic clearance values are usually estimated by measuring the disappearance of the drug as a function of time. Therefore it is necessary to show the relationship of metabolic intrinsic clearance to metabolic stability described in the following paragraph.

Since the mid 1970s, several practical attempts to relate *in vivo* pharmacokinetics to *in vitro* drug metabolism have been documented [6, 7, 11, 17]. Rane et al.[7] first developed the concept of **intrinsic metabolic clearance** (CL_{int}). They demonstrated that *in vitro* metabolism rates correlate with hepatic extraction ratios determined from isolated perfused rat livers for a selected set of model compounds [7, 11]. More

recently, the issue of *in vitro* and *in vivo* correlations has been reviewed systematically [18, 19].

According to Houston et al.[19], intrinsic clearance is defined as the proportionality constant between drug concentration at the enzyme site and rate of metabolism as described by *equation 3*:

$$\text{Rate of metabolism} = \text{CL}_{\text{int}} * C_e \quad (3)$$

Rearrangement of (3) leads to *equation 4*

$$\frac{\text{Rate of metabolism}}{C_e} = \text{CL}_{\text{int}} \quad (4)$$

As enzyme catalyzed reactions follow Michaelis-Menten kinetics, rates of metabolism can be related to the concentration at the catalytic site, maximum velocity of reaction (V_{max}), and a constant, known as the **Michaelis constant** (K_m). K_m is defined as the substrate concentration at half maximal velocity of the reaction [11]:

$$\text{Rate of metabolism} = v_0 = \frac{V_{\text{max}} \times C_e}{K_m + C_e} \quad (5)$$

Assuming that $C_e \ll K_m$, rearrangement of *equation 5* leads to the following expression:

$$\frac{\text{Rate of metabolism}}{C_e} = \frac{V_{\text{max}}}{K_m} \quad (6)$$

Finally, *equating 4* and *6* gives:

$$\text{CL}_{\text{int}} = \frac{V_{\text{max}}}{K_m} \quad (7)$$

According to *equation 7* reasonable correlations between *in vivo* PK properties and parameters derived from *in vitro* metabolism studies are possible [11].

1.3.3 Mathematical Concepts

A number of mathematical models have been developed for the prediction of hepatic *in vivo* clearance (**CL_{in vivo}**) on the basis of *in vitro* clearance (**CL_{in vitro}**) data. Most commonly applied models are the “**well-stirred**” and “**parallel-tube**” model (**Fig. 4**). The “well-stirred” model is also known as the venous equilibrium model. It assumes that the drug concentration is constant throughout the hepatic compartment and equal to the outflow concentration [8].

The theory behind the “parallel-tube model” or sinusoidal model is based on an assumed greater uptake of the drug into the hepatocytes at the portal venous end of the tubes. The concentration declines exponentially along the tubes [8].

“The average concentration within the organ is the logarithmic average of C_{in} and C_{out} ” [20]. Applying the theory for the “well-stirred” model, the relationship between hepatic venous concentration C_{out} , incoming mixed arterial and venous blood concentration C_{in} , hepatic blood flow Q_H and intrinsic clearance Cl_{int} is expressed as follows in *equation 8*:

$$C_{out} = C_{in} \cdot \frac{Q_H}{Q_H + f_u \cdot Cl_{int}} \quad (8)$$

Remember that f_u denotes the free fraction of drug in blood. The hepatic organ clearance Cl_H then becomes:

$$Cl_H = \frac{Q_H \cdot f_u \cdot Cl_{int}}{Q_H + f_u \cdot Cl_{int}} \quad (9)$$

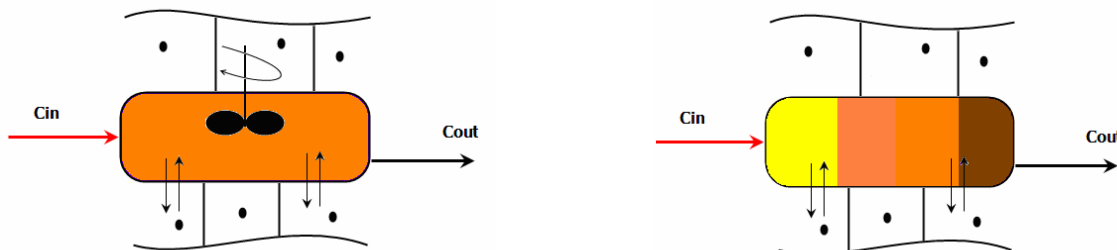


Fig.4 The “well-stirred” or venous equilibrium model (left) and the “parallel tube model” or sinusoidal model (right). The tanks are lined with rows of hepatocytes where the metabolism of the drug is supposed to occur. The small black arrows indicate the exchange [20]

1.4 Assessment of Drug Metabolism *In Vitro* and *In Silico*

Based on theoretical knowledge of drug metabolism, various *in vitro* assays have been developed to study drug metabolism using recombinant enzymes, liver microsomes, fresh and cryopreserved hepatocytes and tissue slices [12]. All *in vitro* models are more or less routinely used for predicting drug clearance and the risk of drug-drug interactions (**DDI**) related to enzymatic inhibition [12].

- Assays based on recombinant enzyme systems provide the simplest *in vitro* model that contains some of the numerous catalyzing enzymes which are produced in the endoplasmic reticulum (ER) of the eukaryotic host cells. The most commonly used recombinant expression systems are the baculovirus and human lymphoblastoid system. The major advantage of such assays is the simplicity. Other advantages are the possibility to study the activity of the specific enzymes separately, and these cell free assays are suitable for High-Throughput (HT)-screening.
A major drawback in using recombinant enzymes is related to varying enzymatic activity in the preparations and these *in vitro* assays only provide information on phase-I metabolism.
- The microsome-based assays are currently the standard *in vitro* model in industry for the estimation of $CL_{in vivo}$. Microsomes are prepared either from animal and/or human tissues and pooled microsomes are typically used to reflect average enzymatic activity found in humans or animals [12].
The major advantage of this model is the relative stability of enzyme activities during prolonged storage.
A major disadvantage is the limited incubation time since enzymatic activities decrease after 2h of incubation. Above all, the supplementation of relevant cofactors and other reaction components is essential so the supplementation with selected cofactors only allows the analysis of the different contributing classes of metabolizing enzymes, such as CYP450s, FMO and UGT.
- A third type of *in vitro* model uses either fresh or cryopreserved hepatocytes. The clearance of a compound can be estimated and predicted because all phase-I and phase-II enzymes and relevant cofactors are present [12]. Additionally, the potential for DDIs can be determined by this *in vitro* model. As a result, human hepatocyte experiments are considered to be very important.
The limited availability of fresh human hepatocytes is a major drawback which has led to research in culturing and cryopreservation of hepatocytes to improve its availability when needed.
- The most complex *in vitro* models are tissue models. These have the major advantage of very closely mimicking the *in vivo* situation. Consequently, tissues are a useful model for the study of the formation of metabolites, although they are not very well established in the prediction of metabolic clearance and DDIs.

Thus far, metabolic stability has always been estimated by one of the *in vitro* models described above. Generally, the time dependent disappearance of a compound is measured and used for the estimation of metabolic stability. However, fewer efforts have been directed towards the relationship between drug structure or properties and their metabolic stability. This is largely due to the limited information on the degraded products generated.

Literature search revealed that hardly any structure-based metabolic stability assessment has been published so far and applied although there is an increasing need for structure based mechanistic understanding of metabolic processes [17].

To overcome the hurdle of long and time consuming development steps in drug discovery and development, several *in silico* approaches towards predictive ADMET-models have been described [17].

Predictive ADMET models exist out of **three main components**:

- 1) A high quality of experimental data is essential for the training of the model.
- 2) Descriptors of molecular structures that can be correlated with the experimental data.
- 3) An appropriate modeling technology has to be available to produce the model [17].

Good experimental ADMET data is not readily available, although amounts of data have been accumulated within the confidential files of big pharmaceutical companies [17]. Hence, published models tend to be built on small datasets which limits their robustness and prediction power [17].

According to Dearden [17], *in silico* prediction of ADMET properties has progressed enormously over the past few years, so most physicochemical properties can be modelled today.

Since the prediction and calculation of ADMET properties is cost- and time effective, it can be expected that the development of increasingly accurate predictive tools will be further advanced [17].

1.5 Biotransformation and Drug Metabolism

1.5.1 Liver and Drug Metabolism

The liver is the major organ responsible for the metabolism and elimination of drugs and xenobiotics. From a physiological point of view, blood flow to this organ has important implications. It is supplied via the hepatic artery arising from the aorta (25%) and via the portal vein (75%) which is a conglomeration of venous returns from the intestines, spleen and mesenteries [21]. The liver is located in between portal and systemic circulation. Thus, the liver will usually receive drugs or xenobiotics entering via the portal system during oral absorption [21].

Specific cells in the liver, hepatocytes, carry out all the chemical reactions which are associated with **phase-I metabolism** (oxidation reactions) [21] and most metabolising enzymes such as CYP450s are located in the endoplasmatic reticulum (**ER**).

1.5.2 Lipophilicity and Metabolism

Most drugs are rather lipophilic. For this reason, the definition of drug metabolism is the conversion of a lipophilic compound to a more hydrophilic compound which can be readily excreted by the kidneys [14, 16]. Lipophilic drug molecules usually undergo extensive metabolism in the liver, resulting in low bioavailability [14, 16].

Compounds which are rapidly removed from the body are defined as compounds of low metabolic stability [12]. Biotransformation of a compound is normally linked with a reduction in lipophilicity and the formation of a metabolite which is usually less active than the parent compound [1, 2, 16]. For hydrophilic drugs ($\log D_{7.4} < 0$), renal clearance is the predominant route of elimination. In contrast to renal clearance, the metabolic clearance increases with increasing $\log D$ and this becomes the major route for lipophilic compounds.

The "rate of metabolism is a function of chemical liability and the ability to enter and leave the active site of the enzyme" [12]. Therefore, lipophilicity is an important physicochemical parameter to be considered in pre-clinical drug discovery.

Lipophilicity is usually expressed as the partition coefficient of a compound between octanol and water [22, 23]. Measuring the distribution of a drug between two immiscible phases indicates the ability of a drug to partition between aqueous phases and lipid biophases depending on its relative concentration and affinity for each phase [24].

Octanol was chosen as a solvent with good polarity and the ability to produce solubility in water to some extent [24]. The polarity of octanol best mimics the chemical constitution of biological membranes as they are rather complex anhydrous lipid phases [24]. Solvents other than octanol (e.g. isobutanol, hexan, cyclohexan) have also been tested [24]. Molecular size and hydrogen bonding capacity are two major molecular properties which contribute to the degree of lipophilicity [22].

Lipophilic compounds are primarily subject to phase-I metabolism whereas hydrophilic compounds more readily undergo phase-II metabolism. Increasing lipophilicity inevitably leads to an increase of the intrinsic clearance so that affinity for metabolising enzymes is enhanced [22, 25] as shown in Fig.5 below:

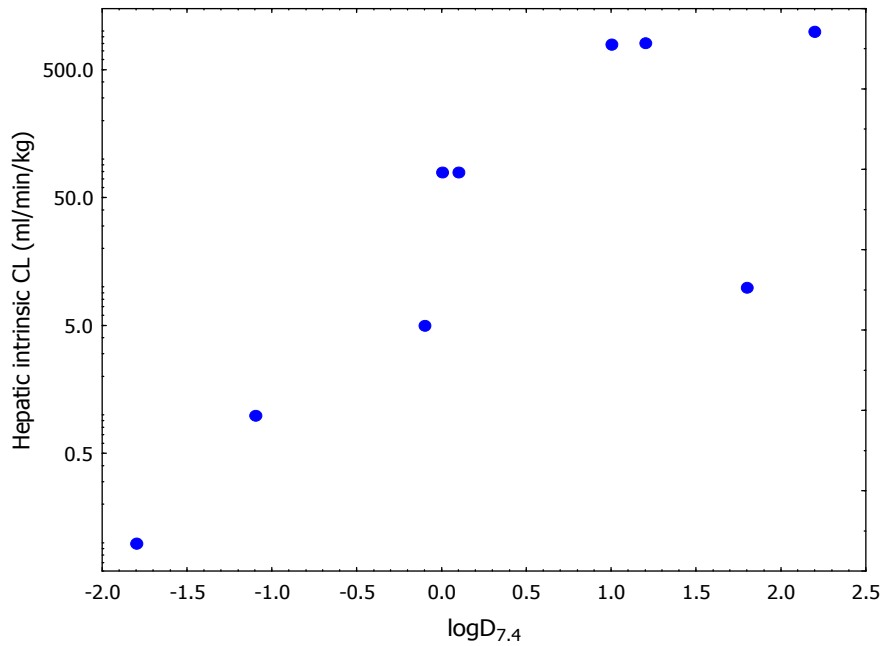


Fig.5 Correlation lipophilicity ($\log D_{7,4}$) with unbound (free) hepatic intrinsic clearance ($CL_{i(a)}$, filled squares) and unbound (free) renal clearance ($CL_{(r)}$ open triangles) adapted from van der Waterbeemd et al.[22]

1.5.3 Phase-I and Phase-II Metabolic Reactions

Drug elimination in the body involves many complex rate processes. Although organ systems have specific functions, the tissues within the organs are not structurally homogenous, and elimination processes may vary in each organ. The volume of the distribution concept is simple and convenient, because all drugs are dissolved and distributed in body fluids. The advantage of the clearance approach is that it applies to all elimination rate processes, regardless of the mechanism for elimination. In addition, for first-order elimination processes, clearance in contrast to drug elimination rate is a constant [2].

Biotransformational processes are usually catalyzed by enzymes. There are very few exceptions where drugs are non-enzymatically metabolized. Although biotransformation enzymes exist in other tissues, e.g. kidney, lung, small intestine and skin also contain biotransformation enzymes, liver tissues remain the most important ones as the highest levels are found there [12, 14, 16].

Generally, drug metabolism can be divided into **phase-I** and **II metabolism**. Phase-I metabolism involves oxidation, reduction and hydrolysis reactions, catalyzed by a number of enzymes. The most important metabolizing enzymes are haem-containing (CYP450) and flavin containing mono-oxygenases (FMO) [12]. Phase-II metabolism enzymes, e.g. UDP-glucuronyltransferases (UGT) and sulfonyletransferases, catalyze conjugation reaction of lipophilic chemicals, for example products of phase-I metabolism processes.

The most common drug biotransformation reactions are listed in Table 1.

Table 1 Common drug biotransformation reactions [16]

PHASE I REACTION	PHASE II REACTION
<i>Oxidation</i>	<i>Glucuronide conjugation</i>
Aromatic hydroxylation	Ether glucuronide
Side chain hydroxylation	Ester glucuronide
N-,O- and S- dealkylation	Amide glucuronide
Desamination	<i>Peptide conjugation</i>
Sulfoxidation, N-oxidation	
N-hydroxylation	<i>Glycine conjugation (hippurate)</i>
<i>Reduction</i>	
Azoreduction	<i>Methylation</i>
Nitroreduction	N-methylation
Alcohol dehydrogenase	O-methylation
<i>Hydrolysis</i>	<i>Acetylation</i>
Ester hydrolysis	<i>Sulfate conjugation</i>
Amide hydrolysis	<i>Mercapturic acid synthesis</i>

Most phase-I reactions are catalyzed by members of the CYP450 superfamily containing a haem moiety (**Fig.6**).

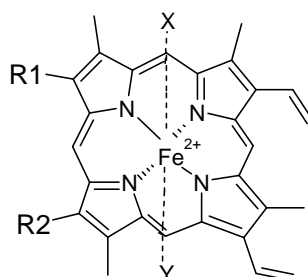


Fig.6 Haem moiety [1]

CYP450 are ubiquitous in nature. To date more than 500 different isoforms of CYP450 have been identified in humans, animals and plants [26]. However, only a few CYP450 isoforms play a significant role in the drug metabolism process [26].

The CYP1A, 2A6, 2B6, 2C, 2D6, 2E1 and the 3A families are the most important isoforms.

Therefore, CYP450 inhibition assays and DDI studies in pre-clinical discovery are performed with these isoforms [12].

The most versatile and abundant CYP450 isoform is 3A4 as it exhibits a large active site with low substrate specificity. It is involved in the metabolism of over 60% of the marketed drugs and also in a high number of significant DDIs [9, 11, 12, 14, 16, 27] so the assessment of metabolic profiles, especially that of CYP3A, plays an important role in pre-clinical drug discovery.

Table 2 Summary of the structural characteristics of human CYP450 substrates [28]

CYP450	Structural characteristics
1A2	Planar molecules, neutral or basic in character
2A6	Diverse relatively small neutral or basic molecules usually containing 1 aromatic ring
2B6	Angular medium-sized neutral or basic molecules with 1-2 hydrogen bond donor/acceptor atoms
2C9	Medium-sized acidic molecules with 1-2 hydrogen bond acceptors
2C19	Medium-sized molecules, mostly basic with 2-3 hydrogen bond acceptors
2D6	Medium-sized basic molecules with protonable nitrogen 5-7 Å from site of metabolism
3A4	Relatively large, structurally diverse molecules

Imipramine is an example for CYP450-mediated metabolism with a known, commercially available active metabolite and fully characterized metabolic pathway (**Fig.7**). Demethylations of imipramine are catalyzed by CYP3A4 and CYP1A2, whereas the hydroxylation is catalyzed by CYP2D6.

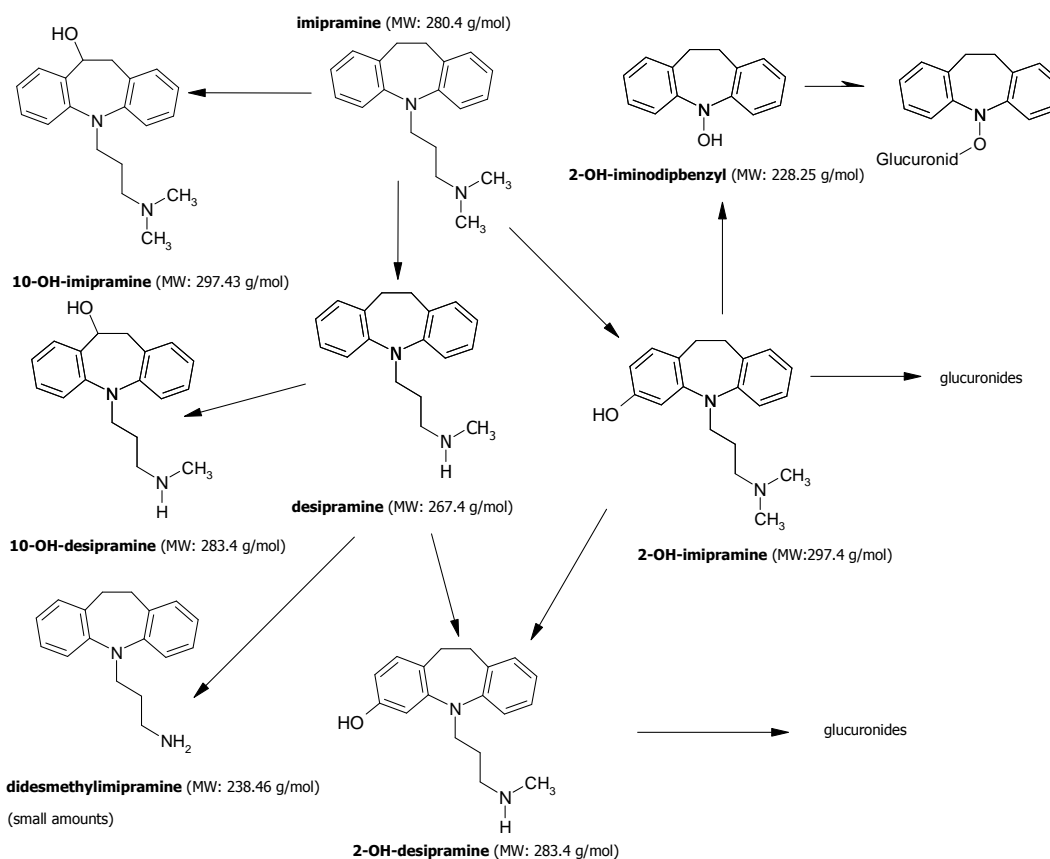


Fig.7 Metabolic pathway of imipramine with known phase-I metabolism and high *in vivo* clearance [29]

For further understanding of CYP450 mediated phase-I metabolism, it is necessary to review the CYP450 catalyzed biotransformation reactions in more detail. Regardless of structural differences in individual CYP450s, the mechanism of the CYP450 catalytic cycle is essentially the same across all isoforms [4].

The **catalytic cycle of CYP450 (Fig.8)** includes the following six steps [1, 4]:

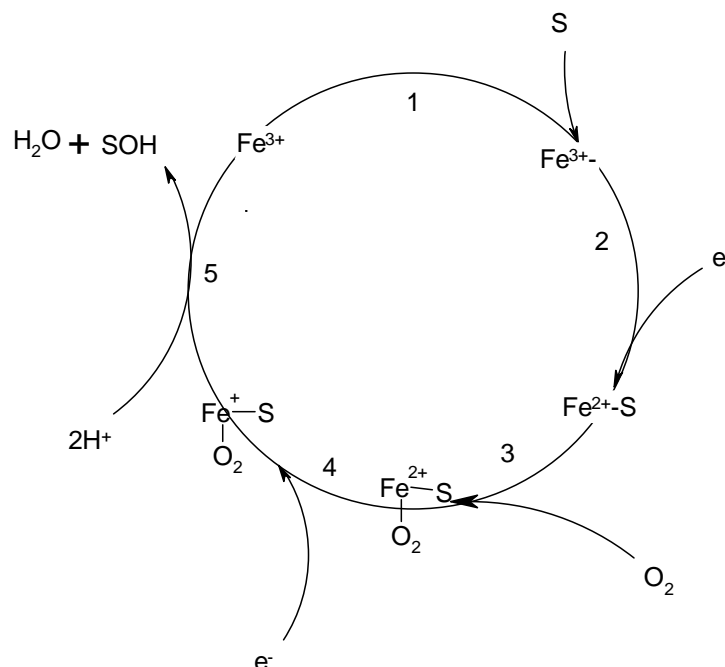


Fig.8 Catalytic cycle of CYP450 as described by Lewis [1, 4]: 1) Substrate binding, 2) First reduction of Fe^{3+} , 3) Oxygen binding 4) Second reduction, 5) Product formation, 6) Product release

1. Substrate Binding

Binding of substrate to the enzyme lowers the redox potential of the CYP450 and induces a shift in the ferric iron spin-state equilibrium towards the high-spin form. Additionally, the desolvation of the active site results in a change in the entropy of the enzyme. "The substrate-bound complex is relatively stable, readily reduced to the Fe^{2+} state because substrate binding lowers the CYP450 redox potential by about 0.1V." [1, 4]

2. First Reduction

The transfer of the first electron from the reductase or redoxin is included in the fastest steps in the catalytic cycle. Substrate binding lowers the redox potential of CYP450. This suggests some co-operation between the binding interaction and the electronic pathway.

3. Oxygen Binding

This step includes the rapid binding of molecular dioxygen to the high-spin Fe^{2+} CYP450-substrate complex. The oxyferrous complex is relatively stable, but the dioxygen is auto oxidizing to superoxide resulting in spectral changes. As a result of oxygen binding to CYP450 the ferrous iron returns to the low-spin configuration and the iron atom moves back into the plane of the porphyrin ring. Activated dioxygen (triplet

ground state) exhibits two unpaired electrons whereas high-spin ferrous CYP450 has only four electrons so significant pairing interactions are expected.

According to Lewis, this is a possible explanation for the relevance of the shift from low- to high-spin which exhibits a high affinity for oxygen. Other electronic factors pertaining to both the ligand and the haem iron must also be important, for example the electron deficient nature of dioxygen and overall negative charge of the Fe (II) haem-cysteinyll complex.

In addition, the haem iron is a good π -donor which facilitates strong binding of π -acceptor ligands such as oxygen, carbon monoxide and nitrogen monoxide.

4. Second Reduction

This rate-determining step is the major pathway for the decomposition of the oxycytochrome CYP450 substrate complex. The addition of a second electron to the oxycytochrome CYP450 complex suggests the formation of a species formally expressed as either $\text{Fe}^{2+}\text{O}_2^-$ or $\text{Fe}^{3+}\text{O}_2^{2-}$. With a bound substrate, the reduced oxycytochrome CYP450 complex undergoes rapid rearrangement to yield the oxygenated substrate and water.

5. Product Formation

An iron (V) oxene ($\text{Fe}=\text{O}$) intermediate is generated as the oxygenating species in CYP450 catalysis, weakening and facilitating cleavage of the dioxygen bond. The second oxygen forms a water molecule by acquiring two protons through rearrangement.

6. Product Release

A more hydrophilic metabolite is released.

Lewis et al. [1] was among the first to consider the correlation between metabolic stability and redox potentials. As reported, the haem moiety seems to play an important role in the set-up for this theory. He also stated that substrate binding lowers the redox potential of CYP450. In addition, the rate of reaction between the haemoprotein and hydrated electrons may be dependent upon a number of different parameters such as MW, number of aromatic residues and the net surface charge. These parameters become important again in *Chapter 4, pp.68* [1].

The source of electrons is either NADH or NADPH depending on the isoform involved [1]. In Fig.9 possible routes of electron transfer for different CYP450 systems are illustrated. It is suggested, however, that electrons may be transferred through a potential gradient from reductant to oxidant species, between the interacting species and terminating in various oxygen redox couples [1].

1.6 Structure of CYP3A4

Crystal structures of CYP450s possess a largely conserved tertiary structural core of amino acid residues, representing the key structural, and functional elements characteristic of CYP450 isoenzymes including several β -sheet elements and many α -helices [1, 25]. An additional helix was observed located at the extreme N-terminus of CYP3A4, but the significance of that helix is yet unknown.

First crystal structures for human CYP3A4, which is the most abundant isoform and metabolizing over 60% of endogenous and exogenous compounds, were reported by Williams et al.[30] and Yano et al.[31] in 2005.

One of the most interesting features of the active site cavity of CYP3A4 is its volume [32]. The active site is defined as "the area within the cytochrome P450 protein that can bind a substrate, giving it access to the active oxygen"[32]. Owing to its relatively large size it has the capacity to oxidize a variety of both, large and small molecules.

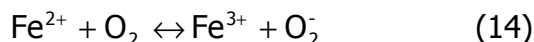
Moreover, when a small molecule binds to CYP3A4, a significant portion of the cavity remains unfilled by the substrate and therefore contacts between the substrate and enzyme are not as extensive [33]. Additionally, the unfilled portion of the cavity is often sufficiently large to bind another substrate or effector molecule, as suggested by kinetic and fluorescence studies on the binding behaviour of CYP450 [33].

Substrates of CYP3A4 or more generally CYP3A have more freedom to find their "catalytically competent" orientations in the active site [34] so CYP3A4 can additionally attack the most favourable chemical position. In the catalysis of other CYP450, substrates spend a significant amount of time in non-productive positions as their active sites are much smaller than that of CYP3A4 [34].

Major routes of catalysis for CYP3A4 are either aliphatic oxidation or N-dealkylation [34]. The major sites of oxidation are allylic positions in the compound [34]. Moreover, catalysis can proceed either by abstracting hydrogen atoms, as is the case in aliphatic carbon hydroxylation, or electrons where circumstances are more favourable [34]. For instance, N-dealkylation of aliphatic tertiary amines by an initial one-electron oxidation is regarded as chemically facile due to low $E_{1/2}$ of those functions[34].

Hence, substrates of CYP3A4 have diverse structures, which significantly complicate the rational prediction of their metabolism and identification of potential DDI [32]. Active sites of other CYP450s, such as 2D6 or 2C9 for instance, are smaller in size in comparison to CYP3A4 [33]. Consequently, substrate specificity is increased and therefore, unlike the case of CYP3A4, structure-activity relationships (**SAR**) for these substrates are feasible.

Binding of CYP450 to substrates triggers an interaction with the CYP450 redox partners by inducing a conformational change [1, 32]. Several spin states are accessed when the first electron is transferred to form the high-spin ferrous state of the CYP450. Molecular oxygen can bind fairly rapidly and easily so that the ferrous state becomes low-spin [1]. Additionally, it was suggested that the CYP450 converts the dioxygen into the superoxide anion by electron transfer from ferrous iron as illustrated in equation 14. [1]. This electron transfer induces the formation of ferric iron from ferrous iron, illustrated in *equation 14*.



Importantly for the activation of the oxygen, the porphyrin ring which encapsulates the iron is a good σ -donor and π -acceptor tetradentate ligand [1, 4]. Lewis and Guengerich's catalytic cycle for CYP450 [1, 4] suggests that the iron peroxide, an intermediate of the haem group during the catalytic cycle, could act as a nucleophilic reagent for the oxygen. Electrophilic oxygenation is more likely carried out by an iron oxene, iron hydroperoxide or an iron hydroxide which potentially exhibits the characteristics of a hydroxyl radical [1, 4]. From the electronic viewpoint, an iron-oxene radical could potentially very well represent the optimum electronic configuration for an electrophilic attack of certain types of substrates such as aromatic compounds and tertiary amines [1, 4].

Substrate binding lowers the CYP450 redox potential [1, 35] and the fact that proton transfer as well as electron transfer is facilitated suggests the participation of several amino residues in the active site cavity of CYP450 being ionizable. Therefore, ionization constants are regarded as one of the most important physicochemical properties besides lipophilicity [4]. The presence of an ionizable group seems to be important for the binding to the active site and the determination of the regioselectivity of the metabolic reaction [1, 4, 32].

Lipophilicity is of great importance in the metabolism of substrates CYP3A4 [4]. Furthermore, CYP3A4 is predominantly hydrophobic [34] so its substrates are rather lipophilic with values ranging from $\log D_{7.4}$ 0.4 to 8 [4].

It should be noted that besides the two physicochemical parameters lipophilicity and ionization potentials, other structural parameters such as redoxchemical behaviour play also an important role in CYP450 mediated conversion processes.

A general overview of electron transfer pathways is provided in Fig.8.

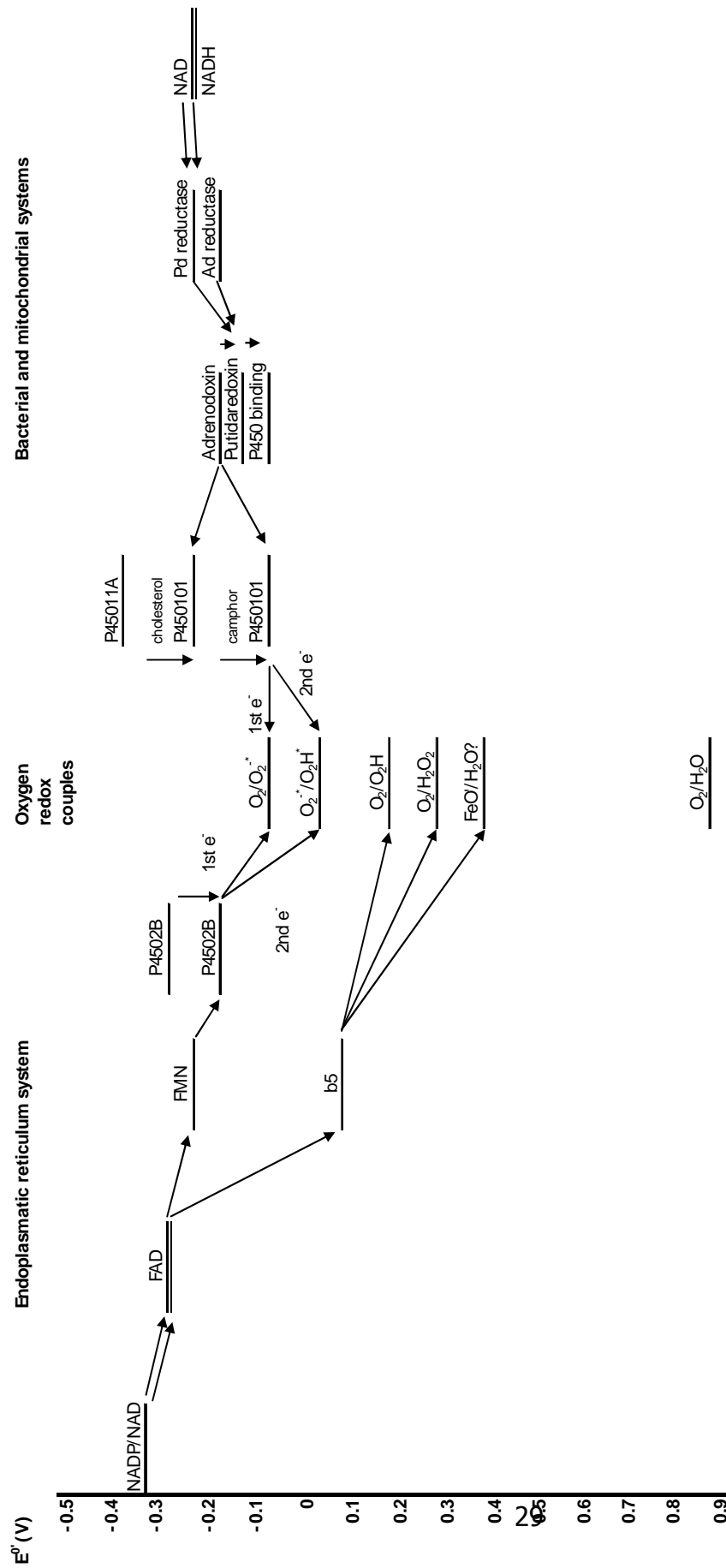


Fig.9 Electronic transfer pathways in various CYP450 systems [1]

1.7 Aim of the PhD-Thesis

Increased failure rates of drug discovery compounds in the last decades established fundamental research activities in the field of ADMET.

With the introduction of systematic metabolic studies in early drug discovery, attrition rates of discovery compounds could be reduced. To date, the estimation and prediction of the discovery compound's metabolic stability is still regarded as a key issue in the drug discovery and development process.

As has been described, early metabolic stability determinations have been primarily focused on assays (microsomal stability, hepatic stability), which usually only delivers information on the rate of metabolism by the determination of the drug disappearance. Currently, these assays are standard in the pharmaceutical industry but they can hardly deliver sufficient information on drug structural aspects influencing the metabolic liability of discovery compounds beside lipophilicity and ionization.

Without doubt, there is a need for a better understanding of the metabolic processes in lead selection and optimisation. A larger focus on structural aspects of drug candidates could probably improve the understanding of metabolic degradation processes and structural-effect relationships.

Most drug candidates and drugs undergo phase-I metabolism processes which are mainly enzymatically catalyzed by the CYP450 superfamily. CYP3A4 is the most important and abundant isoform of this superfamily and is involved in the metabolism of over 60% of known drugs [1, 2]. In comparison to other metabolic active enzymatic systems, the active cavity site of CYP3A4 is relatively large in size and therefore allows the oxidation of various compound classes.

Hence, substrates of CYP3A4 are structurally diverse. Especially in the case of CYP3A4, it is most likely that besides enzymatic activity other factors such as catalytic activity, drug structural and property related parameters additionally play an important role in the prediction of the suitability of drug candidates.

CYP3A4 substrates are more likely to obtain their best electronic orientation in the active cavity site of CYP3A4. Consequently the chemically most liable position of the substrates can be attacked more easily. Simply the ionization potential of a compound is the same energy at its highest occupied electronic energy level $E(\text{HOMO})$. The knowledge of this energy was stated as a first indicator of potential reactivity in the CYP450 system [1, 3].

The substrate's redox potential are an important factor for the PhD-thesis [1, 4].

With the introduction of novel analytical techniques [36-42], new approaches for fast redox behaviour profiling of drug candidates became feasible.

Cyclic voltammetry was the analytical method of choice. It is a fast and reliable electrochemical method for the determination of redoxchemical characteristics of compounds. Standard cyclic voltammetry used to be performed in a single mode, and large compound consumption.

An external collaboration with Gatlik Ltd. (Basel) gave rise to a novel HT-screening system: the **EPSS**, an electroactive pharmaceutical screening system. Redoxactive behaviour of discovery compounds can be screened fast and reliable by that novel HT-cyclic voltammetry system. Measurements under physiological-like conditions as well as low compound consumption of substances are some of its advantages.

Another approach involved the simulation of the two-electron transfer which occurs during the catalytic cycle of CYP450 by redoxreactions. Several redoxactive compounds exhibiting reversible two-electron transfers were identified as redoxindicators (RDI) with the help of cyclic voltammetry.

A redoxchemical based assay for the prediction of metabolic stability was developed with *p*-chloranil as RDI.

Therefore, the aim of the PhD-thesis was the development of fast and easy profiling systems, allowing improvement of the understanding of metabolic processes at the structural level and the identification of compounds/compound classes with a high probability of metabolic instability with focus on phase-I metabolic processes.

The PhD-thesis is structured in a theoretical and an experimental part with the experimental part subdivided into three publishable chapters:

Chapter 2 (pp. 30) contains a detailed description and comparison between classical and HT-cyclic voltammetry.

Chapter 3 (pp. 44) deals with the identification of redoxindicators for the development of a redoxchemical based *p*-chloranil assay.

Chapter 4 (pp. 68) includes the data analysis of results retrieved by cyclic voltammetry and *p*-chloranil assay. It also reports results of the multivariate data analysis (PLS) which was performed for the creation of a suitable model for the prediction of metabolic stability.

EXPERIMENTAL PART

Chapter 2: Description and Comparison of Classical Cyclic Voltammetry with High-Throughput Cyclic Voltammetry for the Determination of Redox Potentials

2.1 Introduction

Cyclic voltammetry was used as an analytical method for the determination of reduction/oxidation potentials (redox potentials). Firstly, cyclic voltammetric measurements were performed in a classical manner. Subsequently, a HT-cyclic voltammetric set-up developed by Gatlik Ltd (Basel) was adapted and applied in the analysis of redoxchemical related metabolic stability determinations.

In the following chapter, a description and comparison of classical cyclic voltammetry and HT-cyclic voltammetry is given. Interpretation of the data will be provided in *Chapter 4 (pp. 68)*.

2.1.1 Background on Electrochemistry

Electrochemistry is comprised of several aspects of molecular sciences. Besides the movement of charges in an electrical field, electron-transfer induced processes are an important issue in chemistry and life sciences [43-48].

Numerous electroanalytical methods have been developed in recent decades such as linear sweep voltammetry, differential pulse voltammetry, paleography, chrono-potentiometry and **cyclic voltammetry (CV)** [43]. In the current study, we have only focused on cyclic voltammetry.

"Cyclic voltammetry is an electrochemical method for studying variable potentials at an electrode involving application of a triangular potential sweep, allowing one to sweep back through the potential region just covered " [44]. In particular, cyclic voltammetry has gained considerable popularity because of its large scope [43]. In addition to thermodynamic data, (i.e. redox potentials), cyclic voltammetry can be utilized to obtain kinetic parameters of electron-transfer induced reactions and provide information on the stability and follow-up transformations of primarily formed intermediates [43, 46].

2.1.2 Experimental Aspects of Cyclic Voltammetry

In Fig.1, a typical sketch of an experimental set-up for CV is illustrated. Normally, an electrochemical cell contains a three-electrode system; a working electrode, an auxiliary electrode and a reference electrode [44]. These electrodes are in contact with an electrolyte, an ionic conductor [44, 47, 49]. The potentiostat sets the control parameters of the experiment and it induces a cyclic linear potential sweep on the working electrode resulting in the characteristic current-potential curve. The potential is measured as a

function of time [43-45, 47]. The electric current at the working electrode is defined as faradaic current due to the electron transfer.

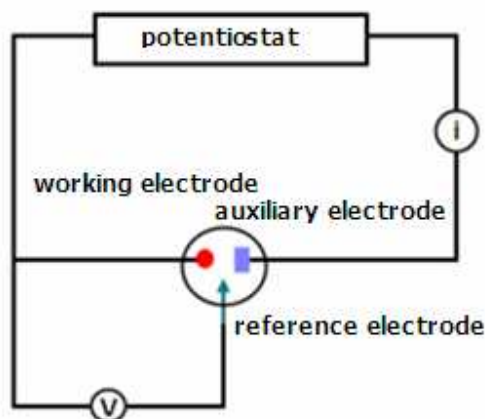


Fig.1 Schematic sketch for a general set-up of an electrochemical cell

The auxiliary electrode is driven by the potentiostat circuit and balances the faradaic process at the working electrode with an electron transfer in the opposite direction [47]. Reference electrodes are used as external references for the experiment and their potentials are calibrated with internal standards such as ferrocene (**FOC**) or ferricyanide (**FeCN**).

The following materials for electrodes are very common: Pt or Au as a working electrode, Pt or Au as an auxiliary electrode and Ag/AgCl or SCE as a reference electrode [44]. Ag/AgCl and SCE reference electrodes are commonly used in experimental aqueous conditions [47].

In CV, the potential applied to the working electrode is scanned in a linear manner between two potential values, E_{\min} and E_{\max} . The electron transfer of the redox reaction occurs on the surface of the working electrode within the predefined potential range. The potential provides qualitative information about the analyte of interest. The surface of the working electrode is more reductant or oxidant depending on the potential applied to it. Therefore, the more negative the potential becomes, the more improved and effective the electrode becomes as a reducing agent and vice versa [48]. Supporting electrolytes, such as TBAP or KCl, enhance conductivity in the electrochemical system [43-45, 47, 48].

The most important parameter in CV is the scan rate, \mathbf{v} :

$$v = \frac{\Delta E}{\Delta t} \quad (1)$$

ΔE : difference between the upper and lower potential limit
 Δt : time

The potential is applied in a saw-tooth manner to the working electrode and the current is monitored as illustrated by Fig.2 [44, 45]:

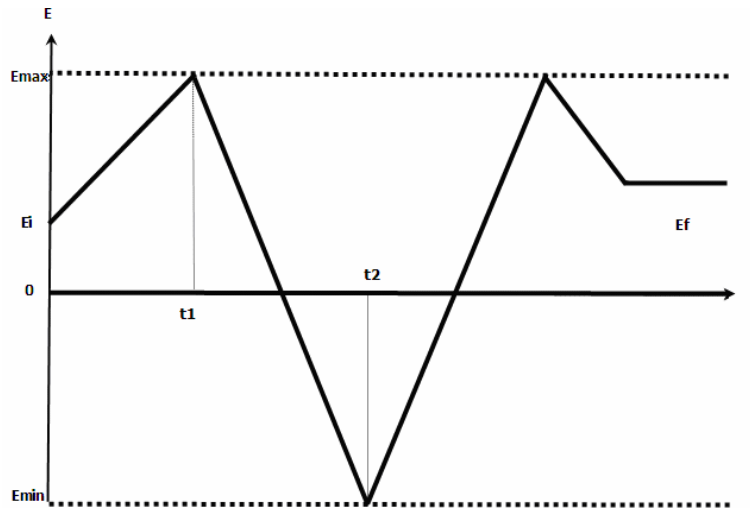


Fig.2 Variation of applied potential with time in cyclic voltammetry, showing the initial potential, E_i , the final potential E_f , maximum E_{max} , and minimum E_{min} potential, The sweep rate $dE/dt=v$. For linear sweep voltammetry consider only one segment. The fact that the initial sweep is positive is purely illustrative.

A common cyclic voltammetric cycle starts at E_i (initial potential); the potential is increased to its upper limit E_{max} at a constant scan rate, and then reversed at t_1 running back to E_{min} . At E_{min} and t_2 , the scan direction of the potential is changed once more and again it is increased to reach E_{max} . The number of cycles is varied depending on the focus of the experiment.

For illustration purposes, a typical cyclic voltammogram for reversible charge transfer is shown in Fig.3.

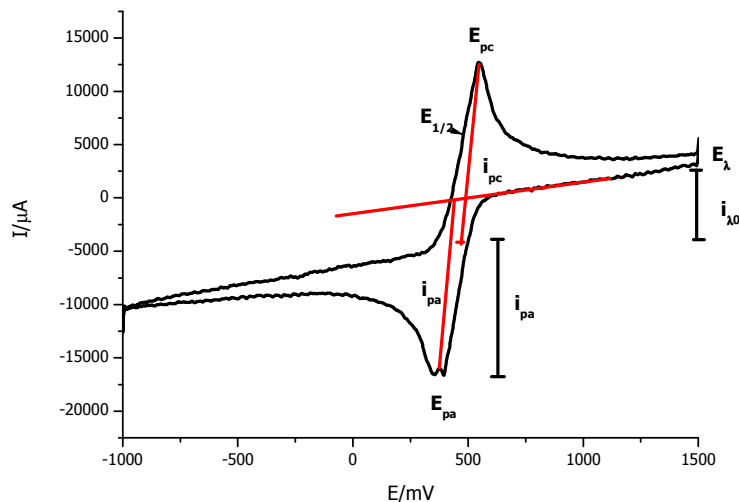


Fig.3 Cyclic voltammogram for a reversible charge transfer, E_{pc} : cathodic peak potential, E_{pa} : anodic potential, E_{λ} : switching potential, $E_{1/2}$: half-wave potential, i_{pc} : cathodic peak current, i_{pa} : anodic peak current, $i_{\lambda 0}$: current at E_{λ} , i_{pa} : anodic peak current at baseline.

Reversible reactions are kinetically rapid oxidation-reduction reactions at an electrode surface under mass-transfer-limited conditions [48]. For diffusion-controlled reactions stirring should be suppressed during the measurement [43-45, 47, 48]. The parameters of greatest interest for a reversible voltammogram are the peak cathodic potential (E_{pc}), the peak anodic potential (E_{pa}), the peak cathodic current (i_{ps}), and the peak anodic current (i_{pa}). The formal redox potential of the voltammetric response provides qualitative information about the redox couple [45].

Quantitative information regarding the concentration of the analyte is obtained from peak heights according to the **Randles-Ševčík**, *equation 2* [43-45, 47, 48]:

$$i_p = 0.443 \frac{n^{3/2} F^{3/2}}{R^{1/2} T^{1/2}} AD^{1/2} C_0^* v^{1/2} \quad (2)$$

i_p : peak current in amperes
 A: electrode area in cm^2
 D: diffusion coefficient in cm^2s^{-1}
 C: concentration in mol cm^{-3}
 V: sweep rate in V/s^{-1}

Not only does *equation 2* illustrate the proportionality of the peak current to the concentration, but more importantly it also predicts that the peak current of a reversible redox process, plotted against the square root of the sweep rate, must vary in a linear fashion. Therefore, the sweep rate or scan rate is an important parameter, as scan rates cannot be increased relative to the redox behaviour.

Consequently, if the anodic peak potential and the cathodic peak potential are of great interest, the normal potential (E°) can be expressed as an average of the anodic peak potential (E_{pa}) and cathodic peak potential E_{pc} , so *equation 2* is valid:

$$E^\circ = \frac{(E_{pa} + E_{pc})}{2} \quad (3)$$

In a reversibly cyclic voltammogram, where $E_{pa} - E_{pc} \sim 59 \text{ mV}$, the peak separation is inversely proportional to the number of electrons transferred, n :

$$\Delta E = (E_{pa} - E_{pc}) = \frac{0.0592}{n} \quad (4)$$

Initially, the shape of the curve resembles that of a linear sweep voltammogram, but after reversal of the sweep there is a rapid change in current on account of the high

concentration of oxidizable species close to the electrode generated on the reductive sweep [44, 45]. When the potential is close to the value which is required to oxidize the reduced species, there is a substantial anodic current until all the oxidation is complete, and the current returns to zero [44, 45].

Fig.4, in contrast, shows an example of an irreversible cyclic voltammogram:

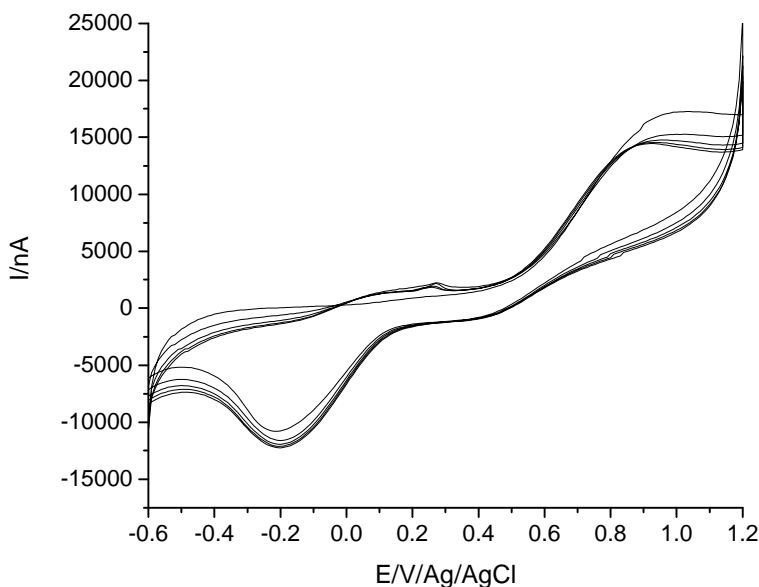


Fig.4 Cyclic voltammogram for an irreversible charge transfer carried out at HT-cyclic voltammetry in aqueous media

Till date cyclic voltammetric measurements have been performed in the classical single mode.

Electro active pharmaceutical screening system (**EPSS**) is a novel way of performing cyclic voltammetry which utilises the classical experimental set-up and three-electrode system. The sensor plate, used with EPSS, contains 96 small electrochemical cells, set in serial. Each of the 96 wells contains a planar three-electrode system.

The system capacity allows the measurement of up to 96 compounds. For the first time, cyclic voltammetry can now be used as a profiling or screening tool. New applications become favourable, for example profiling or screening of drug-like molecules in the early drug development stage.

Therefore, the focus of the current study was the development of a new application based upon the EPSS system with a subsequent technical modification to measure molecules under physiological-like conditions, and a comparison of the classical method and HT-methods.

2.2 Experimental Section

2.2.1 Drugs and Chemicals

p-Chloranil, chloranilic acid, *o*-chloranil, menadione, DDQ, juglone, tetra butyl ammonium perchlorat (TBAP), ferrocene, used in this study were purchased from Fluka (Buchs, Switzerland) and used without further purification. 1, 2-naphthoquinone was obtained from Sigma-Aldrich (Buchs, Switzerland).

Spectroscopic grade dimethylsulfoxide (DMSO) was purchased from Acros and electrochemical grade ACN from Fluka (Buchs, Switzerland). The pH of the solutions, used in the assay, was adjusted with sodium dihydrogen phosphate buffer (NaH₂PO₄) from Fluka (Buchs, Switzerland) at pH 7.4. KCl (analytical grade) was purchased from Merck (Switzerland).

2.2.1.2 Preparation of Sodium Dihydrogen Phosphate Buffer (PB) [50]

3.0 g of NaH₂PO₄ was weighed into a 500 ml volumetric flask and dissolved in 250 ml ultra pure distilled (Invitrogen[®]) water. Next, the exact pH was adjusted to 7.4 with approximately 4.0 ml of 2 M NaOH using a Metrohm[®] 827 pH lab pH-meter and the solution was further diluted with water to 500 ml total volume. In the final step, filtration with Millipore Steritop Express[™] Plus 0.22 μm filter systems was performed to increase stability of the buffer.

2.2.2 Cyclic Voltammetry

Classical Approach. First, cyclic voltammetric measurements were performed with macro electrodes in non-aqueous solvents on a **Metrohm Polarecord E 506** and **VA scanner E 612** with a **VA stand 663** (Metrohm AG, Herisau, Switzerland). The set-up of the electrochemical chamber used in this experiment can be seen in Fig.1. Measurements were carried out in acetonitrile (**ACN**) and in DMSO at room temperature. Supporting electrolyte, 0.01M TBAP was added to enhance conductivity and minimize double-layer effects.

A platinum disk was used as a working electrode and the platinum wire as auxiliary electrode. A standard calomel electrode (SCE) was used for reference. Scan rates ranged from 0.15-0.8 V/s depending on the molecule. Ferrocene (FOC/FOC⁺) was used as an internal reference (E^0 :0.398 V vs. SCE). Sample concentrations varied from 10⁻³ M to 10⁻⁵ M and the total reaction volume was constant at 25.0 ml. A hepes buffer system at pH 7.4 with C_{buffer}: 50.0 mM was used. For the measurement of water-insoluble compounds, a mix of DMSO 100%: water (50:50) was tolerated. The total run time for the measurement of one single compound was 20 min and the system was connected to a computer to enable data analysis by the software *CycloVoltammetrie CycVolt.6.EXE*, Version 3.2.2. [51].

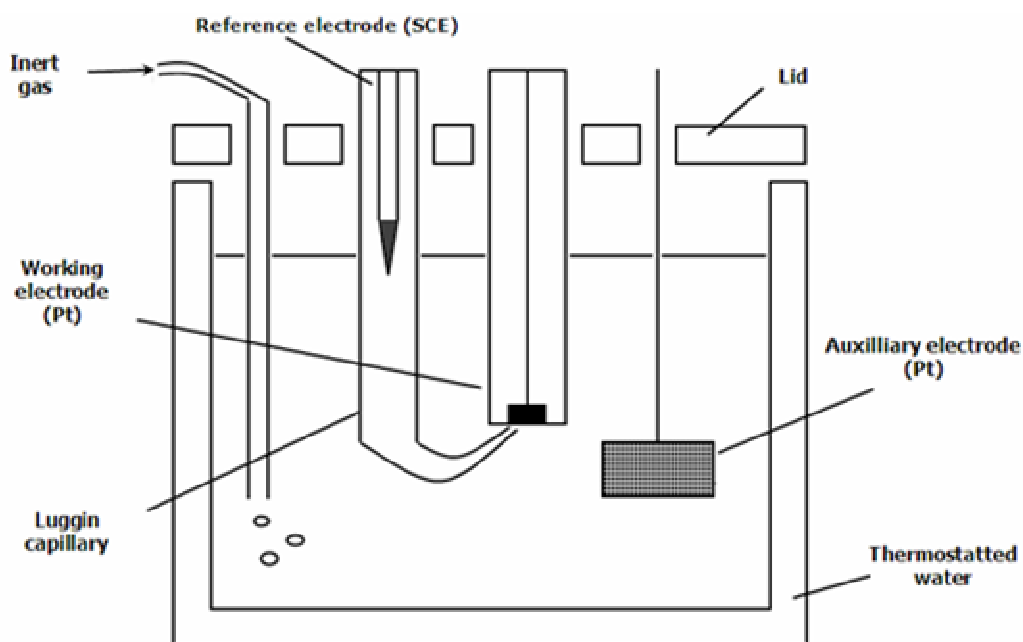


Fig.5 Schematic drawing for an electrochemical cell used in the classical experimental set-up [45]

High-Throughput Approach. Electroactive pharmaceutical screening system (EPSS, Gatlik Ltd., Basel) is a HT-screening system. EPSS was adapted to cyclic voltammetric measurements via the novel integration of potentiostat, multiplexing system and measurement unit into one compartment. Measurements are no longer carried out in electrochemical chambers but on sensor plates instead. These 96-well sensor plates, invented by Gatlik Inc. (Basel, www.gatlik.com) contain three macro-electrodes in each well. Gold is used as both, a working and auxiliary electrode. The reference electrode is a secondary electrode, made of Ag/AgCl. All measurements were carried out at 20°C at pH 7.4 in 0.5 mM PB and 0.0001 mM KCl supporting electrolyte. For the enhancement of solubility of low water-soluble compounds, 10% DMSO was added.

The average scan rate was 0.640 V/s. Ferrocyanide ($\text{FeCN}/\text{FeCN}^+$) and ferrocene (FOC/FOC^+) were used as internal references (E^0 (FOC): 0.252 V vs. Ag/AgCl). Sample concentrations varied from 0.001 mM to 0.0001 mM. Total reaction volume per well can vary from 35.0-55.0 μl depending on the sensor plate type. EPSS was connected to a computer and data was imported into *Excel* and analyzed by a macro provided by Gatlik Ltd.

After the measurement, the sensor plate was cleaned with distilled water and ethanol using a cotton stick. The estimated average lifetime expectancy of a sensor plate is 8 uses before discarding. The total scan time of the whole sensor plate is 45 min, if 96 wells are scanned 5 times with an average scan rate of 0.5 V/s.

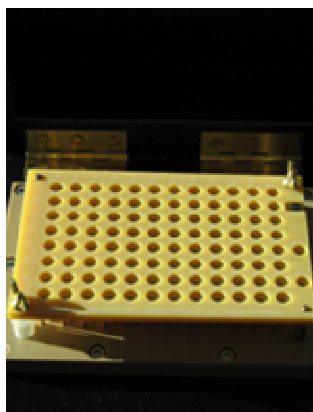


Fig.6 Picture of EPSS sensor plate placed on measurement unit

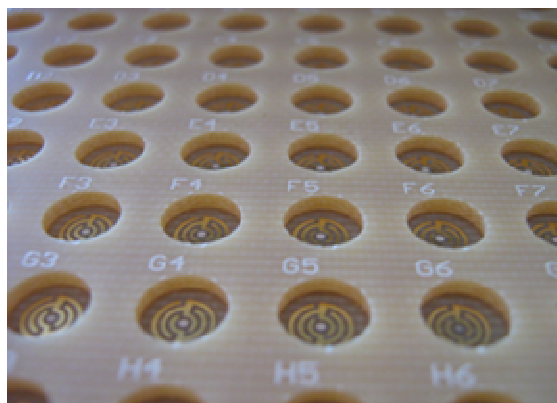


Fig.7 Example of a sensor plate V4 (Gatlik, Basel) with a total well volume of 55 μ l

2.2.3 Data Analysis

All results, acquired in Excel, were transferred to *Origin 7.0* (OriginLab Cooperation, Northampton, USA) for the graphical presentation, whereas all statistical calculations were carried out using *Statistica 7.1* (StatSoft, Tulsa, USA).

2.3 Results

The focuses of the study were first the development of a method using the new EPSS system and second the determination of redoxchemical behaviour of commercially available compounds by cyclic voltammetry. In addition, the results from both, the classical and EPSS methods were compared as depicted in **Fig.8**.

The initial application of EPSS was for the determination of viscosity so our aim was to modify EPSS for our specific purposes, such as the determination of redoxactive behaviour of discovery compounds. Secondly, feasibility was shown by repetition of experiments already conducted using the classical method.

Method development was initiated by following the subsequent experimental strategy: Measurements using the same compounds were repeated with EPSS. The EPSS system used the same experimental conditions as with the classical set-up but important parameters, such as the electrolyte concentration and the sample concentrations, had to be adjusted to conform to reaction requirements of EPSS. Furthermore, these initial experiments were the basis for the development of a method simulating physiological-like conditions with EPSS and the subsequent modification of some technical aspects. Validation and comparison of the EPSS with the classical system was carried out at pH 7.4 in PB at a concentration of 0.5 mM.

Table 1 shows the results, obtained by the classical method and EPSS, including the experimental error.

Table 1 Electrochemical Potentials for commercially available electron acceptors measured by the classical and HT-cyclic voltammetry (number of repetition per compound: 4), values are FOC-corrected. Used buffer system was hepes buffer.

Compound	Reduction potential	
	Classical cyclic voltammetry E_{red} [V], DMSO, Graz	HT- cyclic voltammetry E_{red} [V], buffer, pH:7.4, EPSS
ferrocene (ISTD)	0.368 ± 0.031	0.151 ± 0.012
2,3 dichloro-5,6 dicyano-benzoquinone	0.575 ± 0.006	0.522 ± 0.010
o-chloranil	0.155 ± 0.017	0.010 ± 0.014
p-chloranil	0.078 ± 0.092	-0.131 ± 0.004
chloranilic acid *	-0.220	-0.151 ± 0.003
juglone	-0.433 ± 0.095	-0.454 ± 0.023
1,2-napthoquinone	-0.505 ± 0.036	-0.463 ± 0.03
menadione	-0.615 ± 0.009	-0.612 ± 0.037
chalkon	-1.394 ± 0.004	-1.360 ± 0.051

* Only 1 datapoint could be obtained for chloranilic acid

Therefore, both methods deliver similar results under the described conditions. Fig.8 correlated the values of classical versus HT-methods. The correlation yielded a R^2 : 0.979 with an estimated standard error of 0.0907.

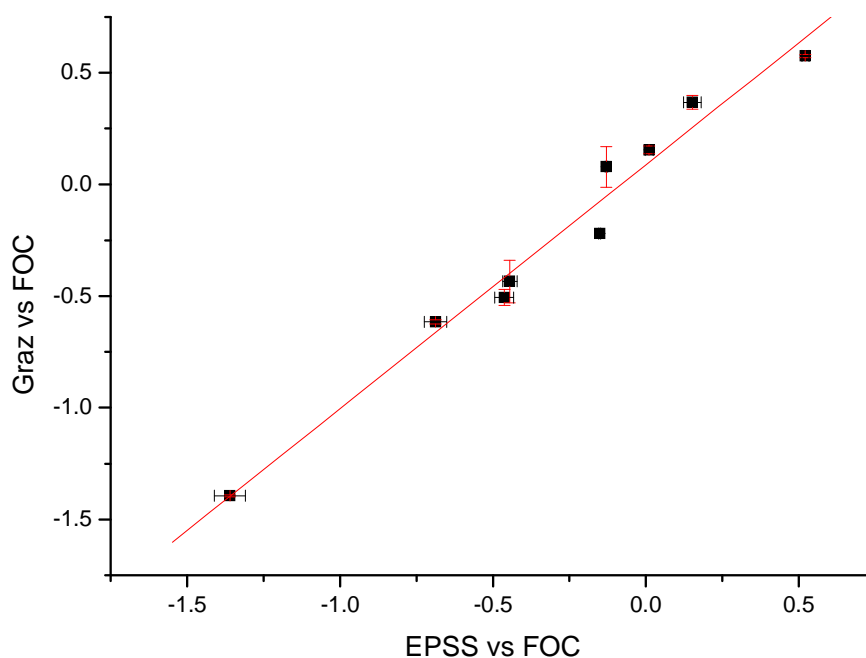


Fig.8 Correlation of data recorded at **classical method** and **EPSS** (HT-method), the correlation yielded a R^2 : 0.9799, $n=9$. Statistical values are as follows: F-value: 342.93, STD error of estimate: 0.0907 intercept: 0.068. Number of cases: $n=9$

2.4 Discussion

The major goals of the current study were the development of a new application of the EPSS system with a subsequent technical modification to measure molecules under physiological-like conditions and the comparison of the classical method with the HT-method.

However, the two methods seemed to be comparable as shown in Fig.8. Looking at this graph, low experimental errors were detectable for both methods. The only explanation for the larger standard deviation with EPSS was the fact that these experiments were performed with an open system. Although all solutions were strongly de-gassed, re-oxygenation was not preventable.

2.4.1 Classical Cyclic Voltammetry

One of the most notable weaknesses of the classical method was the large amounts of solvents required as well as long time-consuming cleaning steps.

25.0 ml of solvent per experiment were needed for the measurement of one single compound. Measurements, classically performed, are not suitable for profiling/screening purposes, as up to two compounds can be measured simultaneously, if a second electrochemical chamber unit is available applied in serial. It is more suitable for deducing specific properties of selected compounds. Solubility was another issue as the threshold concentration was easily infringed. Measurements in aqueous systems, such as hepes buffer, failed because of solubility problems. For most compounds, the solubility threshold concentration was reached. Therefore, no suitable cyclic voltammetric results were obtained when using the PB as solvent.

In the classical experimental set-up (**Fig.5**), the electrochemical chamber was always covered by a lid. Solutions had been degassed 10 min before starting the experiment. Usage of organic solvents (ACN, DMSO) is clearly advantageous for the classical system and ACN of electrochemical grade is usually the solvent of choice for the record of precise and sharp voltammograms, unless the compound is not soluble in ACN.

2.4.2 HT-Cyclic Voltammetry: EPSS

The EPSS method was developed from the assay conditions implemented for the classical one, with the ultimate goal of developing a method for EPSS which can be applied under physiological-like conditions.

After that, EPSS was validated and compared with the classical system by using 9 (8 + 1 internal standard) selected commercially available redoxactive compounds. Major modifications and studies were necessary as volatility and shape of electrode meant it was not possible to apply the classical conditions directly to the EPSS method. For example for EPSS, TBAP had to be replaced by KCl as it seemed to be more advantageous for the enhancement of conductivity in this case. This was particularly beneficial for the Ag/AgCl secondary electrodes which require Cl-ions for conductivity

reasons [52]. With EPSS, disposable sensor plates were used. These were normal conductivity plates with 96 three-electrodes in each well. The total reaction volume amount was 35.0 to 55.0 μl , depending on the sensor plate type.

Covering the sensor plate with plastic or aluminium, failed because of the risk of capillary effect. Moreover, most commercially available foils contain glue on the reverse side so it was most likely the case that the solvent came into contact with the glue. Leaving the system open had the disadvantage that the Ar-degassed reaction solutions were quickly re-oxygenated. Neither ACN, DMSO nor other volatile solvents were expedient.

A clear advantage of EPSS was the possibility of measuring up to 96 compounds simultaneously. Total run time for one sensor plate measuring 96 wells and 5 scans each took 45 min at a scan rate of 0.64 V/s. What is more, even slightly insoluble compounds were measurable in PB as long as the threshold concentration was not reached.

The sensitivity of electrochemical experiments is influenced by the shape of electrodes. At the moment, the electrode shape in our sensor plates is the inter-digitated electrode type, so impurities were easily traced.

2.4.3 Solvent-Related Issues

Normally, electrochemical experiments are first conducted in pure ACN because it produces a curve shape resolution which facilitates easy evaluation of curve shapes and its peak. Secondly, DMSO or any other solvents are used to obtain the same results. Typically, curve resolution and shape is less sharp in DMSO or aqueous solvents.

Initially, hepes buffer was used as reaction solvent for EPSS measurements. However, based on the appearance of unsolicited signals in the blank run indicating hepes buffer as a potential reaction partner, the buffer system was changed to phosphate buffer with all other conditions (concentration, ionic strength and pH value) kept the same.

The reaction solvent of a single compartment system was ACN, DMSO and PB. Interestingly, the results in DMSO obtained from the classical method and results in PB from EPSS correlated well as illustrated in Fig. 8.

2.4.4 Internal Standards

Common internal references were used such as the FeCN-complex for aqueous solutions and FOC for organic solvents [52]. Gagné et al. [52] have described the suitability of internal references such as FOC. Measurements of a reduction potential is facilitated by the use of reliable and universally accepted reference electrodes such as normal hydrogen electrode (NHE), saturated calomel electrode (SCE) and Ag/AgCl electrode.

Unfortunately, they have not been able to find any good reference electrodes that work for any aqueous phases as measurements in aqueous media have not been extensively researched so far.

For this reason, the usage of an internal standard like FOC as well as FeCN-complex is clearly advantageous [52].

The cyclic voltammetric experiment is performed without FOC or FeCN first. FOC/ FeCN is added to the reaction solution and the experiment is then repeated [52]. Both the FOC and FeCN-complexes have a characteristic curve shape, showing reproducible reversible electrochemical behaviour. The redox potential of FOC is the absolute zero of the experiment so all formal cyclic voltammetric redox potentials are usually referred against internal standards e.g. FOC or FeCN.

Solubility of FOC is an issue in the physiological-like conditions as FOC is completely insoluble in aqueous media. The addition of 10% DMSO decreases the risk of precipitation. Experiments with 5% FOC resulted in no signals. In the case of aqueous conditions, FeCN should be preferably used.

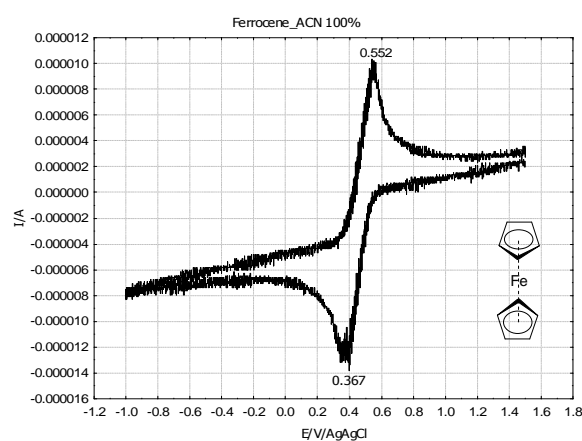


Fig.9 Cyclic voltammogram *ferrocene* in **acetonitrile**, scanning from 0.6 to 1.0 V with a scan rate of 0.8 V/s, signals retrieved by **classical cyclic voltammetry**

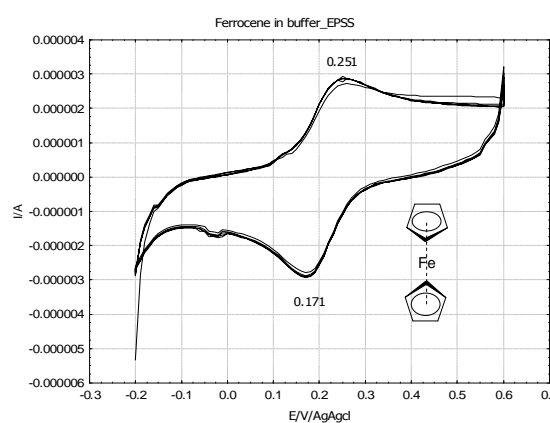


Fig.10 Cyclic voltammogram *ferrocene* in **phosphate buffer**, scanning from -0.3 to 0.8V with a scan rate of 0.64 V/s, signals retrieved by **EPSS**, HT-cyclic voltammetry

Solvent induced differences in the curve shape can also be investigated in Fig.9 and Fig.10. The cyclic voltammogram of FOC (Fig.9) conducted in ACN showed much sharper resolution than the cyclic voltammogram of FOC in PB (Fig.10).

Interestingly, cyclic voltammetry at slow scan rates results in reversible behaviour, while faster scan rates reveal quasi-reversible behaviour [43, 47, 52].

2.4.5 Further Approaches in Electrochemistry

Not many comparisons between classical and HT-cyclic voltammetry measurement are reported in literature. Shi et al. [53] described an electrochemical method to carry out experiments on microelectrodes based on microchips.

Recently, a literature search to obtain references with descriptions of similar systems such as EPSS has not revealed any results.

Another approach to applying electrochemistry for profiling or screening purposes is an electrochemical flow-cell coupled to LC/MS (**EC/LC/MS**) [40, 54]. Karst et al. [40]

investigated the suitability of this method for the fast detection of electrochemical behaviour when performing a LC/MS experiment. This electrochemical flow-cell is commercialized by ESA.INC (Chelmsford, USA).

Again, unknown concentrations and time are two main disadvantages to this method. The flow-cell is coupled with LC/MS so it is a part of one single run, which does not give much time for the compound to react electrochemically [36, 40, 55]. Furthermore, this system does not work under physiological-like conditions due to the required use of polar eluents in most LC/MS experiments and, thin-layer or wall-jet cells have a reputation for being contaminated very easily by reaction side products [36, 40].

The use of phosphate buffer is not possible, since it induces the risk of precipitation inside the instrument. In comparison with EPSS, this method does not provide any further information on the redoxreaction type. Gun et al. [55] showed that EC/LC/MS could be used as a powerful tool for the investigation of complex electrochemical transformations.

In principal, EC/LC/MS is a useful tool for a quick answer of unspecific electrochemical questions related to mass changes detectable in mass spectra. However, for the retrieval of comprehensive information on the redox behaviour, the strongest recommendation is to use EPSS.

2.5 Conclusions and Perspectives

For the first time, a HT-tool for the electrochemical profiling or screening of redoxactive molecules is available. Up to 96 samples can be measured in parallel to enable rapid determination of electrochemical characteristics. Tedious cleaning steps can be avoided, as the sensor plates are disposable. If problems related to measurements in volatile solvents can be resolved, the EPSS would be a good profiling or screening system for early drug discovery. Moreover, for the specific studies of the redoxchemical behaviour of compounds, EPSS is suitable as both the number and rate of scans can be optimized with relation to the experimental focus.

Although EC/LC/MS seemed to be more advantageous being coupled to LC/MS, it does not really permit experiments under physiological-like conditions and quantitative analysis of concentrations is not possible. Although numerous publications about EC/LC/MS are available, results have never been reported for an extended dataset. EC/LC/MS is more suitable for the rapid determination of unspecific redox behaviour resulting in mass changes whereas EPSS provides the information on the redox kinetics and the time-dependent change of the compound [36, 40].

The shape of the electrodes is the major determinant for specificity and concentration related issues. Currently the inter-digitated electrodes are used, allowing low concentration for the experimental set-up. One potential application of this technique is the measuring of a compound's electrochemical stability in physiological systems. However, the range of potential explicit applications of EPSS still needs to be investigated.

Literature search revealed that electrochemistry has become recognized as a suitable tool for research in early drug discovery phase or bioelectrochemistry [36, 40, 56].

Smith et al. [56, 57] have described an interesting approach in their review article to determine the redoxchemistry of the amyloid- β -peptide (a precursor for Alzheimer's disease) by EC/LC/MS. The growing significance of electrochemistry is illustrated by a number of publications which use electrochemistry to model phase-I metabolism [36, 40, 55].

Chapter 3: Redoxchemical Approach for the Prediction of Metabolic Stability

3.1 Introduction

In *Chapter 2* (pp. 33) the development of the method for HT-cyclic voltammetry has been already discussed. This method could be useful in supporting the electrochemical approach for compound profiling based on the relationship between redox potentials and metabolic stability.

In the following chapter, focus is mainly on the development of an assay based on a redoxchemical process by using a simple to handle redoxindicator (**RDI**), and the application of the results in the quantification and prediction of metabolic stability. This chapter deals with the development of a redox chemical process based on *p*-chlorine and describes analytical and compound related challenges that were encountered.

The most commonly occurring quinones are benzoquinones, naphthoquinones and anthraquinones. They are predominant in nature and are important components of several functional biological systems such as electron transport chains and protein carboxylation. Some quinones, such as ubiquinones, coenzyme Q and vitamin K, are metabolically significant [58]. The name "quinone" refers to compounds containing benzoquinone isomers as part of their structure [58]. Their carbonyl groups are more ketene-like, and although their structure is derived from aromatic compounds, they are not aromatic [58]. Halogenated quinones such as ***p*-chloranil** (2, 3, 5, 6 tetrachloro-1, 4-dibenzoquinone) or **DDQ** (dichloro-diquino-dimethane) are often used as strong oxidizing agents in organic chemistry.

Quinone chemistry is similar to that of α - β -unsaturated ketones. Their redox features are broadly based on the electrophilic reactivity determined by the carbonyl groups and the reaction of polarized double bonds with nucleophiles [58]. Quinones are involved in two different types of redox transitions, namely reactions involving only electron transfer and reactions nucleophilic addition, implying either oxidation or reduction of the quinoid ring. Quinones, in our case *p*-chloranil, are one or two electron acceptors. These one or two-electron transfer mechanisms can be observed in reversible two-peak cyclic voltammograms. Estimated reduction potentials of *p*-chloranil and juglone were E_{red} : -0.131 V vs. FOC (EPSS) and E_{red} : -0.454 V vs. FOC (EPSS) respectively.

An extensive literature search of molecules with well-documented electrochemical properties was conducted. Subsequently, nine compounds with a reduction potential close to that of CYP450 and a radical intermediate were selected for CV-measurements.

p-Chloranil (**Fig.1**) satisfied these criteria:

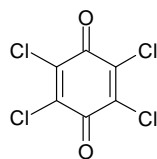


Fig.1 2,3,5,6-tetrachloro-1,4-dibenzoquinone (***p*-chloranil**)

The goal of the current study was the development of a HT-screening assay based on redoxchemical interactions. The assay should provide data simulating redox behaviour as observed in biological systems with focus on metabolic stability. Therefore, a strong electron acceptor such as *p*-chloranil was chosen as suitable component.

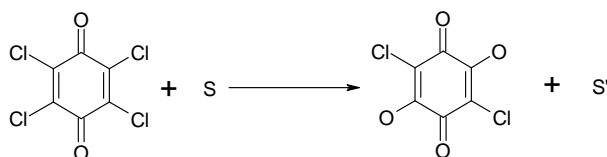


Fig.2 General reaction pathway of *p*-chloranil with a sample S

3.2 Experimental Section

3.2.1 Drugs and Chemicals

p-Chloranil, chloranilic acid, *o*-chloranil, menadione, DDQ and juglone used in this study were purchased from Fluka (Buchs, Switzerland) and used without purification. 1, 2-naphthoquinone, imipramine, ciprofloxacin, venlafaxin, verapamil, paroxetine and loratadine were obtained from Sigma-Aldrich (Buchs, Switzerland). All other compounds, namely sertraline, prochlorperazine, desipramine, nitrendipine, 5-methoxy psoralen and 8-methoxy coumarin were obtained from an internal compound depository.

Internal compounds with CL_high_mic were obtained as 100% DMSO stock solutions from an internal compound depository. Dopamine, pyrocatechine and spectroscopic grade DMSO were purchased from Acros (Belgium). The pH of the reaction solutions was adjusted with phosphate buffer (PB) (Merck) at pH 7.4.

3.2.1.1 Preparation of Sodium Dihydrogen Phosphate Buffer

A detailed description of the buffer preparation is provided in *Subchapter 2.2.1.2 (p.35)*.

3.2.1.2 Preparation of *p*-Chloranil Solution

A 10.0 mM (2.45 mg/ml) *p*-chloranil stock solution was prepared by dissolving 2.45 mg *p*-chloranil in 1 ml DMSO 100%. The stock solution was further diluted with 980 μ l DMSO 100% to a 0.2 mM working solution.

3.2.2 Methods

3.2.2.1 Cyclic Voltammetry

In *Chapter 2, Subchapter 2.2, p.38*, Materials and Methods for cyclic voltammetry have already been described more detail. Thus, there is no repetition in *Chapter 3*.

3.2.2.2 UV-Spectroscopy

Primary UV-spectroscopic measurements were conducted using a *SPECTRAmax Plus 384 v1.18 Feb01 2005* (serial number: MN 03536) for 96 or 384 UV-well plates and *SoftMax[®] Pro 4.8* (Molecular Devices Cooperation) for data analysis (both Molecular Devices Cooperation).

3.2.2.3 LC/MS Equipment: Agilent 1100 Series and 6140

The LC/MS system **Agilent 1100 Series** (Agilent Technologies, Waldbronn, Germany) comprised of a DE 23930947 column oven, DE 23902690 auto sampler, two DE 43619228 and DE 23913504 binary pumps and used an Agilent Extend C18, 1.8 μm , 4.6x50 mm analytical column maintained at a temperature of 60 °C, a DE 54200390 80 Hz Full spectral Ultra Fast LC diode array UV detector and a G1946D MSD SL single quad MS with API-ESI as ionization source.

For separations with basic eluents, a Waters Xbridge[®] C₁₈ 2.5 μm , 4.6 x 75 mm analytical column was used because its detection range covered a pH range from 1-12. Data was acquired using an interface and the chromatograms analysed using *Agilent Chemstation[®] Rev.B.03.01 (317)*.

The LC/MS system **Agilent 1200 Series with 6140 MSD** (Agilent Technologies, Waldbronn, Germany) comprised of a TCC SL column oven, DE 23902690 auto sampler, two binary pumps SL, Agilent Eclipse Plus[®] C18 1.8 μm , 2.1x50 mm analytical column maintained at a temperature of 60 °C and a DAD SL 80 Hz Full spectral Ultra Fast LC diode array UV detector with a 10 mm measurement unit and a G1946D MSD single quad MS with API-ESI as ionization source.

Agilent Eclipse Plus[®] C18 1.8 μm , 2.1x50 mm was identified as suitable for rapid resolution. Data was acquired using an interface and the chromatograms were analysed using the software as described above.

3.2.2.4 LC/MS Method: Agilent 1100 Series and 6140

For **Agilent 1100 Series**, a linear mobile phase gradient (1.0 ml/min) consisting of water (**A**): ACN (**B**): formic acid (65:35:0.1) was run. After 0.4 Min to 1.0 Min the gradient reached its maximum of water (**A**): ACN (**B**): formic acid (5:95:0.1) before returning to starting conditions. The column was equilibrated with 65% **A** during 0.5 min prior to next injection. Total runtime was 2.5 min. Detection of the analytes was by in-line UV-detection at 254, 280, 292, 310, 320 nm.

For **Agilent 1200 Series with 6140 MSD** the gradient, run for this assay consisted of solvent **A** 95% water +0.1% formic acid and solvent **B** 5% ACN + 0.1% formic acid. The gradient profile was 5- 95%**B** for 0.6 min at 1.0 ml/min and the column was equilibrated with 95% **A** for 0.2 min prior to each injection. Total runtime was 2.5 min. Detection of the analytes was by inline UV-detection at 254, 292, 310 and 320 nm.

3.2.2.5 MS-Parameters for Agilent 1100 and 6140 Series

Mass spectrometric parameters for the instruments of **1100 Series** and **6140 Series** were similar except for the peak width and step size. With **6140** the step-size was set at 0.15 min and peak width was at 0.05 min. The capillary voltage was 3500 V (positive and negative electrode). Standard conditions were used for the spray chamber (13 L/min, flow of drying gas at 300°C and 60 psig for nebuliser pressure). Mass detection was set up for a range of molecular weights between 150 and 600 g/mol using a

fragmentor voltage of 150 V and a peak width of 0.1 Min. All mobile phases were freshly prepared before each run due to stability issues. Peak height ratios between pure sample and sample+*p*-chloranil were used for quantitative analysis.

3.2.3 Final conditions for the sample preparation

p-Chloranil solution was prepared as described detailed in *Subchapter 3.2.1.2* (*p.49*). Total reaction volume was 100.0 μl containing 5.0 μl 0.01 mM *p*-chloranil, a 5.0 μl 0.01 mM sample and a 90.0 μl 50 mM PB. Samples, obtained in the 5 mM 8.0 μl format were prepared and diluted with 100% DMSO to the working solution concentration (0.2 mM). All liquids were degassed with Ar gas for 20 min to remove oxygen from the solution. Further steps in sample preparation were automated and performed with a Tecan Gemini[®] robotic system. UV-half area plates were covered with an aluminium foil which was pre-pierced to allow the robotic system to fill the wells. In the final step, *p*-chloranil was pipetted to each well to start the incubation. The system was incubated for 30 min and 30.0 μl 0.1 M HCl was added to adjust the final pH to 6.5. Subsequently, aliquots of the reaction volume were transferred into a NUNC 96 Agilent HPLC plate and covered with a pierceable foil. Finally, the LC/MS experiment was begun. In Fig.3, the sample procedure is illustrated graphically:

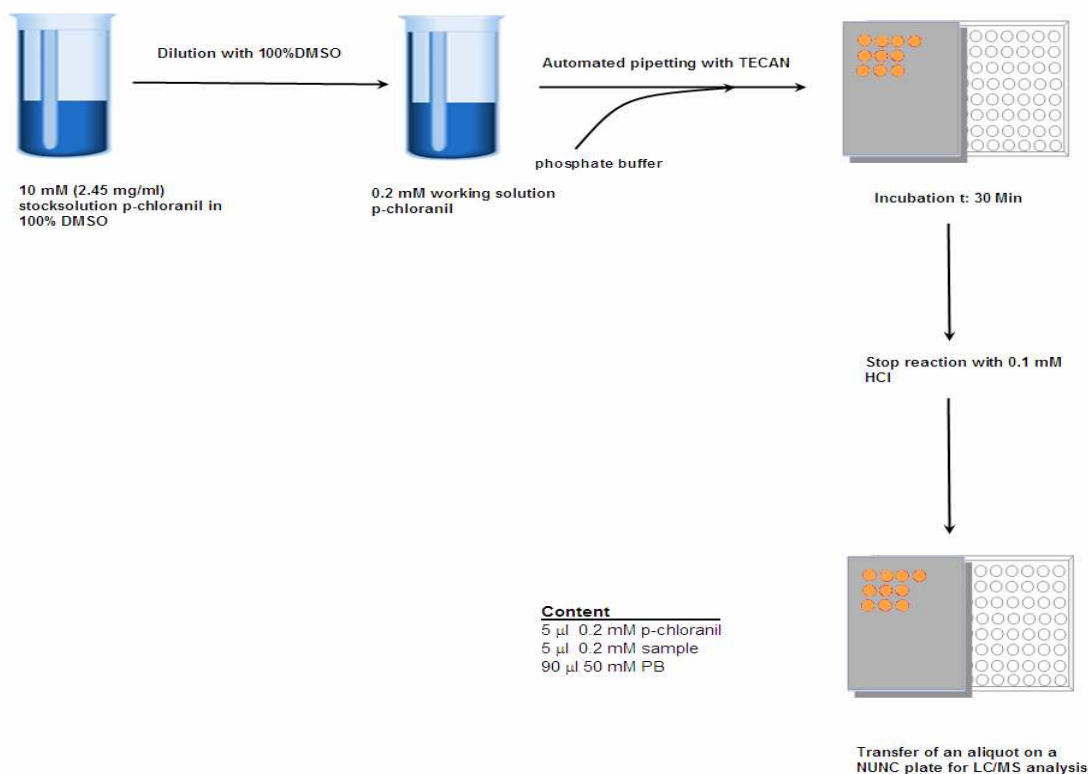


Fig.3 The principal steps of the sample preparation for *p*-chloranil assay

3.2.4 Assay Optimisation

The method was optimized by analysis of the time dependency, substrate and RDI dependency.

Time dependent product formation was investigated by selecting seven different time points (5, 20, 75, 90, 140, 170 and 210 min). Results are presented in Fig.11 (page 59). Time dependency of substrate and RDI concentrations were investigated using similar procedures (**Fig.11**) by varying substrate and RDI concentration at constant time. Eight different substrate and RDI concentrations (0.1, 0.075, 0.05, 0.025, 0.01, 0.005, 0.0025 and 0.001 mM) were chosen. All other parameters remained unchanged. Measurements were performed in triplicate.

3.2.5 Data Analysis

All results, acquired in Excel, were transferred to *Origin 7.0* (OriginLab Cooperation, Northampton, USA), whereas all statistical calculation were made with *Statistica 7.1* (StatSoft, Tulsa, USA). The peak heights of the sample before and after 30 min incubation with *p*-chloranil were compared. The difference between the two peak heights was expressed as percentage decrease of compound (%CPD_{dis}).

3.3 Results and Discussions

The major goal of the current study was the development of a fast and reliable redoxchemical assay to measure discovery compounds under physiological-like conditions using *p*-chloranil as the RDI and LC/MS as an analytical technique. This assay should simulate redox behaviour of compounds in biological systems. Consequently, the strong electron acceptor *p*-chloranil was chosen to interact with compounds from early drug discovery.

Initially, the assay was designed for UV-spectroscopy using a 96-well plate reader but soon transferred to LC/MS due to interferences of absorptions maxima (λ_{\max}) of sample and RDI.

Mass spectrometry (MS) was only used for structure determination or crosschecking. Almost all the experiments were conducted with a chromatographic system of the *Agilent 1100 series*. With the introduction of *Agilent 6140* RRLC with fast MSD, a modern and further developed version of *Agilent 1100 Series*, experiments were repeated and compared. The major difference between the two LC/MS systems was sensitivity and scanning speed for peak detection.

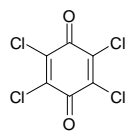
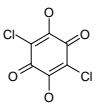
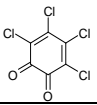
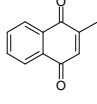
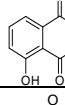
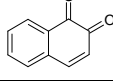
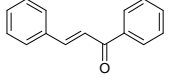
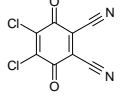
3.3.1 Selection of *p*-Chloranil

Preliminary experiments before beginning of this study were conducted with *p*-chloranil. Polar and non-polar solvents such as acetonitrile (ACN), ethanol (EtOH) and dimethylsulfoxide (DMSO) and different analytical or experimental conditions were tested. However, aqueous conditions had not been tested previously in the preliminary experiments. Furthermore, *p*-chloranil exhibited certain oxidation ability in terms of reactions with sample solutions.

Chemically, *p*-chloranil is a π -acceptor, showing high electron affinity due to its tetrachlorosubstitution [59]. Cl has a strong negative inductive effect on the quinoid ring. For that reason, *p*-chloranil was taken as a key structure for a literature data search conducted with *Beilstein* (MDL CrossFire Commander Version 7.9 SP2 (Build 46)) [60]. Selection criteria were either compounds including quinoid structures or small compounds with well-documented electrochemical properties.

This data is collected and a selection of 9 compounds is depicted in **Table 1**. Only 8 compounds are shown in Table 1, as the ninth compound is the internal standard FOC. Potentials are illustrated either in half-wave potentials or peak potentials. The entire information is given in the appendix.

Table 1 Literature data of selected compounds with documented electrochemical data

Compound	MW	Structure	E-Pot [61]	Solvent	Method	Lit.Ref
<i>p</i>-chloranil	245.88		-0.33	ACN	CV	[62-72]
			0.35	ACN		
			-0.88	DMF	CV	
			0.78	MeOH	Pot.Tit	
			0.24	CH ₂ Cl ₂	CV	
			0.312	C ₆ H ₆		
chlorac	208.99		0.42	H ₂ O	CV	[65, 73-78]
ochlor	254.88		0.833	C ₆ H ₆		[65, 79, 80]
			0.794	H ₂ O		
mena	172.18		-0.225		P	[58, 81-84]
			-0.277		CV	
jug	174.16		0.22	DMSO	CV	[65, 81, 85]
			0.45			
12naphQ	158.16		0.579	EtOH		[65]
chalk	208.26		-0.62	H ₂ O	P	[86, 87]
			-1.0061			
			-1.19	Buffer	P	
DDQ	227.01					

Data in **Table 1** was identified as fairly inconsistent. Comprehensive information regarding experimental conditions or technical details was rarely provided. Consequently, the above eight compounds were measured using cyclic voltammetry, covering a range from -1.0 V to ~1.0 V, and ferrocene (FOC) as internal standard.

Initial cyclic voltammetric experiments were only possible in ACN and DMSO due to the classical CV method. However, with the introduction of HT-cyclic voltammetry, measurements under physiological-like conditions were possible.

The goal of the electrochemical study was the identification of a set of compounds covering a broad range of reduction potentials and ideally exhibiting a value close to the CYP450's (E_{red} : -0.25 V) and reversible electrochemical behaviour [88].

The entire results of the CV-measurements have already been presented in Table 1 of *Chapter 2, p.41*.

Juglone and *p*-chloranil (**Fig.4** and **Fig.5** respectively) were identified as examples for the CV-measurements reported previously. Hence, their reduction potentials were in a range which was expedient for successful sample oxidations. Naturally, there were differences regarding the experimental and literature values which were due to different electrode materials and experimental conditions.

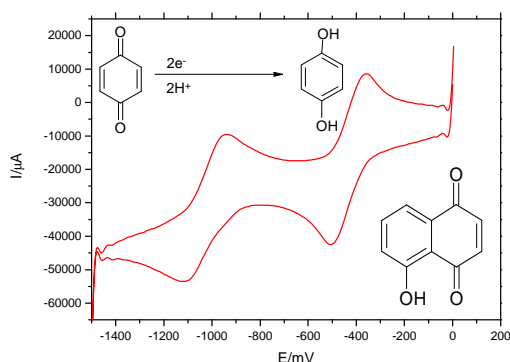


Fig.4 Cyclic voltammogram of 0.01 mM **juglone** measured in 100% DMSO at a scan rate of 150 mV/s in a range from 600 mV to -1000 mV using classical CV

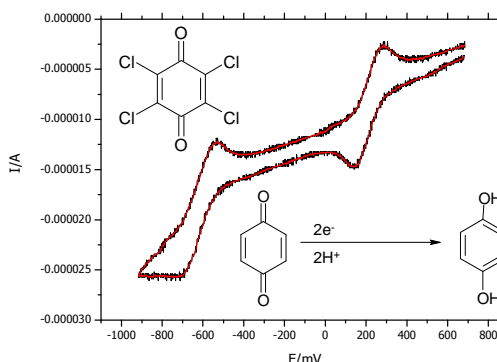


Fig.5 Cyclic voltammogram of 0.01 mM ***p*-chloranil** measured in 100% DMSO at a scan rate of 150mV/s in a range from 600 mV to -1000 mV using classical CV

Initial assay development and validation was carried out with **juglone** (5-hydroxy-1, 4-naphthoquinone) as it showed reversible two-electron accepting behaviour. Its λ_{\max} was determined as 424 nm in PB.

Continuing experiments of juglone with commercially available compounds indicated juglone's oxidizing properties were not strong enough for a significant change of UV-spectra. The lack of substituents with strong negative inductive effects is one of the reasons why it is a weaker oxidant. For this reason, juglone was exchanged for *p*-chloranil.

Further optimisations of concentration and reaction volumes enabled the re-introduction of *p*-chloranil as a strong oxidant. What is more, the initial solubility problem of *p*-chloranil was solved by the determination of its threshold concentration by reducing concentrations. Its λ_{\max} was determined at 292 nm in PB and the λ_{\max} of its hydroquinone (HQ) at 310 nm.

With the extension of the dataset from commercially available compounds to discovery compounds, the low λ_{\max} of 292 nm soon appeared to be an obstacle as most discovery compounds have a λ_{\max} in a similar range. Thus, interferences of UV spectra were to be expected. To facilitate differentiation and strengthen the significance of this assay, the analytical technique was transferred from UV-spectroscopy to LC/MS. For data analysis, the peak height of the sample alone was compared with peak height of the sample after incubation with *p*-chloranil. Quantification via peak area was not appropriate due to

occasionally appearing broad peaks. MS measurements, performed in the full scan mode, were required for additional structural information.

3.3.2 Stability of *p*-Chloranil

3.3.2.1 Light Influence

Factors affecting the stability of *p*-chloranil were studied. The influence of light was tested by an experiment using an aluminium cover for UV plates. The analytical method of choice was UV-spectroscopy.

The experimental set-up involved preparation of two sample plates at the final sample preparation conditions, one of which was provided with an additional light-protecting cover.

Protecting *p*-chloranil from light achieved more stability. After 40 min, 25.43% of *p*-chloranil was degraded in the absence of a light protecting cover whereas light protection increased the stability of *p*-chloranil by at least to 10%, as illustrated in Fig.6. Time in min (x-axis) was plotted against the natural logarithmic quotient of the absorption at the specific time point divided by absorption at time point $t=0$ (y-axis). Following this experiment, all tubes containing *p*-chloranil were protected from light with aluminium foil.

In addition, *p*-chloranil was always added last, to ensure the same starting point for the incubation.

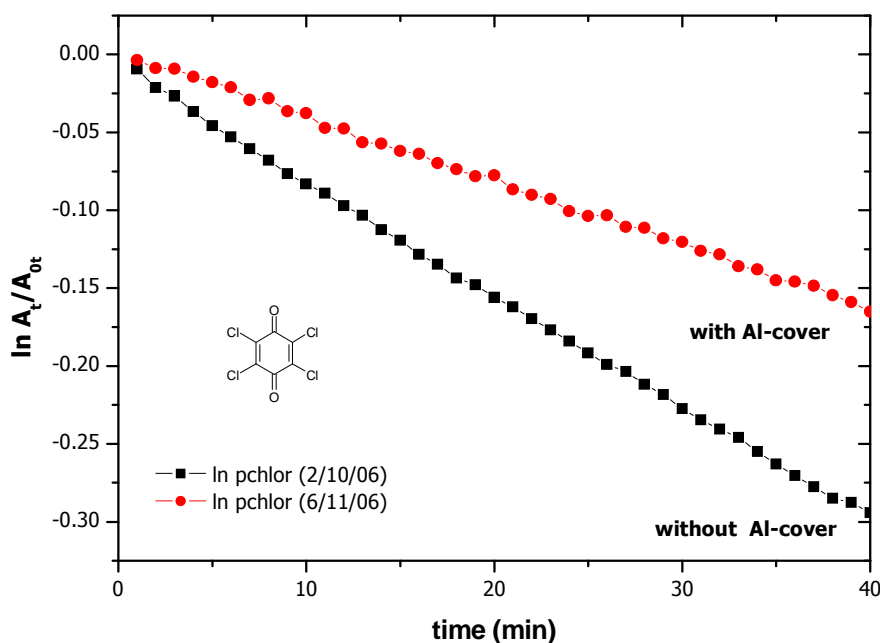


Fig.6 Influence of light on the degradation of *p*-chloranil using an aluminium (Al) cover. A kinetic measurement during 40 min was performed using three different wavelengths (292 nm, 310 nm and 650 nm). Measurements at 650 nm were necessary to crosscheck solubility of compounds. The measurement interval was 1 min and OD_{\min} was set 0, OD_{\max} at 1. The *p*-chloranil sample without Al-cover showed at higher degree of degradation (25.43%) than the sample with Al-cover (15.43 %).

3.3.2.2 pH-Related Influences

Kinetic experiments of *p*-chloranil in aqueous media with neutral to slightly alkaline pH values indicated pH related degradation. Consequently, for the evaluation of potential pH-related influences on the absorbance spectra of *p*-chloranil, an experiment was launched at two different pH values (6.5 and 7.4) with similar experimental conditions to that of Sarr et al. [89, 90]. All reaction solutions were purged heavily with Ar to avoid oxygen influence. By decreasing the pH value, decomposition was either slowed down or even stopped as illustrated in Fig.7.

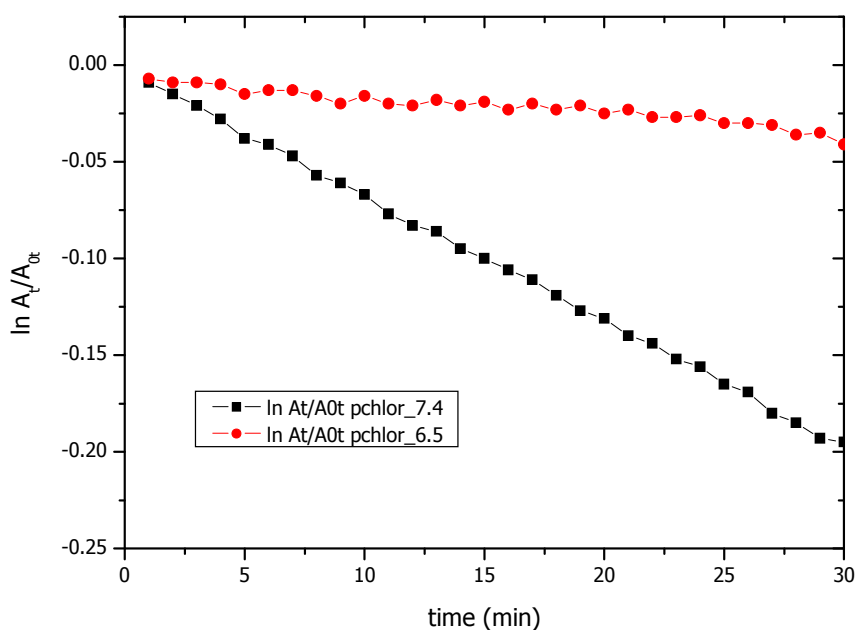


Fig.7 Influence of pH value on the degradation of *p*-chloranil using aluminium cover. Measurement was done with UV-Vis-spectroscopy performing a kinetic measurement over 40 min using three different wavelengths at 292 nm, 310 nm and 650 nm. 650 nm was necessary to crosscheck solubility of compounds. The measurement interval was 1 min with OD_{min} was set at 0, OD_{max} at 1.

According to Hancock and Bishop [91, 92] hydrolysis of *p*-chloranil produces chloranilic acid. Sarr et al. [89] intensively studied the behaviour of *p*-chloranil in aqueous media in the pH range from 6.5 up to 9 with observed change in absorbance spectra. Raymond et al. [93] also reported the fast degradation of *p*-chloranil in aqueous media. In Fig.8 the degradation of *p*-chloranil to chloranilic acid as described in the publication of Veltsitas [94] is shown.

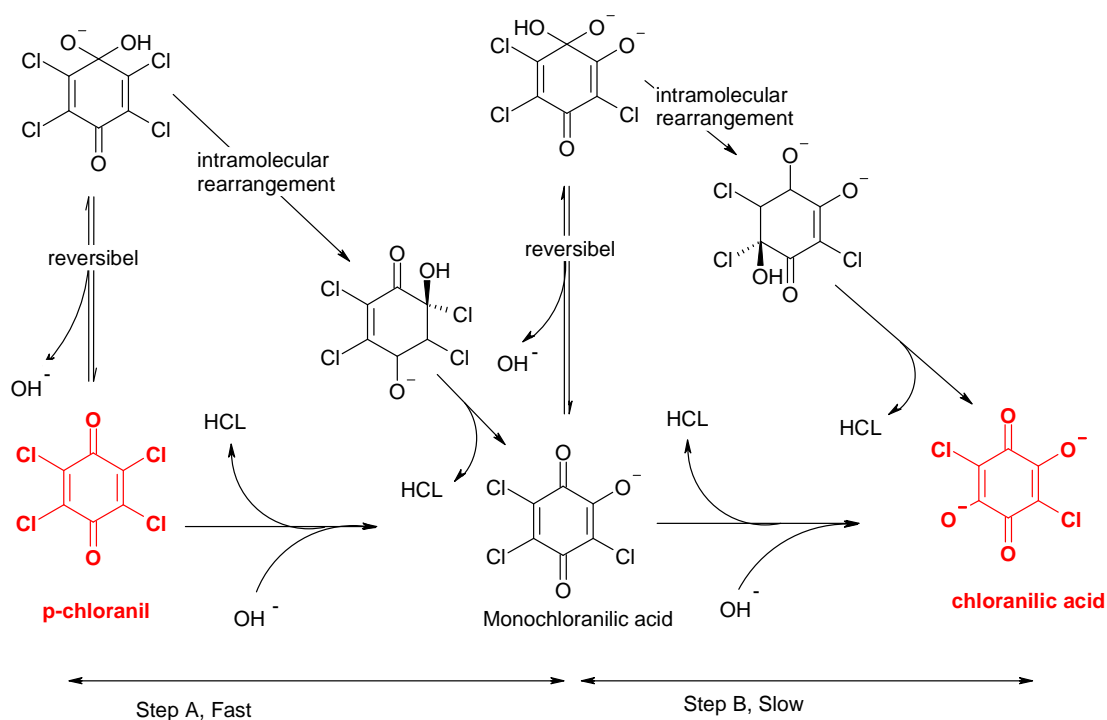


Fig.8: Degradation of *p*-chloranil to chloranilic acid according to Veltsitas [94]

Furthermore, a new step was introduced into the sample preparation procedure. After $t=30$ min, the incubation of *p*-chloranil/ sample was terminated by adding $30.0 \mu\text{l}$ 0.1 M HCl to reach the final pH of 6.5 and make an LC/MS experiment feasible, as degradation was no longer proceeding.

3.3.2.3 Physical Stability of *p*-Chloranil

In addition, the ageing of solid *p*-chloranil should be taken into account. The *p*-chloranil powder is hygroscopic and undergoes rapid decomposition to its hydroquinone (**HQ**). In practice, any given container of a *p*-chloranil sample should not be used for longer than 2-3 months after opening.

A constant Ar atmosphere covering the powder in the container was found to slow down degradation. The difference between freshly opened powder and older powder are illustrated in Fig.9.

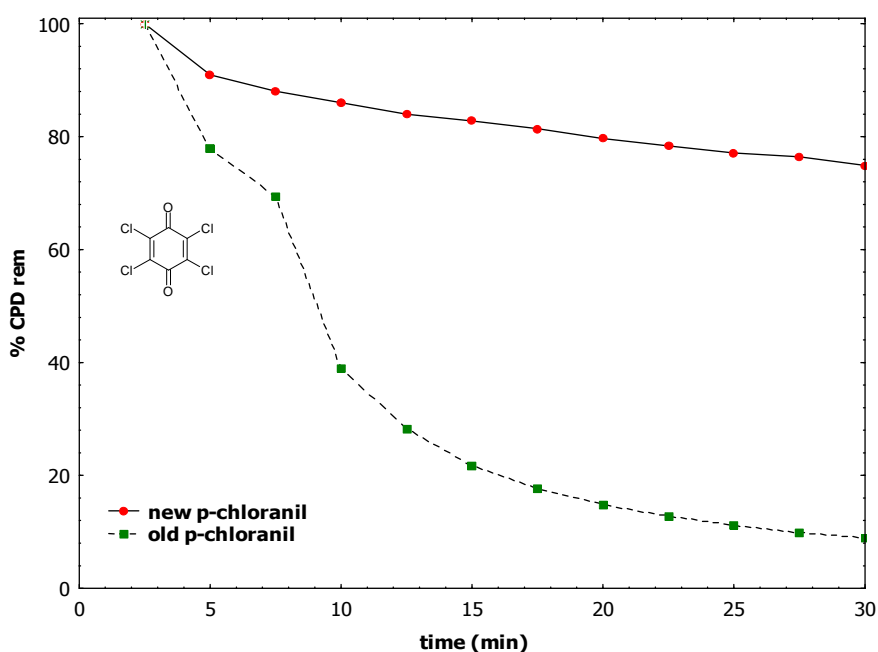


Fig.9: Degradation kinetics of *p*-chloranil measured with Agilent 6140 under the conditions mentioned in Material and Methods, pp.46

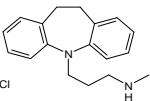
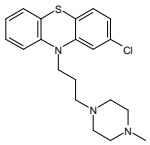
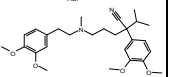
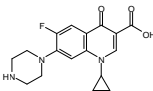
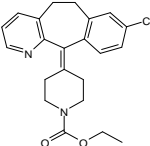
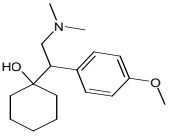
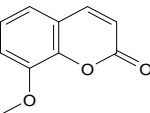
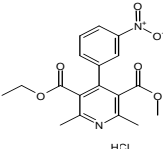
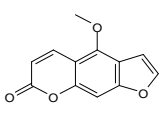
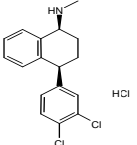
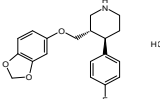
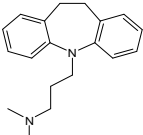
Two *p*-chloranil solutions were prepared containing either fresh *p*-chloranil in 100% DMSO or old *p*-chloranil in 100% DMSO solutions at a concentration of 0.01 mM and subsequently measured chromatographically.

Measurements were conducted by multiple injections. The curve with green points represents the old *p*-chloranil after multiple injections, whereas the curve with red dots represents the freshly opened powder.

3.3.3 Compound Selection Procedure

A set of 12 commercially available compounds (**Table 2**) with reportedly high *in vivo* clearance (**CL_{in vivo}**) were chosen for the reaction with *p*-chloranil. These compounds covered a broad range of CL_{in vivo} [16] from 0.1 to 50 ml/min/kg and were incubated under the assay conditions described previously. Besides structural diversity, one of the major selection criteria was a high microsomal instability.

Table 2 Structures of commercially available compounds with their CL_{mic} [16]

NAME	STRUCTURES	CL _{mic_rat} [μl/min/mg protein]			
desipramine		777.67	prochlorperazine		973
verapamil		650	ciprofloxacin		4.8
loratadine		434.91	venlafaxine		643.67
8-Me-Coumarin		225.54	nitrendipine		66.13
5-Me -Psoralen		1033.67	sertraline		97.75
paroxetine		2.15	imipramine		2180

Five of these commercially available compounds with particularly high $CL_{in vivo}$ were used for incubations with *p*-chloranil and measured kinetically by UV-spectroscopy. The obtained results are presented in Fig.10.

Following first-order kinetics, the ratio of the term $\ln A_t/A_{ot}$ (A stands for absorption) is plotted versus time (min).

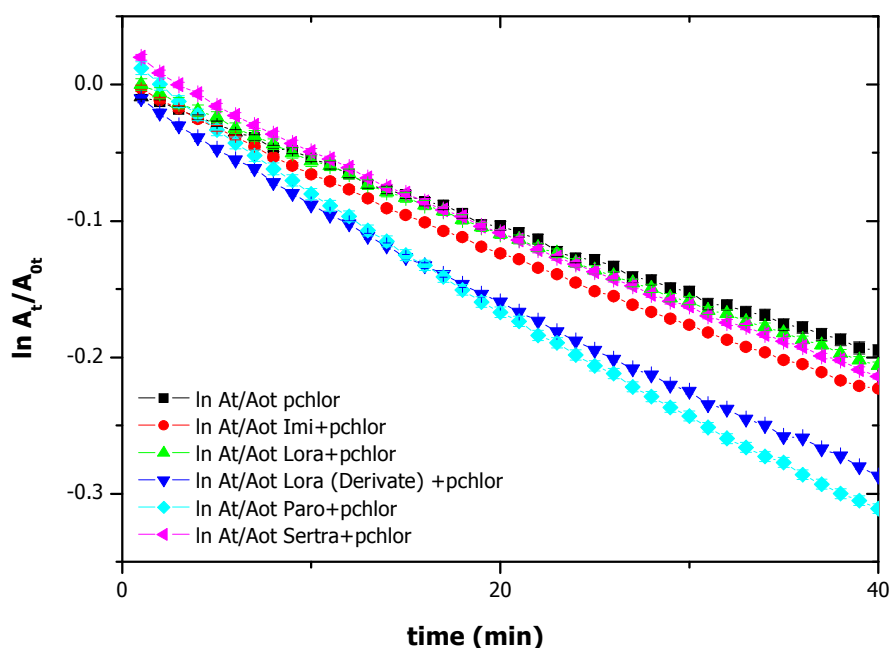


Fig. 10 Degradation kinetics of five commercially available compounds [loratadine (lora), imipramine (imi), loratadine derivative (lora+derivative), paroxetine (paro) and sertraline (sertra)] after their incubation with *p*-chloranil at equimolar concentrations of 0.01 mM.

3.3.4 Assay Set-Up

Several experiments modulating RDI, sample concentration, incubation time and assay conditions were performed to optimise reaction conditions.

Fig.11 illustrates an example of the evaluation of concentration dependency on rate for pure *p*-chloranil and loratadine (lora), imipramine (imi) and sertraline (sertra) incubated with *p*-chloranil respectively. These commercial compounds were chosen as examples due to the good availability of their major metabolites.

Equimolar conditions of 0.01 mM substrate and *p*-chloranil were appropriate as a linear plot of k vs. time was observed. Initially, assay development was carried out with juglone, another quinone showing reversible redoxchemical behaviour, but soon replaced by *p*-chloranil because juglone did not exhibit the expected oxidation capability.

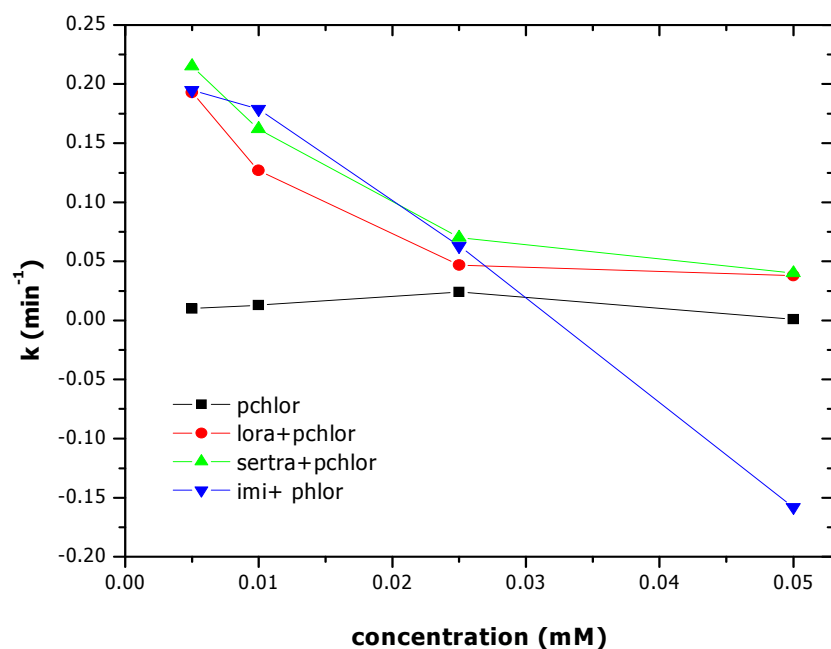


Fig. 11: Concentration dependency of three different commercially available compounds loratadine (lora), imipramine (imi), sertraline (sertra) and RDI *p*-chloranil at equimolar concentration of 0.01 mM. The reaction followed first order kinetics. The λ_{max} was chosen for *p*-chloranil at 320 nm. The number of cases was $n=4$. The incubation length was set to 30 min.

Concentration (substrate and *p*-chloranil) dependent behaviour was similar to that of juglone so when the concentration dependency experiment was repeated, only single measurements per concentration were performed. Thus, no error bars are presented in Fig.11.

Finally, the assay set-up was as follows: sample concentration at 0.01 mM, RDI concentration at 0.01 mM, 10% DMSO, PB and an incubation time of $t=30$ min. The reaction was stopped by adding 30.0 μl 0.1 M HCl to the reaction solution decreasing the pH to its final value of 6.5 and inhibiting the formation of hydroquinone (HQ) or trichlorhydroquinone (TCHQ).

3.3.5 Assay Validation: Reproducibility, Robustness

Reproducibility and robustness are two important criteria for a stable assay set-up. For that reason *inter-day* as well as *intra-day* variability of *p*-chloranil was evaluated.

First of all, consistency in retention times was checked. The retention times (**RT**) of *p*-chloranil were 1.105 min for *Agilent 6140 Series* and 0.552 min for *Agilent 1100 Series* respectively.

Table 3 illustrates the RSD % for 13 injections of *p*-chloranil on various days and months.

Table 3: Relative standard deviation of *p*-chloranil for its retention times for Agilent 1100 Series

Retention times (RT: 0.552 min)	average	SD	RSD %
<i>p</i> -chloranil (n=13)	0.551	0.006	1.086

Fig.12 is a representative example with *p*-chloranil of the chromatograms recorded with the **Agilent 1200 Series with 6140 MSD**.

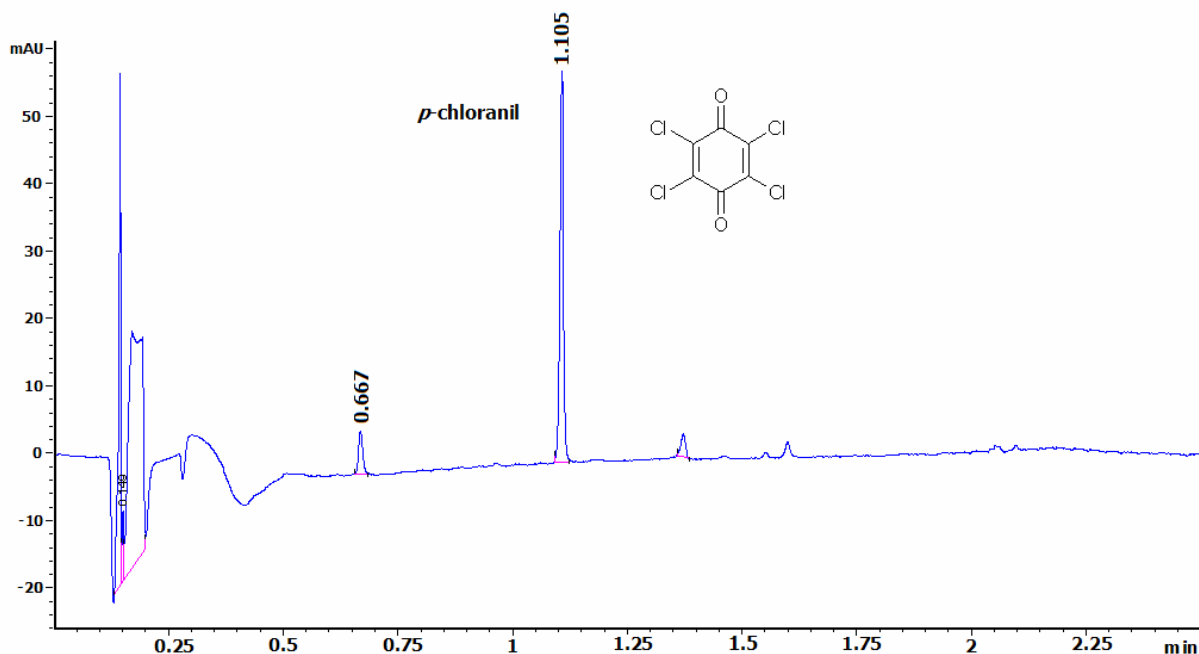


Fig.12: Representative chromatogram of *p*-chloranil measured with Agilent 1200 series and 6140 MSD. The gradient run for this assay consisted of 95% **A** (water +0.1% formic acid) and solvent 5% **B** (ACN + 0.1% formic acid). The gradient schedule is 5- 95% **B** for 0.6 min at 1.0 ml/min. The column is re-equilibrated with 95% **A** during 0.2 min prior to next injection. Total run time was 2.5 min. Detection of the analytes was by inline UV-detection at 254,292, 310, and 320.

The assay was validated on different days with various batches of freshly prepared *p*-chloranil. The results of this validation are presented in Table 4. For the calculation of the RSD of the intra-day variation, the average of a triple experiment was taken, whereas for the calculation of inter-day variation, the averages of two days were taken. These experiments were performed chromatographically and measured in triplicate.

Table 4 Intra-day, inter-day assay variability for *p*-chloranil (RDI) alone

Analyte	Concentration (mM)	Intra-day variation (RSD,%) *	Inter-day variation (RSD,%)
<i>p</i>-chloranil (n=3)	0.01	5.38	3.19
	0.01	3.19	2.57
	0.01	1.15	3.41
	0.01	3.19	3.41

* Inter-day variations are the mean of triple experiments of two days

Fig.13 illustrates a representative chromatogram of an internal sample (K5_2nd). It proves the effect of *p*-chloranil on the sample, as after 30 min only 70% of the initial concentration of K5_2nd remained.

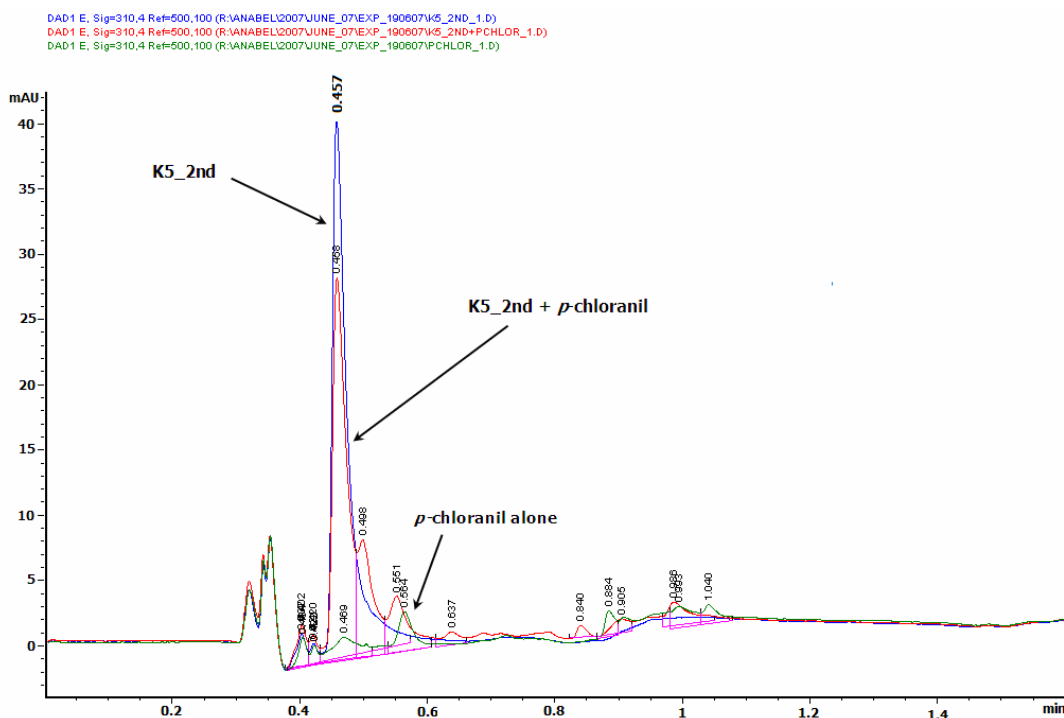


Fig.13 Example of a chromatogram measuring K5_2nd after the incubation $t=30$ min with *p*-chloranil. Measured with Agilent 1100 series and MSD. The gradient run for this assay consisted of **A** (water + 0.1% formic acid) and **B** (ACN + 0.1% formic acid). The gradient schedule is 5-95% **B** for 0.6 min at 1.0 ml/min. The column is re-equilibrated with **A** 95% for 0.2 min prior to next injection. Total runtime was 2.5 min. Detection of the analytes was by inline UV-detection at 254,292, 310, and 320 nm.

3.3.6 Reaction Products of *p*-Chloranil and MS

As previously described in Materials and Methods (*Subchapter 3.2, pp 49*) the ionization source used was API-ESI. Assay development also increased experience in the handling of *p*-chloranil and an understanding of its reaction pathway.

MS-measurements for *p*-chloranil were challenging, because for successful detection of signals in the negative scan mode, *p*-chloranil had to convert into its tetrachlorosubstituted hydroquinone first. Characteristic isotopic patterns for Cl allowed easier interpretation.

In Fig.14 a calculated isotopic pattern for **tetrachlorohydroquinone** TCIHQ (MW: 247.89) is provided.

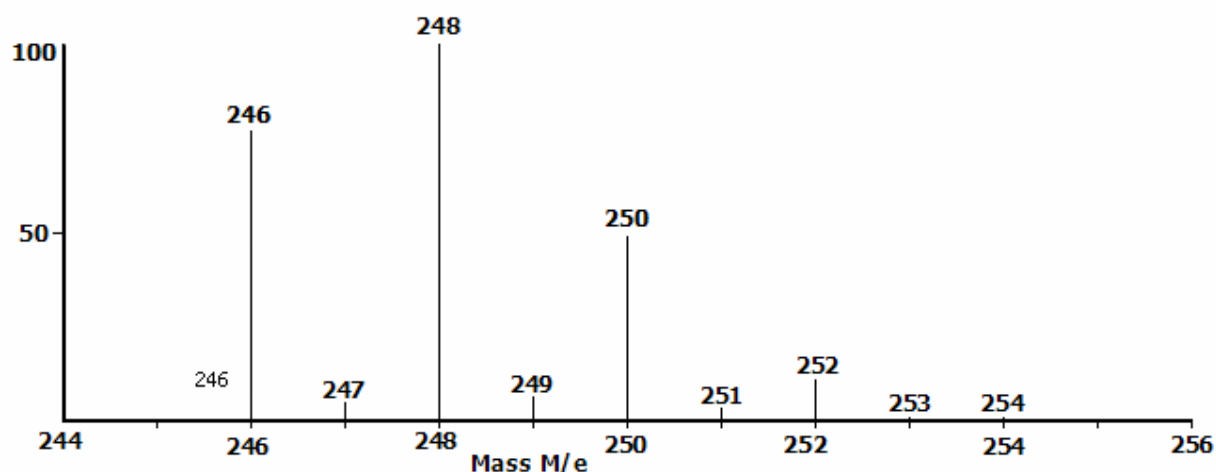


Fig.14 Calculated isotopic pattern for **tetrachlorohydroquinone (TCIHQ)** using a web calculating tool [95]

Chloranilic acid has been identified as one of the reaction products of *p*-chloranil in aqueous media. The absorption maximum of chloranilic acid occurs at λ_{\max} : 320 nm in PB which is close to that of *p*-chloranil (λ_{\max} at 292 nm) as mentioned previously. By UV-spectroscopy, differentiation of those peaks was unfeasible, but chromatographic separation enabled their visualization. This observation was confirmed by direct injection of chloranilic acid.

In Fig. 14 and 15, the calculated isotopic patterns of tetrachlorohydroquinone (**TClHQ**) and chloranilic acid are shown as a basis for the comparison with the experimental results retrieved.

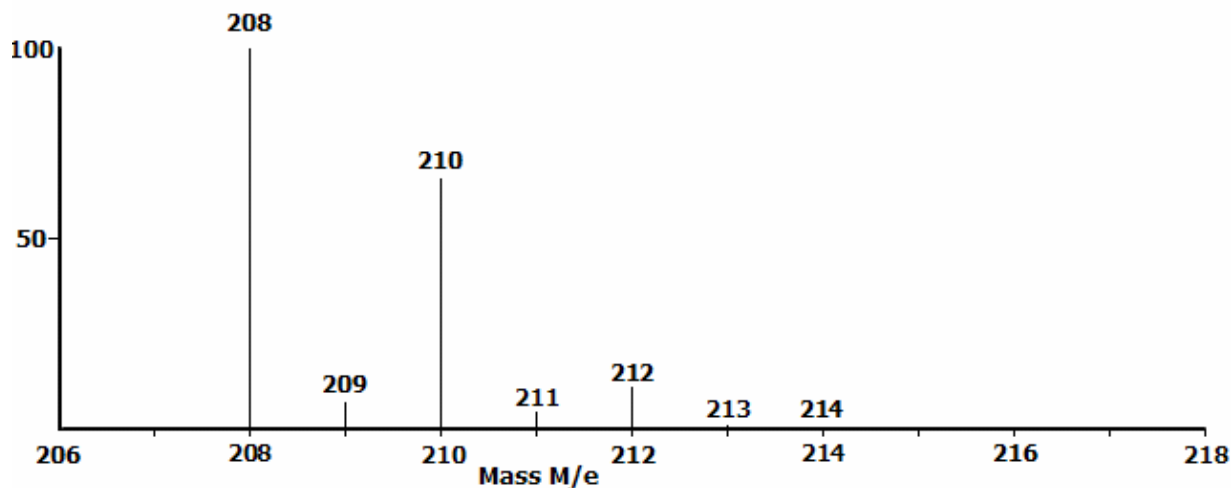


Fig.15 Calculated of isotopic pattern for **chloranilic acid (chlorac)** using a web tool [95]

In Fig.16 two isotopic patterns are depicted, the ones of both TClHQ and chloranilic acid. The typical isotopic pattern for both tri- and tetrachlorosubstitution are visible for TClHQ, but masses at 208.9 suggested the formation of chloranilic acid (208.9 g/mol). Closer inspection of the isotopic pattern of chloranilic acid retrieved experimentally suggested a trichlorosubstitution but the expected mass for trichlorosubstitution does not correlate with the MW as shown in Fig.16. No satisfactory explanation was available for this effect. TClHQ was injected to better understand the mixed isotopic pattern with *p*-chloranil as shown in Fig.19.

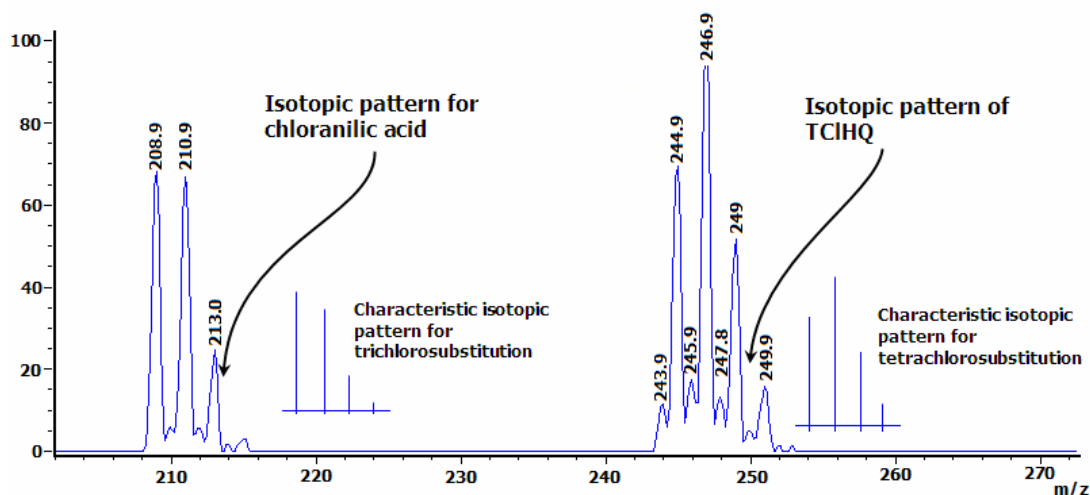


Fig.16 Isotopic pattern of **TClHQ** and **chlorac** measured with **Agilent 6140** Series. The gradient run for this assay consisted of **A** (95% water +0.1% formic acid) and solvent **B** 5% (ACN + 0.1% formic acid). The gradient schedule was 5- 95% **B** for 0.6 min at 1.0 ml/min. The column was re-equilibrated with 95% **A** for 0.2 min prior to next injection. Total runtime was 2.5 min. Detection of the analytes was by inline UV-detection at 254,292, 310, 320 nm. Standard conditions for MS were used.

Following this, more isotopic patterns of *p*-chloranil are shown. Fig.17 illustrates the calculated values whereas Fig.18 and 19 provide an overview of isotopic patterns retrieved from our experiments:

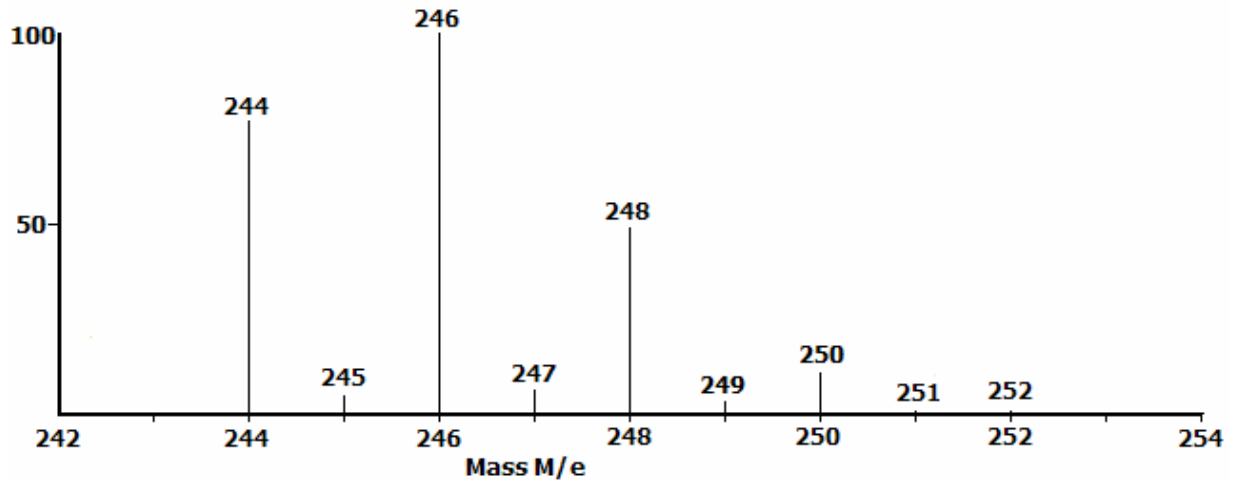


Fig.17 Calculated isotopic pattern of *p*-chloranil using a web tool [95]

Freshly prepared *p*-chloranil was analyzed via LC/MS and the result is shown in Fig.18. It exhibited the characteristic tetrachlorosubstitution pattern.

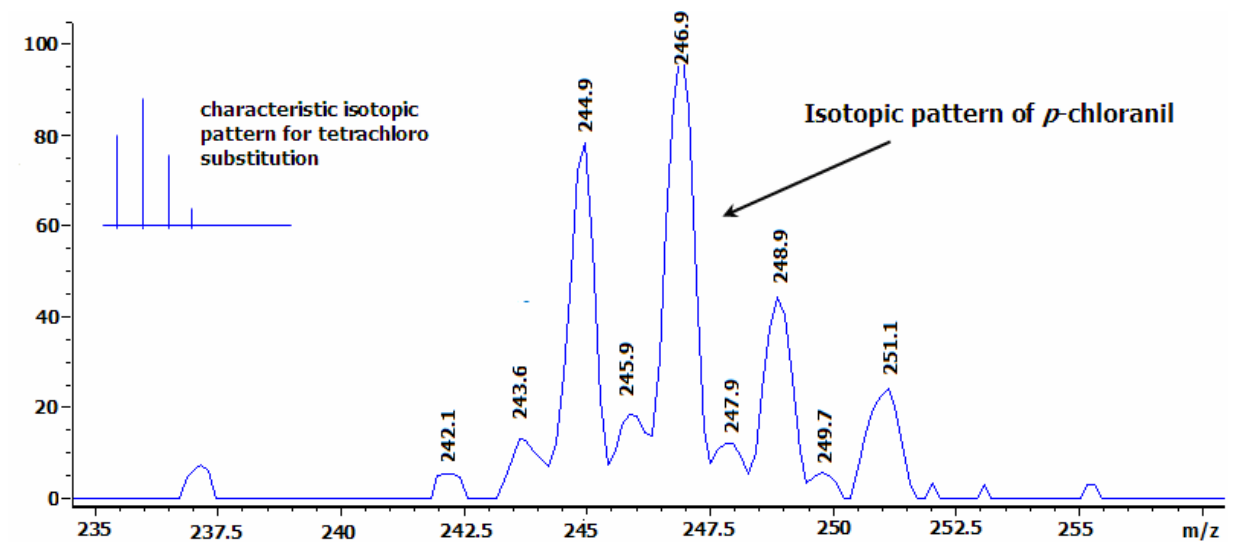


Fig.18 Isotopic pattern of fresh *p*-chloranil analysed with **Agilent 6140** Series. The gradient run for this assay consisted of **A** (95% water +0.1% formic acid) and solvent **B** 5% (ACN + 0.1% formic acid). The gradient schedule was 5- 95% **B** for 0.6 min at 1.0 ml/min. The column was re-equilibrated with 95% **A** for 0.2 min prior to next injection. Total runtime was 2.5 min. Detection of the analytes was by inline UV-detection at 254,292, 310, 320 nm. Standard conditions for MS were used.

In Fig.19 there is obviously a difference in the isotopic pattern as the characteristics for tetrachlorosubstitution are no longer visible.

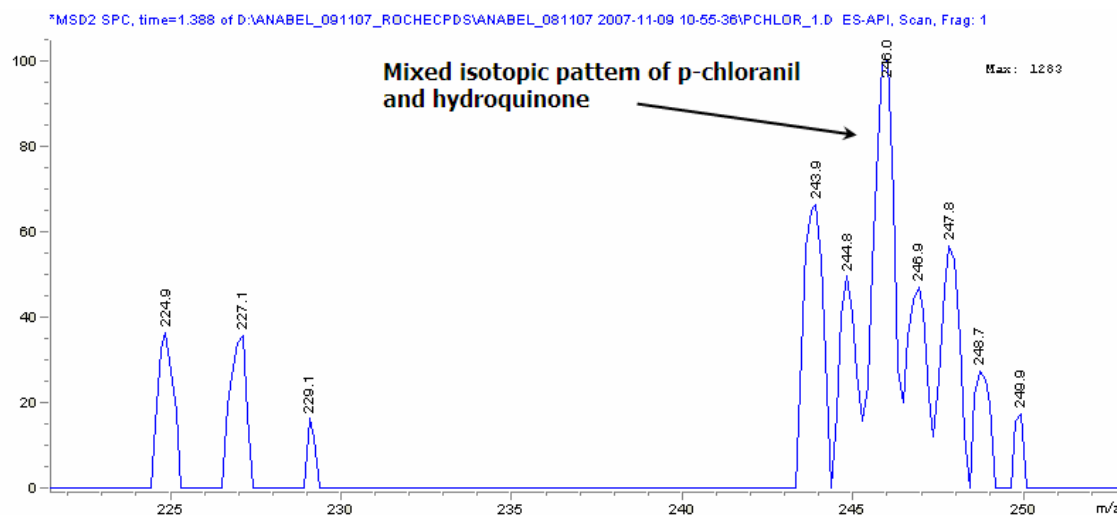


Fig.19 Isotopic pattern of mixture of *p*-chloranil and TCIHQ analyzed with Agilent 6140 Series. The gradient run for this assay consisted of **A** (95% water +0.1% formic acid) and solvent **B** 5% (ACN + 0.1% formic acid). The gradient schedule was 5- 95% **B** for 0.6 min at 1.0 ml/min. The column was re-equilibrated with 95% **A** for 0.2 min prior to next injection. Total runtime was 2.5 min. Detection of the analytes was by inline UV-detection at 254,292, 310, 320 nm. Standard conditions for MS were used.

In order to confirm these observations, the study with *p*-chloranil and its reaction behaviour was repeated in another internal lab at F. Hoffmann-La Roche with more sophisticated equipment (*Appendix, Results from p-Chloranil Studies pp. 115, [96, 97]*) Colleagues from the department *Applied Analytical Methods, section Molecular Structure Research* at F. Hoffmann-La Roche agreed to analyze the reaction products of *p*-chloranil and determine its reaction behaviour under our assay conditions.

The results are attached in the appendix [96, 97]. One of their major results was the identification of tetrachlorohydroquinone which was probably formed by oxidation of *p*-chloranil in the ionization source of LC/MS/MS. They also discovered that direct flow injection of *p*-chloranil into MS did not enhance the formation of hydroquinone.

They repeated direct flow injection of *p*-chloranil dissolved in ACN/MeOH and the isotopic pattern was in accordance with a tetrachloride-substitution. Moreover, direct flow injection of *p*-chloranil, dissolved in PB, also revealed an isotopic pattern characteristic of tetrachloride substitution. Both ACN and PB, which were used for the chromatographic experiment, did not contain of any modifiers. Subsequent experiments with standard experimental LC/MS conditions revealed a mixture of isotopic patterns of HQ and *p*-chloranil. Formic acid in the mobile phase (added to increase the ionization of the compounds), probably contributes to the decomposition of *p*-chloranil in the ionization source. The results of their experiments were similar to those already retrieved by our lab. A major finding was the immediate formation of HQ once the LC/MS experiment was launched. However, there also seemed to be a time dependent

formation of HQ and TCHQ documented with chromatograms found in the appendix. In summary, our results were confirmed by those of our colleagues.

One of their recommendations was to avoid API-ESI or formic acid as a modifier. API-ESI was described in the literature as difficult to handle with regard to other issues [89]. Sarr et al. [89] reported that most likely a basic environment is created due to the enrichment of hydroxide ions during electro spray ionization. Moreover, he stated that the environment in the electro-spray chamber seemed to be sufficient for alkaline hydrolysis [89]. Finally, an example for complete decomposition of *p*-chloranil is shown in Fig.20. A similar one was published by Sarr et al.[89].

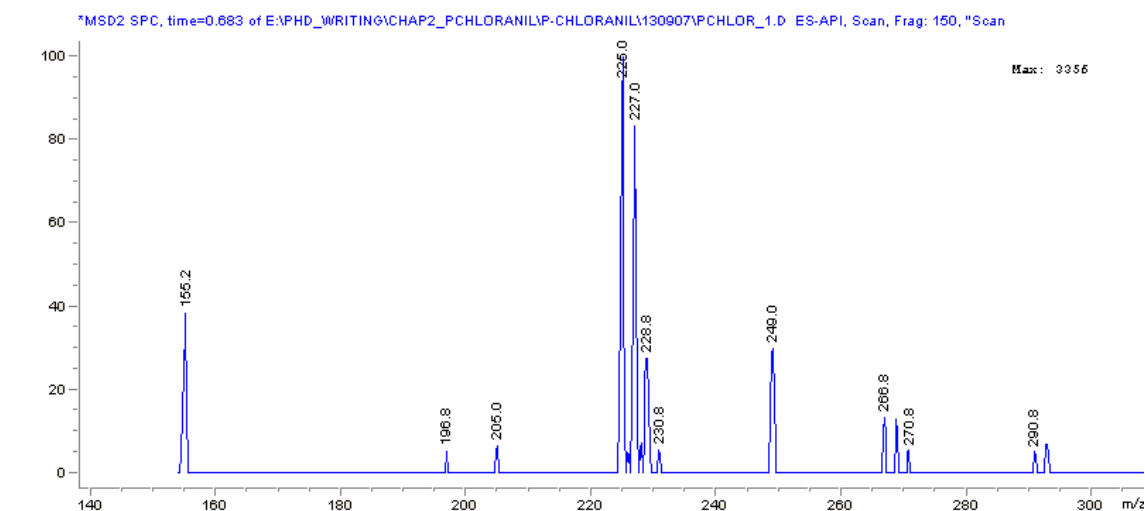


Fig.20 Example for decomposition of *p*-chloranil after short incubation in aqueous medium at pH 7.4 with **Agilent 6140** Series. The gradient run for this assay consisted of **A** (95% water +0.1% formic acid) and solvent **B** 5% (ACN + 0.1% formic acid). The gradient schedule was 5- 95% **B** for 0.6 min at 1.0 ml/min. The column was re-equilibrated with 95% **A** for 0.2 min prior to next injection. Total runtime was 2.5 min. Detection of the analytes was by inline UV-detection at 254,292, 310, 320 nm. Standard conditions for MS were used.

3.4 Conclusions and Perspectives

p-Chloranil is a compound with complex reaction behaviour due to its tetrachloride-substitution. Assay development was therefore accompanied with numerous challenges and working with *p*-chloranil required some precautions.

Solutions of *p*-chloranil should always be prepared freshly before each experiment and stored in the dark. In addition all reaction solutions should be degassed with Ar before use.

As *p*-chloranil is inexpensive, it is advantageous to exchange the bottle of powder regularly if used intensively, or at least ensure that the powder is always stored under Ar atmosphere.

Intensive investigations revealed that quantification by peak height comparison of sample and sample after *p*-chloranil incubation offered reasonable results. Quantification via peak area was not possible as occasionally broad peaks occurred.

The assay per se works, if quantification is based on the disappearance of the sample. Its experimental results will be further discussed in *Chapter 4* (p.71).

Clearly advantageous for the *p*-chloranil assay are the low amounts of compound required for the assay. Including a final DMSO concentration of 10% in the final assay conditions enabled concentrations of 0.01 mM for both *p*-chloranil and most internal samples.

The assay showed reasonable reproducibility and robustness, expressed in a small SD. If the assay set-up is taken for further research, a replacement of *p*-chloranil with a compound with similar oxidant properties but less complex reaction behaviour in aqueous media could be advantageous. *o*-Chloranil is a potential compound for the replacement of *p*-chloranil as *o*-chloranil exhibits a more positive reduction potential as *p*-chloranil ($E_{\text{red (ochlor)}}$ vs. FOC: 0.010 V), but literature has not reported any complex reaction behaviour in aqueous media.

For the routine application of the assay, only LC is necessary as MS is only used for the answering of structure specific questions. Additionally, in case of the lack of chromophoric structures, MS-analysis can be used to detect metabolite formation. If MS is used routinely for quantification, a replacement of modifier should be considered because of a tendency for formic acid (FA) adducts formation in API-ESI/MS.

Hence, this assay may be suitable for applications in early drug discovery and complement microsomal clearance information if the currently existing problems are solved. Results which were obtained in the current chapter will be further discussed in *Chapter 4* (p.68).

Chapter 4: Prediction of Metabolic Stability by Redoxchemical and Electrochemical Approaches

Results obtained from the electrochemical (*Chapter 2, pp.33*) and redoxchemical approach (*Chapter 3, pp.47*) for the early metabolic stability profiling of discovery compounds are further discussed in the following chapter.

4.1 Introduction

Due to extensive biotransformation, insufficient metabolic stability of discovery compounds is still a major bottleneck in the drug discovery process [13]. Numerous *in vitro* approaches have been introduced in the past few years for the early determination of metabolic profiles.

The primary aim of metabolic studies is the detection of a compound's most likely site of metabolism, enabling compound modification in the early stages of the drug discovery process.

Metabolic stability is a term widely used in the description of the rate and extent of metabolism of a compound [12]. For example, a compound with a low degree of metabolic stability is rapidly and extensively metabolized [11].

Usually, metabolic stability studies involve the determination of two pharmacokinetic parameters: ***in vitro* half-life** ($t_{1/2}$) and **intrinsic clearance** (Cl_{int}) which are used for the description of metabolic stability.

The intrinsic clearance is based on three basic parameters: the blood flow through the organ (Q), the intrinsic capability of the organ to clear the drug (Cl_{int}) and the limitation on drug uptake into the clearing organ [12, 98].

Applying the theory of the "well-stirred" model, the relationship between hepatic venous concentration C_{out} , incoming mixed arterial and venous blood concentration C_{in} , hepatic blood flow Q_H and intrinsic clearance Cl_{int} is expressed as follows:

$$Cl_H = \frac{Q_H \cdot f_u \cdot Cl_{int}}{Q_H + f_u \cdot Cl_{int}} \quad (1)$$

Clearance and its relationship to metabolic stability have already been discussed extensively in *Chapter I, pp. 12*, of this thesis and will not be further mentioned hereafter.

4.1.1 Biotransformation and CYP450

Most drugs with a low degree of metabolic stability are usually associated with extensive biotransformation reactions.

Biotransformation is defined as the conversion of a lipophilic to a more hydrophilic compound which can be readily excreted by the kidneys [12, 22, 23].

Generally, biotransformation is divided into phase-I and phase-II metabolism. Phase-I metabolism involves oxidation, reduction and hydrolysis reactions and is catalyzed by a number of enzymes. Phase-II metabolism involves conjugation reactions, so biotransformation is normally linked with a reduction in lipophilicity and the formation of a metabolite that is less active than the parent compound [99]. Most phase-I reactions are catalyzed by cytochromes P450 (CYP450).

CYP450s are enzymes of a superfamily with a haem-containing moiety [39]. Some of these isoforms exhibit high substrate specificity, based on the structural diversity in the active site of the enzyme, which perform essential biosynthetic functions such as steroid synthesis [35, 39, 100].

Only a few CYP450 isoforms play a significant role in the drug metabolism process [26]. These are the isoforms of the CYP1A, 2A6, 2B6, 2C, 2D6, 2E1 and 3A families.

The most versatile and most abundant isoform is CYP3A4 whose most interesting feature is an active site cavity of large volume resulting in a low substrate specificity [32] and a high capacity to oxidize a variety of both small and relatively large compounds [32]. If small molecules are bound to CYP3A4, a significant portion of the cavity remains unfilled by the substrate. Hence, the contact between the substrate and enzyme is not extensive and the unfilled portion of the cavity is sufficiently large to bind another substrate [33]. In such cases, orientation of the substrate to the active site of CYP3A4 is also important.

4.1.2 CYP450 Catalysis

The CYP450 catalysis itself is redoxchemical driven. Electrons obtained from an electron transport chain are needed for the formation of a high-energy oxidizing species [39, 101, 102]. The high-energy oxidizing species is needed for efficient hydroxylation of an inactive C-H bond by the relatively inert oxygen molecule which is in its triplet ground state [39, 100].

Several parameters contribute to the activation of CYP450. Coordination environment and the dielectric setting of the haem are both important as they significantly contribute to the high amount of electron energy required for the activation of the enzyme [1, 35, 39].

For the redoxchemical process of CYP450 catalysis, the haem moiety (**Fig.1**) (iron-protoporphyrin) is very important as it is the electroactive component of CYP450 [39].

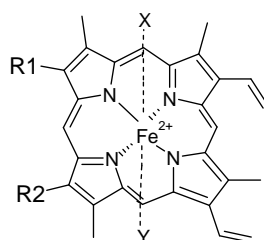


Fig.1 Haem moiety [1]

In the substrate-free form of CYP450, six coordination sites around the iron atom are offered by the haem moiety. The nitrogen atoms of the tetrapyrrole macrocycle occupy the four lateral sites whereas the proximal site is occupied by a sulfur atom of the thiolate (cysteine) group and the distal site by a weakly bound water molecule [39].

Substrate binding lowers the redox potential of CYP450 [1, 35]. Above all, the fact that electron transfer is facilitated suggests the participation of several ionizable amino residues in the active site [1].

Lewis et al. [1, 35] suggested a correlation between the ionization energy and redoxchemical potential.

The ionization potential is the energy which is needed to abstract an electron. Ionization potential of a compound are equal to the energy of the compound's highest occupied electronic level [1, 35]. This energy can indicate the potential reactivity in the CYP450 system so this knowledge is useful for further structure modifications.

4.1.3 Aim of the Study

Substrates of CYP3A4 are rather diverse in their structures and rather lipophilic in nature with values ranging from $\log D_{7.4}$ 0.4 to 8. Therefore CYP3A4 is involved in the metabolism of over 60% of marketed drugs today and also in a high number of significant drug-drug interactions (DDI) [9, 11, 12, 14, 16, 27].

Prediction of CYP3A4 metabolism is complicated. In general, metabolic stability determinations are based on the rate of disappearance of the parent drug in the presence of human liver microsomes or hepatocytes and its subsequent classification into high, medium or low metabolic stability [12, 21, 23, 39].

But the identification of certain structural fragments for CYP3A4-catalyzed metabolism usually is not possible by these experiments.

Additionally, unlike other CYP450 isoforms e.g. CYP2D6, structure-activity relationships (SAR) of CYP3A4 substrates have not been feasible so far.

Currently, very little is known about CYP3A4 crystal structures [31]. Although there are some publications available about crystal structures of substrate-free CYP3A4, the purpose of the amino acid residues in the whole enzyme is yet unknown [30, 31].

De Graaf et al. [25] have also published an integrative approach to model CYP450 *in silico* although to date nobody has provided suitable tools for the prediction of CYP3A4 catalyzed metabolism.

Hence, our approach was the estimation of the electronic nature of CYP3A4 by measuring the E_{ox} and correlating CL_{mic_rat} vs. E_{ox} -potential. The analytical method of choice was HT-cyclic voltammetry. A detailed description of method development and modification of EPSS has already been provided in *Chapter 2 (pp. 33)*.

A second approach was a redoxchemical one as it involved mimicking the two-electron transfer which occurs by redoxreactions during the catalytic cycle of CYP450.

Several redoxactive compounds with reversible two-electron transfer behaviour were identified as potential redoxindicators by cyclic voltammetric measurements (RDI) and a redoxchemical based assay was developed. In our case the development was carried out with *p*-chloranil, a quinoid redoxindicator.

Therefore, the aim of the PhD-thesis was the development of fast and easy profiling systems, allowing to improve on a long term perspective the understanding of metabolic processes at the structural level and the identification of compounds/compound classes with high probability to be metabolically instable with focus on phase-I metabolic processes.

4.2 Experimental Section

Information regarding the chemicals used, buffer composition and preparation and preparation of *p*-chloranil solution has already been described previously in *Chapter 3, Subchapters 3.2, pp.45*.

4.2.1 Selection Procedure of Datasets

Two datasets were collected. The first dataset consisted of 35 drug-like commercially available compounds as only these 35 compounds were found to have high *in vivo* clearance in human. Known phase-I metabolism was the main selection criterion for this dataset to exclude other ways of elimination or metabolism. Although human *in vivo* clearance was published for these marketed drugs, no information on microsomal rat clearance (CL_{mic_rat}) was available [16]. Therefore, these compounds were measured internally in the department of DMPK, F. Hoffmann-La Roche for consistent CL_{mic_rat} data.

The second dataset consisted of 65 drug-like molecules which were extracted from the internal data repository. In this instance, selection criteria were availability and CL_{mic_rat} data. These compounds showed CL_{mic_rat} ranging from 200 up to 3000 $\mu\text{l}/\text{min}/\text{mg}$ protein.

Sometimes, the oxidation potentials of the compound have not been measurable because their E_{ox} laid outwith the experimental range.

Additionally, several commercial compounds and internal discovery compounds had to be omitted due to chemical instability. Therefore the final dataset consisted of 53 compounds (12 commercial compounds and 41 in-house compounds).

Structures of commercially available compounds have been already presented in **Table 2** (*Chapter 3, Subchapter 3.3.3 p.60*).

4.2.2 Collection of Structural, Metabolic and Electrochemical Information from Literature

The aim of the literature search was the identification of recurring structures which are responsible for phase-I metabolism. These structures were the basis for a SAR, shown in **Table A** in the appendix.

Availability of data regarding electrochemical potential of commercially available drugs was checked by an extensive literature search. The **Human Drug Database (HDDB)**, an internal database, contained entries derived from Dollery [29], PDR [29] and Goodman and Gilman's [103].

All drug molecules in **HDDB** have been collected and fragmented by *in silico* methods. With the aid of daylight software (Daylight, Aliso Viejo, California, USA) the results were clustered into groups of structurally obtained information (*CI*), cluster number (*CI_num*) and number of fragments (*No_frag*) and a new database called *HDDB_fragments* was

created. This database included 809 fragments retrieved by the fragmentation performed previously.

Furthermore, in **Beilstein** database (MDL CrossFire Commander Version 7.9 SP2 (Build 46)) a general search for entries of molecules was launched with the criteria: *MW* ≤ 500 and *electrochemical characteristics (POT)*.

This electrochemical information was stored in a new database called **Beilstein_frag**. Subsequently, the **HDDB** and **Beilstein_frag databases** were cross-referenced, resulting in the assignment of the electrochemical properties of 138 drug-like molecules in the **Beilstein_frag_database**.

In addition, a substructure search of the fragments against the **Beilstein_frag** database was performed.

All *in silico* operations were performed on Linux systems. The results have been collected in several tables. All collected information is attached in the appendix of this thesis (**Tables B, C, D, and E** in the *Appendix*).

Additionally, information on phase-I metabolism has been collected for the 138 molecules. Again, these tables are attached in the appendix. The fragment-based table contains of several co-generic series which have been selected to observe the **structure activity relationship (SAR)** using an in-house tool called *RoSARa*.

The whole literature search process is shown schematically in Fig.2.

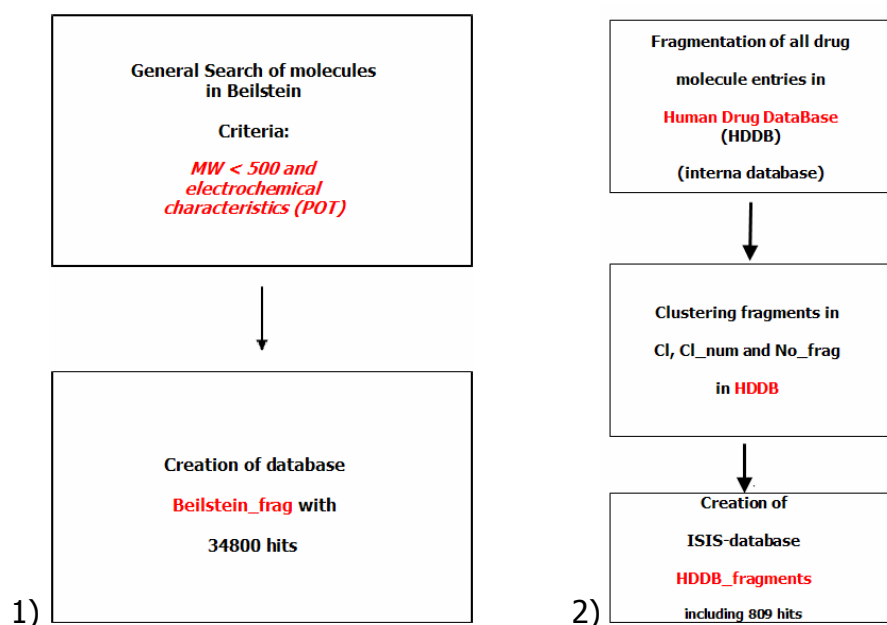


Fig.2 Data retrieval using MDL CrossFinder Commander and Human Drug Database (HDDB). In 1) the initial literature search was conducted using Beilstein. In 2) the retrieved data of 1) was further clustered and analyzed.

4.2.2.1 Descriptors for *In Silico* Prediction

25 *Property based descriptors* were assumed to influence both the microsomal clearance (CL_{mic_rat}) and the electrochemical potentials (E_{ox}). With the exception of CL_{mic_rat} and the E_{ox}, all 23 other descriptors were calculated.

These were used to express the molecular size, polarity, flexibility (number of rotatable bonds), rigidity, electronic properties, formation of hydrogen bonds (number of donor and accepting atoms), hydrophilicity (hphil surf, hphil volume) and lipophilicity (PSA, clogP) (MOLOC Software systems, Switzerland) of the molecules.

Quantum mechanical descriptors have been calculated with the program *ParaSurf'07* (CEPOS InSilico Ltd., Bedford, UK).

4.2.3 Methods

Detailed information on the equipment of LC/MS determination, method and parameters has already been provided in *Chapter 3, Subchapter 3.2.2.2, pp. 49*.

Additionally, information on the experimental set-up of EPSS and its conditions has already been provided in *Chapter 2, Subchapter 2.2.2, and pp. 38*.

Sample preparation procedure and incubation conditions were previously described in *Chapter 3, pp. 49* and therefore are not further discussed here.

4.2.4 Data Analysis

PLS was used as computational approach to analyze complex datasets using *SIMCA+11* (Version 11.0.0.0, Jun 12, 2005, Umetrics AB, Sweden) [104]. According to Wold et al. [105], "PLS is an abbreviation for partial least square modeling in latent variables or projection to latent structures".

PLS can be seen as a particular regression technique for modeling the association between X and Y. It is a useful technique for dealing with both complicated and approximate relationships within datasets [105]. For the current study, the evaluation of the dependency between two parameters such as the CL_{mic_rat} and the E_{ox} was of major importance.

4.3 Results and Discussions

The aim of this study was the invention of methods which are fast and reliable for the determination and prediction of metabolic stability. These methods were based on redoxchemistry and electrochemistry. Method invention descriptions have been provided in *Chapters 2 (pp. 33)* and *Chapters 3 (pp. 47)*.

The identification of recurrent structures in relationship to high CL_{mic_rat} and low oxidation potential, preferably in the range of the CYP450's oxidation potential was of great importance.

4.3.1 Literature Search Results

An extensive literature search was conducted regarding the collection of marketed drugs with known electrochemical activity. Hence, diverse datasets were collected as they contained information from the whole century. For more facile interpretation of this data, additional information on the solvent or type of reference electrodes used in the experiment is required but was not provided. Due to the lack of this information, none of these tables were shown in this paper.

Chosen compounds were measured electrochemically in our lab environment.

4.3.2 Redoxchemical Results

An assay was developed for the prediction of metabolic stability which is based on redoxchemical processes.

The redoxchemical reversible catalytic CYP450 process is the basis for the selection of *p*-chloranil as redoxindicator (RDI). The selection process of the *p*-chloranil and assay development has already been described in more detail in *Chapter 3 (pp. 47)*.

Quantitative analysis was done by LC/MS via comparison of peak heights. The results of the 53 compounds analysed are shown in **Fig.3**. CL_{mic_rat} is plotted vs. the percentage decrease in compound concentration after the incubation (t= 30 min) with *p*-chloranil but it does not correlate well. However there is a general trend visible of increasing loss of compound with increased CL_{mic_rat}.

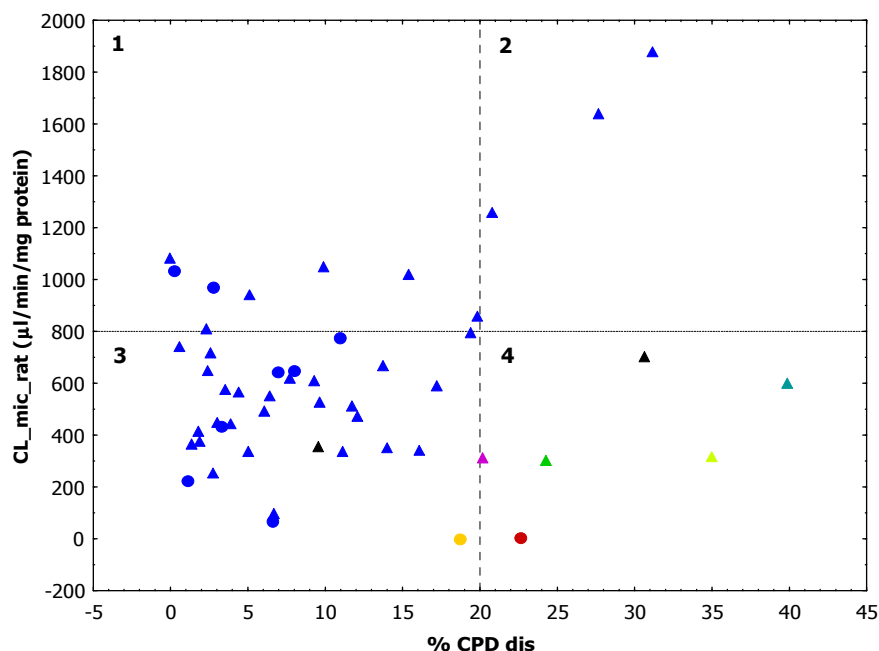


Fig.3 Comparison of *p*-chloranil assay and microsomal rat clearance. Percentage of compound disappeared (%CPD_{dis}) was plotted vs. microsomal rat clearance (CL_{mic_rat}). Dots represent commercial compounds and triangles stand for internal compounds.

Among these 53 compounds, 41 compounds were internal discovery compounds and 12 were commercially available compounds, all with known high CL_{mic_rat}.

For interpretation, the graph was subdivided into four subdivisions.

The reaction behaviour of *p*-chloranil was rather complex as has been discussed previously in *Chapter 3* (pp. 47)

Regarding the quantification with *p*-chloranil, Slifkin's [90] and Veltistas [94] proposal to quantify *p*-chloranil in aqueous media via its hydrolytic conversion to the chloranilic acid in neutral to basic solution was attempted. However, further experiments in aqueous media proved the impracticality of this proposal.

Several additional possibilities for the suitable quantification of the *p*-chloranil assay were investigated. Firstly, the theoretical CL_{mic_rat} was calculated using the "well-stirred" model conditions.

Usually, the weight of the liver and concentration of the protein are essential for the calculation of the theoretical CL_{mic_rat}. We have therefore proposed replacing the weight of liver and concentration of protein with the concentration and MW of *p*-chloranil. Some initial results were promising but using this approach for data analysis did not appear to be reproducible. This was largely due to the problems caused by quantification via *p*-chloranil and therefore further investigations were conducted.

The second quantification approach involved monitoring the amount of chloranilic acid generated during the sample incubation process with *p*-chloranil.

The observed hydrolytic conversion of *p*-chloranil at pH 7.4 by Slifkin [90], Veltsistas [94] and our lab was the basis for the second quantification approach although a reasonable correlation was also not possible by this method.

The third and simplest quantification approach was the comparison between the peak height of pure sample and sample after incubation with *p*-chloranil. Taking peak heights seemed to be more appropriate than quantification via peak area since this was not always good because of occasionally occurring broad peaks. This is probably due to the complex reaction behaviour of *p*-chloranil.

In the following paragraphs several possibilities for the lack of correlation between CL_{mic_rat} and %CPD disappeared are discussed.

The first discussion concerns compounds appearing in subdivision 2. All compounds in this subdivision contain an indol ring system as scaffold.

Taking a closer look at the compounds in the 2nd subdivision of Fig.3, the highest located one (E5_2nd) contains a thiophene fragment with a CL_{mic_rat} of 1878 (μl/min/mg), whereas compounds 2 (G5_2nd) and 3 (M5_2nd) following subsequently, have the same 1-(methylamino)-3-phenylbutane substituent at a different in position on the indol ring (Fig.4).

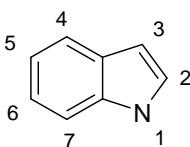


Fig.4 Scaffold indol

Interestingly, performing a 1-(methylamino)-3-phenylbutane substitution at position 4 instead of 3 leads to a higher %CPD_{dis} and hence, CL_{mic_rat} is also increased. It is likely that position 3 is more liable to oxidative metabolism. Consider the two former compounds, G11_2nd and K9_2nd; in all 4 compounds position 3 is blocked.

Like compounds 2 and 3 just discussed, G11_2nd also has an indol-ring as scaffold, with a methanesulfonyl-benzen substituent at position 3 and piperazin at position 7. K9_2nd too has an indol-ring but a (2, 6-dichlor-phenyl)-methyl-sulfide substituent on position 3 and piperazine at position 5.

Hence, all compounds differed in respect to their CL_{mic_rat}. It was assumed that the sulfonyl moiety lead to a lower clearance of CL_{mic_rat} of only 90 μl/min/mg.

K9_2nd with a CL_{mic_rat} of 701 μl/min/mg is represented by the grey dot in subdivision 4, but an explanation for its small percentage of compound decrease after incubation with *p*-chloranil is not readily available. However, it is not an outlier in Fig.3. On one hand, the sulfide provides two lone pairs which could contribute to a reaction, but on the other hand, the piperazine at position 5 makes the molecule metabolically more stable.

Compounds in subdivision 3 were considered to be relevant in the prediction of metabolic stability.

Seven compounds in subdivision 4 are coloured individually, as these appear as outliers in Fig.3 but not for EPSS in Fig.9 (p.80).

In Fig.5, two structures of the coloured compounds are shown:

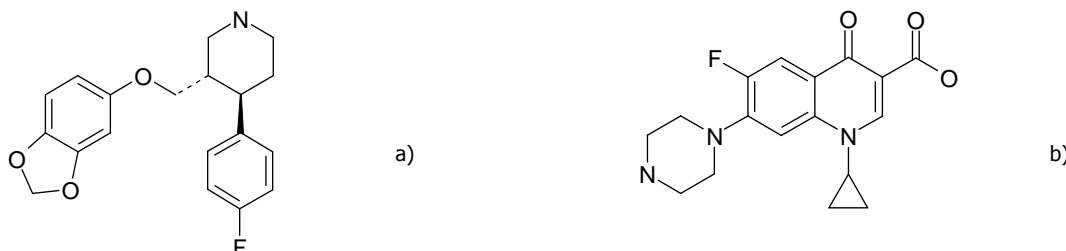


Fig.5 Outliers: a) paroxetine (yellow)

b) ciprofloxacin (red)

Structures and physicochemical properties of these compounds in Fig.9 were closely examined within the group of outliers and explanations have been sought.

One possibility is the assumption of a classical acid-base reaction taking place. At neutral pH conditions, *p*-chloranil was assumed to convert to chloranilic hydroquinone as observed experimentally in our labs and described in *Chapter 3* (pp. 47).

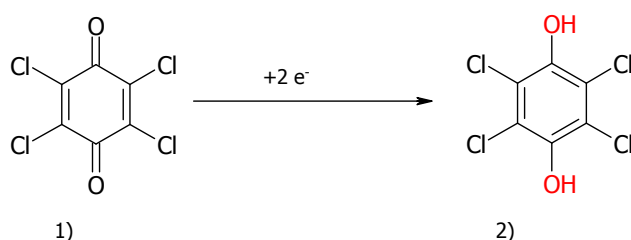


Fig.6 Conversion of *p*-chloranil to its hydroquinone at pH: 7.4. Each hydroxyl group exhibits a pK_a value: 1) pK_{a1} : 5.25 2) pK_{a2} : 6.56

Considering the pK_a values of **hydroquinone (HQ)**, the first pK_a of the hydroxyl group is at 5.25 and the second at 6.56, suggesting an acid-base reaction. The pK_a values have been taken from an internal database of experimental data. Moreover, at pH: 7.4, the HQ was negatively charged and thus could either react with the basic part of zwitterions or the bases themselves.

This offers one possible explanation for the coloured outliers since only two of seven coloured compounds were either acidic or zwitterionic, while the remaining compounds were bases.

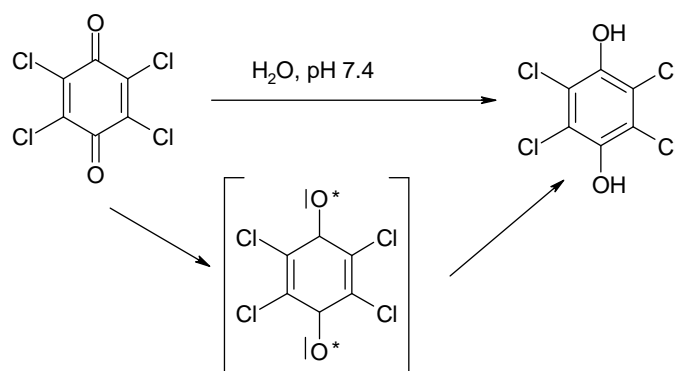


Fig.7 Reaction pathway of *p*-chloranil via radical intermediate in aqueous media at pH 7.4

The example of paroxetine shows the complexity of the reaction behaviour of *p*-chloranil. Probably, *p*-chloranil is activated by a hydroxyl ion forming the radical intermediate of *p*-chloranil as shown in Fig.7. Furthermore, it is likely that the hydroxyl radical is affecting the lone pair of the piperidine nitrogen, creating a double bond in the piperidine ring system which then can be readily oxidized by *p*-chloranil. However, the oxidation can also take place in the α -position of the nitrogen in the piperidine ring.

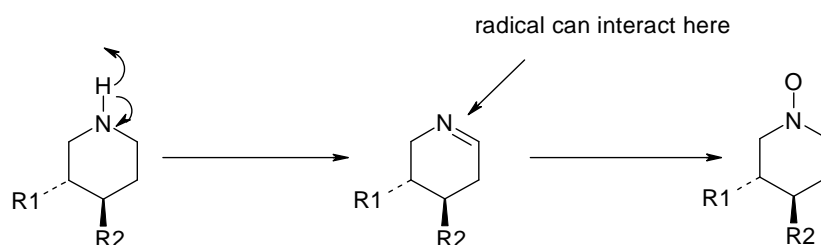


Fig.8 Possible explanation of increased compound instability of paroxetine. Paroxetine was only indicated as fragment

Analysis of the metabolic pathway of paroxetine indicates that the only site of metabolism is at the 1, 3-dioxolane moiety. Other sites besides the secondary nitrogen of the piperidine ring which are liable to oxidation are not available. Chemical reactions usually differ from enzymatic reactions and it is probable that in enzymatic reactions only the dioxolane moiety is affected, whereas chemical oxidations with *p*-chloranil give no conclusive results.

4.3.3 Electrochemical Results

A second assay for the prediction of metabolic stability was performed electrochemically using the same dataset of 53 compounds as for the *p*-chloranil assay. Results by cyclic voltammetry (CV) were additionally used for the prediction of metabolic stability. In Fig.9, a correlation can be seen between CL_{mic_rat} vs. E_{ox}. The coloured dots are those compounds which have been identified as outliers in Fig.3.

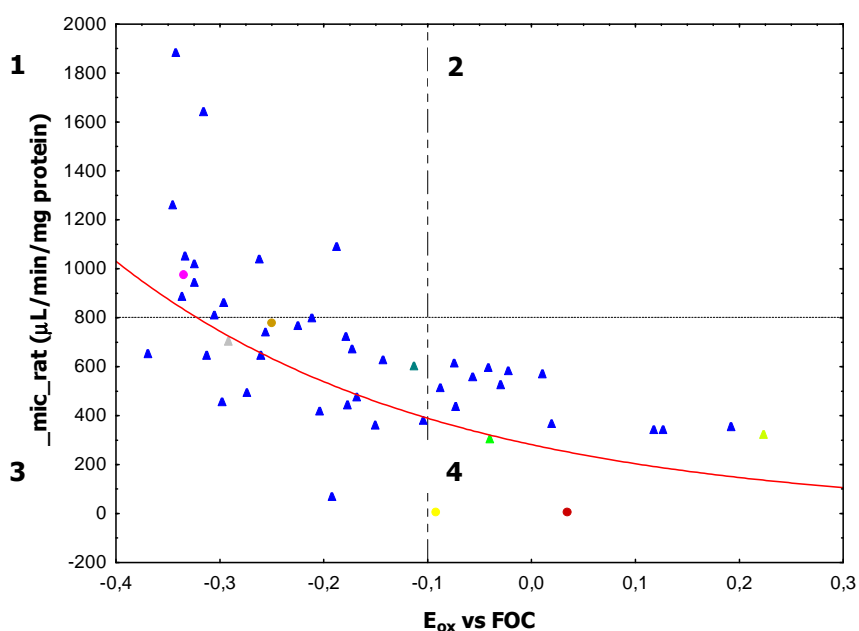


Fig.9 Correlation of E_{ox}-potential referred versus ferrocene (FOC) against microsomal rat clearance. Dots represent commercially available compounds, triangles internal compounds. Apart from the pink and brown dot, the other coloured dots represent compounds which have been identified as outliers in the plot of the *p*-chloranil assay [101].

Dividing Fig.9 into four subdivisions enabled an easier interpretation, with -0.1 V set as a limit for metabolically unstable compounds. Hence, the more negative the electrochemical potential, the more CL_{mic_rat} and metabolic instability were increased. Therefore it was suggested to define that range (subdivisions 1 and 3) as an alert range, where compounds should be re-examined and modifications made if necessary. LC/MS was used only in context of structural determinations and verifications.

There were two examples in subdivision 1 and 3, prochlorperazine (pink dot) (**Fig.10**) and desipramine (brown dot) (**Fig.11**) which are both commercially available compounds. It is known for both drugs that they are metabolized via cytochrome P450. They act against psychiatric disorders. Prochlorperazine belongs to the class of antipsychotic agents and is a highly potent neuroleptic. Desipramine is a tricyclic antidepressant.

According to Toledo et al. [106], imipramine and desipramine, its active metabolite, exhibited an irreversible voltammogram as visible in Fig.11.

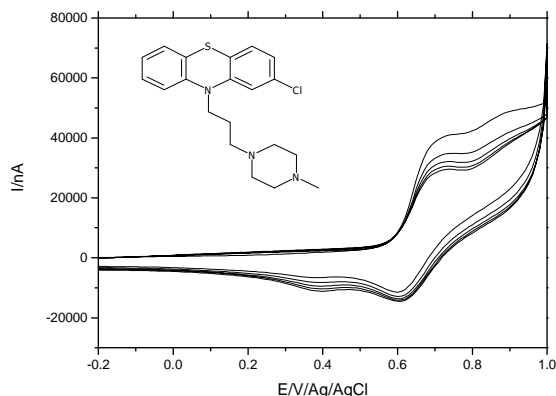


Fig.10 First example for compounds in Fig.9: *prochlorperazine* measured with EPSS at a scan rate of 0.640 V/s in a scan range from -0.5 to 1.0 V, No. of scans n= 5 in 5 mM HB, pH: 7.4

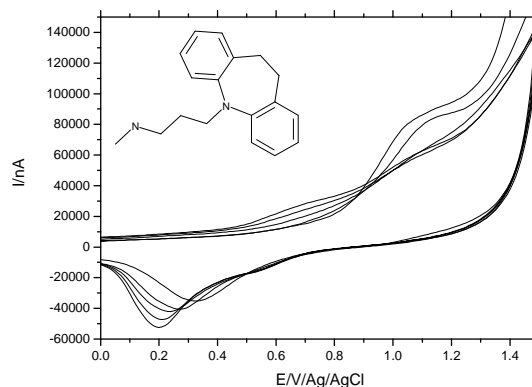


Fig.11 Second example for compounds in Fig.9: *desipramine* measured with EPSS at a scan rate of 0.640 V/s in a scan range from 0 to 1.5V, No. of scans n=5 in 5 mM HB, pH: 7.4

4.3.4 Mass Spectrometric Confirmation of Successful Electrochemical Conversion

In Fig.13 and 14 the chromatographic separation and MS results of an internal compound are shown as an example for successful electrochemical conversion. The isoxazole ring is required for a compound's successful redoxreaction. In Fig.12, a potential pathway is suggested for the observed demethylation after cyclic voltammetry.

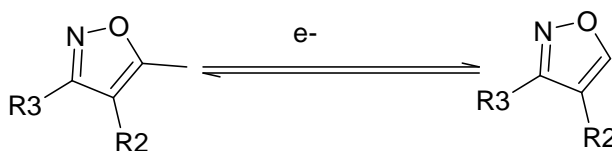


Fig.12 Demethylation reaction of an in-house compound

The blue peak represents the sample without electrochemical treatment, whereas the red peak is the sample after cyclic voltammetry at a different retention time indicating generation of a new, demethylated product.

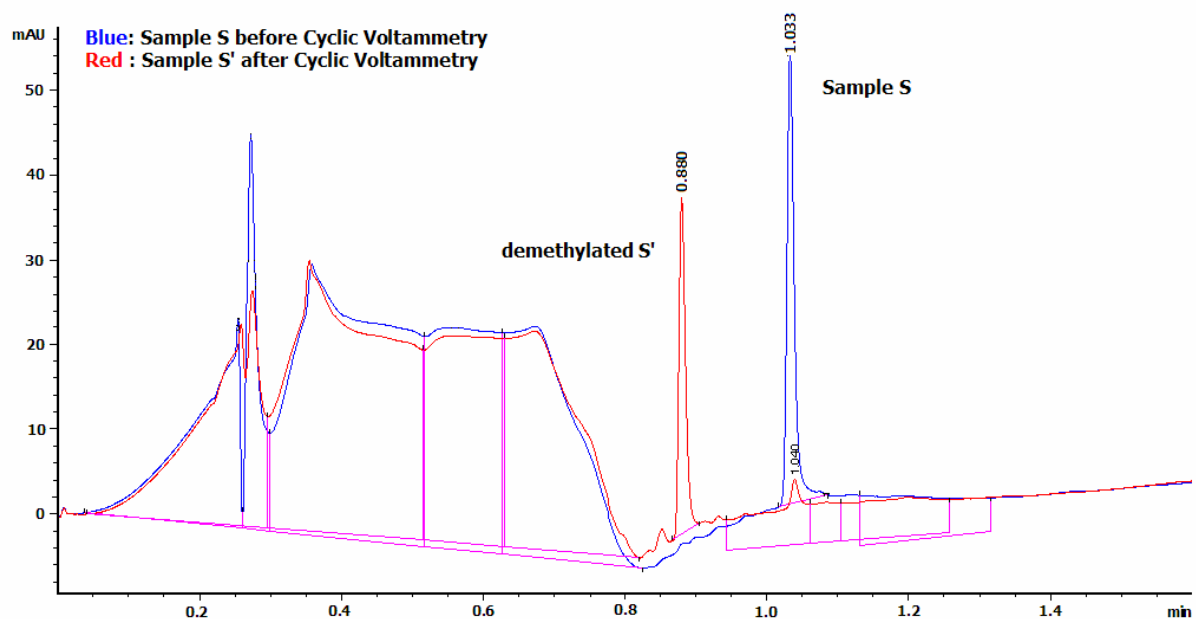


Fig.13 Example of an internal compound for the appearance of a demethylated compound after electrochemical oxidation; LC-result, *Agilent 1100 series MSD SL* at conditions described in Materials and Methods, *Chapter 4*.

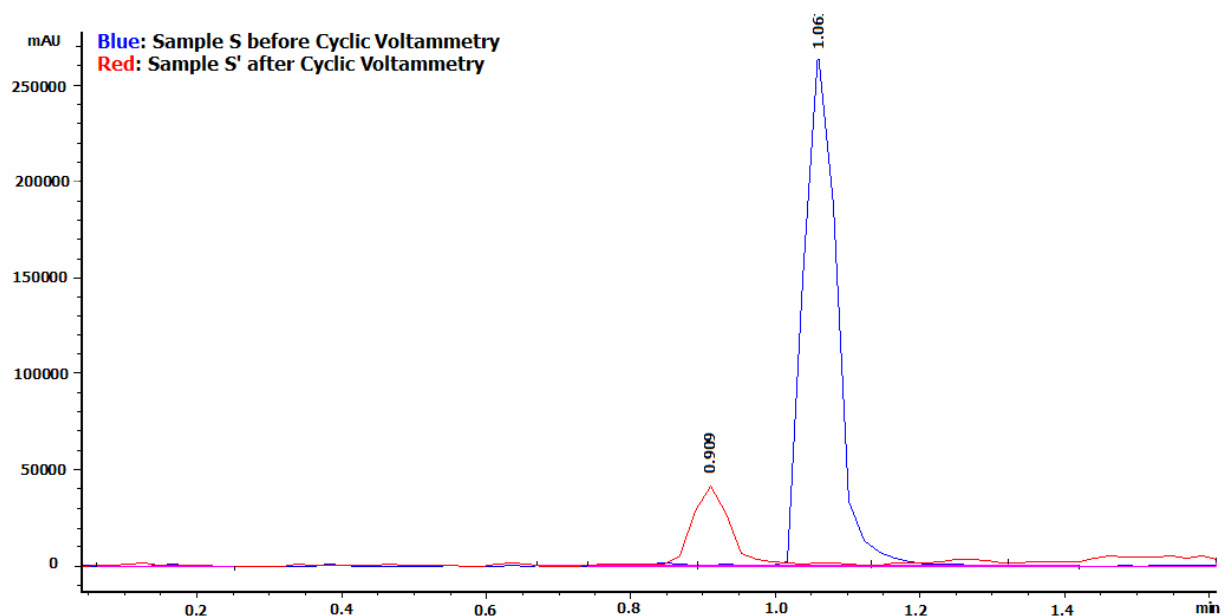


Fig.14 Example of an internal compound for the appearance of a demethylated compound after electrochemical oxidation; MS-result using *Agilent 1100 series MSD SL* at conditions described in Materials and Methods, *Chapter 4*.

Very often, cyclic voltammetric measurements were subsequently analyzed by LC/MS. Frequently only low amounts of demethylated or hydroxylated metabolites were found which made quantification difficult sometimes. Most of the time no clear baseline

separation between metabolite S' and sample S occurred so newly generated masses were only detectable by *extracted ion chromatograms*.

4.3.5 Statistical Determinations using PLS-Analysis

The intention of PLS-analysis was the facilitation of the interpretation of complex datasets. Due to the promising correlation in Fig.9, the electrochemical data was further analyzed. Furthermore, PLS analysis should disclose dependencies between the CL_{mic_rat} and physicochemical properties if any physicochemical parameter could sufficiently describe the CL_{mic_rat} .

Based on the results of the *p*-chloranil assay shown in Fig.3, several PLS models have been created. Subsequently, a model with CL_{mic_rat} as an independent y-variable and PSA, hydrophilicity parameters and $\%CPD_{dis}$ as the x-variable was created with a $R^2:0.128$ and $Q^2: 0.097$. As expected, results showed a lack of correlation and no further results or graphs were shown in this context.

Furthermore for EPSS, several PLS-models have been calculated for the entire dataset of 53 compounds using CL_{mic_rat} as an independent parameter.

In Table 1, an overview of these PLS models are provided for EPSS:

Table 1 Overview of PLS models (CL_{mic_rat}) with CL_{mic_rat} as independent variable was used as independent variable) using E_{ox} as input result

Model	$r^2 Y$	q^2	P	Comment
M1	0.496	0.481	1	all 53 compounds
M2	0.443	0.426	1	only bases extracted of 53 compounds

In **model 1 (M1)**, all 53 compounds were included. CL_{mic_rat} was the independent variable (y-variable) and all the other parameters such as PSA, charge and hydrophilicity were set as x-variables. E_{ox} was identified as the most predominant parameter significantly influencing the CL_{mic_rat} . The model was validated with 20 permutations and no better model was subsequently obtained as illustrated in Fig.15.

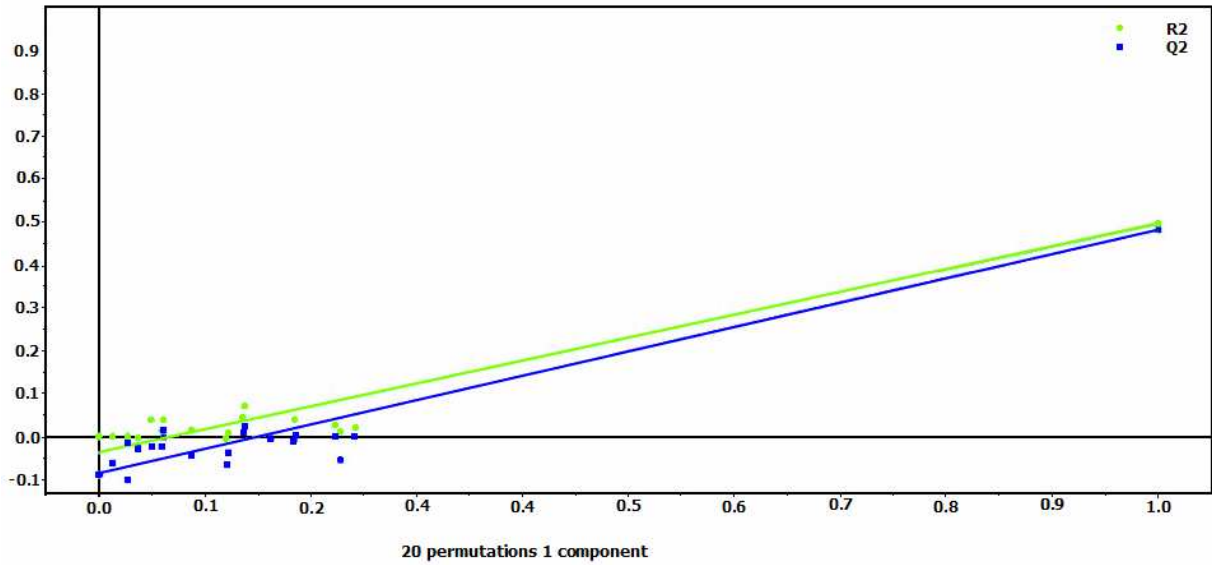


Fig.15 Permutation plot 20 permutations 1 component, CL_mic_rat (ml/min/mg protein): R^2 : (0.0, -0.0363), Q^2 : (0.0, -0.0834)

To verify that none of the 23 physicochemical parameters could describe the CL_mic_rat too, a loading plot was created. This plot (Fig.16) shows that E_{ox} is the predominant parameter but charge also has a significant influence. For understanding and interpretation, the 53 compounds have been subdivided based on their ionization constants (pK_a).

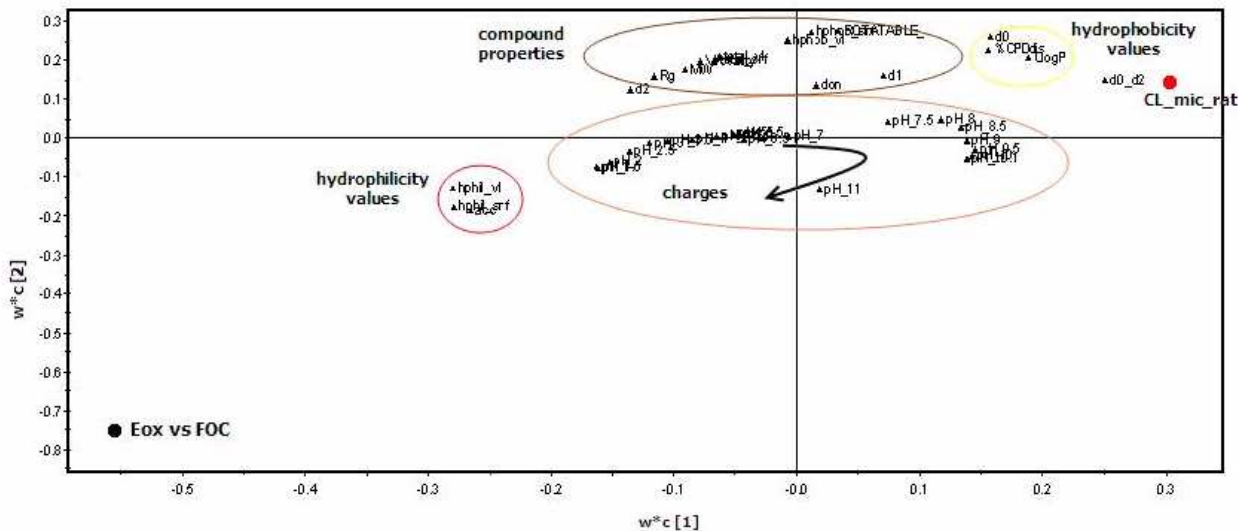


Fig.16 Loading scatter plot with R^2 [61]: 0.1479437, R^2 [61] : 0.185738

Only the group of bases was large enough for the calculation of a second **model 2 (M2)** created following the same procedure as for M1. E_{ox} was again identified as predominant parameter.

Finally a model (**M1**) was created showing a one-to-one correlation of CL_{mic_rat} and E_{ox} .

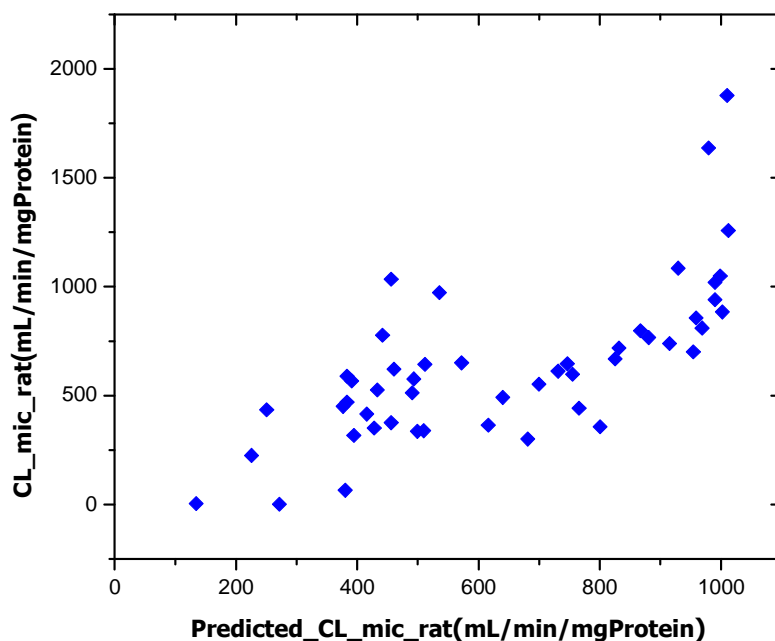


Fig.17 M1 a computational model, created by *RoSARa*. The R^2 was 0.496, the Q^2 : 0.481 and 1 variable.
Equation for M1: $CL_{mic_rat} = -E_{ox} + c$

All relevant physicochemical properties including charges were calculated for 53 compounds. In the PLS-analysis each property was set as the x variable in turn with E_{on} as the independent variables and several models were created. The best model was M1, illustrated by an **observed vs. predicted values plot** in Fig.17 (*Table E* in the Appendix shows all the relevant values) with E_{ox} acting as predominant parameter for the description of CL_{mic_rat} . Its coefficient exhibited a negative value; the more negative the oxidation potential, the higher the CL_{mic_rat} .

Several other models with lower R^2 and Q^2 values were created too. The best model after M1 was the correlation between E_{ox} and *acc*.

If a model was created without E_{ox} as independent variable, a model with very low R^2 was retrieved.

A logarithmic fit has also been investigated for possible quantification of E_{on} and CL_{mic} (Fig.9)

EPSS has proved to be a useful tool for the estimation of metabolic stability in early pre-clinical development. M1 could be used as appropriate model to predict the correlation between CL_{mic_rat} and E_{ox} .

Of course, a dataset of 53 compounds is not sufficient and future focus in this study should be the enlargement of the current dataset.

4.3.6 Comparison of Classical and Novel Determination/Prediction of Metabolic Stability

The introduction of EPSS, a HT-tool, made electrochemical screening of redoxactive molecules feasible for the first time. Up to 96 samples could be potentially measured in parallel allowing a fast determination of electrochemical characteristics. Promising results in Fig.9 suggest its application in pre-clinical development, such as the ranking or grouping of compounds related to their redox characteristics, which have been proven to be related to their metabolic stability.

Several approaches for the determination and mimicking of phase-I metabolism with electrochemistry were recently performed and described [37, 42, 54, 107, 108]. Karst [40, 41], Jurva [37, 42] and Johansson [38] gained lots of knowledge in the field of EC/LC/MS, an electrochemical flow chamber coupled to LC/MS.

Although EC/LC/MS seemed to be more advantageous at first glance, it did not really work well under physiological-like conditions because chromatographic methods still required large amounts of nonpolar solvents and quantitative questions in terms of concentrations could not be sufficiently answered. EC/LC/MS seemed to be more suitable for the rapid determination of unspecific redox behaviour resulting in mass changes whereas EPSS provided the information concerning the redox kinetics and the time-dependent change of the compound concentration [36, 40].

Jurva et al. [37, 40] reported several issues in terms of the EC-flow through cell which have prevented routine use so far. This included insufficient quality of instrumentation and the requirement of tight control of the vaporizer temperature due to thermo spray mass spectrometry [37]. As a result, temperature regulation was a major source of error due to difficulties associated with compound stability and the handling of the systems.

Johansson [38], a member of Jurva's staff, published another method to mimic phase-I metabolism using EC/LC/MS [37] and suggested several methods for oxidation reactions using EC/LC/MS [37]. Moreover, they reported that results obtained electrochemically were concordant with results from microsomal incubations [37]. However, their electrochemical approach showed some limitations [109-111]. Some CYP450-mediated reactions were not imitable by electrochemistry, specifically those compounds containing aliphatic components [37]. EC/LC/MS exhibited another problem: the dilemma of the electrolyte concentration. On one hand, electrolytes were needed to provide better electrochemical conversion, but on the other hand high concentrations of electrolytes resulted in increased background and decreased sample signals if EC was combined with LC/MS [37].

Our aims differed to that of Jurva, Karst and Johansson, as we intended to obtain a valuable model for the prediction of metabolic stability whereas Jurva, Karst and Johansson [37, 38, 40-42, 54, 112] were more focused on mimicking phase-I metabolism. Of course, phase-I metabolism was the major criterion for the selection of our drug candidates too but as has already been stated, the major focus was on the correlation of E_{ox} vs. CL_{mic_rat} shown in Fig.9.

For selectivity and significance, separation of electrochemical and chromatographic determinations was more advantageous for EPSS. With EPSS, cyclic voltammetric measurements were performed and/or samples were further analyzed in LC/MS by transfer of samples. Moreover, EPSS allowed working under physiological-like conditions and the study of the rate of reaction between nucleophiles and electrophiles [37]. However, EPSS did not give any information on regioselectivity, but subsequent LC/MS-analysis showed clearly if demethylations had taken place after CV [37]. Obviously, aliphatic structures were not affected easily by electrochemical oxidation [37] most likely due to the high energy barrier which needed to be overcome for aliphatic hydroxylation [37]. High energy barriers would have resulted in a high electrochemical potential which could not be obtained in our experiments [37].

Although the number of lead series was increased due to the introduction of combinatorial chemistry, the number of new chemical entities has decreased.

Moreover, metabolism studies used to be performed in very late phases of pre-clinical development, when the number of compounds had already been reduced [12, 37]. With the introduction of the parallel approach to drug discovery, metabolism studies were performed earlier requiring simple, fast and reliable screening tools [12, 37]. Metabolic stability and toxicological issues are still the bottleneck for most discovery compounds. It is therefore essential to develop a tool to reduce the number of inappropriate metabolically unstable compounds [37]. Our approach in comparison to the current standard involving the liver microsome and hepatocyte incubations is faster in performing the assay and less susceptible to variations in experimental conditions.

One major disadvantage of our electrochemical approach is the fact that oxygen is a disturbing factor. Therefore, all reaction solutions were degassed by Ar intensively before use. The major advantage of EPSS is data retrieval within a short period of time without the need for biological materials. Sample preparation for EPSS was less complicated than for liver microsomes incubations as liver microsomes (LM) have to be created in an elaborate procedure. Moreover LM incubations required supplementation of relevant cofactors for the initiation of the reactions. Limited time of storage and incubations were accounted as major disadvantage of LM incubations, but this technique is advantageous since it provides a first glimpse of specificity. Above all, metabolic stability determination via EPSS could be easily performed in very early stages of pre-clinical development.

4.4 Conclusions and Perspectives

Both approaches for the investigation of early metabolic stability profiling are novel. Neither the redoxchemical nor the electrochemical one have been published so far, even though several experimental attempts in electrochemistry were conducted to determine phase-I metabolism of compounds. One analytical approach was the electrochemical flow-cell coupled to LC/MS.

Cyclic Voltammetry, particularly HT-cyclic voltammetry (EPSS) allowed physiological-like conditions. For the first time, a relationship between the electrochemical oxidation potential and microsomal rat clearance could be demonstrated. PLS-analysis was used to analyse complex datasets and revealed E_{ox} as a predominant parameter if CL_{mic_rat}

was set as independent variable. As a result EPSS can be applied in early drug discovery phases for early compound profiling of discovery compounds.

For further validation of this approach, the dataset should be increased up to hundreds of compounds to improve predictability.

This new technique enables a fast, non-biological measurement of the electrochemical behaviour of a compound as a first indicator for reactivity in CYP450 mediated metabolism.

The redoxchemical approach was less successful. The *p*-chloranil assay set-up was well defined but reproducible results were hindered by the fact that *p*-chloranil itself showed a complex reaction behaviour in aqueous media.

The example of paroxetine (*Chapter 4, Fig.8, p.82*) demonstrated that the redoxreaction with *p*-chloranil did not suggest a potential pathway of metabolism. Although the microsomal rat clearance of paroxetine was low, the compound loss after the incubation with *p*-chloranil was high. Till date, a suitable explanation for that finding was not available.

Moreover, a correlation between CL_{mic_rat} and %CPD_{dis} could not be seen. We would rather speak of a trend which is certainly visible in Fig.3 (*Chapter 4, p.71*).

Therefore, an interesting modification of the *p*-chloranil assay could be a replacement of *p*-chloranil. As previously mentioned *o*-chloranil is a potential compound as it exhibits a positive reduction potential but is similar to *p*-chloranil structural wise.

Further studies on *p*-chloranil in aqueous media are required to gain a better understanding of its reaction products. The experimental set-up of this assay can be easily used as basis for further improvements.

Both approaches are novel and promising for early metabolic stability compound profiling and are worth for continuing studies.

To conclude the investigations of the PhD-thesis, the goals of this thesis have been met. A fast reliable and non-biological method for the ranking of compounds according to their electrochemical characteristics establishing a link to metabolic stability could be **developed**.

Chapter 5: Final Considerations and Perspectives

The drug discovery and development process is still accompanied by several challenges although highly sophisticated *in vitro* models and *in silico* prediction models are applied early.

Drug metabolism, for example, does account for one of the problems in drug discovery and drug development.

A large fraction of discovery compounds are lipophilic which make them liable to oxidative metabolism most likely enzymatically catalyzed by CYP450.

After a paradigm shift at the end of 90s, metabolism profiling was loaded in front of other drug optimisation activities.

With comprehensive compound profiling in early phases of drug discovery, metabolically instable structures can be identified and subsequently optimized.

So far, metabolic stability determinations have been conducted on a biological basis.

Usually in these assays subcellular hepatic fractions (microsomes) or hepatocytes are used. Above all, conducting these assays is time consuming and gained results typically only deliver information on the rate of metabolism but little information on the resulting products at the structural level.

Both experimental approaches for early metabolic stability profiling of discovery compounds are novel and described by the PhD-thesis. Till date none of the HT-approaches, neither the redoxchemical nor the electrochemical using cyclic voltammetry have been published.

The redoxchemical approach was challenging. The evaluation and optimisation of a suitable experimental set-up, which results can be used for the theoretical CL_{mic} calculations, were hindered by the fact that *p*-chloranil showed a complex reaction behaviour in aqueous media.

Some compounds showed an increased loss of compound but did not correlate in respect to their microsomal clearance. It was described on the example of paroxetine in *Chapter 4 (pp.68)*.

Further investigations on the degradation of *p*-chloranil in aqueous media or replacement of *p*-chloranil vs. *o*-chloranil are recommendable.

Some publications about the EC/LC/MS method to simulate phase-I metabolism are known.

These research groups have never focused on cyclic voltammetry as analytical alternative to EC/LC/MS. This was probably due to the unavailability of suitable technical modifications of the classical experimental set-up.

With the introduction of EPSS, new methods and experimental approaches became feasible. Cyclic Voltammetry, particularly HT-cyclic voltammetry (EPSS) allows aqueous conditions for the determination of redox potentials.

By the application of EPSS, a relationship between the electrochemical oxidation potential and microsomal rat clearance can be demonstrated. A statistical method for data analysis, PLS, was used to analyse complex datasets and revealed E_{ox} as a predominant parameter.

Obtained results support the application of EPSS in early drug discovery for compound profiling with focus on metabolic stability.

This new technique enables a fast, non-biological measurement of the electrochemical behaviour of a compound as a first indicator for reactivity in CYP450 mediated metabolism.

For further validation of this approach, the dataset should be increased up to hundreds of compounds to improve predictability. Currently, only 53 compounds have been used.

Advantage of this approach is time and low amounts of compounds necessary.

Moreover, obtained results call EPSS for toxicological problems. The electrochemical measurements of GSH-adduct formations could be another topic as numerous compounds are also failing due to GSH- adduct formations.

Both assays are fast and easy to perform. If the number of compounds in the dataset is increased and *p*-chloranil is replaced by another redoxactive compound, it will be an attractive tool to implement in early ADME of pre-clinical drug discovery.

6. References

1. Lewis, D.F.V., *Cytochromes P450: Structures Functions and Mechanisms*. 1996, London: Taylor & Francis. 348.
2. Coleman, M.D., *Human Drug Metabolism: An Introduction*. 1st ed. 2005, Birmingham: Wiley. 275.
3. Lewis, D.F.V., et al., *Molecular Modelling of CYP3A4 From an Alignment With CYP102: Identification of Key Interaction between Putative Active Site Residues and CYP3A- Specific Chemicals*. *Xenobiotica*, 1996. 26(10): p. 1067-1086.
4. Guengerich, F.P. and T.L. Macdonald, *Mechanisms of Cytochrome P450 Catalysis*. *Federation of American Societies for Experimental Biology Journal*, 1990. 4: p. 2453-2459.
5. Mutschler, E., et al., *Arzneimittelwirkungen*. 2004, Stuttgart: Wissenschaftliche Verlagsgesellschaft GmbH. 1186.
6. Masimirembwa, C.M., U. Bredberg, and T.B. Andersson, *Metabolic Stability for Drug Discovery and Development: Pharmacokinetic and Biochemical Challenges*. *Clinical Pharmacokinetics*, 2003. 42(6): p. 515-28.
7. Rane, A., G.R. Wilkinson, and D.G. Shand, *Prediction of Hepatic Extraction Ratio from In Vitro Measurement of Intrinsic Clearance*. *Journal of Pharmacology and Experimental Therapeutics*, 1977. 200(2): p. 420-424.
8. Rowland, M. and T. Tozer, *Clinical Pharmacokinetics-Concepts and Application*. 3rd ed. 1995, USA: Lippincot, Williams & Wilkins. 602.
9. Thompson, T.N., *Early ADME in Support of Drug Discovery: The Role of Metabolic Stability Studies*. *Current Drug Metabolism*, 2000. 1: p. 215-241.
10. <http://www.novartis.com/research/drug-discovery.shtml>.
11. Thompson, T.N., *Optimisation of Metabolic Stability as a Goal of Modern Drug Design*. *Medicinal Research Reviews*, 2001. 21(5): p. 412-449.
12. Baranczewski, P., et al., *Introduction to Early In Vitro Identification of Metabolites of New Chemical Entities in Drug Discovery and Development*. *Pharmacological Reports*, 2006. 58: p. 341-352.
13. Kola, I. and J. Landis, *Can the Pharmaceutical Industry Reduce Attrition Rates?* *Nature Reviews Drug Discovery*, 2004. 3(8): p. 711-5.
14. Gombar, V.K., I.S. Silver, and Z. Zhao, *Role of ADME Characteristics in Drug Discovery and their In Silico Evaluation: In Silico Screening of Chemicals for their Metabolic Stability*. *Current Topics in Medicinal Chemistry*, 2003. 3: p. 1205-1225.
15. Herman, J.L., *Generic Approach to High Throughput ADME Screening for Lead Candidate Optimisation*. *International Journal of Mass Spectrometry*, 2004. 238: p. 107-117.
16. Shargel, L., S. Wu-Pong, and A. Yu, *Applied Biopharmaceutics & Pharmacokinetics*. 5th ed. 2005, USA: Mc Graw-Hill Companies. 893.

References

17. Dearden, J.C., *In Silico Prediction of ADMET Properties: How Far Have We Come?* Expert Opinion on Drug Metabolism & Toxicology, 2007. 3(5): p. 635-639.
18. Lave, T., P. Coassolo, and B. Reigner, *Prediction of Hepatic Metabolic Clearance Based on Interspecies Allometric Scaling Techniques and In Vitro-In Vivo Correlations*. Clinical Pharmacokinetics, 1999. 36(3): p. 211-231.
19. Houston, B.J., *Utility of In Vitro Drug Metabolism Data in Predicting In Vivo Metabolic Clearance*. Biochemical Pharmacology, 1994. 47(9): p. 1469-1479.
20. Gabriellson, J. and D. Weiner, *Pharmacokinetic & Pharmacodynamic Data Analysis: Concepts and Applications*. 4th ed. 2006: Swedish Pharmaceutical Society. 1254.
21. Yan, Z. and G.W. Caldwell, *Metabolism Profiling, and Cytochrome P450 Inhibition & Induction in Drug Discovery*. Current Topics in Medicinal Chemistry, 2001. 1: p. 403-425.
22. Testa, B., et al., *Pharmacokinetic Optimisation in Drug Research*. 2001, Zürich: Wiley-VCH. 655.
23. Valko, K. and D.P. Reynolds, *High-Throughput Physicochemical and In Vitro ADMET Screening, A Role in Pharmaceutical Profiling*. American Journal of Drug Delivery, 2005. 3(2): p. 83-100.
24. Florence, A.T. and D. Attwood, *Physicochemical Principles of Pharmacy*. 4th ed. 2006, London: Pharmaceutical Press. 492.
25. de Graaf, C., N.P.E. Vermeulen, and K.A. Feenstra, *Cytochrome P450 In Silico: An Integrative Modeling Approach*. Journal of Medicinal Chemistry, 2005. 48(8): p. 2725-2752.
26. Rendic, S. and F.J. Di Carlo, *Human Cytochrome P450 Enzymes: A Status Report Summarizing their Reactions, Substrates, Inducers, and Inhibitors*. Drug Metabolism Reviews, 1997. 29: p. 413-580.
27. Riley, R.J. and K. Grime, *Metabolic Screening In Vitro: Metabolic Stability, CYP Inhibition and Induction*. Drug Discovery Today: Technologies, 2004. 1(4): p. 365-372.
28. Lewis, D.F.V. and M. Dickins, *Substrate SARs in Human P450s*. Drug Discovery Today, 2002. 7(17): p. 918-925.
29. Dollery, C., *Therapeutic Drugs*. 2nd ed. Vol. 1. 1999, Edinburgh: Churchill Livingstone.
30. Williams, P.A., *Crystal Structures of Human Cytochrome P450 3A4 Bound to Metyrapone and Progesterone*. Science, 2004. 305: p. 683-686.
31. Yano, J.K., *The Structure of Human Microsomal Cytochrome P450 3A4 Determined by X-Ray Crystallography to 2.05 Å Resolution*. Journal of Biological Chemistry, 2004. 279: p. 38091-38094.
32. Scott, E.E. and J.R. Halpert, *Structures of Cytochrome P450 3A4*. Trends in Biochemical Sciences, 2005. 30(1).
33. Johnson, E.F. and D.C. Stout, *Structural Diversity of Human Xenobiotic-Metabolizing Cytochrome P450 Monooxygenases*. Biochemical and Biophysical Research Communications, 2005. 338: p. 331-336.
34. Smith, D.A. and B.C. Jones, *Speculations on the Substrate Structure-Activity Relationship (SSAR) of Cytochrome P450 Enzymes*. Biochemical Pharmacology, 1992. 44(11): p. 2089-2098.

References

35. Lewis, D.F.V., *Human Cytochromes P450 Associated with the Phase 1 Metabolism of Drugs and other Xenobiotics: A Compilation of Substrates and Inhibitors of the CYP1, CYP2 and CYP3 Families*. Current Medicinal Chemistry, 2003. 10: p. 1955-1972.
36. Jurva, U., H.V. Wikstroem, and A.P. Bruins, *Comparison between Electrochemistry/ Mass Spectrometry and Cytochrome P450 Catalyzed Oxidation Reactions*. Rapid Communications in Mass Spectrometry, 2000. 17: p. 800-810.
37. Jurva, U., et al., *Comparison between Electrochemistry/ Mass Spectrometry and Cytochrome P450 Catalyzed Oxidation Reactions*. Rapid Communications in Mass Spectrometry, 2003. 17: p. 800-810.
38. Johansson, T., L. Weidolf, and U. Jurva, *Mimicry of Phase I Drug Metabolism- Novel Methods for Metabolite Characterization and Synthesis*. Rapid Communications in Mass Spectrometry, 2007. 21: p. 2323-2331.
39. Fleming, B.D., et al., *Recent Progress in Cytochrome P450 Enzyme Electrochemistry*. Expert Opinion on Drug Metabolism & Toxicology, 2006. 2(4): p. 581-589.
40. Karst, U., *Electrochemistry/ Mass Spectrometry (EC/MS)- A New Tool to Study Drug Metabolism and Reaction Mechanisms*. Analytical Methods, 2004. 43: p. 2476-2478.
41. Lohmann, W. and U. Karst, *Generation and Identification of Reactive Metabolites by Electrochemistry and Immobilized Enzymes Couples On-Line to Liquid Chromatography/ Mass Spectrometry*. Analytical Chemistry, 2007. 79: p. 6831-6839.
42. Madsen, K.G., et al., *Development and Evaluation of an Electrochemical Method for Studying Reactive Phase-I Metabolites: Correlation to In Vitro Drug Metabolism*. Chemical Research in Toxicology, 2007. 20: p. 821-831.
43. Heinze, J., *Cyclic Voltammetry-" Electrochemical Spectroscopy"*. Angewandte Chemie, 1984. 23(11): p. 831-918.
44. Atkins, P. and J. de Paula, *Physical Chemistry*. 7th ed. 2002, New York: W. H. Freeman and Company. 1140.
45. Brett, C.M.A. and A.M. Brett Oliveira, *Electrochemistry: Principles, Methods and Applications*. 5th ed. 2002, Coimbra, Portugal: Oxford Science Publications. 427.
46. Cannon, R.D., *Electron Transfer Reaction*. 1st ed. 1981, London: Butterworth.
47. Gosser Jr., D.K., *Cyclic Voltammetry: Simulation and Analysis of Reaction Mechanisms*. 1st ed. 1993, New York: VCH. 155.
48. Petrovic, S., *Cyclic Voltammetry of Hexachloroiridate (IV): An Alternative to the Electrochemical Study of the Ferricyanide Ion*. The Chemical Educator, 2000. 5(5): p. 7.
49. Hush, N.S., *Reaction of Molecules at Electrodes*. 2nd ed. 1974, London: Wiley-Interscience.
50. www.liv.ac.uk/buffers.
51. Landgraf, S., *CycloVoltammetrie CycVolt.6.EXE*. Tu Graz, Graz.
52. Gagne, R.R., *Ferrocene as an Internal Standard for Electrochemical Measurements*. Inorganic Chemistry, 1979. 19: p. 2854-2855.

References

53. Shi, M., et al., *Immunoassays Based on Microelectrodes Arrayed on a Silicon Chip for High Throughput Screening of Liver Fibrosis Markers in Human Serum*. *Biosensors and Bioelectronics*, 2006. 21(12): p. 2210-2216.
54. van Leuwen, S.M., et al., *Prediction of Clozapine Metabolism by On-line Electrochemistry/ Liquid Chromatography/ Mass Spectrometry*. *Analytical and Bioanalytical Chemistry*, 2005. 382: p. 742-750.
55. Gun, J., et al., *Studies on the Reduction of [(C5Me5)2Mo2O5] in Methanol/Water/Acetate Solutions by On-Line Electrochemical Flow-Cell and Electrospray Mass Spectrometry*. *Journal of Solid State and Inorganic Chemistry*, 2003: p. 482-492.
56. Smith, D.G., R. Cappai, and K.J. Barnham, *The Redox Chemistry of the Alzheimer's Disease Amyloid β -Peptide*. *Biochimica et Biophysica Acta*, 2007. 1768: p. 1976-1990.
57. Hensley, K., et al., *Electrochemical Analysis of Protein Nitrotyrosine and Dityrosine in the Alzheimer Brain Indicates Region-Specific Accumulation*. *Journal of Molecular Neuroscience*, 1998. 18(20): p. 8126-8132.
58. Brunmark, A. and E. Cadenas, *Redox and Addition Chemistry of Quinoid Compounds and its Biological Implications*. *Free Radical Biology & Medicine*, 1989. 7(4): p. 435-77.
59. Frontana, C., et al., *Substituent Effect on a Family of Quinones in Aprotic Solvents: An Experimental and Theoretical Approach*. *Journal of Physical Chemistry A*, 2006. 110: p. 9411-9419.
60. Rau, J., H.J. Knackmuss, and A. Stolz, *Effects of Different Quinoid Redox Mediators on the Anaerobic Reduction of Azo Dyes by Bacteria*. *Environmental Science and Technology*, 2002. 36: p. 1497-1504.
61. *Physicians' Desk Reference*. 55th ed, Montvale: Medical Economics Company. 3506.
62. Akutagawa, T., *Multiplex Proton-Transfer and Electron-Transfer Natures Based on the 2, 2'-Bi-1*h*-Imidazole System. I. Acid Dissociation Constants and Redox Properties in Solution*. *Journal of the Chemical Society of Japan*, 1995. 68: p. 1753-1773.
63. Aumueller, A. and S. Huenig, *N, N'-Dicyanoquinonediimines- a New Class of Compounds, II: Comparison of Redox Properties with Those of Quinones and Tetracyanoquinodimethanes*. *Justus Liebig's Annalen der Chemie*, 1986: p. 165-176.
64. Bartak, D. and R.A. Osteryoung, *The Redox Behaviour of the Tetrachloro-*p*-Benzoquinone-Tetrachlorohydroquinone System in Molten Aluminium Chloride Sodium Chloride Solvents*. *Journal of Electroanalytical Chemistry*, 1976: p. 69-83.
65. Conant, J.B. and A. Fieser, *Reduction Potentials of Quinones, II. The Potentials of Certain Derivatives of Benzoquinone, Naphthoquinone and Anthraquinones*. *Journal of the American Chemical Society*, 1924. 46: p. 1858-1881.
66. D' Souza, F., *Molecular Recognition via Hydroquinone-Quinone Pairing: Electrochemical and Singlet Emission Behaviour of [5, 10, 15-Triphenyl-20 (2, 5-Dihydroxy-phenyl) Porphyrinato] Zinc (II)-Quinone Complexes*. *Journal of the American Chemical Society*, 1996. 118: p. 923-924.
67. Maslak, P., *Mesolytic Scission of C-C Bonds as a Probe for Photoinduced Electron Transfer Reaction of Quinones*. *Journal of Organic Chemistry*, 1996. 61: p. 2647-2656.

References

68. Murty, K., *Potentiometric and Visual Estimation of Some Quinones with Titanium (III)-Chloride*. Indian Journal of Chemistry, 1982. 21A: p. 756-757.
69. Coenjarts, C. and J.C. Scaiano, *Reaction Pathways Involved in the Quenching of the Photoactivated Aromatic Ketones Xanthone and 1-Azaxanthone by Polyalkylbenzenes*. Journal of the American Chemical Society, 2000. 122(15): p. 3635-3641.
70. Pal, S., *Schiff Base Linked Ferrocenyl Complexes for Second-Order Nonlinear Optics*. Journal of Organometallic Chemistry, 2000. 604: p. 248-259.
71. Hunter, W.H. and D.E. Kvalnes, *An Optical Method for the Study of Reversible Organic Oxidation-Reduction Systems. A. p-Benzoquinones*. Journal of the American Chemical Society, 1932. 54: p. 2869-2881.
72. Peover, M.E., *Reduction Potentials and Intermolecular Charge-Transfer Spectra of Organic Acceptor Molecules. IV. Nitrobenzenes*. Transactions of the Faraday Society, 1964. 60: p. 479.
73. Konopik, N., *Spektrophotometrische Bestimmung der Dissoziationskonstanten von Chloranilsäure*. Monatshefte für Chemie, 1970. 101: p. 1591-1596.
74. Nazarenko, *Dissociation Constants of Chloranilic Acid*. Journal of General Chemistry USSR (Engl. Transl.), 1965. 35.
75. Schwarzenbach, *Redoxgleichgewichte, Aciditätsgleichgewichte und die Absorptionsspektren bei Oxychinonen*. Helvetica Chimica Acta, 1941. 24: p. 617-638.
76. Weissbart, J. and P. van Rysselberghe, *Polarographic Behaviour of Chloranilic Acid*. Journal of Physical Chemistry, 1957. 61: p. 765-767.
77. Demuth and Meyer, *Ueber Nitroethylalkohol*. Justus Liebigs Annalen der Chemie, 1891. 263: p. 28-49.
78. Nishi, S. and M. Matsuda, *Studies on the Carbanions Affected by Neighbouring Sulfur Groups. I. Effect of the Oxidation Number of Sulfur Atom on Ion Pairing and Electron Transfer of the Alkali Metal Fluorenyl Carbanions Substituted in Position 9 with Phenyl Sulfur Groups*. Journal of the American Chemical Society, 1979. 101: p. 4632-4636.
79. Raju, *Reductimetric Determination of Some Quinones with Iron (II)*. Indian Journal of Chemistry, 1993. 32A: p. 1012-1014.
80. Kvalnes, D.E., *An Optical Method for the Study of Reversible Organic Oxidation Reduction System V. o-Benzoquinones*. Journal of the American Chemical Society, 1934. 56: p. 2487-2489.
81. Nurmi, J. and P.G. Tratnyek, *Electrochemical Properties of Natural Organic Matter (Nom, Fraction of Nom and Model Biogeochemical Electron Shuttles)*. Environmental Science & Technology, 2002. 36(617-624).
82. Giles, G., et al., *Electrochemical In Vitro and Cell Culture Analysis of Integrated Redox Catalysts, Implications for Cancer Therapy*. Chemical Communications, 2003. 16: p. 2030-2031.
83. Hugg, J.W.H., A.K. Macbeth, and F.L. Winzor, *The Coloring Matters of Drosera Whittakeri, Part IV. The Reduction Potentials of Some Naphthoquinones*. Journal of Chemical Society, 1936(1457-1462).
84. Shalev, H. and D.H. Evans, *Solvation of Anion Radicals: Gas-Phase vs. Solution*. Journal of the American Chemical Society, 1989. 111(7): p. 2667-2674.

References

85. Wallenfels, K. and W. Moehle, *Die Reduktionspotentiale-Oxidationspotentials der Napthoquinone*. Chemische Berichte, 1943. 76: p. 924-396.
86. Arnett, E.M. and C.F. Dooty, *Solvent Effects in Organic Chemistry. II. Sulfolane-A Weakly Basic Aprotic Solvent of High Dielectric Constant*. Journal of the American Chemical Society, 1964. 86(409-411).
87. Sristava, M.M., M. Singh, and S.N. Sristava, *Polarographic Studies on Kinetics of Electrode Reaction of Benalacetophenone*. Indian Journal of Chemistry, 1984. 23: p. 591-592.
88. Lewis, D.F.V. and J.M. Pratt, *The P450 Catalytic Cycle and Oxygenation Mechanism*. Drug Metabolism Reviews, 1998. 30(4): p. 739-786.
89. Sarr, D.H., et al., *Decomposition of Tetrachloro-1, 4-Benzoquinone (p-Chloranil) in Aqueous Solution*. Environmental Science and Technology, 1995. 29(11): p. 2735-2740.
90. Slifkin, M.A., R.A. Sumner, and J.G. Heathcote, *The Interactions of Chloranil in Aqueous Solvents-I, the Absorption Spectrum of Chloranil in 50 % Aqueous Ethanol*. Spectrochimica Acta, 1967. 28A: p. 1751-1756.
91. Hancock, J.W. and C.E. Morrell, *Trichlorohydroxyquinone*. Tetrahedron Letters, 1962. 22: p. 987-988.
92. Bishop, C.A. and L.K.J. Tong, *Reversible Addition of Hydroxide Ion to Quinones*. Tetrahedron Letters, 1964. 41: p. 3043-3048.
93. Raymond, K.S., A.K. Grafton, and R.A. Wheeler, *Calculated One-Electron Reduction Potentials and Solvation Structures for Selected p-Benzoquinones in Water*. Journal of Physical Chemistry B, 1997. 101: p. 623-631.
94. Veltsistas, P.G., M.I. Karayannis, and M.A. Koupparis, *Potentiometric Determination of p-Chloranil and the Kinetic Study of its Alkaline -Hydrolysis, Using a Chloranilate Selective Electrode*. Talanta, 1994. 41(10): p. 1725-1733.
95. www2.sisweb.com/mstools/isotope.
96. Stolz, S. and H. Dollt, *HR-MS Metabolismus*. 2007, Analytical Department, Metabolite ID, F. Hoffmann-La Roche: Basel. p. 6.
97. Ruf, I. and H. Dollt, *p-Chloranil and Chloranilic Acid Study*. 2006, Applied Analytical Methods, Section Molecular Structure Research: Basel. p. 20.
98. Obach, S.R., *The Prediction of Human Clearance from Hepatic Microsomal Metabolism Data*. Current Opinion in Drug Discovery and Development, 2001. 4(1): p. 36-44.
99. Bouchard, G., et al., *Ionic Partition Diagram of the Zwitterionic Antihistamine Cetirizine*. Helvetica Chimica Acta, 2001. 84(2): p. 375-387.
100. Ortiz de Montellano, P.R., *Cytochrome P450: Structure, Mechanism, and Biochemistry*. 2005, New York, USA: Kluwer Academic/ Plenum Publisher.
101. Bistolos, N., et al., *Cytochrome P450 Biosensors-A Review*. Biosensors and Bioelectronics, 2005. 20(12): p. 2408-2423.

References

102. Udit, A.K. and H.B. Gray, *Electrochemistry of Heme-Thiolate Proteins*. Biochemical and Biophysical Research Communications, 2005. 338(1): p. 470-476.
103. Hardman, J.G., et al., *Goodman & Gilman's: The Pharmacological Basis of Therapeutics*. 9th ed. 1996, New York: McGraw-Hill. 1905.
104. Eriksson, L., et al., *Multi-and Megavariate Data Analysis, Part I Basic Principles and Applications*. 2nd ed. 2006: Umetrics. 424.
105. Wold, S., et al., *Multi-Way Principal Components- and PLS-Analysis*. Journal of Chemometrics, 1987. 1: p. 41-56.
106. de Toledo, R.A., et al., *Use of Graphite Polyurethane Composite Electrode for Imipramine Oxidation- Mechanism Proposal and Electroanalytical Determination*. Analytical Letters, 2006. 39: p. 507-520.
107. Volk, K.J., R.A. Yost, and A. Brajtertothm, *Electrochemistry On-line Mass Spectrometry for the Study of Biological Redoxreactions*. Analytical Chemistry, 1992. 64: p. A21-A33.
108. Deng, H.T. and G.J. Van Berkel, *A Thin-Layer Electrochemical Flow-Cell Coupled On-line with Electrospray-Mass Spectrometry for the Study of Biological Redoxreactions*. Electroanalysis, 1999. 11: p. 857-865.
109. Brookes, B.A., et al., *Voltammetric Sensing of Thiols. The Electrocatalytic Oxidation of 4-Acetamidophenol in the Presence of Cysteine: A Mechanistic Rotating Disk Electrode Study*. Journal of Physical Chemistry: B, 2001. 105: p. 6361-6366.
110. Roussel, H.T., et al., *Mechanistic Aspects of On-line Electrochemical Tagging of Free L-Cysteine Residues during Electrospray Ionisation for Mass Spectrometry in Protein Analysis*. Springer Series in Chemical Physics, 2003. 4: p. 200-206.
111. Roussel, C., et al., *On-line Cysteine Modification for Protein Analysis: New Probes for Electrochemical Tagging Nanospray Mass Spectrometry*. Journal of Electroanalytical Chemistry, 2004. 570: p. 187-199.
112. Johnson, K.A., et al., *Chemical and On-Line Electrochemical Reduction of Metalloproteins with High-Resolution Electrospray Ionization Mass Spectrometry Detection*. Analytical Chemistry, 2001. 73: p. 803-808.
113. www.medterms.com.
114. www.bio.hw.ac.uk/edintox/glossall.htm.
115. en.wikipedia.org/wiki/Xenobiotics.
116. www.chemdiv.com/en/Information/glossary/.
117. <http://chemistry.about.com/library/glossary/>.
118. www.iupac.com.
119. Scully, F., D.M. Oglesby, and H.J. Buck, *Cyclic Voltammetry of Organic and Inorganic N-Chloramines in Aqueous Solution*. Analytical Chemistry, 1984. 56: p. 1449-1451.

References

120. Somich, C., et al., *Photoinitiated Electron-Transfer Reactions of Aromatic Imides with Phenylcyclopropanes. Formation of Radical Ion Pair Cycloadducts. Mechanism of the Reaction.* Journal of Organic Chemistry, 1990. 55(9): p. 2624-2630.
121. Tanko, J.M. and R.E. Drumright, *Radical Ion Probes. 2. Evidence for the Reversible Ring Opening of Arylcyclopropylketyl Anions. Implications for Mechanistic Studies.* Journal of the American Chemical Society, 1992. 114(5): p. 1844-1854.
122. Utlely, J.H.P. and G.G. Rozenberg, *Electroorganic Reactions. Part 56: Anodic Oxidation of 2-Methyl- and 2-Benzyl-naphthalenes: Factors influencing Competing Pathways.* Tetrahedron, 2002. 58(26): p. 5251-5265.
123. Mori, M., H. Hatta, and S.I. Nishimoto, *Stereoelectronic Effect on One-Electron Reductive Release of 5-Fluorouracil from 5-Fluoro-1-(2'-Oxocycloalkyl) Uracils as a New Class of Radiation-Activated Antitumor Prodrugs.* Journal of Organic Chemistry, 2000. 65(15): p. 4641-4647.
124. Moressi, M.B., M.A. Zon, and H. Fernandez, *Electrochemical Oxidation of 6-Propionyl-2-(N, N-Dimethylamino) Naphthalene (Prodan) in Acetonitrile on Pt Electrodes: Reversible Dimerization of Prodan Radical Cations.* Canadian Journal of Chemistry, 2002. 80(9): p. 1232-1241.
125. Wartini, A.R., et al., *Intramolecular Electron Transfer between 2, 5-Dimethoxy-1, 4-phenylene Units in Paracyclophane Radical Cations.* European Journal of Organic Chemistry, 1998. 1998(1): p. 139-148.
126. Yudin, A.K., et al., *F8BINOL, an Electronically Perturbed Version of BINOL with Remarkable Configurational Stability.* Organical Letters, 2000. 2(1): p. 41-44.
127. Yasuda, M., et al., *Photoamination of Alkenyl-naphthalenes with Ammonia via Electron Transfer.* Bulletin of the Chemical Society of Japan, 1998. 71(7): p. 1655-1660.
128. Onodera, K., et al., *Mechanistic Considerations on Photoreaction of Organic Compounds via Excitation of Contact Charge Transfer Complexes with Oxygen.* Tetrahedron, 1985. 41(11): p. 2215-2220.
129. Sakamoto, M., et al., *Intermolecular Electron Transfer from Naphthalene Derivatives in the Higher Triplet Excited States.* Journal of the American Chemical Society, 2004. 126(31): p. 9709-9714.
130. Antonello, S. and F. Maran, *Dependence of Intramolecular Dissociative Electron Transfer Rates on riving Force in Donor-Spacer-Acceptor Systems.* Journal of the American Chemical Society, 1998. 120(23): p. 5713-5722.
131. Zweig, A., A.H. Maurer, and B.G. Roberts, *Oxidation, Reduction, and Electrochemiluminescence of Donor-Substituted Polycyclic Aromatic Hydrocarbons.* Journal of Organic Chemistry, 1967. 32(5): p. 1322-1329.
132. Fukuzumi, S., I. Nakanishi, and K. Tanaka, *Multielectron Oxidation of Anthracenes with a One-Electron Oxidant via Water-Accelerated Electron-Transfer Disproportionation of the Radical Cations as the Rate-Determining Step.* Journal of Physical Chemistry A, 1999. 103(50): p. 11212-11220.
133. Sauro, V. and M. Workentin, *The Redox Properties of Ferrocenyl-Substituted Aryl Azines.* Canadian Journal of Chemistry, 2002. 80: p. 250-262.
134. Wood, P.D. and L.J. Johnston, *Photoionization and Photosensitized Electron-Transfer Reactions of Psoralens and Coumarins.* Journal of Physical Chemistry A, 1998. 102(28): p. 5585-5591.

References

135. Orlov, Y.E. and A.P. Prokopenko, *Polarography of Natural Coumarins*. Journal of General Chemistry USSR (Engl. Translation), 1970. 28: p. 5585-5591.
136. Holmes, H.L. and D.J. Currie, *Polarographic Half-Wave Potentials and UV-Absorption Spectra of some Conjugated Heteratomic Compounds*. Canadian Journal of Chemistry, 1969. 7: p. 4076-4083.
137. Gaidukevich, A., T. Zhukova, and A. Kravchenko, Journal of General Chemistry USSR (Engl. Translation), 1986. 56: p. 1887-1891.
138. Jockusch, S., et al., *Photoinduced Energy and Electron Transfer between Ketone Triplets and Organic Dyes*. Journal of Physical Chemistry A, 1997. 101(4): p. 440-445.
139. Tabner, B.J. and J.R. Yandle, *A Correlation of Half-Wave Reduction Potentials with Theoretical Calculations for Some Nitrogen -Containing Heteromolecules in Dimethylformamide*. Journal of the Chemical Society: A, 1968: p. 381-382.
140. Andrieux, C., et al., *Electron Transfer Catalyzed Reactions: Electrochemical Induction of the Hydrogen Atom Transfer Oxidation of Alcohols and Other Substrates by Aromatic Halides*. Journal of the American Chemical Society, 1987. 109: p. 1518-1525.
141. Al-Khuzzaii, S., et al., *Interaction of the Quinoline Derivative with Coenzyme Q10*. Zeitschrift für Naturforschung, 1979. 34: p. 1003.
142. Lai, R.F., L. Lu, and S.B. Jenekhe, *Synthesis, Cyclic Voltammetric Studies and Electrogenerated Chemiluminescence of a New Donor- Acceptor Molecule: 2, 7-[Bis [4-Phenyl-2-Quinoliny]] -10-Methylphenothiazine*. Journal of the American Chemical Society, 2001. 123: p. 9112-9118.
143. Casimir, D.J. and L.E. Lyons, *Polarographic Reduction of Some Heterocyclic Molecules Part I. The Reduction of Cinchoninic Acid*. Journal of the Chemical Society: A, 1950: p. 783-785.
144. Pandrey, G., S. Rani, and G. Lakshmaiah, *Direct Carbon-Carbon Bond Formation Strategy at the α -Position of Tertiary Amines by Photoinduced Electron Transfer (PET) Processes*. Tetrahedron Letters, 1992. 33: p. 5107-5110.
145. Fournier, F., J. Berthelot, and Y.L. Pascal, *Hydrodimerisation Electrochimique de Cetonnes Aromatiques Encombrees en Milieu Aprotique et en Presence de Chlorure de Chrome*. Tetrahedron, 1984. 40(2): p. 339-347.
146. Bertram, J., M. Fleischmann, and D. Pletcher, *The Anodic Oxidation of Alkanes in Fluorosulphonic Acid; a Novel Synthesis of [a] [b]-Unsaturated Ketones*. Tetrahedron Letters, 1971. 12(4): p. 349-350.
147. Manecke, G. and W. Huebner, *Reaktion Von Benzochinone-(1, 4) mit Diazomethan Und Vinyldiazomethan*. Tetrahedron Letters, 1971. 26: p. 2443-2446.
148. Driebergen, R.J., et al., *Electrochemistry of Potentially Bioreductive Alkylating Quinones Part I. Electrochemical Properties of Relatively Simple Quinones, as Model Compounds of Mitomycin and Aziridinylquinones-Type1 Antitumour Agents*. Analytica Chimica Acta, 1990. 233: p. 251-268.
149. Mazur, M. and G.J. Blanchard, *Photochemical and Electrochemical Oxidation Reactions of Surface Bound Polycyclic Aromatic Hydrocarbons*. Journal of Physical Chemistry, 2004. 108: p. 1038-1045.
150. Reddy, G., et al., *Electrochemical Reduction Behaviour of 1-Amino-9, 10-Anthraquinone*. Journal of the Indian Chemical Society, 1992. 69: p. 737-740.

References

151. Tai, S., S. Hayashida, and N. Hayashi, *Photoinduced Electron-Transfer Reaction of Naphthalocyanine*. Journal of the Chemical Society, Perkin Transactions 2: Physical Organic Chemistry, 1991. 10: p. 1637-41.
152. Gupta, N. and H. Linschitz, *Hydrogen-Bonding and Protonation Effects in Electrochemistry of Quinones in Aprotic Solvents*. Journal of the American Chemical Society, 1997. 119: p. 6384-6391.
153. Loveland, J.W. and G.R. Dimeler, *Anodic Voltammetry to +2.0 Volts. Application to Hydrocarbons and Oxidation Stability Studies*. Analytical Chemistry, 1961. 33(9): p. 1196-1201.
154. Kitagawa, T., et al., *Amphoteric Redox Nature of p-Benzoquinones with Donor- and Acceptor-Substituents*. Chemical Letters, 1990. 6: p. 897-900.
155. Kruppa, A.I., et al., *EPR and AM1 Study of the Structure of the Radical Anion of Ionone*. Journal of Physical Chemistry A, 1999. 103(10): p. 1414-1418.
156. Bratu, C. and A.T. Balaban, *Electrochemistry of Carbonium Ions. I. Electrochemical Oxidation of 1, 5-Diketones*. Revue Roumaine de Chimie, 1965. 10: p. 1001-1008.
157. Cheng, J.P., et al., *Energetics of Multistep versus One-step Hydride Transfer Reactions of Reduced Nicotinamide Adenine Dinucleotide (NADH) Models with Organic Cations and p-Quinones*. Journal of Organic Chemistry, 1998. 63(18): p. 6108-6114.
158. Bellec, C., et al., *Chemical and Electrochemical Reductions of 5H-Benzopyrano [1] [4, 3-d] Pyrimidines*. Journal of Heterocyclic Chemistry, 1990. 27(3): p. 551-5.
159. Bordwell, F. and W.Z. Liu, *Equilibrium Acidities and Homolytic Bond Dissociation Energies of N-H and/or O-H bonds in N-Phenylhydroxylamine and its Derivatives*. Journal of the American Chemical Society, 1996. 118: p. 8777-8781.
160. Bordwell, F.G., X.M. Zhang, and J.P. Cheng, *Bond Dissociation Energies of the Nitrogen-Hydrogen Bonds in Anilines and in the Corresponding Radical Anions. Equilibrium Acidities of Aniline Radical Cations*. Journal of Organic Chemistry, 1993. 58(23): p. 6410-6416.
161. Malmstrom, J., et al., *The Antioxidant Profile of 2, 3-Dihydrobenzo[b] Furan-5-ol and its 1-Thio, 1-Seleno, and 1-Telluro Analogues*. Journal of the American Chemical Society, 2001. 123(15): p. 3434-3440.
162. Mizuno, K., M. Ishii, and Y. Otsuji, *Photoinduced Alkylation of Five-Membered Heteroaromatic Compounds via Electron-Transfer Reaction: Heterodimer Cation Radical Intermediacy*. Journal of the American Chemical Society, 1981. 103(18): p. 5570-5572.
163. Waltman, R.J., A.F. Diaz, and J. Bargon, *Substituent Effects in the Electropolymerization of Aromatic Heterocyclic Compounds*. Journal of Physical Chemistry, 1984. 88(19): p. 4343-4346.
164. Nakayama, J. and K. Kuroda, *Synthesis and Reactivities of a Highly Strained Thiophene with Two Fused Four-Membered Rings, 1,2,4,5-Tetrahydrodicyclobuta[b,d]Thiophene*. Journal of the American Chemical Society, 1993. 115(11): p. 4612-4617.
165. Rudzinski, W.E., Y. Zhang, and X. Luo, *Mass Spectrometry of Polyaromatic Sulfur Compounds in the Presence of Palladium(II)*. Journal of Mass Spectrometry, 2003. 38(2): p. 167-173.
166. Konno, A., et al., *Electrolytic Transformation of Fluoroorganic Compounds. 5. Anodic Cyanation of 2, 2, 2-Trifluoromethylamines*. Journal of Organic Chemistry, 1990. 55: p. 1952-1954.

References

167. Dawid, W., H. Scholl, and R. Skowronski, *Electrode Reactions of Some Piperidine Derivatives*. Polish Journal of Chemistry, 1984. 58: p. 497-502.
168. Benoit, R. and P. Pichet, *Acid-Base Reactions in Sulfolane*. Journal of Electroanalytical Chemistry and Interfacial Electrochemistry, 1973. 43.
169. Nelsen, S.F., et al., *One-Electron Oxidation of Trialkylsulfenamides*. Journal of the American Chemical Society, 1982. 104: p. 6641-6646.
170. Bent, L., et al., *Chemical Constitution, Electrochemical, Photographic and Allergenic Properties of p-Amino-N-Dialkylines*. Journal of the American Chemical Society, 1951. 73: p. 3100-3101.
171. Borsari, M., et al., *Substituent Effects in the Reduction Behaviour of Thio- and Oxopyridines in Non-Aqueous Solvents*. Australian Journal of Chemistry, 2003. 56: p. 1223-1238.
172. Karpinets, A.P. and V.D. Bezuglyi, *Study of the Effect of Depolarizer Structure and the Nature of the Mixed Solvent on the Polarographic Reduction of Organic Compounds. IV. Polarographic Study of the State of Ketones in Methanol-Benzene Solutions*. Journal of General Chemistry USSR (Engl. Translation), 1980. 50(6): p. 1379-9.
173. Vieth, B. and W. Jugelt, *Electrochemical Synthesis of Nitrogen Heterocyclic Compounds. XVIII. Cathodic Behavior of Bisenaminones*. Zeitschrift für physikalische Chemie, 1984. 265(5): p. 947-58.
174. Rao, P.S. and E. Hayon, *Redox Potentials of Free Radicals. III. Reevaluation of the Method*. Journal of the American Chemical Society, 1975. 97(11): p. 2986-2989.
175. Allen, W., R.L. Pasternak, and W. Seaman, *Polarographic Determination and Evidence for the Structure of Leucovorin*. Journal of the American Chemical Society, 1952. 74(13): p. 3264-3269.
176. Dixon, B.G. and G.B. Schuster, *Chemiluminescence of Secondary Peroxy Esters*. Journal of the American Chemical Society, 1981. 103(11): p. 3068-3077.
177. Svaan, M. and V.D. Parker, *Temperature Effects on Electrode Processes. II. The Entropy of Formation of Ion Radicals of Heteroaromatic Compounds*. Acta Chemica Scandinavica, Series B, 1982. B36(6): p. 351-5.
178. Pearson, A.J. and A.M. Gelormini, *Manipulation of the Reduction Potentials of Wurster's Blue Derivatives via Steric and Conformational Effects*. Tetrahedron Letters, 1997. 38(29): p. 5123-5126.
179. Rudenko, A.P. and F. Pragst, *Electrochemical Oxidation of Organic Compounds in Fluorosulfonic Acid. XIII. Oxidative Reaction of Aromatic Compounds in Acidic Systems based on FSO₃H and CF₃COOH*. Russian Journal of Organic Chemistry, 1997. 34: p. 1589-1620.
180. Malik, W. and R. Jain, *On the Polarographic Reduction of 2-Aminobenzothiazoles*. Journal of the Indian Chemical Society, 1982. 59(4): p. 558-61.
181. Colonna, M., L. Greci, and M. Poloni, *Electrophilic Ipso Substitutions. Part 3. Reactions of 3-Substituted Indoles, 4-Substituted N, N-Dimethylanilines, and 1- and 3-Substituted Indolizines with Nitrous Acid*. Journal of the Chemical Society, Perkin Transactions 2: Physical Organic Chemistry, 1984. 2: p. 165-9.
182. Supin, G.S., et al., *Polarography of N, N'-Disubstituted Derivatives of Parabanic Acid*. Journal of General Chemistry USSR (Engl. Translation), 1977. 47(5): p. 1202.

References

183. Kato, S. and G. Dryhurst, *Electrochemical Oxidation of some 5-Substituted Barbituric Acids at the Pyrolytic Graphite Electrode: Electrochemical Synthesis of 5, 5'-Substituted Hydurilic Acids*. Journal of Electroanalytical Chemistry, 1977. 79(2): p. 391-399.
184. Shishkina, N.A., et al., *Structure and Basicity of Phenolic Mannich Bases*. Bulletin Academia Scientific USSR Division Chemical Sciences (Engl. Transl.), 1976. 6: p. 1259-64.
185. Iversen, P.E., *Organic Electrosyntheses. III. Reduction of N-Nitrosamines*. Acta Chemica Scandinavica, Series B, 1971. 25(6): p. 2337-40.
186. Renaud, P. and S. Schubert, *Radical Reductive Alkylation of Enamines with Chloromethyl p-Tolyl Sulfone*. Angewandte Chemie, 1990. 102(4): p. 416-417.
187. Hartmann, H., P. Gerstner, and D. Rohde, *A Simple Route to N-Arylated 2-Aminothiophenes as a New Class of Amorphous Glass Forming Molecules*. Organical Letters, 2001. 3(11): p. 1673-1675.
188. Kotha, S. and A. Kuki, *A New Synthetic Approach to Unusually Electron Rich α -Amino Acids*. Journal of the Chemical Society, Chemical Communications, 1992. 5(404-6).
189. Goyal, R.N., et al., *Effect of Methyl Groups on the Oxidation of Xanthine and Correlation of Oxidation Potentials with Frontier Molecular Orbital Energies*. Indian Journal of Chemistry, Section A: Inorganic, Bio-inorganic, Physical, Theoretical & Analytical Chemistry, 2000. 39A(9): p. 953-963.
190. Goyal, R.N. and A. Rastogi, *Oxidation Chemistry of 3, 7-Dimethylxanthine - a Central Behavioral Stimulant at Solid Electrodes*. Croatica Chemica Acta, 2000. 73(2): p. 495-509.
191. Hashimoto, S., *Mechanism of Fluorescence Quenching of Pyrene with Purines in Polar Media: Formation of the Pyrene Triplet State via Exciplex Formation*. Journal of Physical Chemistry, 1993. 97(15): p. 3662-3667.
192. Svyatkina, D.L.D. and G. Kurov, Journal of General Chemistry USSR (Engl. Translation), 1988. 58: p. 2357-2360.

7. Abbreviations

ACN:	acetonitrile
DMSO:	dimethylsulfoxide
DDQ:	dichlorodicyanoquinomethan
<i>p</i> -chlor:	<i>p</i> -chloranil
chlor ac:	chloranilic acid
jug:	juglone
HT:	high-throughput
RDI:	redoxindicator
CPD:	compound
Cl:	chlorine
FOC:	ferrocene
CV:	cyclic voltammetry
PB:	phosphate buffer
HB:	hepes buffer
CL_mic_rat:	rat microsomal clearance
CL_mic:	microsomal clearance
ER:	endoplasmatic reticulum
<i>in vivo</i> CL:	<i>in vivo</i> clearance
E _{ox} :	electrochemical oxidation potential
HLM:	human liver microsomes
HP:	hepatocytes
LC/MS:	L iquid C hromatography- M ass S pectrometry
EC/LC/MS:	E lectrochemistry- L iquid C hromatography- M ass S pectrometry
EC:	Electrochemistry
CV:	cyclic voltammetry
ADME:	acronym for absorption, distribution, metabolism and elimination.
V _{max} :	velocity of reaction
DDI:	drug-drug interaction

Abbreviations

K_m	Michaelis constant
CYP450:	Cytochrome P450
FMO:	flavin-monooxygenases
UGT:	UDP-glucuronyltransferases
DDI:	drug-drug interaction
MW:	molecular weight
PK:	pharmacokinetic properties
EPSS:	electro active pharmaceutical profiling/screening system
SCE:	standard calomel electrode
Ag/AgCl:	silver/silver chloride electrode
FeCN:	ferrocyanide
o-chlor:	o-chloranil
1,2-naphQ:	1,2-naphthoquinone
mena:	menadione
chalk:	chalkon
Au:	gold
Ag:	silver
KCl:	potassium chloride

8. Glossary

ADMET:	absorption, distribution, metabolism, elimination and toxicology
Cl_{int} :	intrinsic clearance. This describes the enzyme catalysed removal of a drug by the system and therefore is not influenced by other physiological determinants of clearance, such as hepatic blood flow.
CYP450:	cytochrome P450. These enzymes are involved in the oxidative metabolism of a high proportion of marketed drugs
K_m :	the Michaelis-Menten constant describing the affinity of a substrate for an enzyme. The K_m is equal to the substrate concentration at which the reaction rate is half maximal.
Discovery compounds:	term for compounds in pre-clinical development, belonging to the lead series identified
Signal transduction:	"A basic process in molecular cell biology involving the conversion of a signal from outside the cell to a functional change within the cell" [113].
Pharmacokinetics:	"This is the science which describes quantitatively the uptake of drugs by the body, their biotransformation, their distribution, metabolism, and elimination from the body. Both total amounts and tissue and organ concentrations are considered" [114].
Pharmacodynamics:	This is a scientific discipline, which is a part of pharmacology and deals with the effect of drugs on tissues and organs [5].
Xenobiotic:	A xenobiotic is a chemical which is found in an organism but which is not normally produced or expected to be present in it [115].
Bioavailability:	The percentage of drug that is detected in the systemic circulation after its administration [116].
Half life ($t_{1/2}$):	The time required to convert one half of a reactant to product [117].

Cyclic voltammetry:	Electrochemical technique for studying variable potential at an electrode involving of a triangular potential sweep
Working electrode:	An electrode that serves as a transducer responding to the excitation and the concentration of the substance of interest in the solution investigated, and that permits the flow of current sufficiently large appreciable changes of bulk composition within the ordinary duration of a measurement.
Reference electrode:	A nonpolarizable electrode that generates highly reproducible potentials; examples are the calomel electrode, silver-silver chloride electrode, and mercury pool [44].
Auxiliary electrode:	Auxiliary electrodes are used for the transfer of electric current to the working electrode [44]
Potentiostat:	An electronic instrument that controls the voltage difference between a working electrode and a reference electrode both contained in an electrochemical cell. The control is implemented by injecting current into the cell through an auxiliary electrode. The potentiostat measures the current flow between the working and auxiliary electrodes [118].

Figure Index

Chapter 1

Fig.1 Adapted from Mutschler, a schematic overview on the fate of a drug after oral application, Page 12

Fig.2 Typical reasons for failures in 1991, Page 13

Fig.3 The drug discovery and drug development process, Page 14

Fig.4 The "well-stirred" or venous equilibrium model (left) and the "parallel tube model" or sinusoidal model (right). The tanks are lined with rows of hepatocytes where the metabolism of the drug is supposed to occur. The small black arrows indicate the exchange, Page 17

Fig.5 Correlation Lipophilicity ($\log D_{7,4}$) with unbound (free) hepatic intrinsic clearance ($CL_{i(a)}$, filled squares) and unbound (free) renal clearance ($CL_{(r)}$, open triangles) adapted from van der Waterbeemd et al., Page 21

Fig.6 Haem moiety, Page 23

Fig.7 Metabolic pathway of imipramine with known phase-I metabolism and high in vivo clearance, Page 24

Fig.8 Catalytic cycle of CYP450 after Lewis: 1) Substrate binding, 2) First reduction of Fe^{3+} 3) Oxygen binding 4) Second reduction 5) Product formation 6) Product release, Page 25

Fig.9 Electronic transfer pathways in various CYP450 systems, Page 29

Chapter 2

Fig.1 Schematic sketch for a general set-up of an electrochemical cell, Page 34

Fig.2 Variation of applied potential with time in cyclic voltammetry, showing the initial potential, E_i , the final potential E_f , maximum E_{max} , and minimum E_{min} potential, The sweep rate $dE/dt=v$. For linear sweep voltammetry consider only one segment. The fact that the initial sweep is positive is purely illustrative. Page 35

Fig.3 Cyclic voltammogram for a reversible charge transfer, E_{pc} : cathodic peak potential, E_{pa} : anodic potential, E_{switch} : switching potential, $E_{1/2}$: half-wave potential, i_{pc} : cathodic peak current, i_{pa} : anodic peak current, $i_{\text{red}0}$: current at E_{red} , i_{pa} : anodic peak current at Baseline. Page 35

Fig.4 Cyclic voltammogram for an irreversible charge transfer carried out at HT-cyclic voltammetry in aqueous media, Page 37

Fig.5 Schematic drawing for an electrochemical cell used in the classical experimental set-up, Page 39

Fig.6 Picture of EPSS with a sensor plate placed on the measurement unit, Page 40

Fig.7 Example of a sensor plate V4 (Gatlik, Basel) total well volume of 55 μl Page 40

Fig.8 Correlation of data recorded at **classical method** and **EPSS** (HT-method), the correlation yielded a R^2 : 0.9799. Statistical values are as follows: F-value: 342.93, STD error of estimate: 0.0907 intercept: 0.068. Number of cases: n=9, Page 41

Fig.9 Cyclic voltammogram *ferrocene* in **acetonitrile**, scanning from 0.6 to 1.0 V with a scan rate of 0.8 V/s, signals retrieved by **classical cyclic voltammetry**, Page 44

Fig.10 Cyclic voltammogram *ferrocene* in **phosphate buffer** scanning from -0.3 to 0.8V with a scan rate of 0.64 V/s, signals retrieved by **EPSS**, HT-cyclic voltammetry, Page 44

Chapter 3

Fig.1 2,3,5,6-tetrachloro-1,4-dibenzoquinone (***p*-chloranil**), Page 48

Fig.2 General reaction pathway of *p*-chloranil with a sample S, Page 48

Fig.3 The principal steps of the sample preparation for *p*-chloranil assay, Page 51

Fig.4 Cyclic voltammogram of 0.01 mM **juglone** measured in 100% DMSO at a scan rate of 150 mV/s in a range from 600 mV to -1000 mV using classical CV, Page 55

Fig.5 Cyclic voltammogram of 0.01 mM ***p*-chloranil** measured in 100% DMSO at a scan rate of 150mV/s in a range from 600 mV to -1000 mV using classical CV, Page 55

Fig.6 Influence of light on the degradation of *p*-chloranil using an aluminium cover. A kinetic measurement during 40 min was performed using three different wavelengths (292nm, 310nm and 650 nm). Measurements at 650 nm were necessary to crosscheck solubility of compounds. The measurement interval was 1 min and OD_{min} was set 0, OD_{max} at 1. The chloranil sample without Al-cover showed at higher degree of degradation (25.43%) than the sample with Al-cover (15.43 %), Page 56

Fig.7 Influence of pH value on the degradation of *p*-chloranil using aluminium cover. Measurement was done with UV-Vis-spectroscopy performing a kinetic measurement during 40 min using three different wavelengths at 292nm, 310nm and 650 nm. 650 nm was necessary to crosscheck solubility of compounds. The measurement interval was 1 min and OD_{min} was set 0, OD_{max} at 1. Page 57

Fig.8 Degradation of *p*-chlorine to chloranilic acid according to Sarr, Page 58

Fig.9 Degradation Kinetics of *p*-chloranil measured with Agilent 6140 under the conditions mentioned in Material and Methods, Page 59

Fig.10 Degradation kinetics of five commercially available compounds [loratadine (lora), imipramine (imi), loratadine derivative (lora+derivative), paroxetine (paro) and sertraline (sertra)] after their incubation with *p*-chloranil at equimolar concentrations of 0.01 mM, Page 61

Fig.11 Concentration dependency of three different commercially available compounds as loratadine (lora), imipramine (imi), sertraline (sertra) and as RDI *p*-chloranil at equimolar concentration of 0.01 mM. The reaction followed first order kinetics. The λ_{max} was chosen for *p*-chloranil at 320 nm. The number of cases was n=4. The incubation length was set to 30 min., Page 62

Fig.12 Representative chromatogram of *p*-chloranil measured with Agilent 1200 series and 6140 MSD. The gradient run for this assay consisted of **A** 95% water +0.1% formic acid and solvent **B** 5 % ACN + 0.1% formic acid. The gradient schedule is 5- 95% **B** for 0.6 min at 1.0 ml/min. The column is re-

equilibrated with 95% A during 0.2 min prior to next injection. Total run time was 2.5 min. Detection of the analytes was by inline UV-detection at 254,292, 310, and 320, Page 62

Fig.13 Example of a chromatogram measuring K5_2nd after the incubation t=30 min with p-chloranil. Measured with Agilent 1100 series and MSD. The gradient run for this assay consisted of **A** (water +0.1% formic acid) and solvent **B** (ACN + 0.1% formic acid). The gradient schedule is 5- 95% **B** for 0.6 min at 1.0 ml/min. The column is re-equilibrated with 95% A for 0.2 min prior to next injection. Total runtime was 2.5 min. Detection of the analytes was by inline UV-detection at 254,292, 310, and 320 nm, Page 64

Fig.14 Calculated isotopic pattern for **tetrachlorohydroquinone (TCIHQ)** using a web calculating tool, Page 65

Fig.15 Calculated of isotopic pattern for **chloranilic acid (chlorac)** using a web tool, Page 66

Fig.16 Isotopic pattern of **TCIHQ** and **chlorac** measured with **Agilent 6140** Series. The gradient, run for this assay consisted of **A** 95% water +0.1% formic acid and solvent **B** 5% ACN + 0.1% formic acid. The gradient schedule is 5- 95% **B** for 0.6 min at 1.0 ml/min. The column is re-equilibrated with 95% A during 0.2 min prior to next injection. Total runtime was 2.5 min. Detection of the analytes was by inline UV-detection at 254,292, 310, 320 nm. Standard conditions for MS were used, Page 66

Fig.17 Calculated isotopic pattern of **p-chloranil** using a web tool, Page 67

Fig.18 Isotopic pattern of fresh **p-chloranil** immediately analyzed after preparation with **Agilent 6140** Series. The gradient, run for this assay consisted of 95% **A** (water +0.1% formic acid) and solvent 5% **B** (ACN + 0.1% formic acid). The gradient schedule is 5- 95% **B** for 0.6 min at 1.0 ml/min. The column is re-equilibrated with 95% A during 0.2 min prior to next injection. Total runtime was 2.5 min. Detection of the analytes was by inline UV-detection at 254,292, 310, 320 nm. Standard conditions for MS were used. Page 67

Fig.19 Isotopic pattern of mixture of **p-chloranil** and **TCIHQ** with **Agilent 6140** Series. The gradient, run for this assay consisted of **A** 95% water +0.1% formic acid and solvent **B** 5% ACN + 0.1% formic acid. The gradient schedule is 5- 95% **B** for 0.6 min at 1.0 ml/min. The column is re-equilibrated with 95% A during 0.2 min prior to next injection. Total runtime was 2.5 min. Detection of the analytes was by inline UV-detection at 254,292, 310, 320 nm. Standard conditions for MS were used. Page 68

Fig.20 Example for decomposition of **p-chloranil** after short incubation in aqueous medium at pH 7.4 with **Agilent 6140** Series. The gradient, run for this assay consisted of 95% **A** (water +0.1% formic acid) and solvent 5% **B** (ACN + 0.1% formic acid). The gradient schedule is 5- 95% **B** for 0.6 min at 1.0 ml/min. The column is re-equilibrated with 95% A for 0.2 min prior to next injection. Total runtime was 2.5 min. Detection of the analytes was by inline UV-detection at 254,292, 310, 320 nm. Standard conditions for MS were used, Page 69

Chapter 4

Fig.1 Haem moiety, Page 73

Fig.2 Data retrieval using MDL CrossFinder Commander and Human Drug Database, Page 76

Fig.3 Comparison of p-chloranil assay and microsomal rat clearance. Percentage of compound disappeared (%CPD_{dis}) was plotted vs. microsomal rat clearance (CL_{mic_rat}), Page 79

Fig.4 Scaffold indol, Page 80

Fig.5 Outliers: a) paroxetine (yellow) b) ciprofloxacin (red). Page 81

Fig.6 Conversion of *p*-chloranil to its hydroquinone at pH: 7.4. Each hydroxyl group exhibits a pK_a value: 1) pK_{a1} : 5.25 2) pK_{a2} : 6.56, Page 81

Fig.7 Reaction pathway of *p*-chloranil via radicalic intermediate in aqueous media at pH 7.4, Page 82

Fig.8 Possible explanation of increased compound instability of paroxetine. Paroxetine was only indicated as fragment, Page 82

Fig.9 Correlation of E_{ox} -potential referred versus ferrocene against microsomal rat clearance, Page 83

Fig.10 First example for a compound in Fig.9: *prochlorperazine* measured with EPSS at a scan rate of 0.640 V/s in a scan range from -0.5 to 1.0 V, No. of scans $n=5$ in 5 mM HB, pH: 7.4, Page 84

Fig.11 Second example for a compound in Fig.9. *desipramine* measured with EPSS at a scan rate of 0.640 V/s in a scan range from 0 to 1.5V, No. of scans $n=5$ in 5 mM HB, pH: 7.4 Page 84

Fig.12 Demethylation reaction of an in-house compound Page 84

Fig.13 Example of an in-house compound for the appearance of a demethylated compound after electrochemical oxidation; LC-result, **Agilent 1100 series MSD SL** at conditions described in Materials and Methods, *Chapter 4*. Page 85

Fig.14 Example of an in-house compound for the appearance of a demethylated compound after electrochemical oxidation; MS-result using **Agilent 1100 series MSD SL** at conditions described in Materials and Methods, *Chapter 4*. Page 85

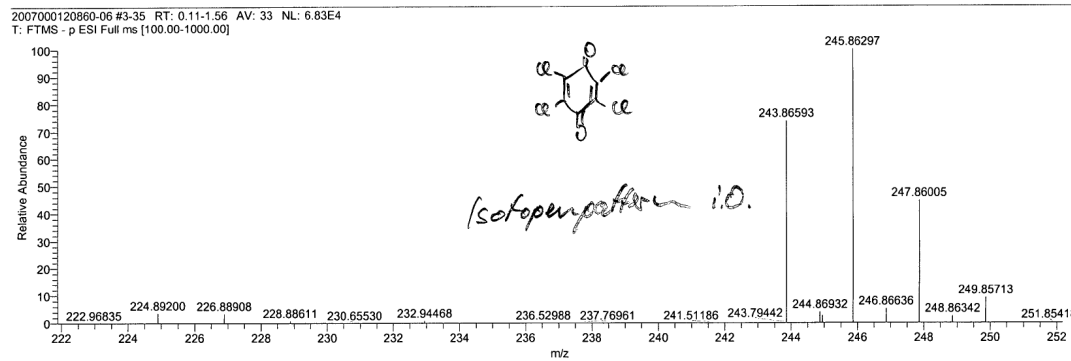
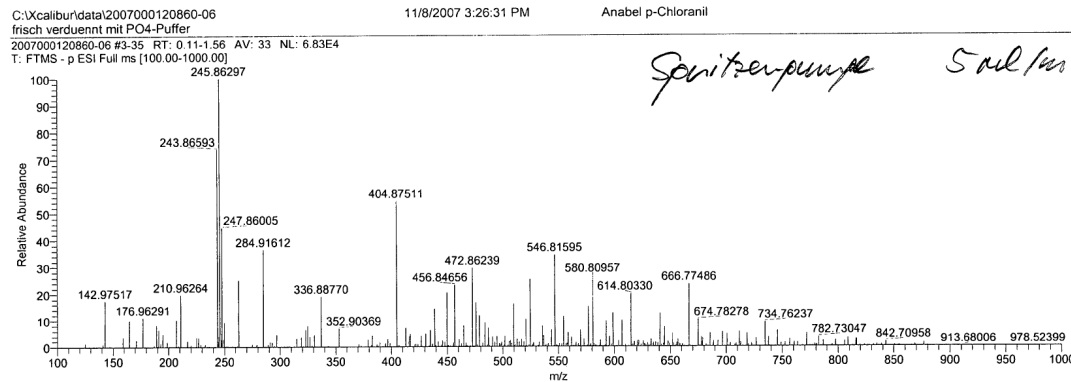
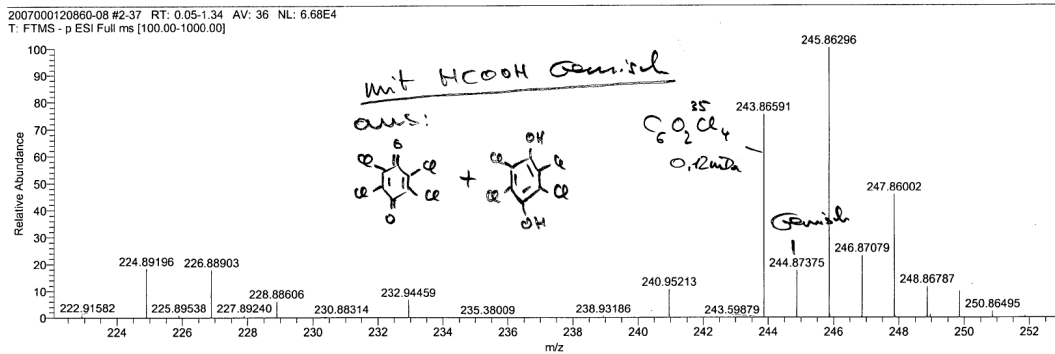
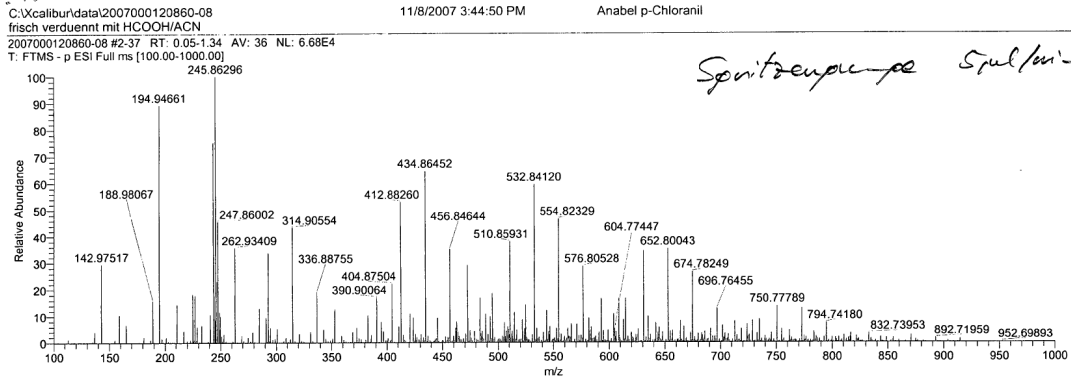
Fig.15 Permutation plot 20 permutations 1 component, CL_{mic_rat} (ml/min/mg protein): R^2 : (0.0, -0.0363), Q^2 : (0.0, -0.0834) Page 87

Fig.16 Loading Scatter plot with R^2 [61]: 0.1479437, R^2 [61]: 0.185738 Page 87

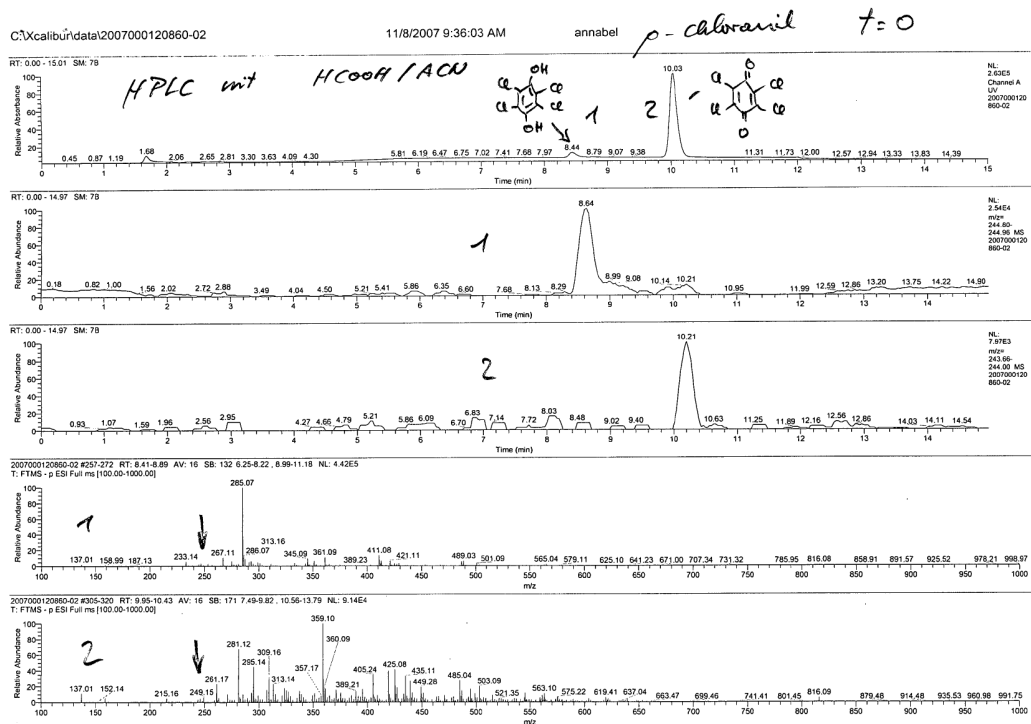
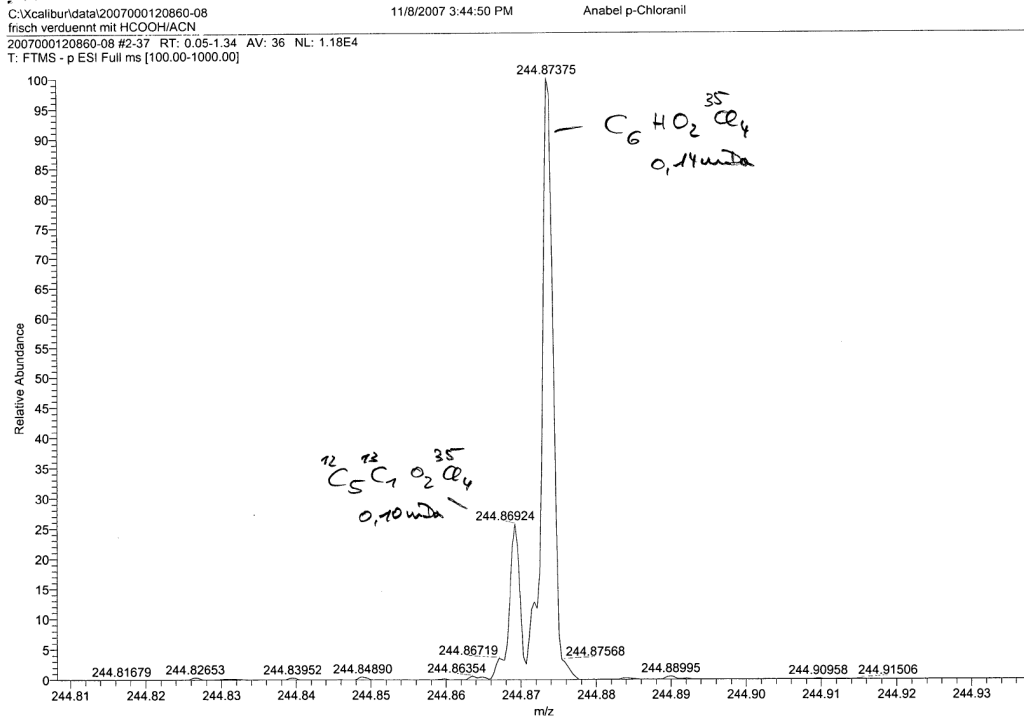
Fig.17 M1 a computational model, created by *RoSARa*. The R^2 was 0.496, the Q^2 : 0.481 and 1 variable. Equation for M1: $CL_{mic_rat} = -E_{ox} + c$ Page 88

APPENDIX

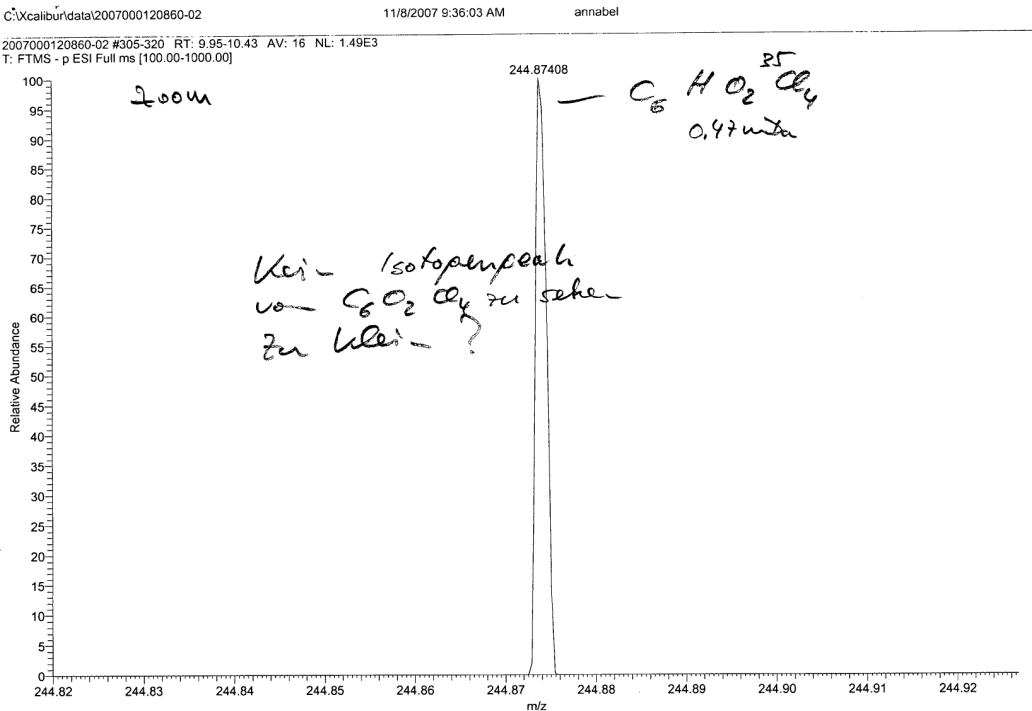
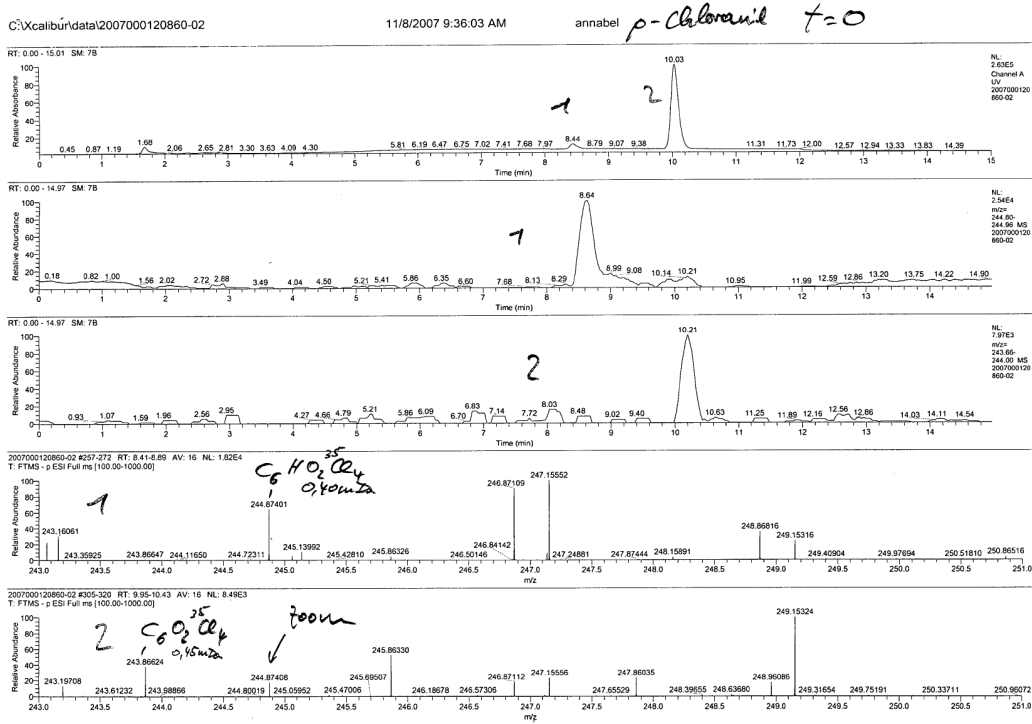
Results from p-Chloranil studies [96] [97]



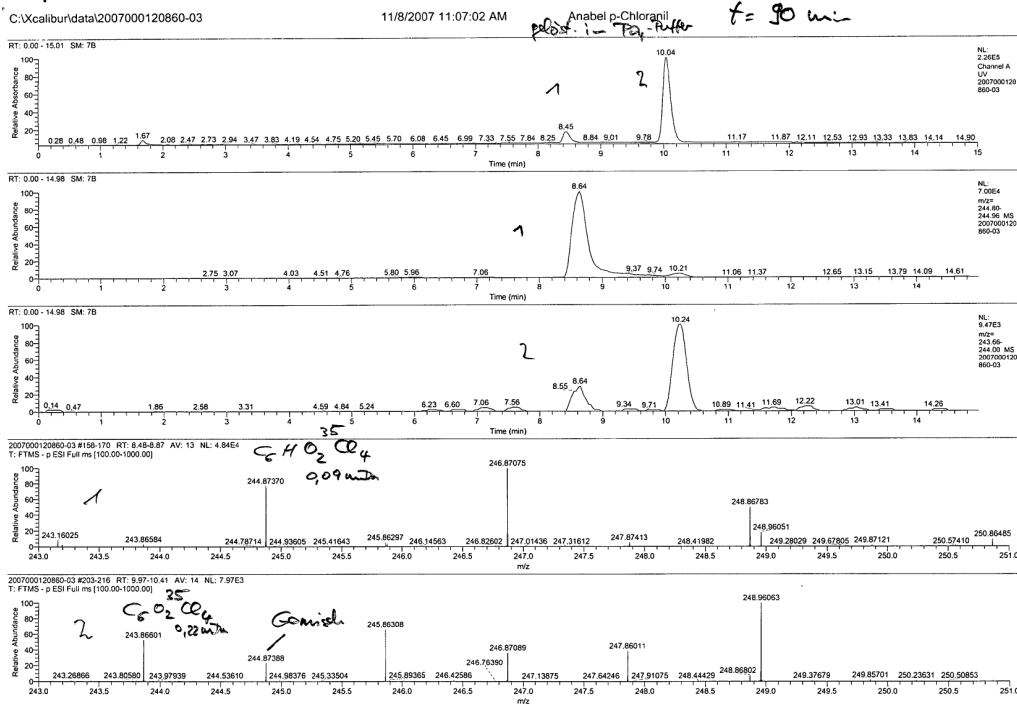
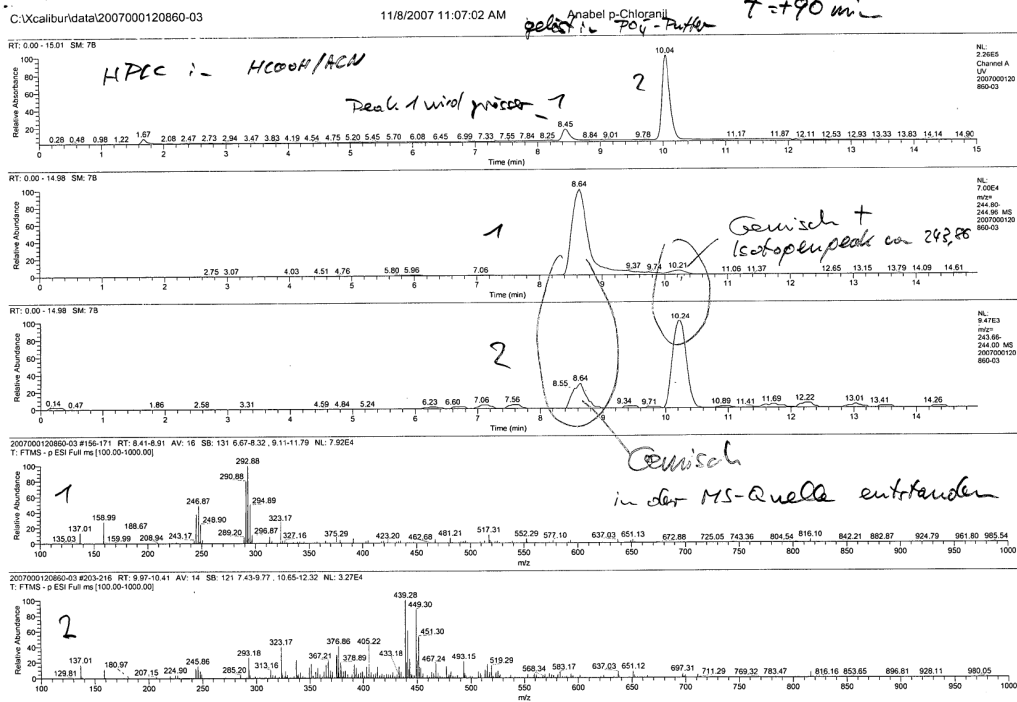
Appendix: Results from *p*-Chloranil studies



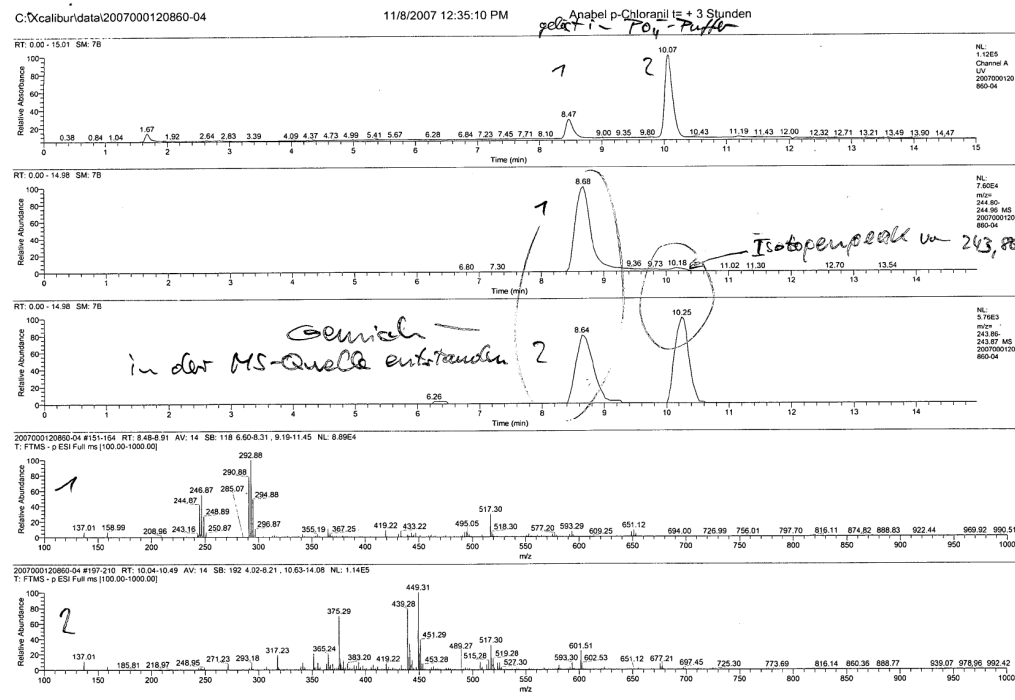
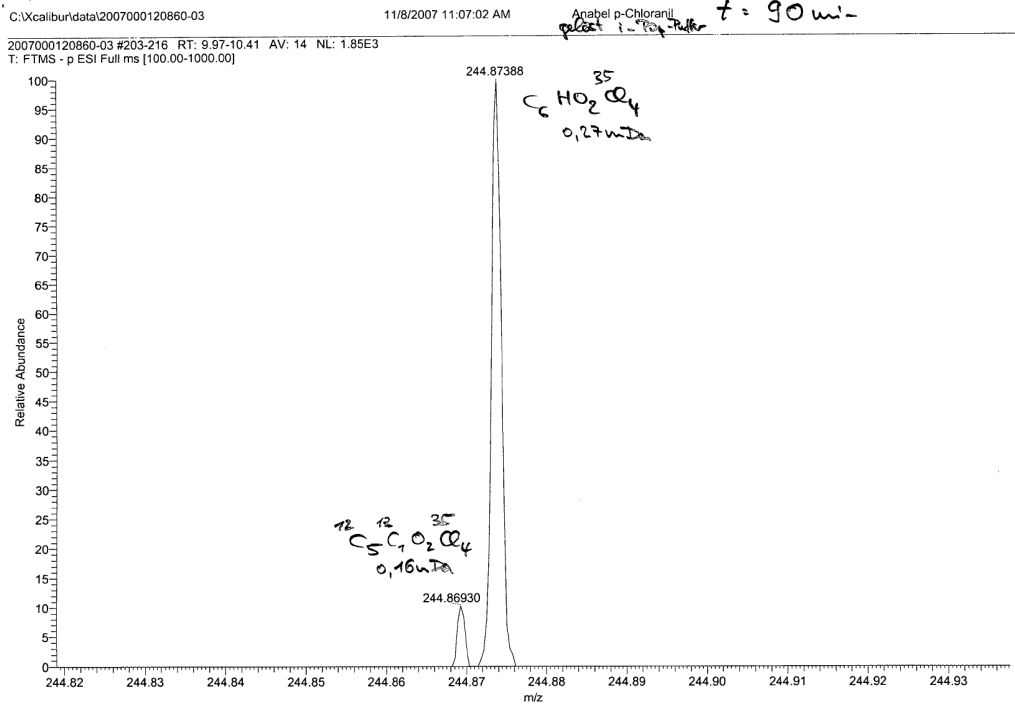
Appendix: Results from *p*-Chloranil studies



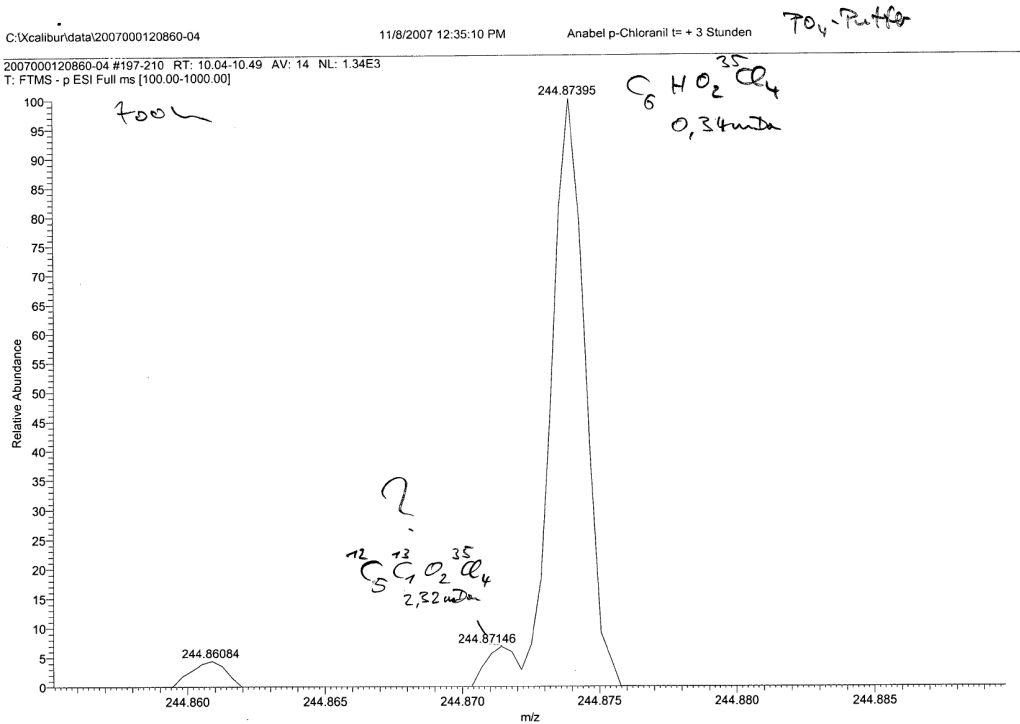
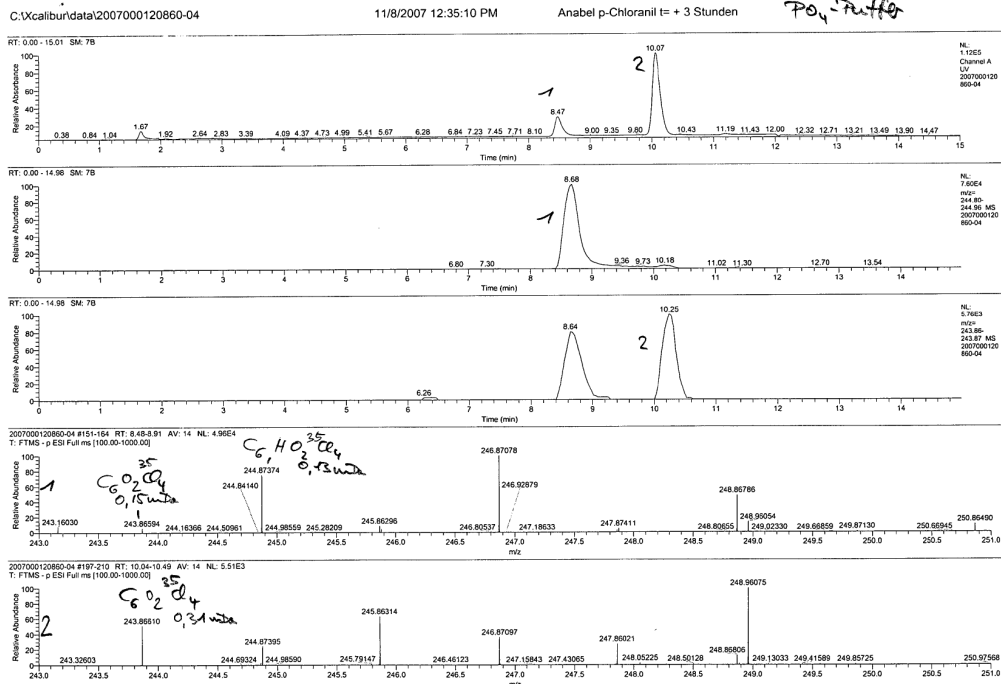
Appendix: Results from p-Chloranil studies



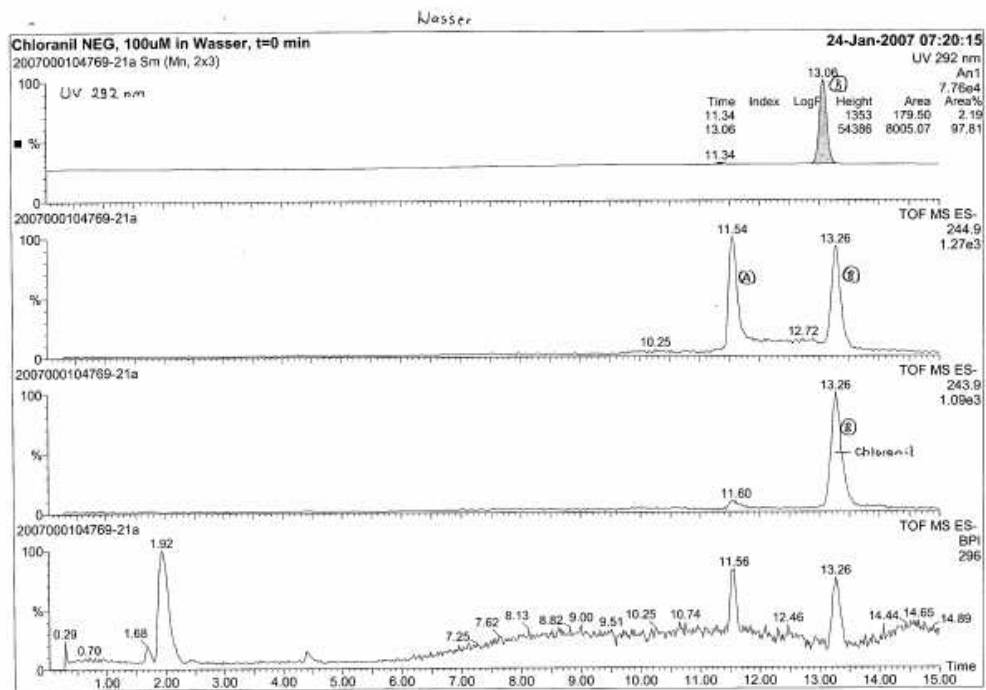
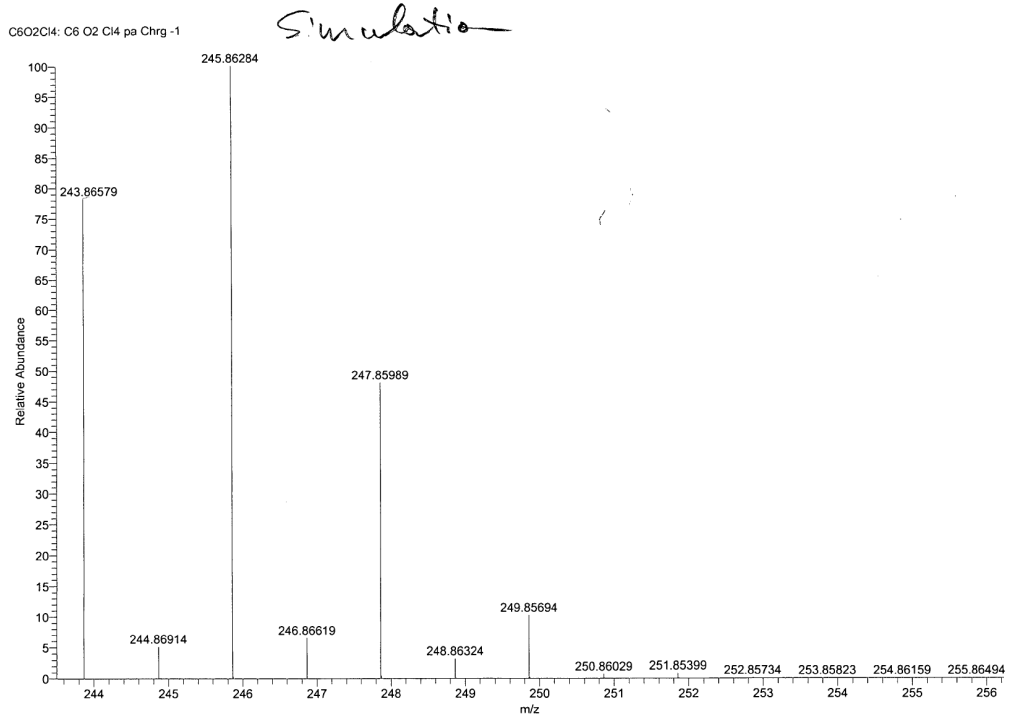
Appendix: Results from *p*-Chloranil studies



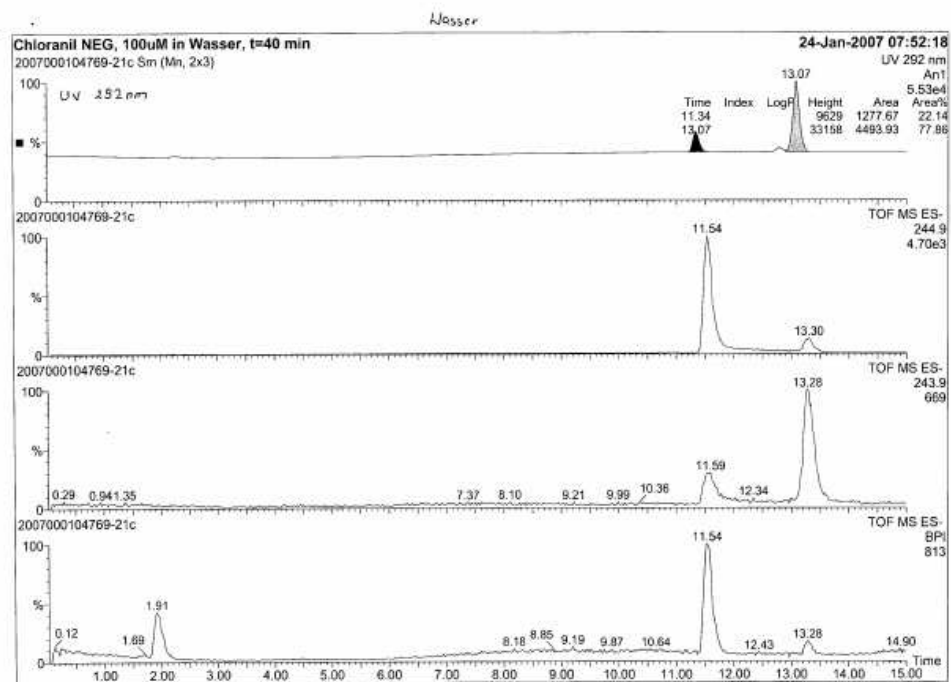
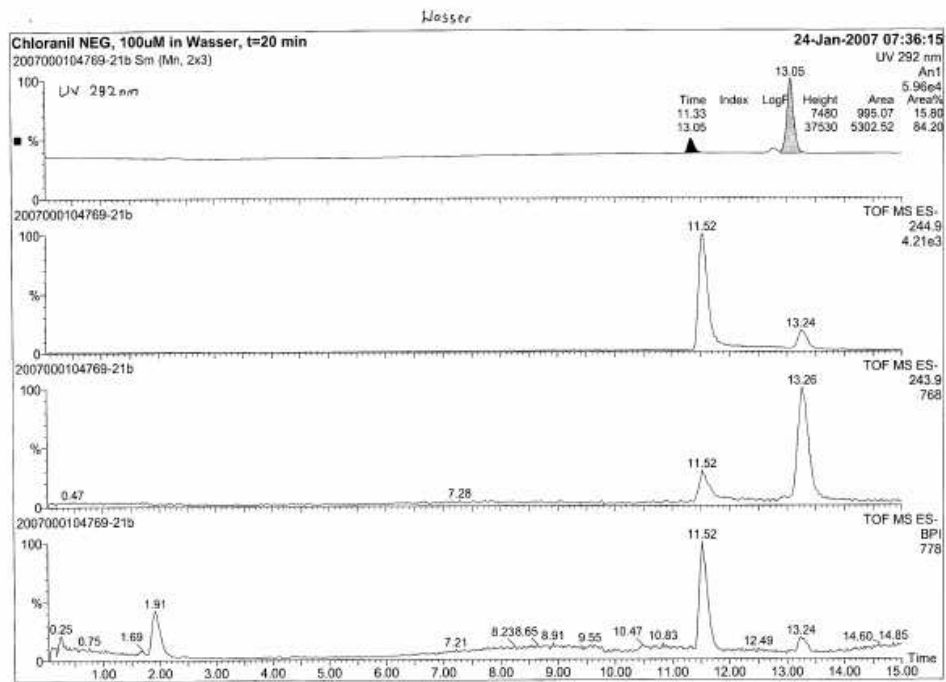
Appendix: Results from *p*-Chloranil studies



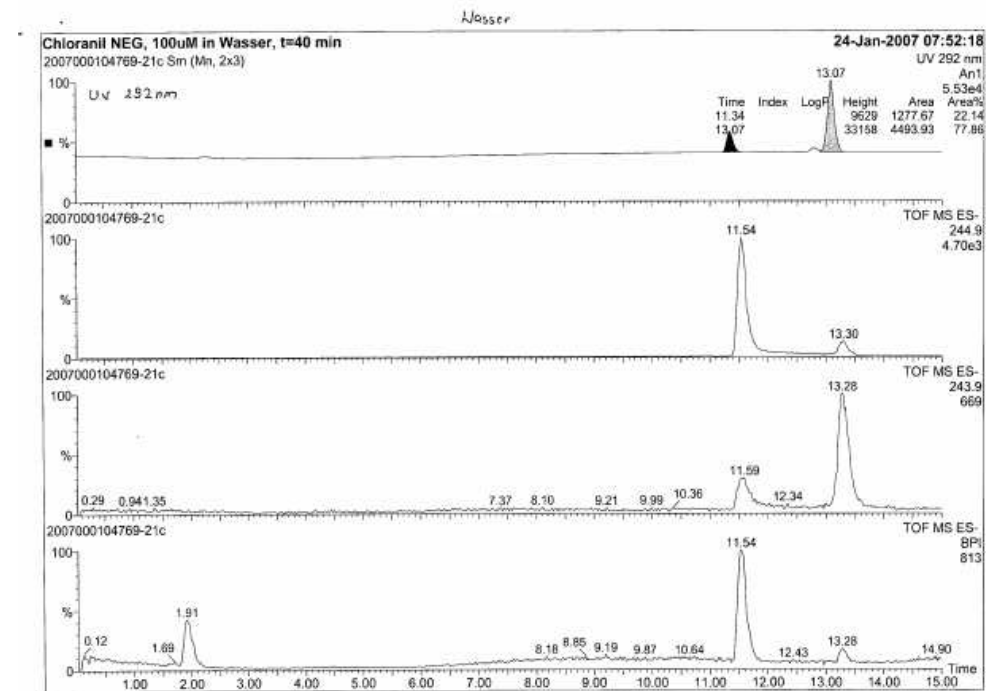
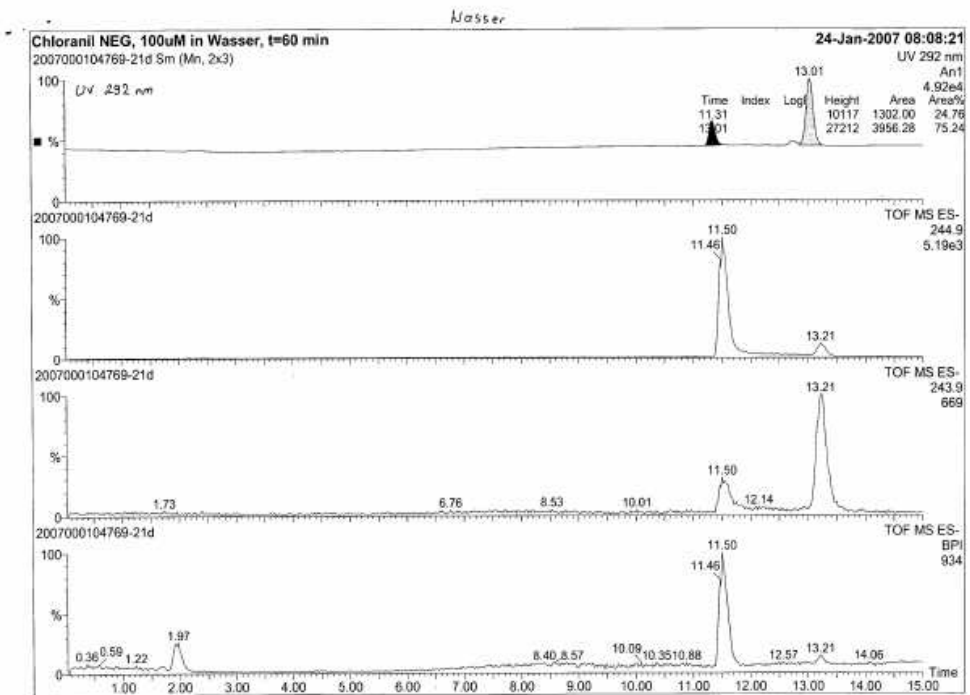
Appendix: Results from *p*-Chloranil studies



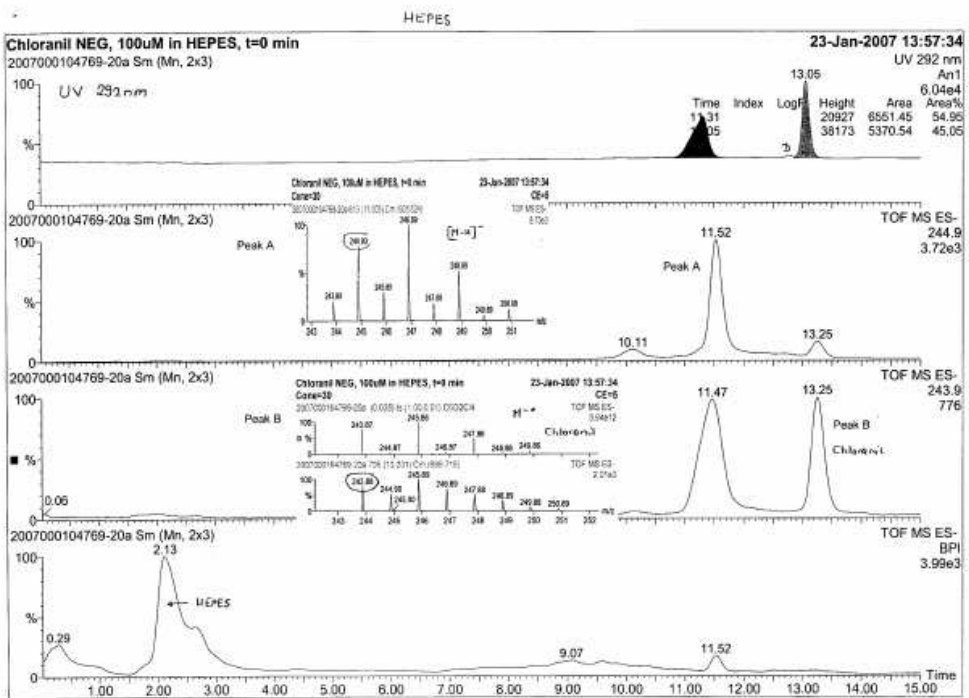
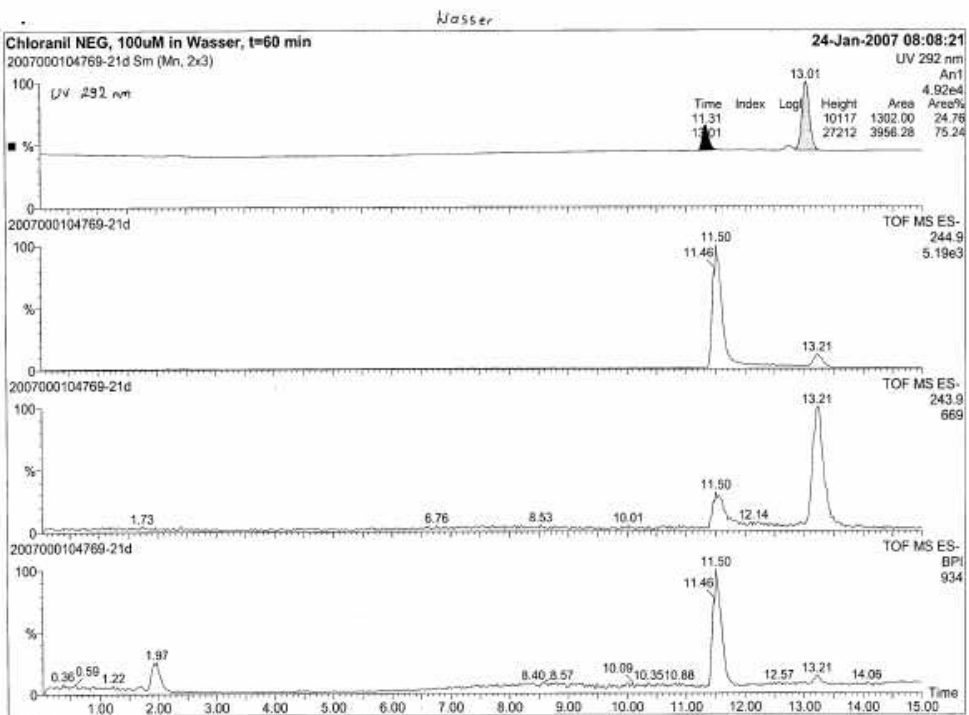
Appendix: Results from *p*-Chloranil studies



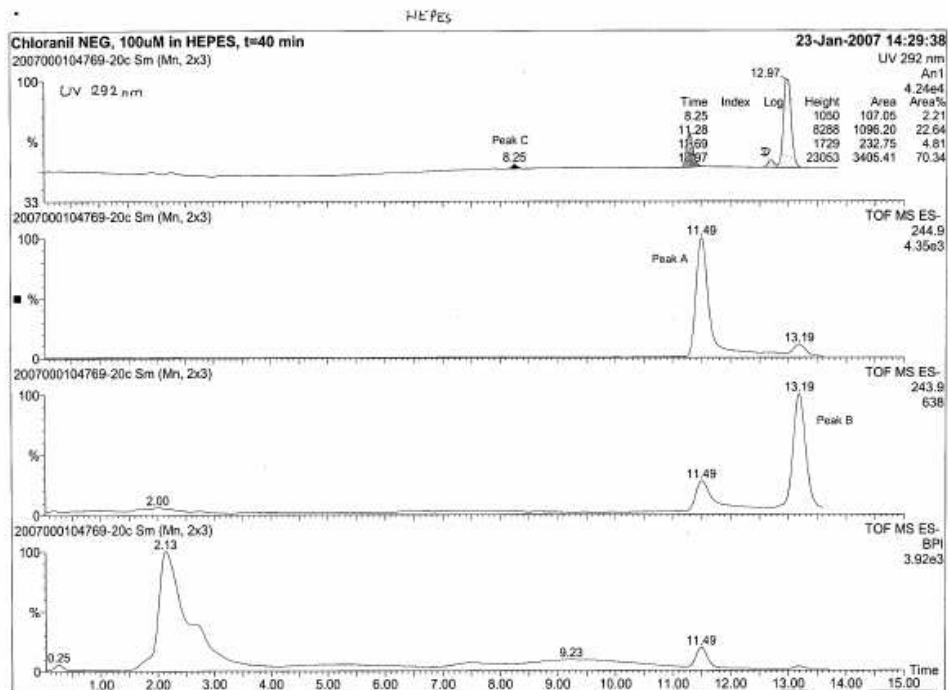
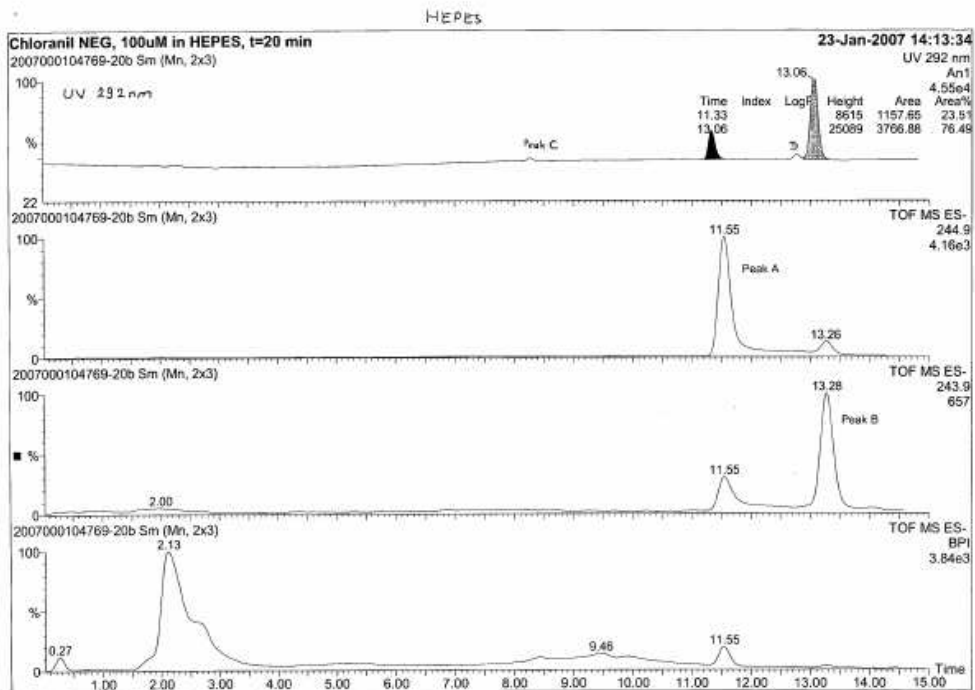
Appendix: Results from *p*-Chloranil studies



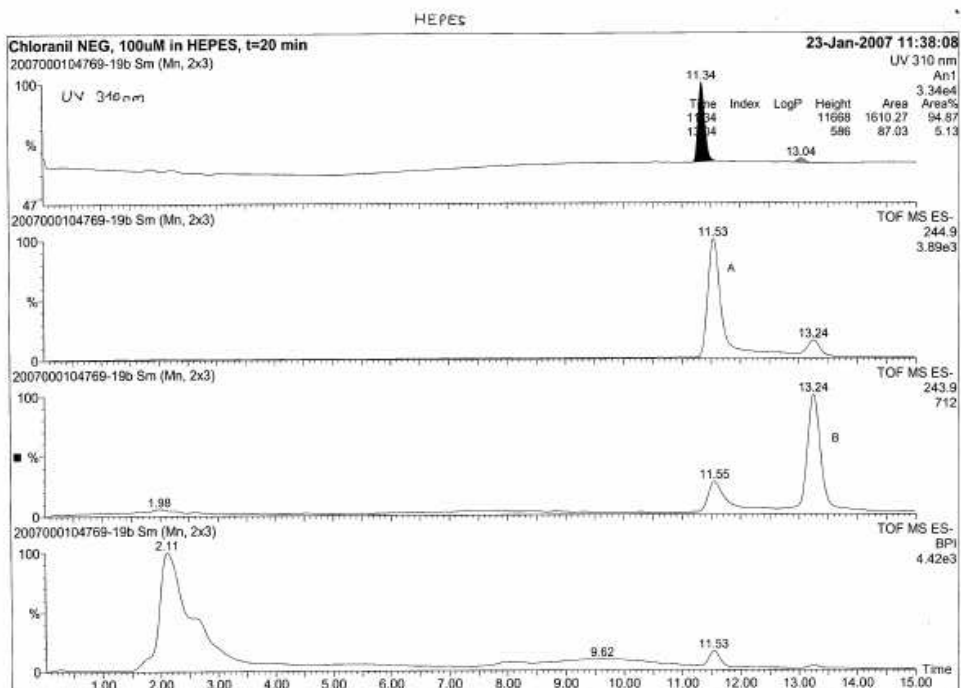
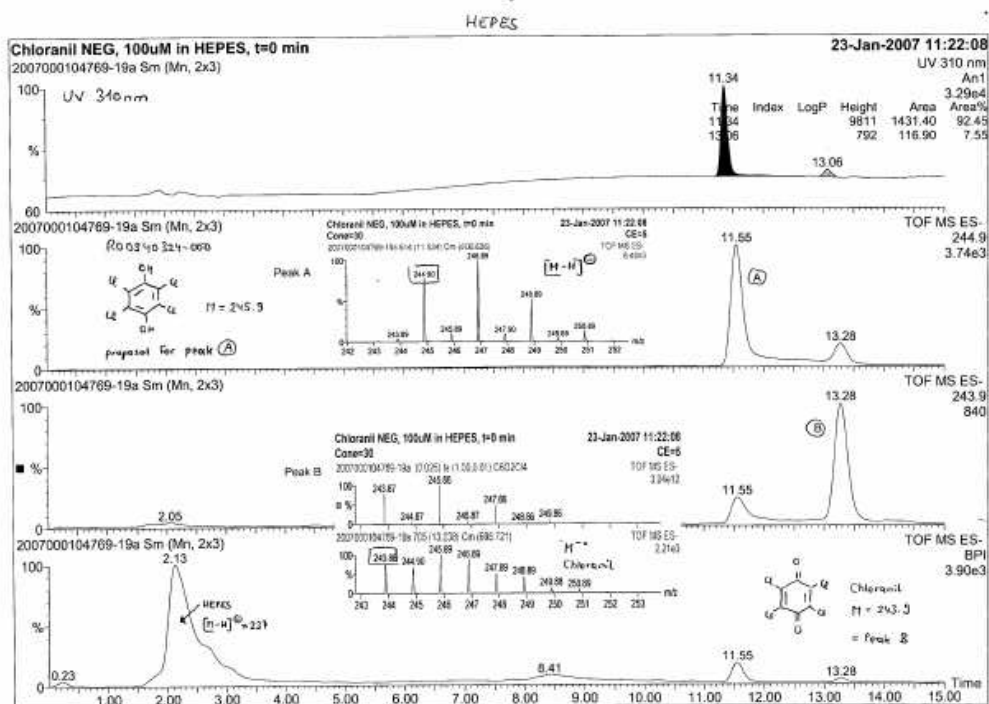
Appendix: Results from *p*-Chloranil studies



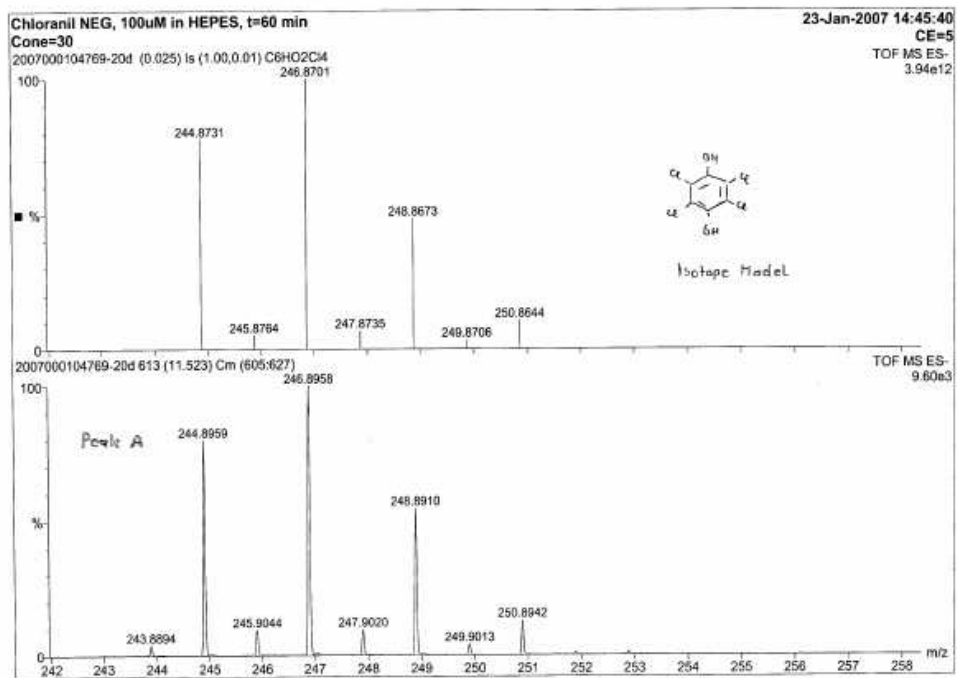
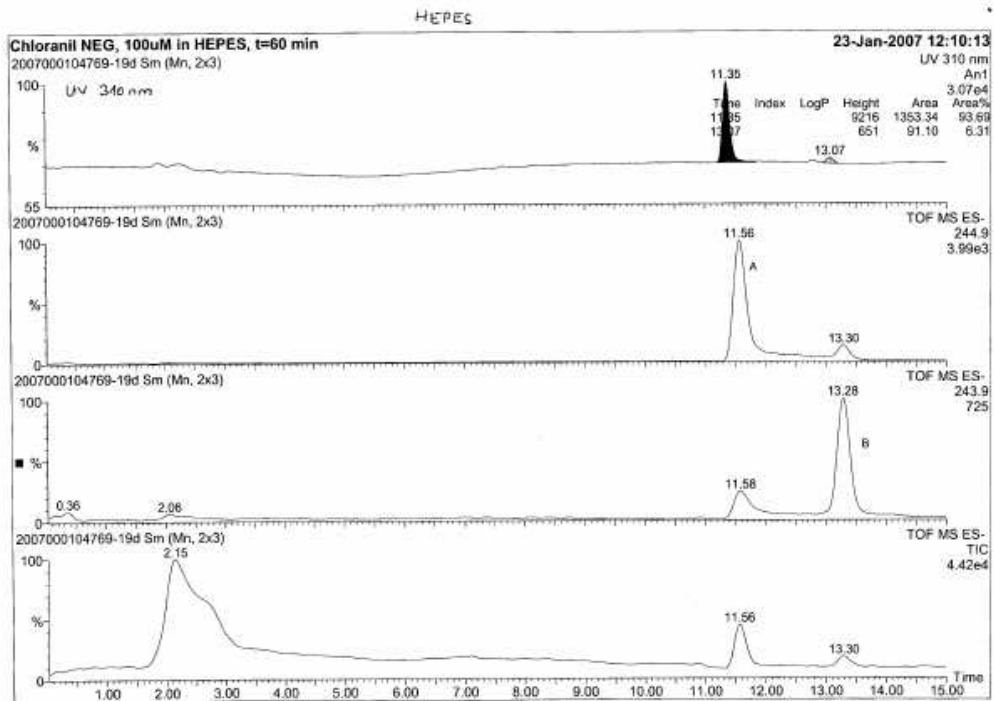
Appendix: Results from *p*-Chloranil studies



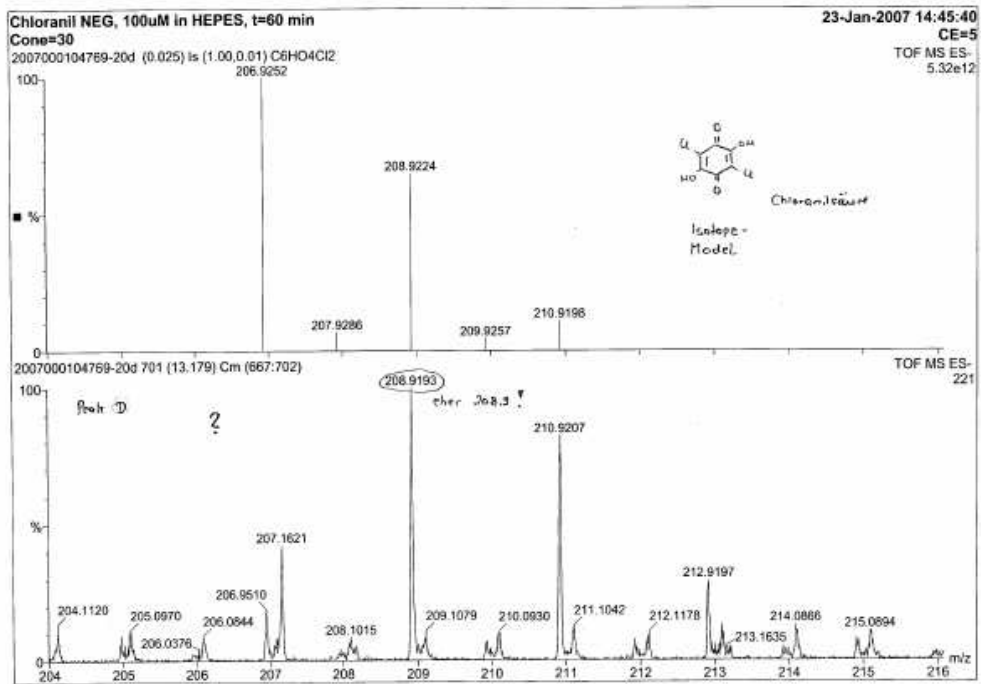
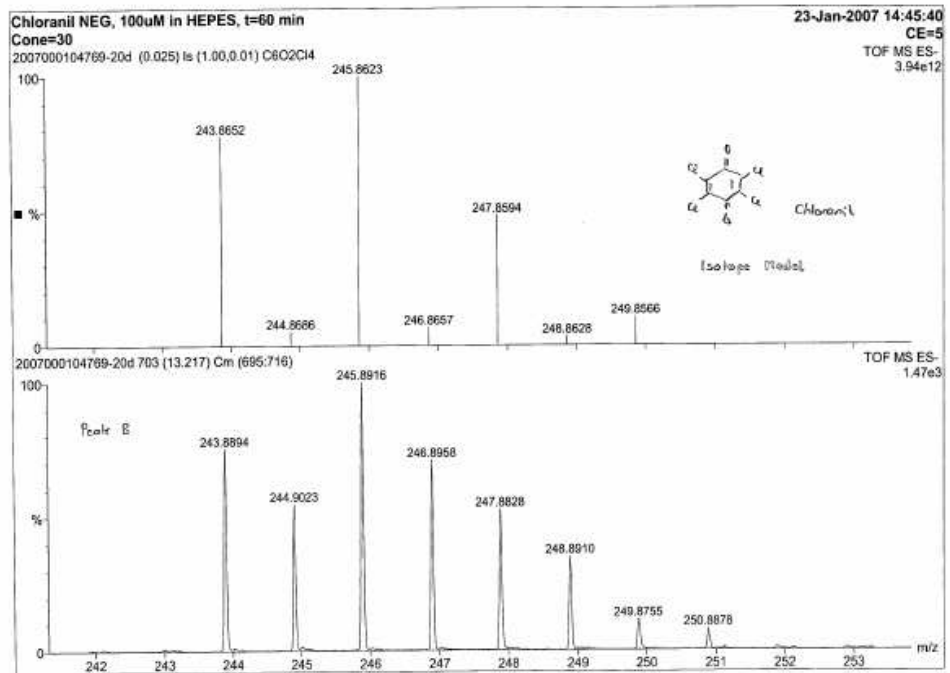
Appendix: Results from *p*-Chloranil studies



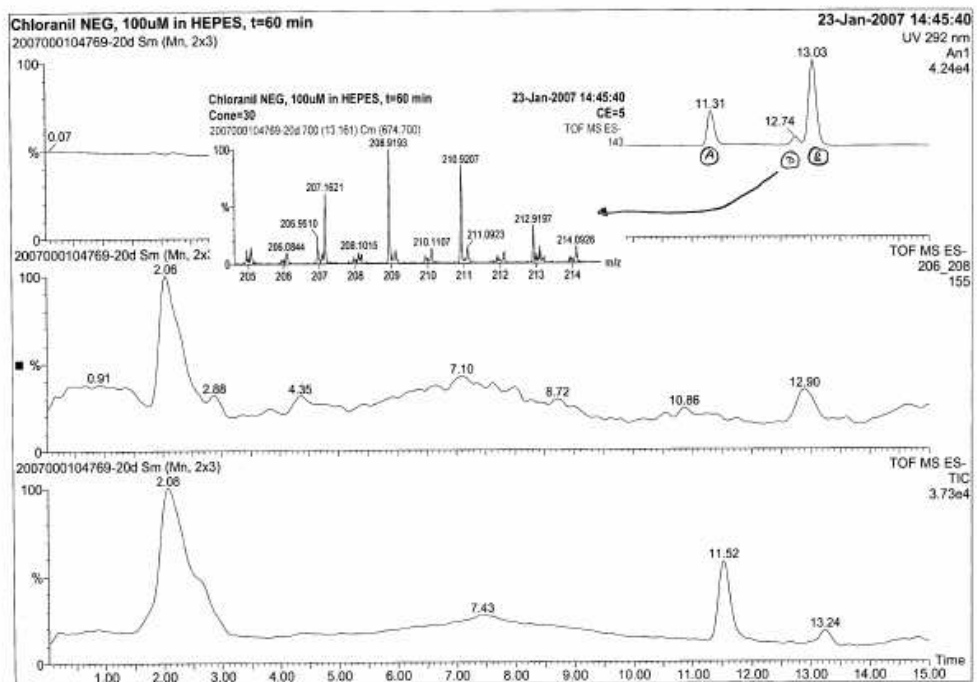
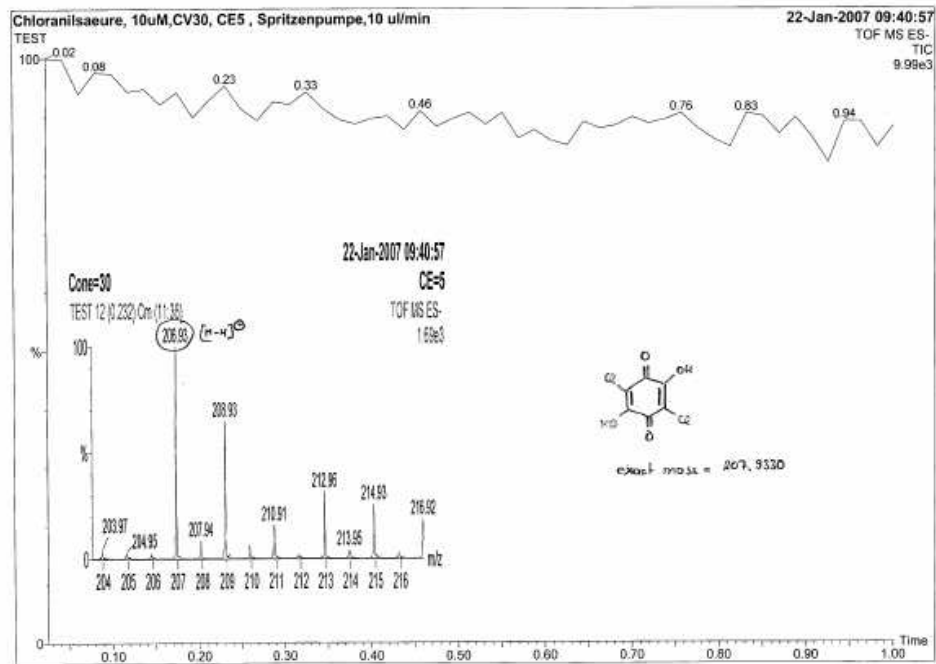
Appendix: Results from *p*-Chloranil studies



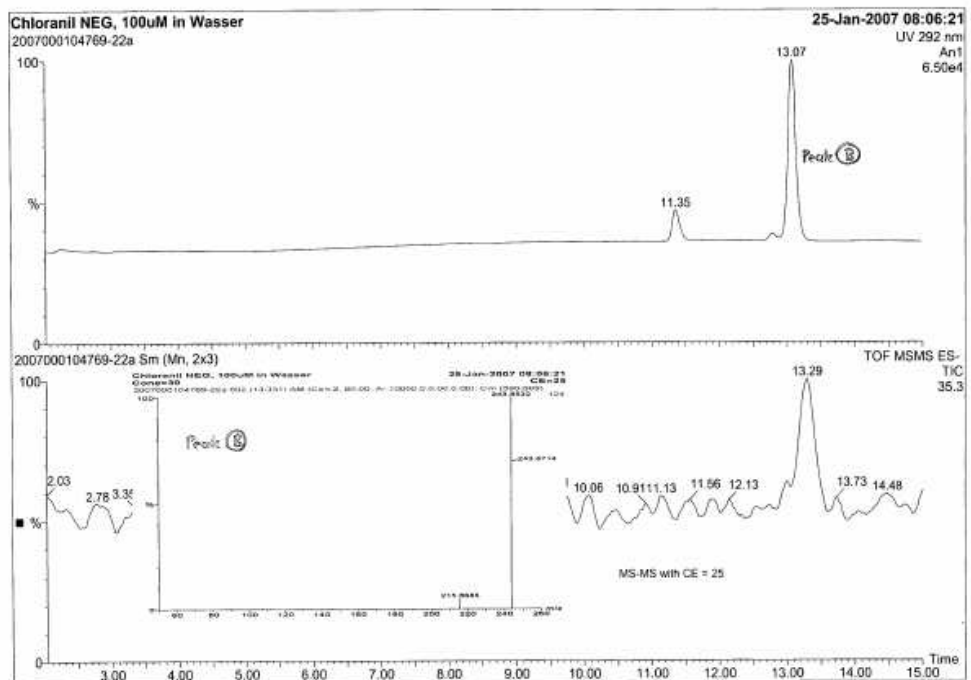
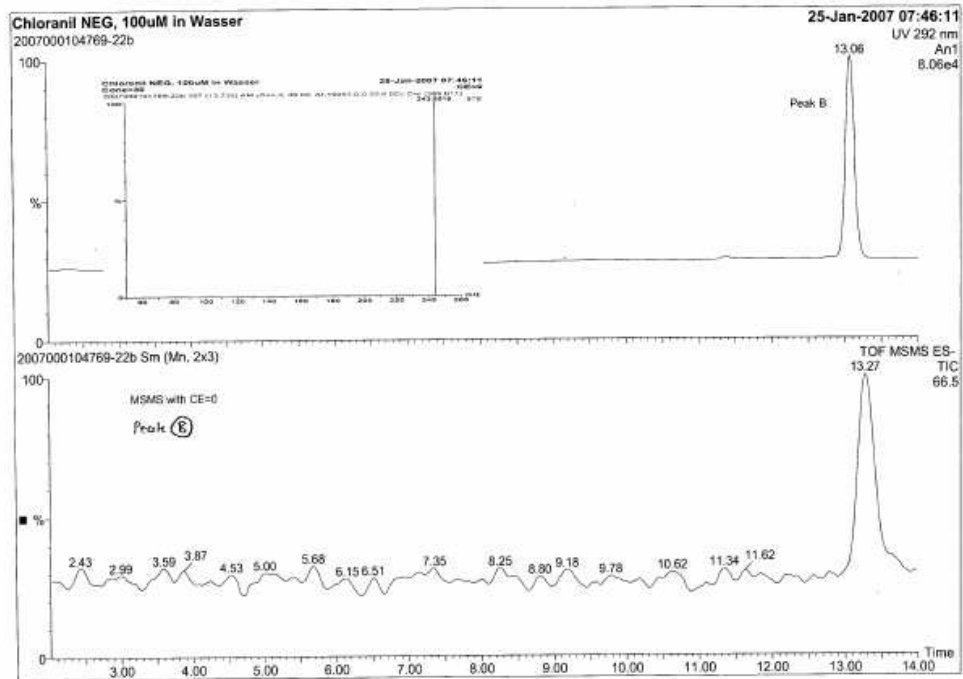
Appendix: Results from *p*-Chloranil studies



Appendix: Results from *p*-Chloranil studies



Appendix: Results from *p*-Chloranil studies



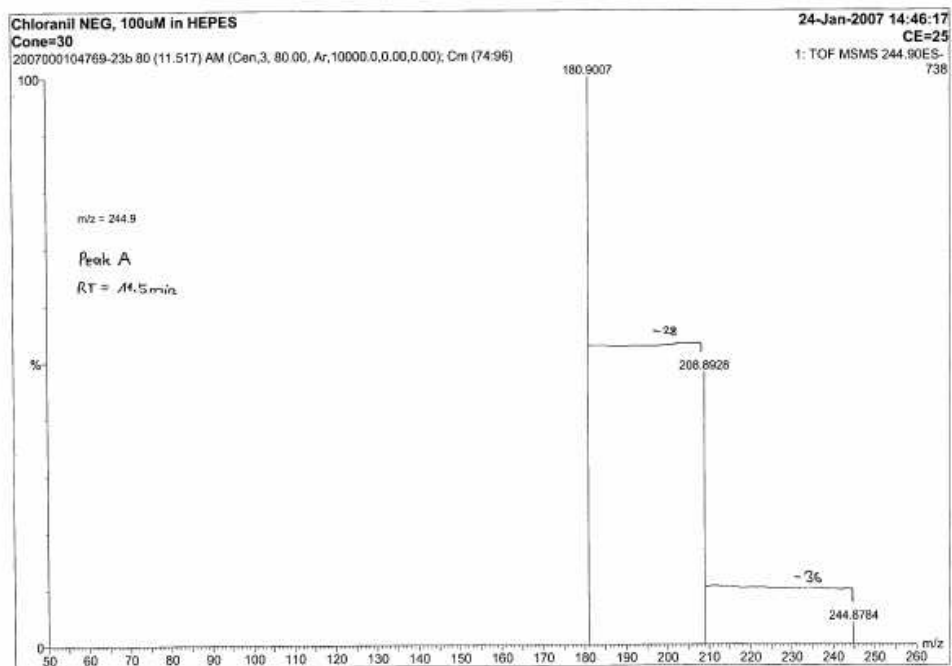


Table A: Structure-Activity Relationships of literature data related to their E_{ox}

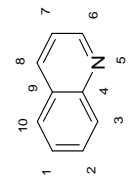
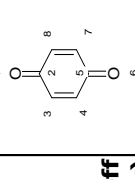
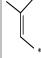
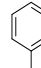
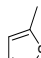
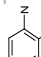
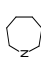

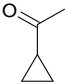

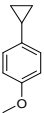
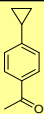
SUBSTITUENT EFFECTS	QUINOLINES	QUINONES	Coeff (Eox)		MORPHOLINES	PIPERIDINES	Coeff (Eox)	Coeff (Eox)
literature data								
	* —	* —N>	-0.216	* —Cl	* —	* —	-0.407	0.365
	[1*]C	[3*]N>C1	[7*]Cl	[1*]C	[1*]C	[1*]C	[1*]C	
Frag_Belstein_Search	* —	* —Cl	-0.146	* —Br	* —NH ₂	* —	0.617	0.331
	[3*]C	[3*]Cl	[7*]Br	[1*]N	[1*]N	[1*]C	[1*]C	
	* —NH ₂	* —Br	0.013	* —		* —OH	-0.407	-0.674
	[3*]N	[3*]Br	[7*]C	[7*]C	[1*]C=C(O)	[1*]O	[1*]O	
	* —OH		0.422	* —Cl		* —Cl	0.197	-0.040
	[3*]O	[3*]c1cccc1	[8*]Cl	[8*]Cl	[1*]c1cccc	[1*]Cl	[1*]Cl	
	* —	* —	0.384	* —Br		* —S>		0.207
	[6*]C	[3*]C	[8*]Br	[8*]Br		[1*]S	[1*]S	
	* —	* —Cl	-0.178	* —			[1*]c1ccc(N)c(C)c1	-0.272
	[8*]C	[4*]Cl	[8*]C	[8*]C			[1*]NCCCCC1	-0.053
	* —C(=O)O	* —Br	[8*]Br	* —NH ₂				
	[8*]C(=O)O	[4*]Br	[8*]N	[8*]N				
		* —	0.013					-0.080
		[4*]C	[4*]C			[2*]C	[2*]C	
		* —NH ₂	-0.178					
		[4*]N	[4*]N					
		* —N>	-0.177					0.216
		[7*]N>C1	[8*]C					
			-0.035					-0.080

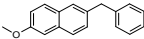
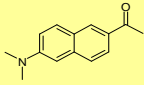
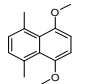
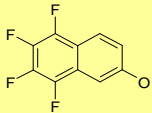
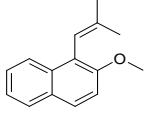
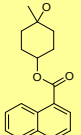
Table B: Fragment-Table [69, 84, 119-192]

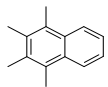
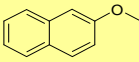
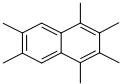
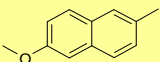
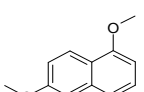
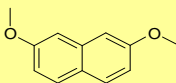
Chemical Name	MW	MF	Structure	E [V]	conditions
index					
» P : polarography » V : voltammetry » CV : cyclic voltammetry » RE : reference electrode » WE : working electrode » AE : auxiliary electrode					
DIBENZO-AZEPINE-DERIVATIVES					
dibenzoylcycloheptene	206.2	C ₁₅ H ₁₀ O		solvent: DMF E _{1/2} (1): -1.52 E _{1/2} (2): -1.96	» P » WE: not described » AE: not described » RE: SCE
5-methylene-5H-dibenzo[a,d]cycloheptene	204.3	C ₁₆ H ₁₂		solvent: ACN E _{1/2} : -2.26 solvent: DMF E _{1/2} : -2.24	» CV » WE: Pt-wire » AE: Pt- wire » RE: NHE
iminodibenzyl	195.3	C ₁₄ H ₁₃ N		E _{ox} : -1.057	» <i>method not very well described</i>
iminostilbene 5H-dibenzo[b,f]azepine	193.3	C ₁₄ H ₁₁ N		solvent: DMSO E _{1/2} : 0.27	» CV ISTD: Ferrocene » WE: Pt-wire » AE: Pt- wire » RE: Ag/AgCl
carbamazepin Tegretol	236.3	C ₁₅ H ₁₂ N ₂ O		solvent: ACN E _p : -2.27	» CV » WE: glassy carbon » RE: Ag/AgCl wire » AE: Pt-wire
iminodibenzyl-5-carbonyl chloride Intermediate of Carbamazepin	257.7	C ₁₅ H ₁₂ ClNO		solvent: ACN E _{1/2} (1): -1.91 E _{1/2} (2): -2.23 solvent: - E _p : -1.955 -2.275	» direct current P/ CV » WE: dropping Hg » AE: Pt- wire » RE: GKE (?) » CV
CYCLOPROPAN - DERIVATIVES					
cyclopropane	42.1	C ₃ H ₆		solvent: ACN E _{1/2} : 3.41	» CV » WE: Pt-wire » AE: Pt- wire » RE: Ag/AgCl
cirazepam benzodiazepincyclopropyl methylamine	339.8	C ₁₉ H ₁₈ ClN ₃ O		solvent: BR-Buffer	» coulometry » WE: stirred Mercury » AE: Graphit in sat KCl » RE: Ag/AgCl
methylcyclopropene	54.1	C ₄ H ₆		solvent: DMF E _{ox} : 2.41	» <i>Not very much information on the electrochemic method !</i>

Appendix: Tables

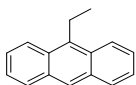
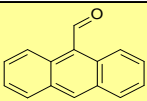
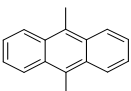
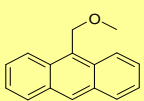
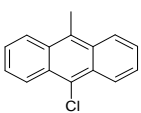
dicyclopopylmethanone	110.2	C ₇ H ₁₀ O		solvent: DMF E _{red} : -3.188	» CV » WE: GCE » AE: Pt-wire coil » RE: Ag/AgCl
1-cyclopropyl-ethanone	84.12	C ₅ H ₈ O		solvent: DMF E _{red} : -3.215	» CV » WE: GCE » AE: Pt-wire coil » RE: Ag/AgCl
1,1-dimethyl-cyclopropane	70.13	C ₅ H ₁₀		solvent: ACN E _{ox} : 2.5	» preparative electrolysis <i>the electrode material has not been described</i>
4-cyclopropylanisole	148.2	C ₁₀ H ₁₂ O		solvent: ACN E _{ox} : 1.42	» CV » WE: Au » AE: Pt-wire » RE: SCE
NOTE! Irreversible Cyclic Voltamograms					
1-(4-cyclopropyl-phenyl)-ethanone	160.22	C ₁₁ H ₁₂ O		solvent: ACN E° : -2.48	» CV » WE: Au » AE: Pt-wire » RE: Ag/AgCl

NAPHTHALENE -DERIVATIVES

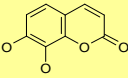
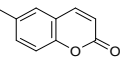
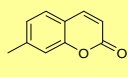
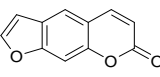
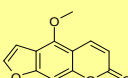
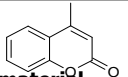
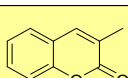
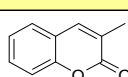
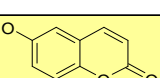
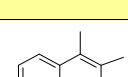
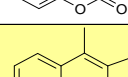
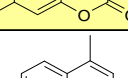
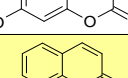
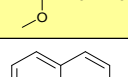
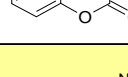
2-benzyl-6-methoxy - naphthalene	248.32	C ₁₈ H ₁₆ O		solvent: ACN E _p /SCE: 1.42	» CV » WE: Pt-blead » AE: Pt-wire coil » RE: Ag/AgCl
6-acetyl-2-dimethylamino naphthalene PRODAN	213.28	C ₁₄ H ₁₅ NO		solvent: ACN E _{ox} : ~ 0.7	» CV ISTD: Ferrocene » WE: Pt-disk » AE: Pt-wire » RE: aq.SCE
1,4-dimethoxy-5,6-dimethylnaphthalene	216.28	C ₁₄ H ₁₆ O ₂		solvent: CH₂Cl₂ E _{ox} : 0.4	» CV ISTD: Ferrocene » WE: glassy carbon » AE: Pt-plate » RE: Ag/AgCl
5,6,7,8-tetrafluonaphth-2-ol	216.13	C ₁₀ H ₄ F ₄ O		solvent: ACN E _{ox} : 1.84	» CV » WE: no info » AE: no info » RE: Ag/AgCl
2-methoxy-1-(2-methyl-1-propenyl)naphthalene	212.29	C ₁₅ H ₁₆ O		solvent: ACN E ^{ox} _{1/2} : 0.9	» Photoanionation
naphthalene-1-carboxylic acid 4-hydroxy-methyl-cyclohexyl ester <i>S.55 Report Fragments_I</i>	284.35	C ₁₈ H ₂₀ O ₃		solvent: ACN E ^{ox} _{1/2} : -1.91	» CV ISTD: Ferrocene » WE: glassy carbon » AE: Pt-plate » RE: Ag/AgCl

1,2,3,4-tetramethyl-naphthalene	184.28	C ₁₄ H ₁₆		solvent: DMSO E _{ox} : 1.55	» CV » WE: Pt-wire » AE: Pt-gauze » RE: SCE
methoxynaphthalene	158.2	C ₁₁ H ₁₀ O		solvent: ACN E _{ox} : 1.41	» CV » WE: Pt-wire » AE: Pt-gauze » RE: Ag/AgCl
1,2,3,4,6,7-hexamethyl-naphthalene	212.33	C ₁₆ H ₂₀			Article is in Russian
2-methoxy-6-methyl-naphthalene	172.23	C ₁₂ H ₁₂ O		solvent: ACN E _p /SCE: 1.41	» CV » WE: Pt-blead » AE: Pt-wire coil » RE: Ag/AgCl
1,6-dimethoxynaphthalene	188.2	C ₁₂ H ₁₂ O ₂		solvent: ACN E _{1/2} (ox): 1.28 E _{1/2} (red): -2.68	» P » WE: dropping Hg (red.) » WE: rotating Pt (oxd.) » RE: SCE
2,7-dimethoxy-naphthalene	188.2	C ₁₂ H ₁₂ O ₂		solvent: ACN E _{1/2} (ox): 1.47 E _{1/2} (red): -2.68	» P » WE: dropping Hg » WE: rotating Pt (oxd.) » RE: SCE

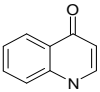
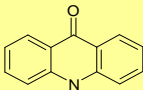
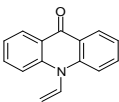
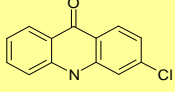
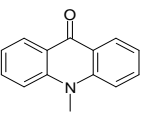
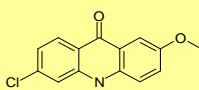
ANTHRACENE-DERIVATIVES *

9-ethyl-anthracene	206.29	C ₁₆ H ₁₄		solvent: ACN E ^o _{ox} : 1.14	» CV ISTD: Ferrocene » WE: Pt-disk » AE: Pt-wire » RE: aq.Ag/AgCl
anthracene-9-carbaldehyde	206.2	C ₁₅ H ₁₀ O		solvent: ACN E ^o ₀ : -1.462	» CV ISTD: Ferrocene » WE: Pt-disk » AE: Pt-wire » RE: aq.Ag/AgCl
9,10-dimethyl-anthracene	206.29	C ₁₆ H ₁₄		solvent: CHCl₃ E ^o _{ox} : 1.16	» CV ISTD: Ferrocene » WE: Pt-disk » AE: Pt-wire » RE: aq.Ag/AgCl
9-methoxymethyl-anthracene	222.29	C ₁₆ H ₁₄ O		solvent: DMSO E _{ox} (A ⁻): -1.635 E _{red} (HA): -2.295	» CV ISTD: Ferrocene » WE: no information » AE: no information » RE: no information
9-chloro-10-methyl-anthracene	226.7	C ₁₅ H ₁₁ Cl		solvent: DMSO E _{ox} (A ⁻): -1.35 E _{red} (HA): -2.207	» CV ISTD: Ferrocene » WE: no information » AE: no information » RE: no information

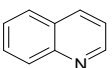
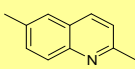
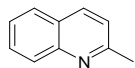
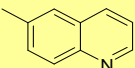
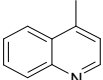
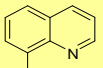
BENZOPYRANON-DERIVATIVES

6-methyl coumarines	160.2	C ₁₀ H ₈ O ₂		solvent: MeOH E _{1/2} : 1.63	» P <i>no further information on the electrode material</i>
5-methoxypsoralen	216.2	C ₁₂ H ₈ O ₄		solvent: H₂O E _{ox} : 1.63 irreversible oxidation	» CV <i>no further information on the electrode material</i>
7-methyl-coumarin	160.2	C ₁₀ H ₈ O ₂		solvent: H₂O E _{ox} : 2.17 irreversible oxidation	» CV <i>no further information on the electrode material</i>
psoralen	186.2	C ₁₁ H ₆ O ₃		solvent: H₂O E _{ox} : 1.89	» CV <i>no further information on the electrode material</i>
7,8-dihydroxy-coumarin	178.1	C ₉ H ₆ O ₄		E _{1/2} : -1.8 pH-dependency	» P <i>no further information on the electrode material</i>
4-methyl-coumarin	160.2	C ₁₀ H ₈ O ₂		E _{1/2} : -1.64	» P <i>no further information on the electrode material</i>
Note! No information concerning solvents or electrode material!					
3-methyl-coumarin	160.2	C ₁₀ H ₈ O ₂		E _{1/2} : -1.68	» P <i>no further information on the electrode material</i>
7-hydroxycoumarin (Umbelliferone)	162.1	C ₉ H ₆ O ₃		E _{1/2} : -1.67	» P <i>no further information on the electrode material</i>
6-hydroxycoumarin	162.1	C ₉ H ₆ O ₃		E _{1/2} : -1.56	» P <i>no further information on the electrode material</i>
3,4-dimethylcoumarin	174.2	C ₁₁ H ₁₀ O ₂		E _{1/2} : -1.73	» P <i>no further information on the electrode material</i>
3,4,7-trimethyl-coumarin	188.2	C ₁₂ H ₁₂ O ₂		E _{1/2} : -1.81	» P <i>no further information on the electrode material</i>
7-hydroxy-4-methyl-coumarin	176.2	C ₁₀ H ₈ O ₃		E _{1/2} : -1.82	» P <i>no further information on the electrode material</i>
8-methoxy coumarin	176.2	C ₁₀ H ₈ O ₃		E _{1/2} : -1.56	» P <i>no further information on the electrode material</i>
coumarin	146.2	C ₉ H ₆ O ₂		E _{1/2} : -1.53	» P <i>no further information on the electrode material</i>
7-aminocoumarin	161.2	C ₉ H ₇ NO ₂		solvent: ethanolic buffer solution E _{1/2} : -1.052	» P » WE: dropping Hg » AE: mercury » RE: SCE

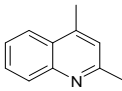
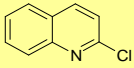
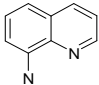
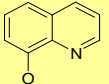
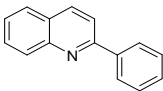
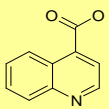
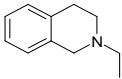
QUINOLINONE

4-quinolinol	145.16	C ₉ H ₇ NO			
9-acridone	195.22	C ₁₃ H ₉ NO		solvent: DMF E _p ^{red} : -2.25	» P » WE: dropping Hg » AE: Pt » RE: SCE
10-vinyl-10H-acridin-9-one	221.26	C ₁₅ H ₁₁ NO		solvent: DMF E _p ^{red} : -2.2	» P » WE: dropping Hg » AE: Pt » RE: SCE
3-chloro-10H-acridin-9-one	229.67	C ₁₃ H ₈ ClNO		solvent: DMF E _p ^{red} : -1.9	» P » WE: dropping Hg » AE: Pt » RE: SCE
10-methyl-10H-acridino-9-one	209.25	C ₁₄ H ₁₁ NO		solvent: ACN E _p ^{ox} : 1.47	» CV » WE: Pt » AE: Pt » RE: SCE
6-chloro-2-methoxy-10H-acridin-9-one	259.69	C ₁₄ H ₁₀ ClNO ₂		solvent: DMF E _p ^{red} : -1.7	» P » WE: dropping Hg » AE: Pt » RE: SCE

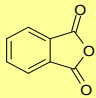
QUINOLINE

quinoline	129.2	C ₉ H ₇ N		solvent: DMF E _{1/2} ^{red} : - 2.18	» P » WE: dropping Hg » AE: Pt » RE: Ag/AgCl
2,6-dimethyl-quinoline	157.21	C ₁₁ H ₁₁ N		solvent: DMF E _{1/2} ^{red} : - 2.31	» P » WE: dropping Hg » AE: Pt » RE: Ag/AgCl
2-methyl-quinoline	143.19	C ₁₀ H ₉ N		solvent: DMF E _{1/2} ^{red} : - 2.2	» P » WE: dropping Hg » AE: Pt » RE: Ag/AgCl
6-methyl-quinoline	143.19	C ₁₀ H ₉ N		solvent: DMF E _{1/2} ^{red} : - 2.19	» P » WE: dropping Hg » AE: Pt » RE: Ag/AgCl
4-methyl-quinoline	143.19	C ₁₀ H ₉ N		solvent: DMF E _{1/2} ^{red} : - 2.25	» P » WE: dropping Hg » AE: Pt » RE: Ag/AgCl
8-methyl-quinoline	143.19	C ₁₀ H ₉ N		solvent: DMF E _{1/2} ^{red} : - 2.22	» P » WE: dropping Hg » AE: Pt » RE: Ag/AgCl

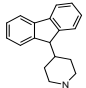
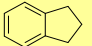

Appendix: Tables

2,4-dimethyl-quinoline	157.21	C ₁₁ H ₁₁ N		solvent: DMF E _{1/2} ^{red} : - 2.82	» P » WE: dropping Hg » AE: Pt » RE: Ag/AgCl
2-chloro-quinoline	163.61	C ₉ H ₆ ClN			» CV » WE: dropping Hg » AE: - » RE: SCE
NOTE! Irreversible reaction					
8-aminoquinoline	144.18	C ₉ H ₈ N ₂		solvent: BR E _{1/2} ^{red} : 1.38	» P » WE: dropping Hg » AE: Pt » RE: SCE
8-hydroxyquinoline	145.16	C ₉ H ₇ N ₀		solvent: BR E _{1/2} ^{red} : 1.28	» P » WE: dropping Hg » AE: Pt » RE: SCE
2-phenyl-quinoline	205.3	C ₁₅ H ₁₁ N		solvent: ACN E _{1/2} ^{red} : -	» CV » WE: Pt-disk » AE: Pt-wire » RE: Ag-wire
quinoline-4-carboxylic acid	173.2	C ₁₀ H ₇ NO ₂		solvent: buffer E _{1/2} ^{red} : 0.795	» P » WE: dropping Hg » AE: Pt » RE: SCE
isoquinoline	161.3	C ₁₁ H ₁₅ N		solvent: ACN E _{1/2} : 1.21	» CV » WE: Pt » RE: Ag/AgCl » AE: Pt

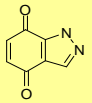
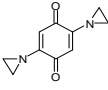
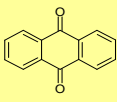
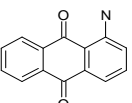
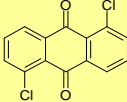
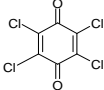
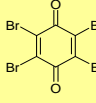
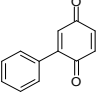
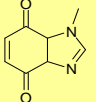
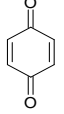
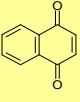
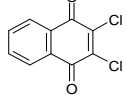
ISOBENZOFURAN

isobenzofuran-1,3-dione	148.12	C ₈ H ₄ O ₃		solvent: ACN E _{1/2} : -2.05	» P » WE: dropping Hg » AE: - » RE: SCE
--------------------------------	--------	--	---	---	---

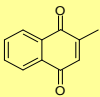
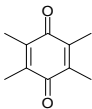
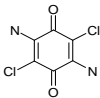
CYCLOPENTAN

1-fluoren-9-yl-piperidine	249.4	C ₁₈ H ₁₉ N		solvent: Me₂SO E _{1/2} : -0.518	
indan-1-one	132.2	C ₉ H ₈ O		solvent: DMF E _{1/2} ^{ox} : 1.97	» CV » WE: Pt » RE: SCE » AE: Pt
cyclopentan	70.1	C ₅ H ₁₀		solvent: fluoro sulphonic acid E _{1/2} : 2.0	» P » WE: Pt » RE: SCE » AE: Pt

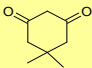
QUINONES/QUINONE-DERIVATIVES

1H-indazole-4,7-dione	148.1	C ₇ H ₄ N ₂ O ₂		solvent: acetic acid E _{1/2} : 0.48	» Redox Titration
2,5-bis-aziridin-1-yl-[1,4]benzoquinone	190.2	C ₁₀ H ₁₀ N ₂ O ₂		solvent: MeOH E _{1/2} : -0.115	» P » WE: dropping Hg » RE: Ag/AgCl » AE: Pt-wire
anthraquinone	208.2	C ₁₄ H ₈ O ₂		solvent: ACN E ^{ox} _{1/2} : 0.9	» CV » WE: Au » RE: Ag/AgCl » AE: Pt
1-amino-anthraquinone	223.2	C ₁₄ H ₉ NO ₂		solvent: MeOH E ^{ox} _{1/2} : -0.24 V	» direct current P » WE: - » RE: - » AE: Pt-wire
1,5-dichloro-anthraquinone	277.1	C ₁₄ H ₆ Cl ₂ O ₂		solvent: CH₂Cl₂ E ^{ox} _{1/2} : -0.84	» CV » WE: Pt » RE: SCE » AE: Pt
p-chloranil	245.9	C ₆ Cl ₄ O ₂		solvent: ACN E _{1/2} : -0.33	» not described
				solvent: CH₂Cl₂ E _{1/2} : 0.24	» CV
p-bromanil	426.7	C ₆ Br ₄ O ₂		solvent: CH₂Cl₂ E ^{ox} _{1/2} : 0.03	» CV » WE: Pt » RE: SCE » AE: Pt
2-methyl-1,4-benzoquinone	184.2	C ₁₂ H ₈ O ₂		solvent: DMF E ^{ox} _{1/2} : 0.44 V	» CV » WE: Pt » RE: SCE » AE: Pt
1-methyl-1H-benzimidazole-4,5-dione	182.2	C ₈ H ₆ N ₂ O ₂		article only available in Russian	
1,4-benzoquinone	108.1	C ₆ H ₄ O ₂		solvent: ACN ΔE: 0.91	» CV
				solvent: DMF E _{1/2} : -0.39	» P
1,4-naphthoquinone	158.16	C ₁₀ H ₆ O ₂		solvent: ACN E ^{ox} _{1/2} : 0.459	» not described
				solvent: ACN E _{1/2} : -0.685	» P
2,3-dichloro-[1,4]naphthoquinone	227.1	C ₁₀ H ₄ Cl ₂ O ₂		solvent: DMF E ^{ox} _{1/2} : 0.53	» CV » WE: Pt » RE: SCE » AE: Pt

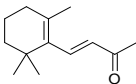
Appendix: Tables

menadione 2-methyl-1,4-naphthoquinone	172.18	C ₁₁ H ₈ O ₂		solvent: - E _{1/2} : -0.225	» P
				solvent: - E _{1/2} ^{pc1} : -0.277	» CV
2,3,5,6-tetramethyl- [1,4]benzoquinone	164.2	C ₁₀ H ₁₂ O ₂		solvent: benzo nitrile E _{1/2} ^{ox} : -0.9	» CV » WE: glassy carbon » RE: Ag/AgCl » AE: Pt-wire
2,3-dihydro-1H-indane	118.2	C ₉ H ₁₀		solvent: ACN E _{1/2} : 1.59	» P » WE: Pt » RE: Ag/AgCl » AE: Pt
2,5-diamino-3,6-dichloro- [1,4]benzoquinone	207.0	C ₆ H ₄ Cl ₂ N ₂ O ₂		solvent: ACN E _{1/2} ^{ox} : -0.72	» CV » WE: Pt » RE: SCE » AE: Pt-wire

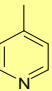
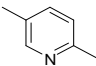
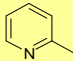
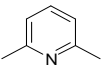
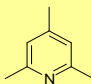
CYCLOHEXAN

5,5-dimethyl- cyclohexane-1,3-dione	140.18	C ₈ H ₁₂ O ₂		solvent: DMSO E _{ox} : -0.23	» P » WE: Pt » RE: Ag/AgCl » AE: Pt
--	--------	---	---	---	--

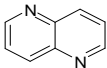
CYCLOHEXENE

	192.3	C ₁₃ H ₂₀ O		solvent: ACN E _{1/2} ^{red} : -1.89	» CV » WE: Pt-wire » AE: Pt-wire » RE: Ag-wire
--	-------	-----------------------------------	---	--	---

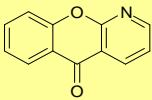
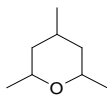
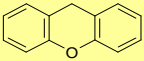
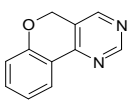
PYRIDINE-DERIVATIVES

4-methyl-pyridine	93.1	C ₆ H ₇ N		solvent: DMF E _{1/2} ^{red} : -2.76	» P » WE: dropping Hg » AE: Pt » RE: Ag/AgCl
2,5-dimethyl-pyridine	107.2	C ₇ H ₉ N		solvent: DMF E _{1/2} ^{red} : -2.82	» P » WE: dropping Hg » AE: Pt » RE: Ag/AgCl
2-methyl pyridine	93.1	C ₆ H ₇ N		solvent: DMF E _{1/2} ^{red} : -2.80	» P » WE: dropping Hg » AE: Pt » RE: Ag/AgCl
2,5-dimethyl-pyridine	107.2	C ₇ H ₉ N		solvent: DMF E _{1/2} ^{red} : -2.85	» P » WE: dropping Hg » AE: Pt » RE: Ag/AgCl
2,4,6-trimethyl-pyridine	121.2	C ₈ H ₁₁ N		solvent: DMF E _{1/2} ^{red} : -2.91	» P » WE: dropping Hg » AE: Pt » RE: Ag/AgCl

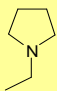
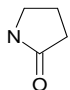
Appendix: Tables

[1,5] naphthyridine	130.2	C ₈ H ₆ N ₂		solvent: DMF E _{1/2} ^{red} : - 1.86	» P » WE: dropping Hg » AE: Pt » RE: Ag/AgCl
----------------------------	-------	--	---	---	--

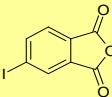
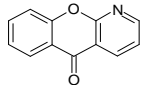
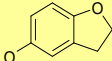
TETRAHYDROPYRAN

chromeno[2,3-b]pyridin-5-one	197.2	C ₁₂ H ₇ NO ₂		solvent: DMF E _{red} ⁰ : - 1.48	» CV » WE: glassy carbon » AE: Pt » RE: Ag/AgCl
2,4,6-trimethyl-tetrahydropyran	128.2	C ₈ H ₁₆ O		solvent: ACN E _{1/2} ^{ox} : - 1.48	» P » WE: Pt » AE: Pt » RE: Ag/AgCl or SCE
xanthene	182.2	C ₁₃ H ₁₀ O		solvent: DMSO E _{red} ⁰ : - 1.36V E _{ox} ⁰ : - 1.76V	» CV » WE: Pt-disk » AE: Pt-wire » RE: Ag/AgCl
5H-benzopyrano-[1][4,3-d]pyrimidine	184.2	C ₁₁ H ₈ N ₂ O		solvent: MeOH E _{1/2} : -1.15 pH: 1.39	» P » WE: dropping Hg » AE: Pt » RE: Ag/AgCl

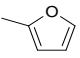
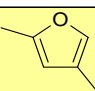
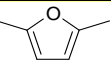
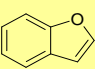
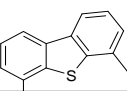
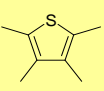
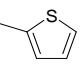
PYRROLIDINE

1-ethyl-pyrrolidine	99.2	C ₆ H ₁₃ N		solvent: ACN E _{1/2} ^{ox} : 1.08	» CV » WE: glassy carbon » RE: SCE » AE: Pt-coil
2-pyrrolidine	85.1	C ₄ H ₇ NO		solvent: DMSO E _{1/2} ^{ox} : 0.03	» CV » WE: Pt » RE: Ag/AgCl » AE: Pt

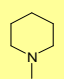
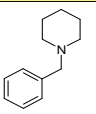
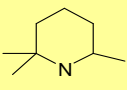
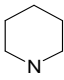
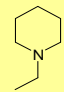
PYRAN

5-iodo-phthalic acid anhydride	274.0	C ₈ H ₃ IO ₃		solvent: buffer E _{1/2} : -1.34	» P » WE: dropping Hg » RE: SCE » AE: Pt
chromeno[2,3-b]pyridin-5-one	140.2	C ₈ H ₁₂ O ₂		solvent: ACN E _{RED} ⁰ : - 1.46	» CV » WE: glassy carbon » RE: Ag/AgCl » AE: Pt
2,3-dihydro-benzofuran-5-ol	136.2	C ₈ H ₈ O ₂		solvent: ACN E _{1/2} : 0.66	» CV » WE: glassy carbon » RE: SCE » AE: Pt-coil

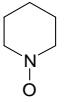
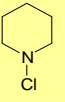
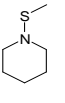
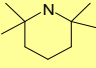
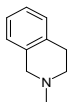
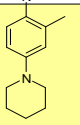
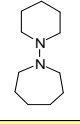
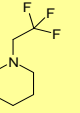
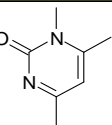
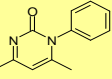
FURAN

2-methyl furan	82.1	C ₅ H ₆ O		solvent: ACN E _{ox} : 1.18	» P » WE: Pt » AE: Pt » RE: Ag/AgCl
2,4-dimethyl furan	96.1	C ₆ H ₈ O		solvent: ACN E _{ox} : 0.90	» P >> for details see above
2,5-dimethyl furan	96.1	C ₆ H ₈ O		solvent: ACN E _{ox} : 0.95	» P >> for details see above
benzofuran	118.1	C ₈ H ₆ O		solvent: ACN E _p : 1.82	» P » WE: Pt » AE: Au » RE: SCE
4,6-dimethyl-dibenzothiophene	212.3	C ₁₄ H ₁₂ S		solvent: ACN E ^{ox} :	» not described
2,3,4,5-tetramethyl-thiophene	140.2	C ₈ H ₁₂ S		solvent: ACN E ^{ox} : 0.89 irreversible reaction	» CV ISTD: Ferrocene » WE: Pt-disk » AE: Pt-wire » RE: Ag/AgCl
2-methyl thiophene	98.2	C ₅ H ₆ S		solvent: ACN E° > 1.8	» CV ISTD: Ferrocene » WE: glassy carbon » AE: Pt-wire » RE: Ag/AgCl

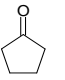
PIPERIDINE

1-methyl piperidine	99.2	C ₆ H ₁₃ N		solvent: ACN E ^{ox} _{1/2} : 1.18	» CV » WE: Pt » RE: SCE » AE: Pt
1-benzyl-piperidine	175.3	C ₁₂ H ₁₇ N		» not described	» not described
2,2,6-trimethyl-piperidine	127.2	C ₈ H ₁₇ N		solvent: H₂O E ^{ox} _{1/2} : - 0.1	» CV » WE: Au » RE: SCE » AE: Pt
piperidine	85.2	C ₅ H ₁₁ N		solvent: H₂O E _{1/2} : 0.422 V	» Potentiometrie » WE: Pt-black electrode » RE: SCE
1-ethyl-piperidine	113.2	C ₇ H ₁₅ N		solvent: H₂O E ^{ox} _{1/2} : 1.1	» CV » WE: Pt » RE: SCE » AE: Pt

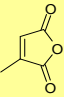
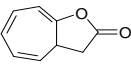
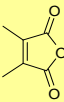
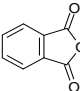
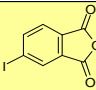
Appendix: Tables

1-hydroxy-piperidine	101.2	C ₅ H ₁₁ NO		solvent: ACN E _{1/2} : -1.26	» CV ISTD: Ferrocene » WE: Pt » RE: Ag/AgCl » AE: Pt
1-chloro-piperidine	119.6	C ₅ H ₁₀ ClN		solvent: PB E _{1/2} : 0.2 irreversible reduction	» CV ISTD: Ferrocene » WE: Pt/glassy carbon » RE: Ag/AgCl » AE: Pt
1-methylsulfanylpiperidine	131.2	C ₆ H ₁₃ NS		solvent: ACN E _{1/2} : 0.81	» CV ISTD: Ferrocene » WE: Au » RE: SCE » AE: Pt
2,2,6,6-tetramethyl-piperidine	141.3	C ₉ H ₁₉ N		solvent: H2O E _{1/2} : - 0.05	» CV ISTD: Ferrocene » WE: Au » RE: SCE » AE: Pt
2-ethyl-1,2,3,4-tetrahydro-isoquinoline	161.3	C ₁₁ H ₅ N		solvent: - E _{1/2} : 1.2	» CV » WE: Pt » RE: SCE » AE: Pt
2-methyl-4-piperidino-aniline	190.3	C ₁₂ H ₈ N ₂		solvent: - E _{1/2} : -0.315 pH: 11	» P » WE: Pt » RE: SCE » AE: Pt
1-piperidine-1-yl-azepane	182.3	C ₁₁ H ₂₂ N ₂		solvent: CH2Cl2 E _p ^o : 0.20	» CV » WE: Pt » RE: SCE » AE: Pt
1-(2,2,2-trifluoro-ethyl)-piperidine	167.2	C ₇ H ₁₂ F ₃ N		solvent: ACN E _p ^o : 0.83	» CV » WE: Pt » RE: SCE » AE: Pt
pyrimidone	138	C ₇ H ₁₀ N ₂ O		solvent: : DMF E _{1/2} ^{red.} : - 2.09	» CV ISTD: Ferrocene » WE: Hg-Stand » AE: Pt-wire » RE: SCE
4,6-dimethyl-1-phenyl-1H-pyrimidine-2-one	200.24	C ₁₂ H ₁₂ N ₂ O		solvent: : DMF E _{1/2} ^{red.} : - 1.94	» CV ISTD: Ferrocene » WE: Hg-Stand » AE: Pt-wire » RE: SCE

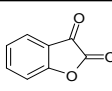
CYCLOPENTANONE

cyclo pentanone	84.12	C ₅ H ₈ O		solvent: : aequ. solution E _{1/2} ^{red.} : - 1.94	» P <i>no further information on the electrode material</i>
------------------------	-------	---------------------------------	---	---	---

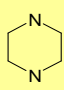
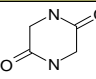
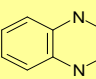
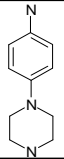
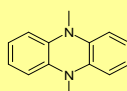
FURANONE

3-methyl-2,5-furandione	112.08	C ₅ H ₄ O ₃		solvent: MeOH/Benze E _{1/2} : -0.72	» P » WE: Hg-Stand » AE: - » RE: SCE
cyclohepta[b]furan-2-one	146.15	C ₉ H ₆ O ₂		solvent: ACN E ^{ox} : 1.13	» CV » WE: Pt » AE: Pt-wire » RE: Ag/AgCl
3,4-dimethyl-2,5-furandione	126.11	C ₆ H ₆ O ₂		solvent: DMF/Bu₄NP Ep: -1.99	» CV » WE: Hg coated Pt-disk » AE: Pt-wire » RE: Ag/AgCl
isobenzofuran-1,3-dione	148.12	C ₈ H ₄ O ₃		solvent: MeOH/Benze E _{1/2} : -1.12	» P » WE: Hg-Stand » AE: - » RE: SCE
4-iodo-phthalic acid anhydride	274.01	C ₈ H ₃ IO ₃		solvent: buffer E _{1/2} : -1.34	» P » WE: Hg-Stand » AE: - » RE: SCE

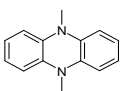
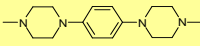
LACTONE

benzofuran-2,3-dione coumarandione	148.12	C ₈ H ₄ O ₃		solvent: DMSO E ^{red} _{1/2} : -0.65	» P » WE: Hg-Stand » AE: - » RE: SCE
---	--------	--	---	---	---

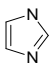
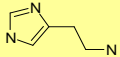
PIPERAZINE

piperazine	86.1	C ₄ H ₁₀ N ₂		solvent: - E _{1/2} (1): -1.96/68 E _{1/2} (2): -2.32/62	» CV » WE: dropping Hg » RE: SCE » AE: Pt-wire
piperazine-2,5-dione	114.1	C ₄ H ₆ N ₂ O ₂		solvent: H₂O E _k ⁰ : 0.4 pH: 7.0	<i>no further information on the method at all</i>
1,2,3,4-tetrahydro-quinoline	134.2	C ₈ H ₁₀ N ₂		solvent: buffer E _{1/2} : 0.05 V	» P <i>no further information on the electrode material</i>
4-piperazino-aniline photographic dye	177.3	C ₁₀ H ₁₅ N ₃		solvent: aqu.sol E _{1/2} : -0.304 pH: 11	» P » WE: Pt » RE H-electrode » AE: -
5,10-dimethyl-5,10-dihydro-phenazine	210.3	C ₁₄ H ₁₄ N ₂		solvent: ACN E _{1/2} : 0.14	» CV » WE: Pt » RE: SCE » AE: Pt-wire

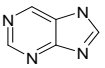
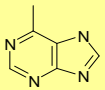
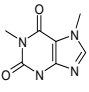
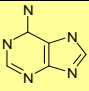
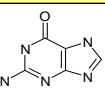
Appendix: Tables

5,10-dimethyl-5,10dihydrophena	212.3	C ₁₄ H ₁₆ N ₂		solvent: ACN E _p : -0.06 rev. potential	» V » WE: Pt » RE: Ag/AgCl » AE: Pt-wire
1,4-bis(4-methylpiperazino)benz	274.4	C ₁₆ H ₂₆ N ₄		solvent: ACN E _p : 0.246	» V » WE: Pt » RE Normal H-electrode » AE: Pt-wire

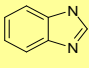
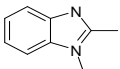
IMIDAZOLE

imidazole	68.08	C ₃ H ₄ N ₂		solvent: ACN E _{1/2} : 1.45	» V » WE: Pt » RE: Ag/AgCl » AE: Pt-wire
2-imidazol-4-ethylamine	111.15	C ₅ H ₉ N ₃		solvent: PB E _{1/2} : 0.05	» CV » WE: modified graphite » AE: Pt-wire » RE: Ag/AgCl

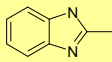
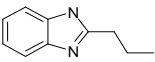
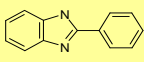
PURINE

purine	120.11	C ₅ H ₄ N ₄			CHECK again
6-methylpurine	134.14	C ₆ H ₆ N ₄		solvent: DMF E _{1/2} : -2.06	» P » WE: Pt » RE: SCE » AE:-
1,7-dimethyl-xanthine	180.17	C ₇ H ₈ N ₄ O ₂		solvent: DMF E _{1/2} : 1.22	» CV » WE: glassy carbon » RE: SCE » AE:Pt
adenine	135.13	C ₅ H ₅ N ₅		solvent: DMSO E _{1/2} : -2.41	» P » WE: Pt » RE: SCE » AE:-
guanine	151.13	C ₅ H ₅ N ₅ O		solvent: DMSO E _{1/2} : -2.76	» CV » WE: glassy carbon » RE Luggin » AE:Pt-sheet

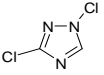
BENZIMIDAZOLE

benzimidazole	118.1	C ₇ H ₆ N ₂		solvent: ACN E _{1/2} : 1.31 irreversible half-wave potential	» V » WE: Pt » RE: Ag/AgCl » AE: Pt
1,2-dimethyl-1H-benzoimidazole	146.2	C ₉ H ₁₀ N ₂		solvent: ACN E _{p/2} ^{1A} : 1.38	» CV ISTD: Ferrocene » WE: glassy carbon » AE: Pt-wire » RE: SCE

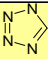
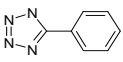
Appendix: Tables

2-methyl-1H-imidazole	132.2	C ₈ H ₈ N ₂		solvent: ACN E _{p/2} ^{1A} : 1.38	» CV ISTD: Ferrocene » WE: glassy carbon » AE: Pt-wire » RE: SCE
2-propyl-1H-benzimidazole	160.2	C ₁₀ H ₁₂ N		solvent: ACN E _{1/2} : 1.83 V irreversible half-wave potential	» V » WE: Pt » RE: Ag/AgCl » AE: Pt
2-phenyl-1H-benzoimidazole	194.2	C ₁₃ H ₁₀ N ₂		solvent: ACN E _p : 1 V	» CV » AE: Pt-wire » RE: Ag/AgCl » WE: Pt

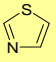
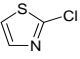
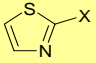
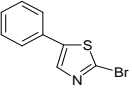
TRIAZOLE

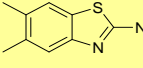
1,3-dichloro-1H-[1,2,4]triazole	137.96	C ₂ HCl ₂ N ₂		solvent: ACN E _{1/2} : -0.1 V	» V » WE: Pt » RE: Ag/AgCl » AE: Pt
--	--------	--	---	--	---

TETRAZOLE

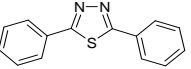
tetrazole	70.05	CH ₄ N ₄			check again
5-phenyl-tetrazole	146.15	C ₇ H ₆ N ₄			

THIAZOLE

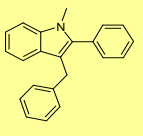
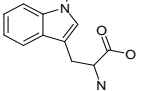
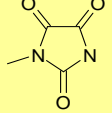
thiazole	82.1	C ₃ H ₃ NS		solvent: ACN E _{1/2} : 1.980 V	» P » WE: Pt » RE: Ag/AgCl » AE: Pt
2-chloro-thiazole	119.6	C ₃ H ₂ ClNS			» P » WE: » RE: SCE » AE: -
2-halogen-thiazole	164.0	C ₃ H ₂ BrNS		solvent: aqu.sol. E _{1/2} (I): 0.24 V E _{1/2} (Br): 0.59 V E _{1/2} (Cl): 0.91 V at pH: 1	» P » WE: » RE: SCE » AE: -
				E _{1/2} (I): 0.70 V E _{1/2} (Br): 1.47 V at pH: 8-10	
5-phenyl-thiazole	161.2	C ₉ H ₇ NS		solvent: ACN E _{1/2} : 1.41 V	» P » WE: Pt » RE: Ag/AgCl » AE: Pt

5,6-dimethyl-benzothiazol-2-ylamine	178.3	C ₉ H ₁₀ N ₂ S		solvent: MeOH/H₂O E _{1/2} : -1.24 V irreversible reaction	» P » WE: Pt » RE: SCE » AE: Pt
--	-------	---	---	---	--

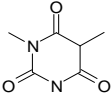
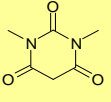
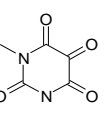
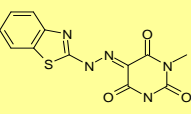
THIADIAZOLE

2,5-diphenyl-Thiadiazole	238.31	C ₁₄ H ₁₀ N ₂ S			
---------------------------------	--------	--	---	--	--

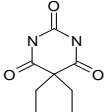
INDOLE-DERIVATIVES

3-benzyl-1-methyl-2-phenylindole	297.4	C ₂₂ H ₁₉ N		solvent: ACN E ^{ox} _{1/2} : 0.51 V	» P » WE: graphit/rotating Pt » RE: Ag/AgCl » AE: -
indolinone 1-methyl-tryptophan	218.3	C ₁₂ H ₁₄ N ₂ O ₂		solvent: H₂O E _{red} : 1.14 V	» Pulse radiolysis
methylparabensäure methyl-Imidazolidintrione	128.1	C ₄ H ₄ N ₂ O ₃		solvent: 40 % EtOH E _{1/2} : -0.74V	» P » WE: dropping Hg » RE: SCE » AE: -

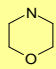
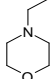
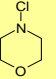
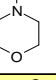
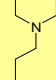
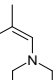
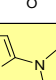
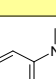
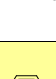
BARBITURIC ACID /-DERIVATIVES

1-5-dimethyl-barbituric acid	156.1	C ₆ H ₆ N ₂ O ₃		solvent: acetic acid and MeOH E ^{ox} _{1/2} : 1.1V	» CV » WE: pyrolytic graphite » RE: SCE » AE: -
1,3-dimethyl-barbituric acid	156.1	C ₆ H ₆ N ₂ O ₃		solvent: acetic acid and MeOH E ^{ox} _{1/2} : 1.58 V	» CV » WE: pyrolytic graphite » RE: SCE » AE: -
alloxan pyrimidine-2,4,5,6-tetraone	142.1	C ₄ H ₂ N ₂ O ₄		solvent: Eimer and Amend Buffer E _{1/2} (1) : -0.115 V E _{1/2} (2) : -0.965 V E _{1/2} (3) : - 1.52 V	» P » WE: » RE: SCE » AE: -
5-(benzothiazol hydrazono)-1,3-	317.3	C ₁₃ H ₁₁ N ₅ O ₃ S		solvent: DMF E _{1/2} : -0.72 V	» P » WE: dropping Hg » RE: SCE » AE: -

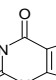
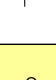
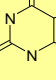
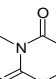
BARBITAL

barbital 5,5-diethyl-pyrimidine-2,4,6-trione	184.2	C ₈ H ₁₂ N ₂ O ₃		solvent: Borate Buffer E _{1/2} : -0.036 V	» P » WE: » RE: SCE » AE: -
---	-------	--	---	--	--------------------------------------

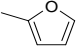
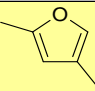
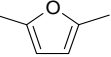
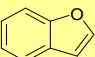
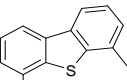
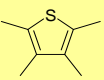
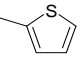
MORPHOLINE

morpholine	87.1	C ₄ H ₉ NO			CHECK AGAIN!
4-ethyl-morpholine	115.2	C ₆ H ₁₃ NO		solvent: EtOH E _{1/2} : 0.19 V	» redox titration
4-chloro-morpholine	121.6	C ₄ H ₈ ClNO		solvent:	
CHECK LITERATURE AGAIN!!					
4-aminomorpholine	102.1	C ₄ H ₁₀ N ₂ O		solvent: EtOH E _{1/2} : 0.8V	» P no further information on the method at all
4-butyl-morpholine	143.2	C ₈ H ₁₇ NO		solvent: EtOH E _{1/2} : 0.203 V	» redox titration
4-(2-methyl-propenyl)-morpholine	141.2	C ₈ H ₁₅ NO		solvent: ACN E _{1/2} : 0.19 V	» P » WE: glassy carbon » RE: Ag/AgCl » AE: Pt
4-thiophen-2-yl-morpholine	169.2	C ₈ H ₁₁ NOS		solvent: ACN E _{ox} : 0.55 V	» no information about the method
4,7-dimethyl-3,4-dihydro-2H-benzo[1,4]oxazine	163.2	C ₁₀ H ₁₃ NO		solvent: ACN E _{1/2} : 0.60 V	» P » WE: no info available » RE: SCE » AE: no info available
4-(4-piperidin-1-yl-phenyl)-morpholine	246.4	C ₁₅ H ₂₂ N ₂ O			

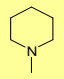
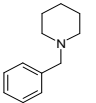
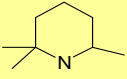
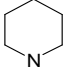
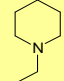
XANTHINES

theobromin	180.2	C ₇ H ₈ N ₄ O ₂		solvent: H₂O PB E _p . 1.3V (low pH-value)	» CV ISTD: Ferrocene » WE: glassy carbon » AE: Pt-wire » RE: SCE
7-methylxanthine	166.1	C ₆ H ₆ N ₄ O ₂		solvent: water with phosphate buffer E _p . 0.925 V	» CV ISTD: Ferrocene » WE: glassy carbon » AE: Pt-wire » RE: SCE
theophyllin	180.2	C ₇ H ₈ N ₄ O ₂		solvent: aq.phosphate buffer E _{ox} : 1.0 V	» CV » WE: pyrolytic graphite » RE: SCE » AE: Pt gauze
caffeine	194.2	C ₈ H ₁₀ N ₄ O ₂		solvent: aq.phosphate buffer E _{ox} : 1.45 V E _{red} : 0.76 V	» CV » WE: pyrolytic graphite » RE: SCE » AE: Pt gauze

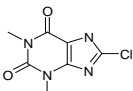
FURAN

2-methyl furan	82.1	C ₅ H ₆ O		solvent: ACN E _{ox} : 1.18	» P » WE: Pt » AE: Pt » RE: Ag/AgCl
2,4-dimethyl furan	96.1	C ₆ H ₈ O		solvent: ACN E _{ox} : 0.90	» P >> for details see above
2,5-dimethyl furan	96.1	C ₆ H ₈ O		solvent: ACN E _{ox} : 0.95	» P >> for details see above
benzofuran	118.1	C ₈ H ₆ O		solvent: ACN E _p : 1.82	» P » WE: Pt » AE: Au » RE: SCE
4,6-dimethyl-dibenzothiophene	212.3	C ₁₄ H ₁₂ S		solvent: ACN E ^{ox} :	» not described
2,3,4,5-tetramethyl-thiophene	140.2	C ₈ H ₁₂ S		solvent: ACN E ^{ox} : 0.89 irreversible reaction	» CV ISTD: Ferrocene » WE: Pt-disk » AE: Pt-wire » RE: Ag/AgCl
2-methyl thiophene	98.2	C ₅ H ₆ S		solvent: ACN E° > 1.8	» CV ISTD: Ferrocene » WE: glassy carbon » AE: Pt-wire » RE: Ag/AgCl

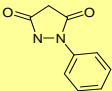
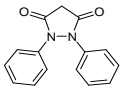
PIPERIDINE

1-methyl piperidine	99.2	C ₆ H ₁₃ N		solvent: ACN E ^{ox} _{1/2} : 1.18	» CV » WE: Pt » RE: SCE » AE: Pt
1-benzyl-piperidine	175.3	C ₁₂ H ₁₇ N		» not described	» not described
2,2,6-trimethyl-piperidine	127.2	C ₈ H ₁₇ N		solvent: H₂O E ^{ox} _{1/2} : - 0.1	» CV » WE: Au » RE: SCE » AE: Pt
piperidine	85.2	C ₅ H ₁₁ N		solvent: H₂O E _{1/2} : 0.422 V	» Potentiometrie » WE: Pt-black electrode » RE: SCE
1-ethyl-piperidine	113.2	C ₇ H ₁₅ N		solvent: H₂O E ^{ox} _{1/2} : 1.1	» CV » WE: Pt » RE: SCE » AE: Pt

Appendix: Tables

8-chlorotheophylline	214.6	C ₇ H ₇ ClN ₄ O ₂		solvent: ACN E _{1/2} ^{ox} : 1.82 V irreversible oxidation process	» CV » WE: - » RE: SCE » AE: -
-----------------------------	-------	---	---	--	---

PYRAZOLIDINE

pyrazolidine	176.17	C ₉ H ₈ N ₂ O ₂			
1,2-diphenyl-pyrazolidine	252.27	C ₁₅ H ₁₂ N ₂ O ₂			

DIOXOLANE

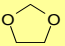
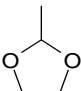
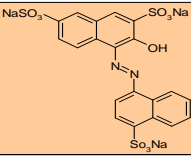
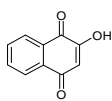
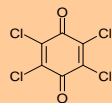
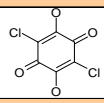
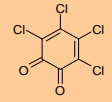
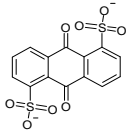
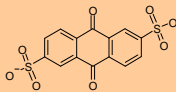
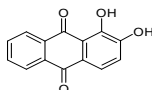
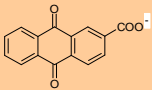
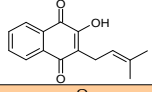
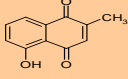
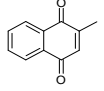
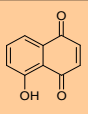
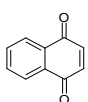
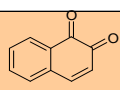
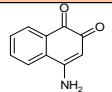
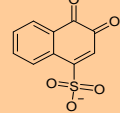
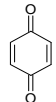
1,3-dioxolane	74.08	C ₃ H ₆ O ₂		solvent: ACN E _{1/2} ^{ox} : -0.9	» CV » WE: glassy carbon » RE: Ag/AgCl » AE: Pt-coil
2-methyl-dioxolane	88.11	C ₄ H ₈ O ₂		solvent: ACN E _{1/2} ^{ox} : -1.15	» CV » WE: glassy carbon » RE: Ag/AgCl » AE: Pt-coil

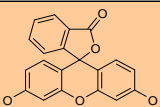
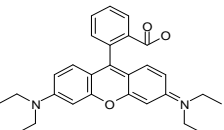
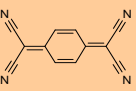
Table C: Colour Compound List

Chemical Name systematic name and trivial name	MW	MF	Structure	Solvent	E_{ox}/E_{red} [V]
P: polarography CV: cyclic voltammetry ACN: acetonitrile					
AZO COMPOUNDS					
amaranth (acid red) 2,7-naphthalenedisulfonic acid	535.49	C ₂₀ H ₁₁ N ₂ O ₁₀ S ₃		solvent: unknown E' ₀ : - 0.250 two electron potential	» P
QUINONES					
lawsone 1,4 naphthalenedione 2-hydroxy-1,4-naphthoquinone	174.16	C ₁₀ H ₆ O ₃		solvent: unknown E _{1/2} : - 0.460	» P
p-chloranil	254.88	C ₆ Cl ₄ O ₂		solvent: unknown E _{1/2} : - 0.330	» P
				solvent: ACN E _{1/2} : - 0.330	method: not described
				solvent: ACN E _{1/2} : 0.350	
				solvent: DMF E' _p : - 0.880	» CV
				solvent: MeOH E _{1/2} : 0.780 to 0.880 growing redox potentials with increasing acidification	method: potentiometric titration
				solvent: CH ₂ Cl ₂ E _{1/2} : 0.240	» CV
chloranilic acid 2,5-dichloro-3,6-dihydroxy-[1,4] benzoquinone	208.99	C ₆ H ₂ Cl ₂ O ₄		solvent: aqu.sol + 0.1N HCl E' ₀ : 0.420	method: not described
o-chloranil tetrachloro-[1,2]benzoquinone	254.88	C ₆ Cl ₄ O ₂		solvent: benzene E' 0: 0.833	method: not described
				solvent: aqu.sol E' 0: 0.794	
anthraquinone-1,5-disulfonate	368.33	C ₁₄ H ₈ O ₈ S ₂		solvent: aqu.sol E' ₀ : 0.239	method: not described

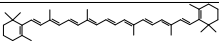
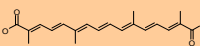
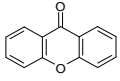
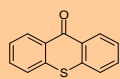
Appendix: Tables

anthraquinone-2,6-disulfonate	368.33	C ₁₄ H ₈ O ₈ S ₂		solvent: aqu.sol E' 0 : 0.228	method: <i>not described</i>
				solvents: 1% Ethanol E _{1/2} : -0.440 to -0.600	» P
				solvent: DMSO	» CV
				ΔEp: 0.130	
alizarin 1,2-dihydroxy-9,10-anthraquinone	240.21	C ₁₄ H ₈ O ₄		solvent: - E' 0: 0.494	method: <i>not described</i>
				solvent: - E _{1/2} : 0.610 to 0.890	method: <i>not described</i>
anthraquinone-2-carboxylate 9,10-dioxo-9,10-dihydro-anthracene-2-carboxylic acid	252.23	C ₁₅ H ₈ O ₄		solvent: - E' 0: 0.208	method: <i>not described</i>
lapachol [1,4]naphthoquinone	242.3	C ₁₅ H ₈ O ₃		solvent: - E' 0 : 0.272	method: titration potentiometric
plumbagin 2-methyl-5-hydroxy-1,4-naphthoquinone	188.18	C ₁₁ H ₈ O ₃		solvent: MeOH E' 0: 0.383	method: <i>not described</i>
menadione 2-methyl-1,4-naphthoquinone	172.18	C ₁₁ H ₈ O ₂		solvent: - E _{1/2} : - 0.225	» P
				solvent: - E'pc1: -277	» CV
				solvent: MeOH E _{1/2} : 0.017 to 0.481	
juglone 5-hydroxy-1,4-naphthoquinone	174.16	C ₁₀ H ₆ O ₃		solvent: DMSO ΔEp: 0.220 (peak1) ΔEp: 0.490 (peak2) E' 0: 0.450	» CV
1,4-naphthoquinone	158.16	C ₁₀ H ₆ O ₂		solvent: ACN E' 0: 0.459	method: <i>not described</i>
				solvent: 0.1 M TBAP +ACN E _{1/2} : -0.685	» P
1,2-naphthoquinone	158.16	C ₁₀ H ₆ O ₂		solvent: aqu.sol E' 0: 0.579	method: <i>not described</i>
4-amino-1,2-naphthoquinone	173.11	C ₁₀ H ₇ NO ₂		solvent: aqu. EtOH E' 0 : 0.440	» P
1,2-naphthoquinone-4-sulfonate	237.21	C ₁₀ H ₅ O ₅		solvent: aqu. sol E' 0: 0.425	method: potentiometric titration
1,4-benzoquinone <i>p</i> -benzoquinone	108.1	C ₆ H ₄ O ₂		solvent: ACN ΔE : 0.910	» CV
				solvent: DMF E _{1/2} : - 0.390	» P

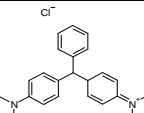
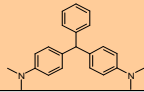
FLUORESCENT MOLECULES

fluorescein 3',6'-dihydroxy-spiro[phthalan-1,9'-xanthen]-3-one	332.31	C ₂₀ H ₁₂ O ₅		solvent: - E ⁰ : -0.572	method: titration
rhodamin	442.56	C ₂₈ H ₃₀ N ₂ O ₃		solvent: - E ⁰ : -0.542 E _{1/2} : -0.852	method: titration
tetracyanoquinodimethane	204.19	C ₁₂ H ₄ N ₄		solvent: - E _p : 0.170	method: <i>not described</i>
				solvent: - E ⁰ : 0.460	method: <i>not described</i>

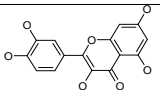
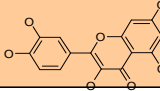
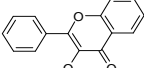
POLYENE

b-b-carotene trans-b-carotene	536.88	C ₄₀ H ₅₆		solvent: - E ₁ : 0.540	» CV
all-trans-crocetin 8,8'-diapo- q,q -carotenedioic acid	536.88	C ₄₀ H ₅₆		solvent: DMF/DMSO/H ₂ O E ⁰ : 0.550 to 0.870	» CV
xanthone xanthen-9-one	196.21	C ₁₃ H ₈ O ₂		solvent: DMF E _{1/2} (1): -1.15 E _{1/2} (2): -1.55 E _{1/2} (3): -2.1	» P
				solvent: - E _{1/2} : -0.910	» CV
				solvent: DMF E _{1/2} : -1.6	» P
thioxanthone thioxanthen-9-one	212.27	C ₁₃ H ₈ OS		solvent: - E _{1/2} : -1.73	» CV
				solvent: - E _{1/2} : -1.62	» CV

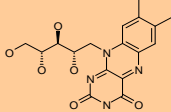
POLYMETHINS

malachitgreen	329.46	C ₂₃ H ₂₅ N ₂ Cl			
leucomalachitgreen	329.46	C ₂₃ H ₂₆ N ₂			

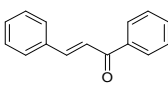
FLAVONOIDES

quercetin	302.24	C ₁₅ H ₁₀ O ₇		solvent: buffer E _{1/2} : -1.62 V	» P
rhamnetin (3,3',4',5-tetrahydroxy-7-methoxyflavon)	316.27	C ₁₆ H ₁₂ O ₇		<i>information about the half-wave potential is only available in Russian!</i>	
flavonol	238.24	C ₁₅ H ₁₀ O ₃		<i>information about the half-wave potential is only available in Russian!</i>	

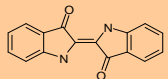
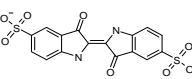
Appendix: Tables

vitamin B2 riboflavin	376.37	$C_{17}H_{20}N_4O_6$		solvent: - $E_{1/2}$: -208	method: <i>not described</i>
---------------------------------	--------	----------------------	---	---------------------------------------	-------------------------------------

CHALKON

chalkon 1,3-diphenyl-acetophenon	208.26	$C_{15}H_{12}O$		solvent: buffer $E_{1/2}$ (1): -0.620 $E_{1/2}$ (2): -1.006 at pH 1.81	» P
				$E_{1/2}$ (1): -1.190 $E_{1/2}$ (2): -1.340 $E_{1/2}$ (3): -1.690 at pH 11.98	

INDIGOID COMPOUNDS

indigo 1H,1H'-[2,2']biindolylidene-2,2'-dione	262.27	$C_{16}H_{10}N_2O_2$		solvent: DMF $E_{1/2}$ (1): -0.780 $E_{1/2}$ (2): -1.260	» CV
indigo carmine 3,3'-dioxo-1,3,1'3'-tetrahydro [2,2']biindolylidene,5,5'- disulfonic acid	420.37 22.99	$C_{16}H_8N_2O_8S_2^{(2-)}$ *2Na ⁽¹⁺⁾		solvent: - E^0 : -0.220	» CV

MISCELLANEOUS

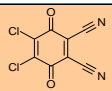
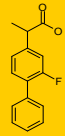
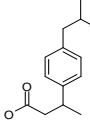
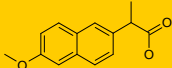
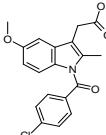
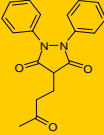
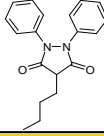
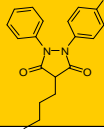
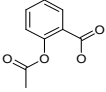
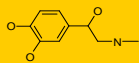
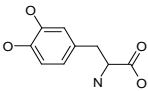
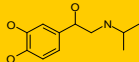
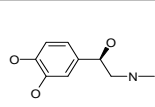
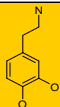
DDQ 2,3-dichloro-5,6-dicyano-1,4-benzoquinone	227.01	$C_8Cl_2N_2O_2$		solvent: - $E_{1/2}$ (1): 0.550	» CV
---	--------	-----------------	---	---	------

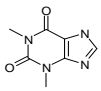
Table D: List

Chemical Name	MF	MW	Structure	E_{pot} [V]	Conditions
ARYLPROPIONIC-DERIVATIVES					
furbiprofen Froben	244.3	$C_{15}H_{13}FO_2$		solvent: EtOH $E_{1/2}$: -1.97 vs SCE $E_{1/2}$: -2.40 vs FC solvent: DMSO $E_{1/2}$: -2.42 vs SCE $E_{1/2}$: -2.82 vs FC	» P » WE: dropping mercury » RE: SCE » AE: Pt-wire
ibuprofen Brufen	206.3	$C_{13}H_{18}O_2$		solvent: EtOH $E_{1/2}$: -2.03 vs SCE $E_{1/2}$: -2.46 vs FC solvent: DMSO $E_{1/2}$: -2.66 vs SCE $E_{1/2}$: -3.06 vs FC	» P for further information: see above
naproxen Aleeve	230.3	$C_{14}H_{14}O_3$		solvent: EtOH $E_{1/2}$: -1.95 vs SCE $E_{1/2}$: -2.38 vs FC solvent: DMSO $E_{1/2}$: -2.39 V vs SCE $E_{1/2}$: -2.79 V vs FC	» P for further information: see above
ARYLACETIC-DERIVATIVES					
indomethacin (Indocid®)	357.8	$C_{19}H_{16}ClNO_4$		solvent: BR (pH: 7.2) E_{p1} : -0.55 E_{p2} : -1.44 E_{p3} : -1.68	» differential pulse voltammetry » WE: droppinn mercury electr. » RE: Ag/AgCl » AE: Pt-wire
PYRAZOLIDINES					
kebutzone	322.4	$C_{19}H_{18}N_2O_3$		solvent: DMSO 1 st cathodic step: $E_{1/2}$: -1.36 2 nd cathodic step $E_{1/2}$: -1.91	» P » WE:dropping mercury » RE: Ag/AgCl » AE: Pt-wire
phenylbutazone Ambene® (D) Butadion® (CH)	308.4	$C_{19}H_{20}N_2O_2$		solvent: DMSO 1 st cathodic step: $E_{1/2}$: -1.37.0 2 nd cathodic step $E_{1/2}$: -1.94	» direct current polarography » WE:dropping mercury » RE: Ag/AgCl » AE: Pt-wire
Oxyphenbutazone main metabolit of phenbutazon	324.4	$C_{19}H_{20}N_2O_3$		solvent: DMSO 1 st cathodic step: $E_{1/2}$: -1.38 2 nd cathodic step $E_{1/2}$: -2.0	» direct current polarography » WE:dropping mercury » RE: Ag/AgCl » AE: Pt-wire
SALICYLIC ACID-DERIVATIVES					
acetylsalicylic acid Aspirin	180.2	$C_9H_8O_4$		solvent: ACN $E_{1/2}$ (1) : -1.64	» P » WE: dropping mercury » RE: silver wire » AE: platinum wire

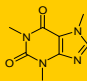
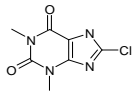
CATECHOLAMINES

epinephrine EpiPen	183.2	C ₉ H ₁₃ NO ₃		solvent: buffer E _{1/2} : 0.380	» normal pulse polarography » WE: carbon » RE: SCE (<i>in Vitro</i>), Ag/AgCl (<i>in Vivo</i>) » AE: Pt-wire
L-Dopa Madopar	197.2	C ₉ H ₁₁ NO ₄		solvent: buffer E _{1/2} : 0.450	» normal pulse polarography » WE: carbon » RE: SCE (<i>in Vitro</i>), Ag/AgCl (<i>in Vivo</i>) » AE: Pt-wire
isoprenaline	211.3	C ₁₁ H ₁₇ NO ₃		solvent: buffer E _{1/2} : 0.370	» V » WE: Au » RE: Ag/AgCl wire » AE: Pt-wire
R-adrenaline	183.2	C ₉ H ₁₃ NO ₃		solvent: buffer E _{1/2} : 0.370	» CV » WE: glassy carbon » RE: Ag/AgCl wire » AE: Pt-wire
dopamin HCL	158.2	C ₈ H ₁₁ NO ₂		solvent: aq. HCl E _{ox} : 0.68 E _{red} : -0.33	» CV » WE: dropping mercury » AE: mercury » RE: SCE

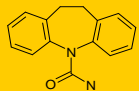
BRONCHODILATATOR

theophyllin	180.2	C ₇ H ₈ N ₄ O ₂		solvent: buffer E _{ox} : 1.0	» CV » WE: pyrolytic graphite » RE: SCE » AE: Pt gauze
--------------------	-------	---	--	---	---

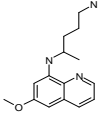
STIMULATING AGENT

caffeine	194.2	C ₈ H ₁₀ N ₄ O ₂		solvent: buffer E _{ox} : 1.45 E _{red} : 0.76	» CV » WE: pyrolytic graphite » RE: SCE » AE: Pt gauze
8-chlorotheophylline	214.6	C ₇ H ₇ ClN ₄ O ₂		solvent: ACN E _{1/2} ox: 1.82 irreversible oxidation	» CV » WE: - » RE: SCE » AE: -

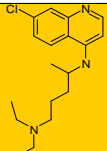
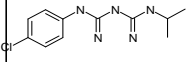
IMINOSTILBEN-DERIVATIVES

carbamazepin Tegretol	236.3	C ₁₅ H ₁₂ N ₂ O		solvent: ACN Ep: -2.27	» CV » WE: glassy carbon » RE: Ag/AgCl wire » AE: Pt-wire
--	-------	--	---	----------------------------------	--

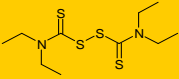
8-AMINO-QUINOLINES

primaquine	259.4	C ₁₅ H ₂₁ N ₃ O			Check literature!
-------------------	-------	--	---	--	-------------------

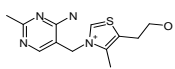
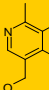
Appendix: Tables

chloroquine Nivaquin	319.9	C ₁₈ H ₂₆ ClN ₃		solvent: - 1 st cathodic step: E _{1/2} : -0.97 2 nd cathodic step E _{1/2} : -1.20	method: -
proguanil Paludrine (Mono) Malarone (Combi)	253.7	C ₁₁ H ₁₆ ClN ₅		solvent: - E _{1/2} : 1.22 V	» P » WE: - » RE: - » AE: -

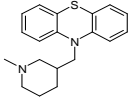
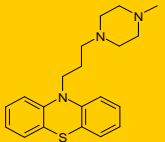
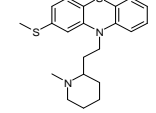
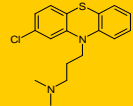
ALDEHYDEHYDROGENASE-INHIBITOR

disulfiram Antabus	296.5	C ₁₀ H ₁₀ N ₂ S ₄		solvent: EtOH E _{1/2} : - 0.4 vs SCE	» P » WE: - » RE: - » AE: -
-------------------------------------	-------	---	---	--	--------------------------------------

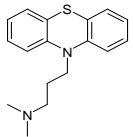
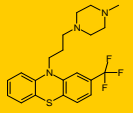
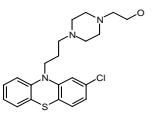
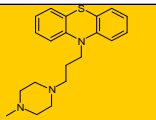
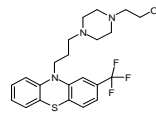
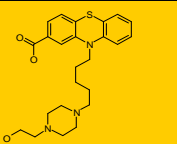
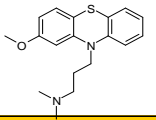
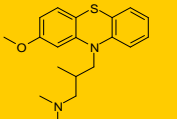
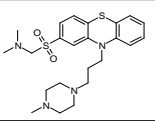
VITAMINES

thiamine Benerva	265.4	C ₁₂ H ₁₇ N ₄ OS		solvent: -	» P » WE: - » RE: - » AE: -
pyridoxine	169.2	C ₈ H ₁₁ NO ₃		solvent: - E _{1/2} : -1.52 V solvent: - E _p : 0.29 V	» CV » differential pulse voltammetry » WE: glassy carbon » RE: Ag/AgCl » AE: Pt-wire

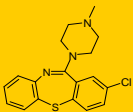
PHENOTHIAZINE-DERIVATIVES

pecazine	310.5	C ₁₉ H ₂₂ N ₂ S		solvent: buffer E _{1/2} : 0.503 solvent: EtOH E _{1/2} : 0.600	» P » WE: rotating gold wire » AE: - » RE: mercury-mercurous sulfate electrode
prochlorperazine	373.9	C ₂₀ H ₂₄ ClN ₃ S		solvent: buffer E _{1/2} : 0.547 solvent: EtOH E _{1/2} : 0.620	» P » WE: rotating gold wire » AE: - » RE: mercury-mercurous sulfate electrode
thioridazine Melleril	370.6	C ₂₁ H ₂₆ N ₂ S ₂		solvent: buffer E _{ox} : 0.58	» Photoionization
chlorpromazine Chlorazine	318.9	C ₁₇ H ₁₉ ClN ₂ S		solvent: buffer E _{1/2} : 0.6	» Photoionization

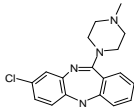
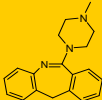
Appendix: Tables

promazine	284.4	$C_{17}H_{20}N_2S$		solvent: buffer E_{ox} : 0.56 solvent: buffer $E_{1/2}$: 0.473 solvent: EtOH $E_{1/2}$: 0.545	» Photoionization » P » H-Cell with mercury-mercurous sulfate reference electrode » oxidations were carried out at a rotating gold wire electrode.
trifluorperazine	407.5	$C_{21}H_{24}F_3N_3S$		solvent: - E_{ox} : 0.66	» CV » WE: adjustable platinum disc embedded in a glass seal » RE: SCE
perphenazine Trilafon	404.0	$C_{21}H_{26}ClN_3OS$		solvent: buffer $E_{1/2}$: 0.619 solvent: EtOH $E_{1/2}$: 0.639	» P
perazine	339.5	$C_{20}H_{25}N_3S$		solvent: - E_{ox} : 0.72	<i>no information about the method the electrodes and the solvent</i>
fluphenazine Dapotum	437.5	$C_{22}H_{26}F_3N_3OS$		solvent: buffer $E_{1/2}$: 0.583 solvent: EtOH $E_{1/2}$: 0.684	» P » WE: rotating gold wire electrode » RE: mercury-mercurous sulfate electrode
acetophenazine	411.6	$C_{23}H_{29}N_3O_2S$			
methopromazine	314.4	$C_{18}H_{22}N_2OS$		solvent: EtOH E_0 : 0.71	» photogalvanical method <i>no information about the method the electrodes and the solvent</i>
methotrimeprazine	328.5	$C_{19}H_{24}N_2OS$			Check literature!
thiopropazine	446.6	$C_{22}H_{30}N_4O_2S_2$			Check literature!

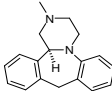
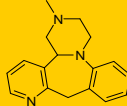
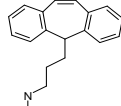
CLOZAPINE-ANALOGUES

clotiapine Entumin	343.9	$C_{18}H_{18}ClN_3S$		solvent: buffer E_p : - 0.920	» CV » WE: carbon paste » AE: carbon paste » RE: Ag/AgCl in 3 M KCl
-------------------------------------	-------	----------------------	---	---	--


Appendix: Tables

clozapine Leponex	326.8	C ₁₈ H ₁₉ ClN ₄		solvent: buffer E _p : -0.375	» CV » WE: carbon paste » AE: carbon paste » RE: Ag/AgCl in 3 M KCl
perlapine	291.4	C ₁₉ H ₂₁ N ₃		solvent: - E _{1/2} : - 1.57 irreversibel half way potential	» P » WE: dropping mercury » AE: Pt-foil » RE: saturated Hg ₂ Cl ₂

TRICYCLIC ANTIDEPRESSANT

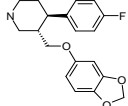
mianserin Tolvon	264.4	C ₁₈ H ₂₀ N ₂		solvent: MeOH E _{ox} : 0.76	» V » WE: glassy carbon » AE: Pt » RE: Ag/AgCl (sat)
mirtazapine Remeron				solvent: MeOH E _{ox} : 0.76	» V » WE: glassy carbon » AE: Pt » RE: Ag/AgCl (sat)
protryptilin	263.4	C ₁₉ H ₂₁ N		solvent: EtOH E _{ox} : 1.85	» CV » WE: glassy carbon » AE: Pt » RE: Ag/AgCl (sat)

NA-REUPTAKE INHIBITOR

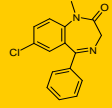
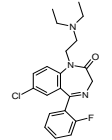
venlafaxine Efexor	277.4	C ₁₇ H ₂₇ NO ₂		solvent: BR E: -1.0 <i>best pH-range:</i> <i>8.0-9.0</i>	» square wave voltammetry » WE: dropping Mercury » AE: glassy carbon » RE: Ag/AgCl (sat)
-------------------------------------	-------	---	---	--	--

Note! a broad range of pH-values have been measured

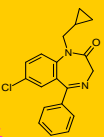
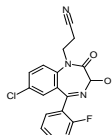
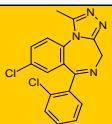
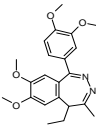
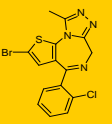
SEROTIN-REUPTAKE INHIBITOR

paroxetine Deroxat	329.4	C ₁₉ H ₂₀ FNO ₃		solvent: BR E _p : 1.15	» CV » WE: glassy carbon » AE: Pt » RE: Ag/AgCl
-------------------------------------	-------	--	---	---	---

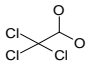
BENZODIAZEPINES

diazepam Valium	284.7	C ₁₆ H ₁₃ ClN ₂ O		solvent: - E _{1/2} : 1.50	» P » WE: dropping Mercury » AE: Pt-wire electrode » RE: SCE
flurazepam Dalmadorm	387.9	C ₂₁ H ₂₃ ClFN ₃ O		solvent: - E _{1/2} : +1.05	» P » WE: Pt-sheet » AE: rotating platinum disk » RE: SCE

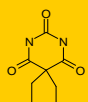
Appendix: Tables

prazepam Demetrim	324.8	C ₁₉ H ₁₇ ClN ₂ O		solvent:- E _{1/2} : -0.6	» P » WE: dropping Mercury » AE: glassy carbon » RE: Ag/AgCl (sat)
<i>Note! Prazepam is hardly soluble in Britton-Robinson Buffer, therefore 10% of DMF was added to increase solubility</i>					
cinolazepam Gerodorm	357.8	C ₁₈ H ₁₃ ClFN ₃ O ₂		solvent:- E _{1/2} (1): -0.58 E _{1/2} (1): -0.84	» coulometry » WE: - » AE: - » RE: Ag/AgCl
<i>half-wave potential changes if the pH-value is increased::> see article</i>					
triazolam Halcion	343.2	C ₁₇ H ₁₂ Cl ₂ N ₄		solvent: EtOH E _{1/2} : -1.38	» V » WE: Pt » AE: Pt » RE: SCE
tofisopam Grandaxin	382.5	C ₂₂ H ₂₆ N ₂ O ₄		solvent:- E _{1/2} : -1.04	» P
Brotizolam Lendormin	393.7	C ₁₅ H ₁₀ BrClN ₄ S			

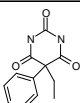
HYPNOTICS

Chloralhydrate Chloraldurat	165.4	C ₂ H ₃ Cl ₃ O ₂		solvent: buffer E _{1/2} : -1.06 E _{1/2} : -1.66	» P » WE: dropping mercury » AE: mercury » RE: SCE
--	-------	--	---	--	---

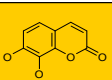
HYPNOTICA

Barbital Veronal (D)	184.2	C ₈ H ₁₂ N ₂ O ₃		solvent: buffer E _{1/2} : -0.03 pH:9.3	» P » WE: dropping mercury » AE: platinum wire » RE: silver wire
---------------------------------------	-------	--	---	--	---

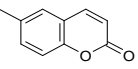
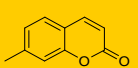
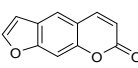
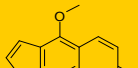
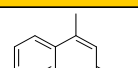
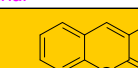
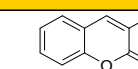
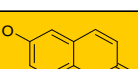
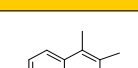
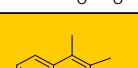
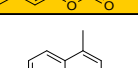
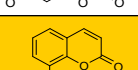
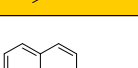
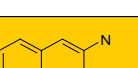
ANTIPILEPTICS/HYPNOTICA

Phenobarbital Luminal	232.2	C ₁₂ H ₁₂ N ₂ O ₃		solvent: ACN E _{1/2} (1): -2.07	» P » WE: dropping mercury » AE: platinum wire » RE: silver wire
--	-------	---	---	--	---

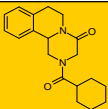
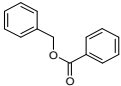
COUMARINES

6-methyl coumarines	160.2	C ₁₀ H ₈ O ₂		solvent: MeOH E _{1/2} : 1.63	» P <i>no further information on the electrode material</i>
----------------------------	-------	---	---	---	--

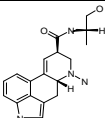
Appendix: Tables

5-methoxy-psoralen	216.2	C ₁₂ H ₈ O ₄		solvent: buffer E _{ox} : 1.63 irreversible oxidation	» CV » WE: - » AE: - » RE: SCE
7-methyl-coumarin	160.2	C ₁₀ H ₈ O ₂		solvent: buffer E _{ox} : 2.17 irreversible oxidation	» CV » for further information: see above
psoralen	186.2	C ₁₁ H ₆ O ₃		solvent: buffer E _{ox} : 1.89	» CV » for further information: see above
7,8-dihydroxy-coumarin	178.1	C ₉ H ₆ O ₄		solvent: - E _{1/2} : -1.8 pH-dependency	» P » WE: - » AE: - » RE: SCE
4-methyl-coumarin	160.2	C ₁₀ H ₈ O ₂		solvent: - E _{1/2} : -1.64	» P » for further information: see above
<i>Note! No information concerning solvents or electrode material</i>					
3-methyl-coumarin	160.2	C ₁₀ H ₈ O ₂		solvent: - E _{1/2} : -1.68	» P » for further information: see above
7-hydroxycoumarin (Umbelliferone)	162.1	C ₉ H ₆ O ₃		solvent: - E _{1/2} : -1.67	» P » for further information: see above
6-hydroxycoumarin	162.1	C ₉ H ₆ O ₃		solvent: - E _{1/2} : -1.56	» P » for further information: see above
3,4-dimethylcoumarin	174.2	C ₁₁ H ₁₀ O ₂		solvent: - E _{1/2} : -1.73	» P » for further information: see above
3,4,7-trimethyl-coumarin	188.2	C ₁₂ H ₁₂ O ₂		solvent: - E _{1/2} : -1.81	» P » for further information: see above
7-hydroxy-4-methyl-coumarin	176.2	C ₁₀ H ₈ O ₃		solvent: - E _{1/2} : -1.82	» P » for further information: see above
8-methoxy coumarin	176.2	C ₁₀ H ₈ O ₃		solvent: - E _{1/2} : -1.56	» P » for further information: see above
coumarin	146.2	C ₉ H ₆ O ₂		solvent: - E _{1/2} : -1.53	» P » for further information: see above
7-aminocoumarin	161.2	C ₉ H ₇ NO ₂		solvent: EtOH E _{1/2} : -1.052	» P » WE: dropping mercury » AE: mercury » RE: SCE

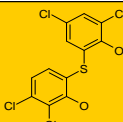
ANTIPARASITAI DRUG

praziquantel Biltricide (D)	312.4	C ₁₉ H ₂₄ N ₂ O ₂			article in Russian
benzylbenzoate ANTISCABIOSUM (D)	212.3	C ₁₄ H ₁₂ O ₂		solvent: ACN E _{1/2} : 2.16	» P » WE: - » AE: - » RE: SCE

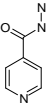
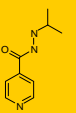
ALKALOIDS

ergometrine maleate	325.4	C ₁₉ H ₂₃ N ₃ O ₂		article missing, has to be rechecked	
----------------------------	-------	---	---	--------------------------------------	--

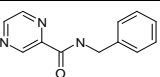
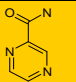
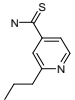
FUNGICIDES

bithionol	356.1	C ₁₂ H ₆ Cl ₄ O ₂ S		will be left out cause of ist toxicity	
------------------	-------	---	---	--	--

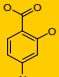
TUBERCULOSTATICS

isoniazid Rimifon	137.1	C ₆ H ₇ N ₃ O		solvent: Buffer E _{1/2} : -1.33	» P » WE: dropping mercury » AE: mercury » RE: SCE
iproniazid	179.2	C ₉ H ₁₃ N ₃ O		solvent: Buffer pH: 2.4 E _{1/2} : -0.624 pH: 8.8 E _{1/2} : -1.236	» P » WE: dropping mercury » AE: mercury » RE: Ag/AgCl (sat)

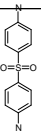
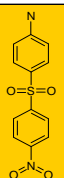
PYRAZINAMIDES

pyrazine-2-carboxylic acid benzylamide	213.24	C ₁₂ H ₁₁ N ₃ O		solvent: DMF E _p : -2.13	» CV » WE: carbon » AE: - » RE: SCE
pyrazindamide Rifater (Combi)	123.1	C ₅ H ₅ N ₃ O		solvent: DMF E _p : -2.11	» CV » WE: carbon » AE: - » RE: SCE
protionamide	180.3	C ₉ H ₁₂ N ₂ S		solvent: - E _{1/2} : -0.9	» P » WE: - » AE: - » RE: SCE

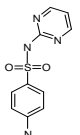
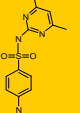
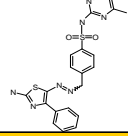
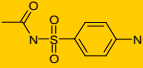
ANTIMYCOBACTERIAL

p-aminosalicylic acid	153.1	C ₇ H ₇ NO ₃			no exact information
------------------------------	-------	---	---	--	----------------------

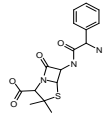
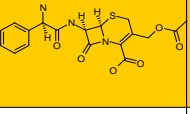
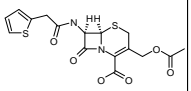
ANTIBIOTICS

pyrimethamine Dapsone ®	248.3	$C_{12}H_{12}N_2O_2S$		solvent: DMF $E_{1/2}$ (1): -2.04 $E_{1/2}$ (2) :-2.50 V solvent: ACN $E_{1/2}$ (1): -2.11 $E_{1/2}$ (2) :-2.32	» P » WE: dropping mercury » AE: - » RE: Ag/AgCl » P » WE: dropping mercury » AE: - » RE: Ag/AgCl
<i>Note! Potential is decreasing when adding the amount of water</i>					
4-(4-nitro-benzenesulfonyl anilin	278.3	$C_{12}H_{12}N_2O_4S$		solvent: DMSO $E_{1/2}$ (1): -2.48 vs the normal hydrogen electrode	» P no information about the electrodes

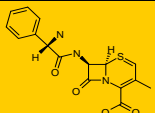
SULFONAMIDES/ ANTIINFECTIVA

sulfadiazine sulfadiazin-Heyl (D)	250.3	$C_{12}H_{12}N_4O_2S$		solvent: ACN $E_{1/2}$ (1) : -1.31 $E_{1/2}$ (2) : -1.58 $E_{1/2}$ (3) : -1.56 $E_{1/2}$ (3) : -1.95	» P » WE: dropping mercury » AE: platinum wire » RE: silver wire
sulfametazine also (sulfadiazine)	278.3	$C_{12}H_{14}N_4O_2S$		solvent: ACN $E_{1/2}$ (1) : -1.45	» P » WE: dropping mercury » RE: silver wire » AE: platinum wire
sulfadimidine	465.6	$C_{21}H_{19}N_7O_2S_2$		solvent: ACN $E_{1/2}$ (1) : -0.56	» P » WE: dropping mercury » AE: platinum wire » RE: silver wire
sulfacetamide Blephamid (D)	214.2	$C_8H_{10}N_2O_3S$		solvent: ACN $E_{1/2}$ (1) : -2.07	» P » WE: dropping mercury » AE: platinum wire » RE: silver wire

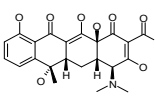
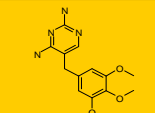
CEPHALOSPORINE-ANTIBIOTICS

ampicillin Ampicillin-STADA (D)	349.4	$C_{16}H_{19}N_3O_4S$			
cefaloglycin	405.4	$C_{18}H_{19}N_3O_6S$		solvent: ACN $E_{1/2}$:-1.60	» P » WE: dropping mercury » AE: mercury » RE: SCE
cefalotin	396.4	$C_{16}H_{16}N_2O_6S_2$		solvent: ACN $E_{1/2}$:-1.53	» P » WE: dropping mercury » AE: mercury » RE: SCE

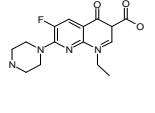
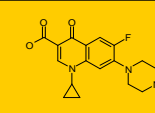
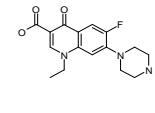
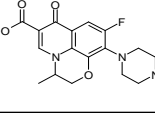
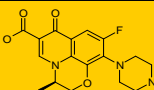
Appendix: Tables

cefalexin	347.4	C ₁₆ H ₁₇ N ₃ O ₄ S		solvent: ACN E _{1/2} : -1.70	» P » WE: dropping mercury » AE: mercury » RE: SCE
------------------	-------	---	---	---	---

TETRACYCLINES

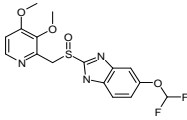
tetracycline	444.4	C ₂₂ H ₂₄ N ₂ O ₈		solvent: DMF no Potential mentioned	» P » WE: dropping mercury » AE: mercury » RE: SCE
trimethoprim (Bactrim® Roche)	290.3	C ₁₄ H ₁₈ N ₄ O ₃		solvent: ACN E _{1/2} : 1.5	» P » WE: rotating Pt-disk » AE: rotating gold disk » RE: SCE

GYRASE-INHIBITORS

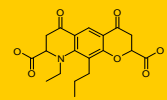
enoxacin Gyramid (D)	320.3	C ₁₅ H ₁₇ FN ₄ O ₃		solvent: - E _{1/2} (1) : -1.43 E _{1/2} (2) : -1.60	» P » WE: dropping mercury » AE: Pt-wire » RE: SCE
				solvent: - E _p (1) : 1.00 no further information on the other electrodes	» CV » WE: graphic electrode
norfloxacin Noroxin ®	319.3	C ₁₆ H ₁₈ FN ₃ O ₃		solvent: - at pH:5.51 E _{1/2} : -1.29 at pH:6.51 E _{1/2} : -1.37	» CV <i>no information on electrodes and solvents</i>
				solvent: - E _{1/2} (1) : -1.48 E _{1/2} (2) : -1.69	» P for further details: see above
pefloxacin Peflacin (D)	333.4	C ₁₇ H ₂₀ FN ₃ O ₃		solvent: - E _{1/2} (1) : -1.53 E _{1/2} (2) : -1.71 E _p (1) : 0.95	» P for further details: see above
ciprofloxacin Ciproxin® electrochemical potential is dependent on the pH-value	331.4	C ₁₇ H ₁₈ FN ₃ O ₃		at pH:6.51 E _{1/2} : -1.21 [V] at pH:10.00 E _{1/2} : -1.74 [V]	» CV <i>no information on electrodes and solvents</i>
ofloxacin Tarivid ®	361.4	C ₁₈ H ₂₀ FN ₃ O ₄		solvent: - E _{1/2} (1) : -1.46 E _{1/2} (2) : -1.67	» P for further details: see above
levofloxacin Tavanic®	361.4	C ₁₈ H ₂₀ FN ₃ O ₄		solvent: -	» P for further details: see above

Appendix: Tables

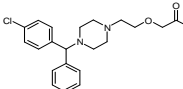
ANTACIDA

pantoprazole Pantozol irreversible oxidation bec.	383.4	$C_{16}H_{15}F_2N_3O_4S$		solvent: BR Ep: 1.175 Ep: 1.080	» CV » WE: carbon paste » AE: Pt wire » RE: Ag/AgCl/3M KCl
---	-------	--------------------------	---	--	---

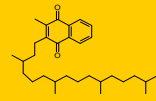
ANTIALLERGICAL /MASTCELL STABILISATING DRUGS

nedocromil sodium Tilarin	375.4	$C_{19}H_{21}NO_7$		solvent: - $E_{1/2}$: -1.01	» P » WE: - » AE: » RE: Ag/AgCl in 3 M KCl
--	-------	--------------------	---	--	---

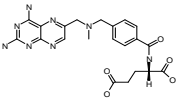
ANTI HISTAMINICA

cetirizine (Zyrtec®)	388.9	$C_{21}H_{25}ClN_2O_3$		solvent: CH₂Cl₂ $E_{1/2}$: ~-0.185	» CV no further details on the electrodes
---	-------	------------------------	---	---	--

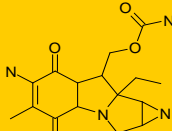
VITAMIN K DERIVATIVE

phytonadione Mephyton (US)	450.7	$C_{31}H_{46}O_2$		solvent: DMF Ep: -1.206 V	» CV » WE: platinum » AE: platinum » RE: Ag/AgC
---	-------	-------------------	---	---	--

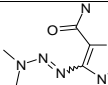
ZYTOSTATICA

methotrexate Methotrexate Lederle bsp.	454.4	$C_{20}H_{22}N_8O_5$			Check Literature!
---	-------	----------------------	---	--	-------------------

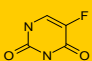
ANTIBIOTIC

mitomycin Mitomycin-C Kyowa	334.3	$C_{15}H_{18}N_4O_5$			» P
--	-------	----------------------	---	--	-----

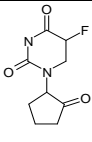
ALKYLATING AGENT

dacarbazine Dacin	182.2	$C_6H_{10}N_6O$		solvent: BR $E_{1/2}$: -1.07 pH: 7.2	» P » WE: dropping mercury » AE: Pt » RE: SCE
------------------------------------	-------	-----------------	---	--	--

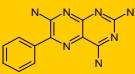
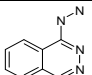
ANTINEOPLASTICAL DRUGS

flouracil Efudix	130.1	$C_4H_3FN_2O_2$		solvent: buffer	» CV » WE: pyrolytic graphite plate » AE: cylindrical Pt-gauze » RE: Ag/AgCl
-----------------------------------	-------	-----------------	---	------------------------	---

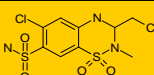
Appendix: Tables

1-(1'-oxocyclopentan-2'yl)-5-fluorouracil	212.2	C ₉ H ₉ FN ₂ O ₃		solvent: DMF E _{red} : -0.48 V irreversible cathodic reduction peaks	» CV » WE: Pt » AE: Pt-wire » RE: Ag/AgCl (sat)
--	-------	--	---	--	---

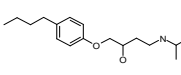
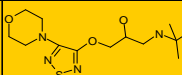
ANTIHYPERTONIC/DIURETIC DRUGS

triamterene	253.3	C ₁₂ H ₁₁ N ₇		solvent: - E _p (1): -0.9 E _p (2): 0.86 E _p (3): 1.3	» P
DYAZIDE (Combination-Drug)					
hydralazine	160.2	C ₈ H ₈ N ₄			» <i>article written in polish !!</i> no further information available

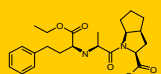
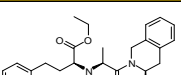
DIURETICS

methylclothiazide	360.2	C ₉ H ₁₁ C ₁₂ N ₃ O ₄ S ₂		solvent: ACN E _{1/2} : -1.58	» P » WE: dropping mercury » AE: platinum wire » RE: silver wire
--------------------------	-------	---	---	---	--

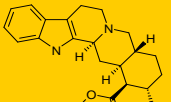
β-RECEPTOR-INHIBITOR

metoprolol	267.4	C ₁₅ H ₂₅ NO ₃		solvent: buffer E _{1/2} : 0.137	» CV » WE: dropping mercury » AE: platinum wire » RE: silver wire
Beloc					
timolol maleate	316.4	C ₁₃ H ₂₄ N ₄ O ₃ S		solvent: - E _{1/2} : 0.154	» CV > for more details see above
Timoptic					
Propranolol				solvent: - E _{1/2} : 0.082	» CV > for more details see above
Inderal					

ACE-INHIBITOR

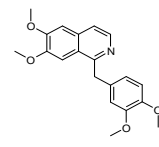
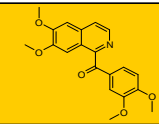
ramipril	416.5	C ₂₃ H ₃₂ N ₂ O ₅		solvent: DMF E _{1/2} : -1.230 at pH: 7.0	» P » WE: dropping mercury » AE: platinum wire » RE: Ag/AgCl
Triatec					
quinapril	438.5	C ₂₅ H ₃₀ N ₂ O ₅		solvent: DMF E _p ^{red} : -1.21	» CV » WE: dropping mercury electrode » AE: Pt-wire » RE: SCE

"AGAINST EREKILE DYSFUNCTION"

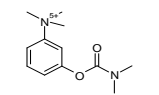
yohimbine	354.5	C ₂₁ H ₂₆ N ₂ O ₃		solvent: MeOH E _{1/2} : 0.838	» coulometry » WE: - » AE: - » RE: SCE
------------------	-------	---	---	--	--

Appendix: Tables

VASODILATOR

papaverine	339.4	C ₂₀ H ₂₁ NO ₄		solvent: - E _{1/2} : -0.085	» CV » for more details see above
papaveraldine	353.4	C ₂₀ H ₁₉ NO ₅			Check again literature

CHOLINESTERASE-INHIBITOR

neostigmine	223.3	C ₁₂ H ₁₉ N ₂ O ₂		solvent: - E _{1/2} : -0.027	» CV » WE: glassy carbon » AE: Pt » RE: Ag/AgCl (sat)
--------------------	-------	---	---	--	--

MISCELLANEOUS

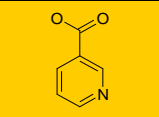
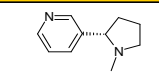
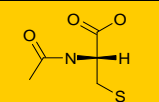
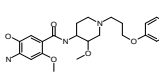
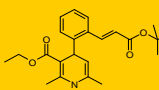
nicotinic acid	123.1	C ₆ H ₅ NO ₂		solvent: - pH: 2.4 E _{1/2} : -1.05 pH: 8.8 E _{1/2} : -1.62	» P » WE: dropping mercury » AE: mercury » RE: Ag/AgCl (sat)
nicotine	162.2	C ₁₀ H ₁₄ N ₂		solvent: buffer E _{1/2} : -1.62	» P » WE: dropping mercury » AE: mercury » RE: Ag/AgCl (sat)
acetylcysteine Fluimucil	163.2	C ₅ H ₉ NO ₃ S		solvent: buffer E _{1/2} (1): -0.41 E _{1/2} (2): -0.595	» P » WE: dropping mercury » AE: Pt » RE: SCE
cisapride	465.95	C ₂₃ H ₂₉ ClFN ₃ O ₄		solvent: buffer E _{ox} : 1.05	no information on the method
lacidipine	455.55	C ₂₆ H ₃₃ NO ₆		solvent: buffer E _p : 0.81	» differential pulse voltammetry » WE: glassy carbon » AE: Pt-wire » RE: Ag/AgCl

Table E: Data of Fig. 17, Chapter 4

Compound **	Predicted microsomal rat clearance [$\mu\text{l}/\text{min}$]	Measured* microsomal rat clearance [$\mu\text{l}/\text{min}$]
8-me-coumarin	298.10	225.54
prochlorperazine	791.14	973.00
verapamil	820.03	650.00
desipramine	687.23	777.67
I13_2nd	587.38	450.63
ciprofloxacin	-98.58	4.80
5-methoxy-psoralen	457.89	1033.67
venlafaxine	1105.12	643.67
loratadine	467.17	434.91
E9_2nd	867.84	766.86
G11_2nd	489.69	590.00
K9_2nd	1051.60	701.00
I11_2nd	382.96	577.00
A11_2nd	645.10	622.00
O13_2nd	288.40	416.00
E5_2nd	1180.15	1878.00
G9_2nd	881.79	739.89
O7_2nd	925.06	857.31
O9_2nd	480.10	646.58
K11_2nd	406.44	566.22
A13_2nd	352.63	513.00
M5_2nd	1321.17	1258.00
I17_2nd	92.98	318.00
A9_2nd	945.83	810.63
I7_2nd	1183.89	941.00
M17_2nd	794.50	301.00
E13_2nd	293.85	471.00
I9_2nd	1017.79	718.62
G5_2nd	1339.36	1637.00
C9_2nd	1152.95	797.00
K13_2nd	1056.41	442.25
A7_2nd	1099.60	1085.19
E11_2nd	914.41	598.24
K19_2nd	721.51	267.75
G15_2nd	263.97	375.82
M7_2nd	1142.01	883.27
E7_2nd	1247.96	1020.39
M11_2nd	920.66	552.31
C11_2nd	453.58	611.78
I15_2nd	761.11	364.20
E17_2nd	647.39	336.16
O11_2nd	383.35	525.89
O15_2nd	231.39	351.62
M15_2nd	360.95	356.73
C13_2nd	479.07	289.40
C7_2nd	729.82	1049.06
C17_2nd	405.35	338.49

* microsomal rat clearance were estimated by the colleagues from the department of DMPK

** compound names containing numbers are codes for internal compounds

Table F: Data of Fig. 3 and 4, Chapter 4

Compound**	CL_{mic_rat} * [mL/min/mg protein]	Eox vs FOC [V]	% CPDdis
E5_2nd	1878.00	-0.32 ± 0.001	31.13 ± 12.43
G5_2nd	1637.00	-0.29 ± 0.113	27.71 ± 25.74
M5_2nd	1258.00	-0.32 ± 0.001	20.78 ± 16.54
A7_2nd	1085.19	-0.16 ± 0.06	
C7_2nd	1049.06	-0.27 ± 0.17	9.94 ± 14.95
E7_2nd	1020.39	-0.30 ± 0.17	15.4 ± 8.33
I7_2nd	941.00	-0.30 ± 0.14	5.14 ± 12.41
M7_2nd	883.27	-0.31 ± 0.19	20.99 ± 16.56
O7_2nd	857.31	-0.27 ± 0.22	19.83 ± 13.81
A9_2nd	810.63	-0.28 ± 0.11	2.29 ± 14.20
C9_2nd	797.00	-0.19 ± 0.10	19.42 ± 19.04
E9_2nd	766.86	-0.20 ± 0.11	
G9_2nd	739.89	-0.23 ± 0.16	0.56 ± 11.36
I9_2nd	718.62	-0.15 ± 0.00	2.59 ± 35.60
K9_2nd	701.00	-0.26 ± 0.07	30.63 ± 14.53
M9_2nd	669.23	-0.15 ± 0.00	13.7 ± 11.81
O9_2nd	646.58	-0.07 ± 0.11	2.39 ± 2.27
A11_2nd	622.00	0.19 ± 0.22	7.73 ± 7.00
C11_2nd	611.78	-0.05 ± 0.01	9.26 ± 14.83
E11_2nd	598.24	-0.08 ± 0.00	39.86 ± 25.18
G11_2nd	590.00	0.22 ± 0.19	17.25 ± 24.20
I11_2nd	577.00	-0.27 ± 0.11	3.52 ± 3.09
K11_2nd	566.22	-0.12 ± 0.15	4.42 ± 3.08
M11_2nd	552.31	-0.20 ± 0.0	6.38 ± 4.39
O11_2nd	525.89	0.22 ± 0.15	9.67 ± 29.54
A13_2nd	513.00	0.16 ± 0.16	11.69 ± 11.78
C13_2nd	491.97	-0.01 ± 0.19	6.09 ± 8.78
E13_2nd	471.00	-0.29 ± 0.28	12.07 ± 8.40
I13_2nd	450.63	0.06 ± 0.38	3.02 ± 1.03
K13_2nd	442.25	0.07 ± 0.04	3.91 ± 5.32
O13_2nd	416.00	0.23 ± 0.11	1.81 ± 3.21
G15_2nd	375.82	0.19 ± 0.19	1.89 ± 2.50
I15_2nd	364.20	0.03 ± 0.00	1.39 ± 2.76
M15_2nd	356.73	-0.12 ± 0.055	9.51 ± 28.03
O15_2nd	351.62	0.17 ± 0.002	13.97 ± 8.10
A17_2nd	341.89		16.11 ± 19.76
C17_2nd	338.49	0.15 ± 0.032	11.12 ± 14.84
E17_2nd	336.16	-0.24 ± 0.206	5.01 ± 4.43
I17_2nd	318.00	0.25 ± 0.05	34.98 ± 46.47
K17_2nd	310.37		20.16 ± 37.82
M17_2nd	301.00	-0.10 ± 0.03	24.23 ± 39.00
A21_2nd	255.63		2.76 ± 2.33
desipramine	777.67	-0.22 ± 0.012	10.91 ± 0.1
verapamil	650.00	-0.24 ± 0.011	7.97 ± 0.15
loratadine	434.91	0.002 ± 0.001	3.26 ± 0.11
8-Me-coumarin	225.54	-0.26 ± 0.003	1.12 ± 2.37
5-Me-psoralen	1033.67	-0.23 ± 0.002	0.20 ± 1.1
paroxetine	2.15 ± 0.064	0.05 ± 0.064	18.70 ± 0.1
sertraline	97.75 ± 0.012		6.67 ± 0
nitrendipine	66.13	-0.15 ± 0.104	6.59 ± 3.3
prochlorperazine	973.00	-0.15 ± 0.002	2.74 ± 3.23
ciprofloxacin	4.80	-0.15 ± 0.006	22.60 ± 3.3
venlafaxine	643.67	-0.08 ± 0.009	6.94 ± 0.1

* microsomal rat clearance were estimated by the colleagues from the department of DMPK

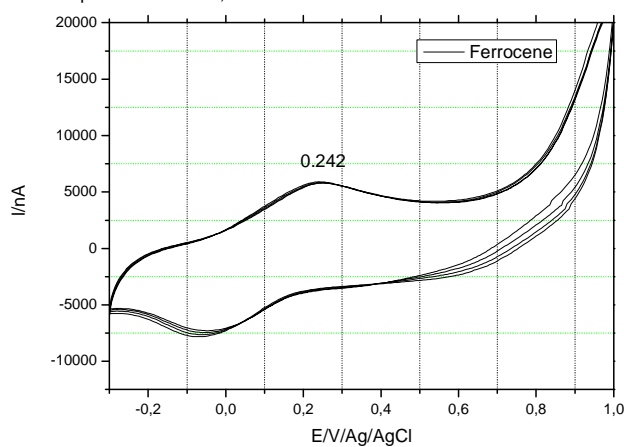
** compound names containing numbers are codes for internal compounds

Table G: Cyclic Voltammograms of compounds used in Fig. 9, Chapter 4

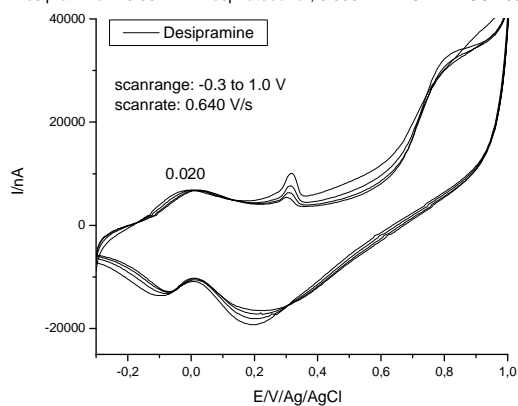
→* Voltammograms are raw data

	E_{ox} [V]	average E_{ox} [V]
ferrocene	0.242	0.241 ± 0.004
	0.245	
	0.237	

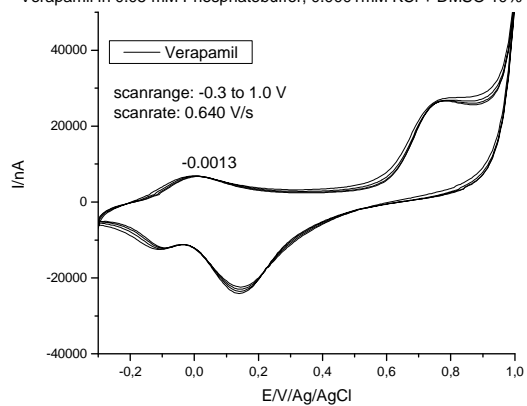
Example for Ferrocene, used as internal standard



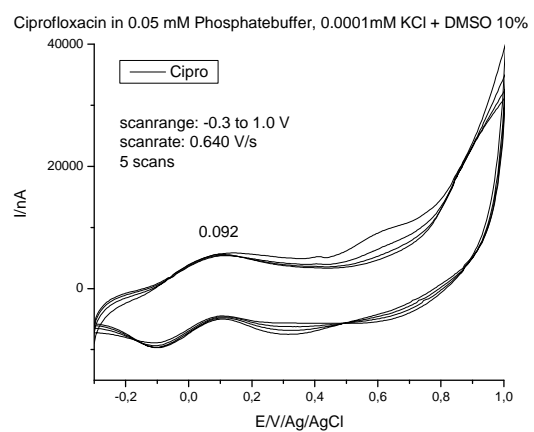
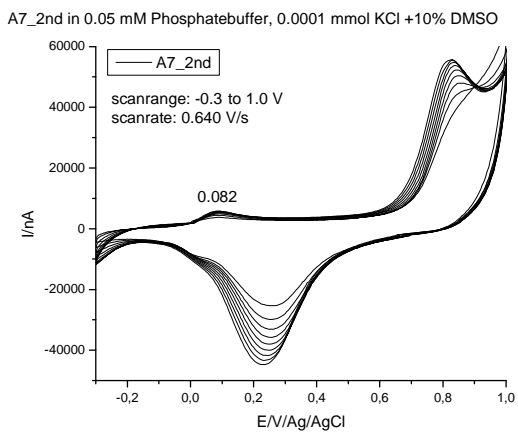
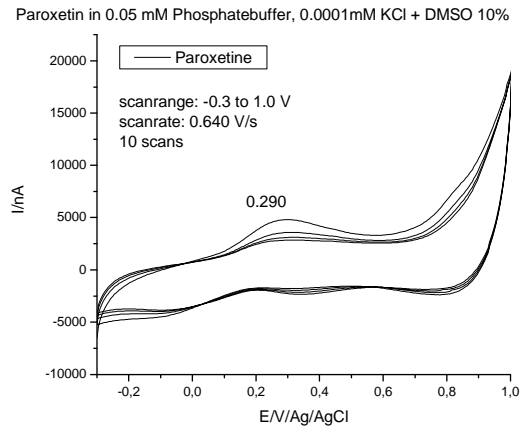
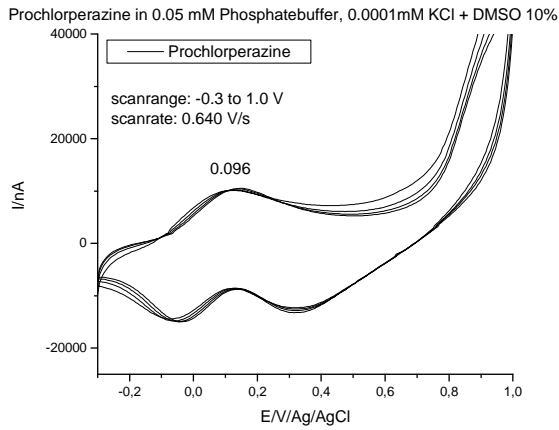
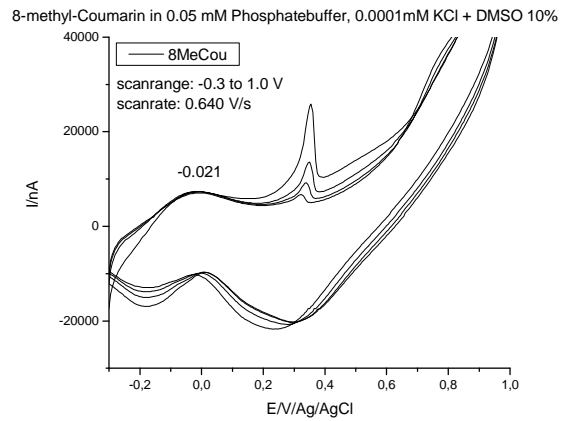
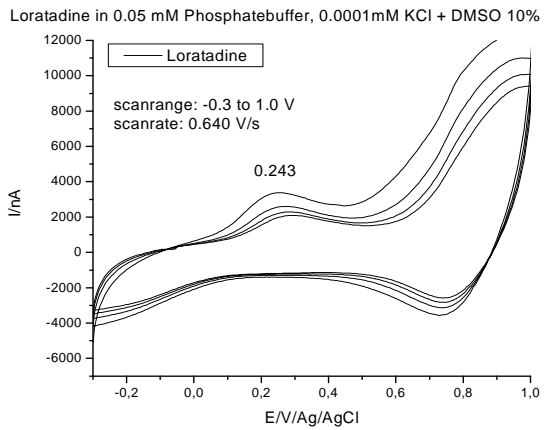
Desipramine in 0.05 mM Phosphatebuffer, 0.0001mM KCl + DMSO 10%



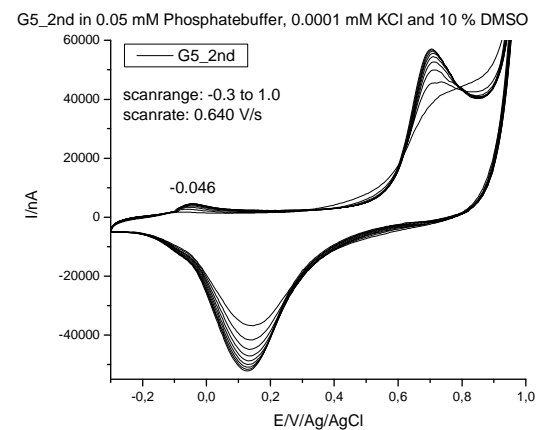
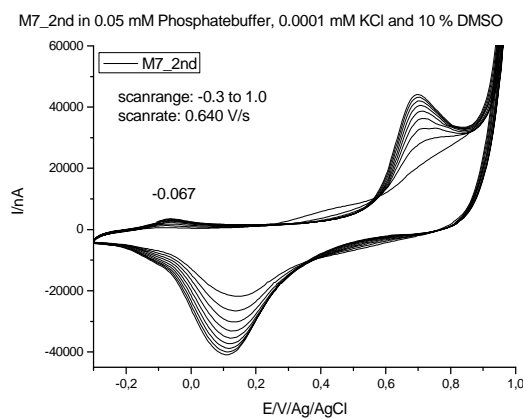
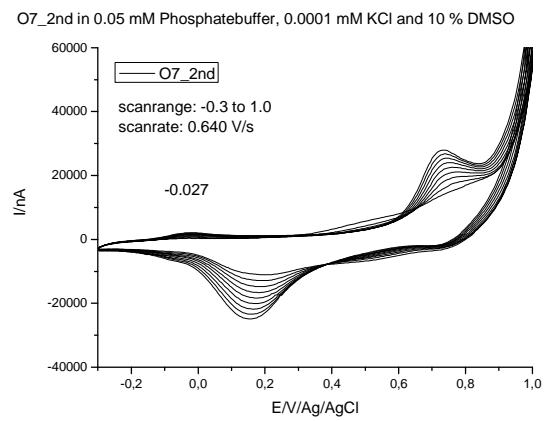
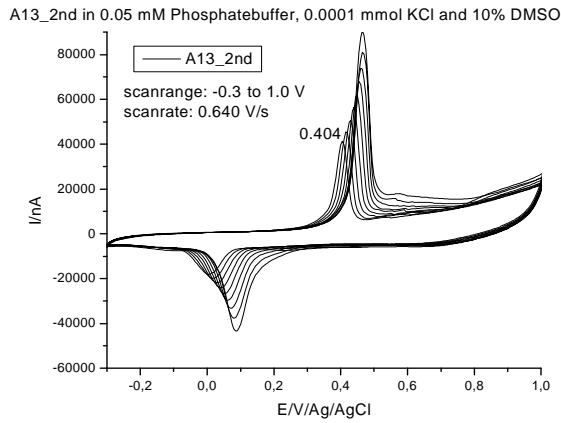
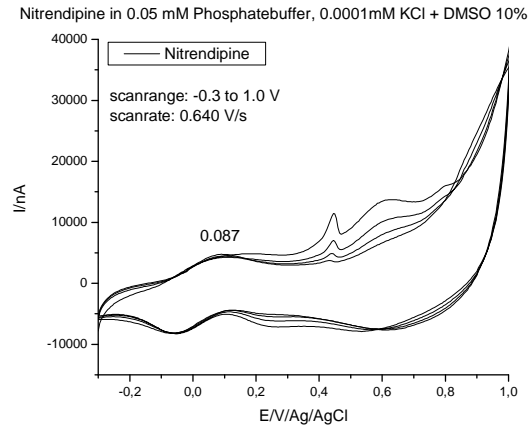
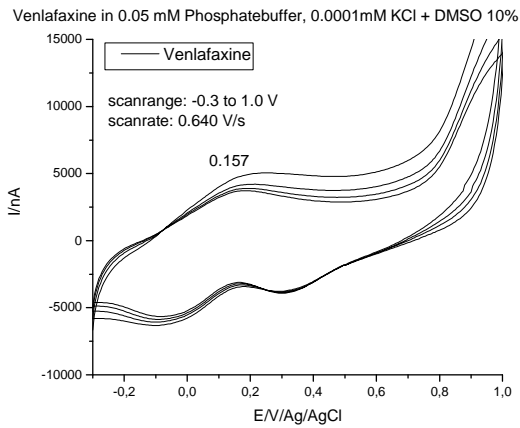
Verapamil in 0.05 mM Phosphatebuffer, 0.0001mM KCl + DMSO 10%



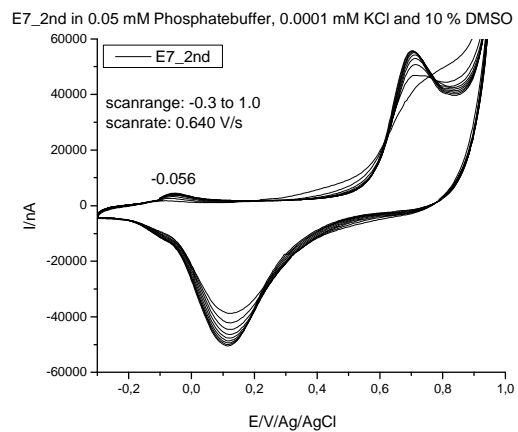
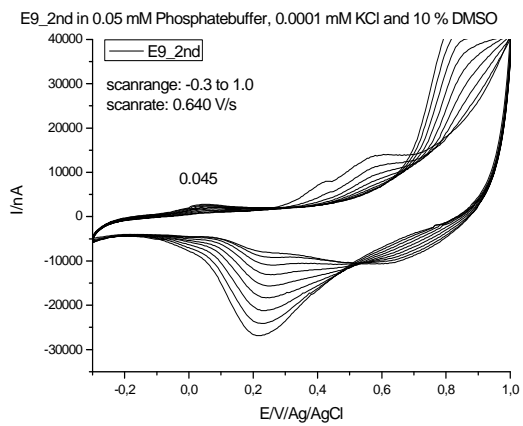
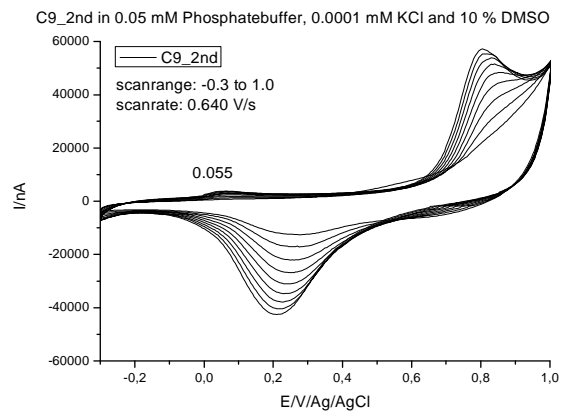
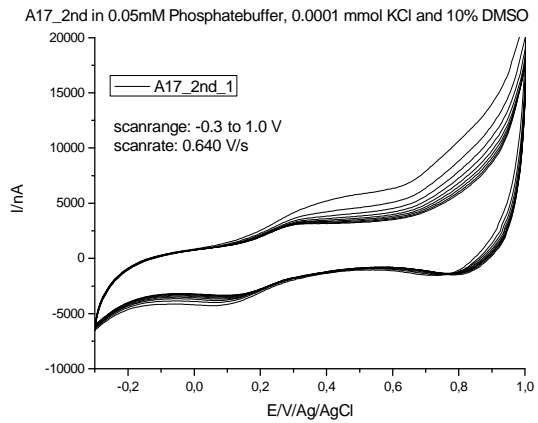
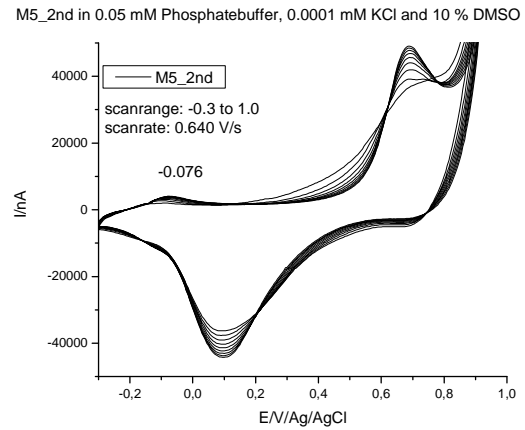
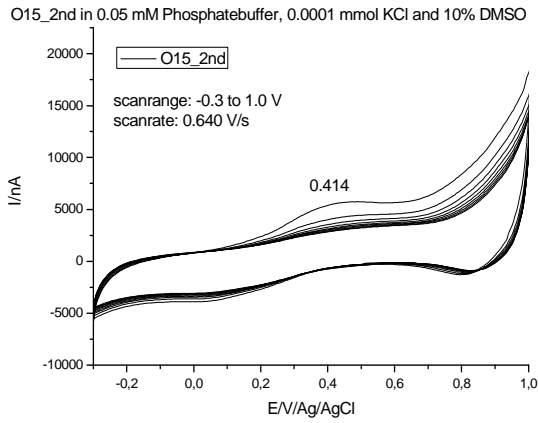
Appendix: Cyclo Voltammograms



Appendix: Cyclo Voltammograms

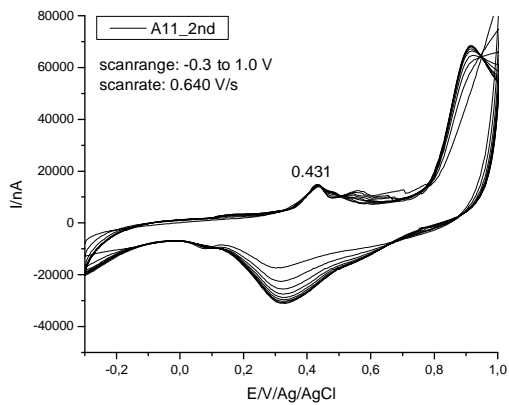


Appendix: Cyclo Voltammograms

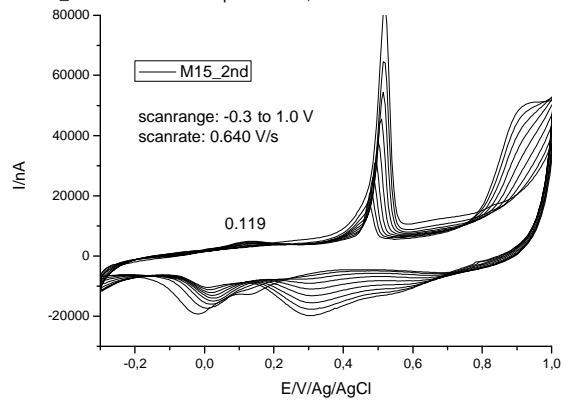


Appendix: Cyclo Voltammograms

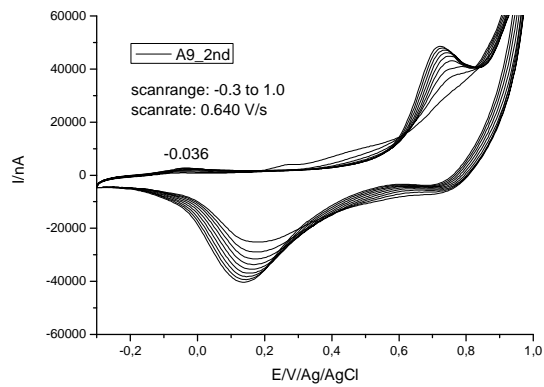
A11_2nd in 0.05 mM Phosphatebuffer, 0.0001 mmol KCl and 10% DMSO



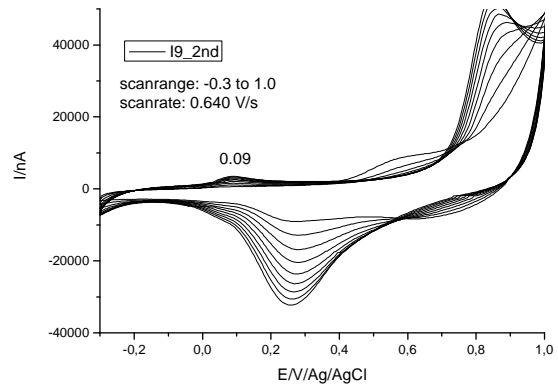
M15_2nd in 0.05 mM Phosphatebuffer, 0.0001 mmol KCl and 10% DMSO



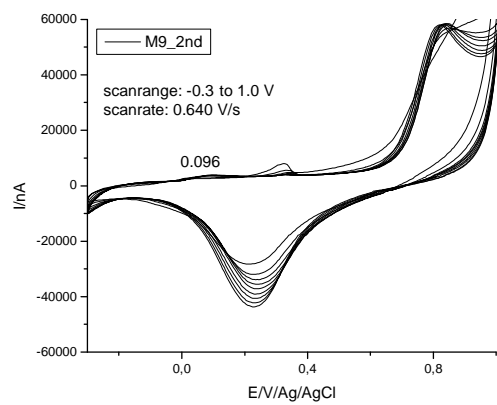
A9_2nd in 0.05 mM Phosphatebuffer, 0.0001 mM KCl and 10 % DMSO



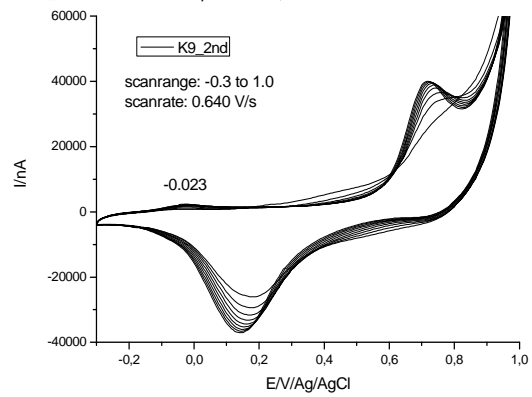
I9_2nd in 0.05 mM Phosphatebuffer, 0.0001 mM KCl and 10 % DMSO



M9_2nd in 0.05 mM Phosphatebuffer, 0.0001 mmol KCl and 10% DMSO

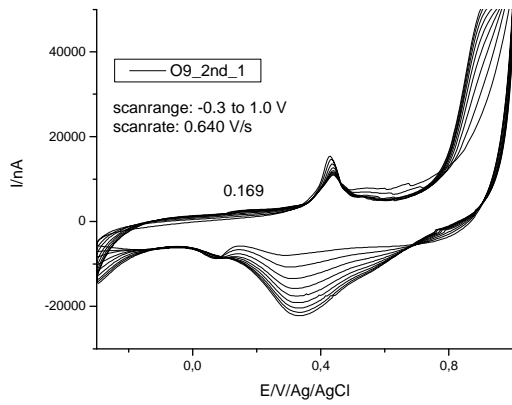


K9_2nd in 0.05 mM Phosphatebuffer, 0.0001 mM KCl and 10 % DMSO

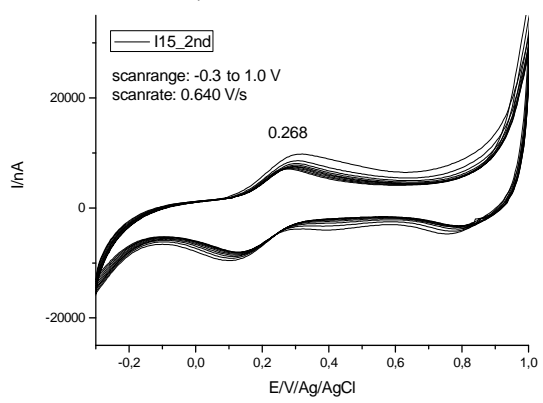


Appendix: Cyclo Voltammograms

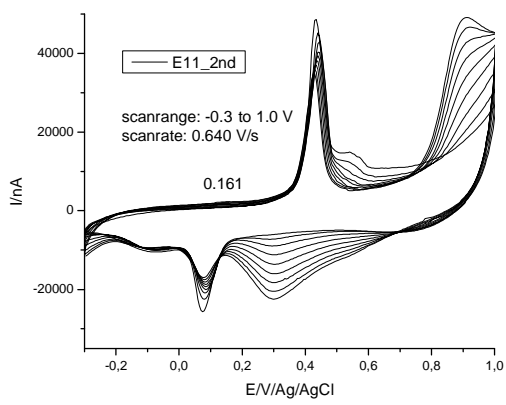
O9_2nd in 0.05 mM Phosphatebuffer, 0.0001 mmol KCl and 10% DMSO



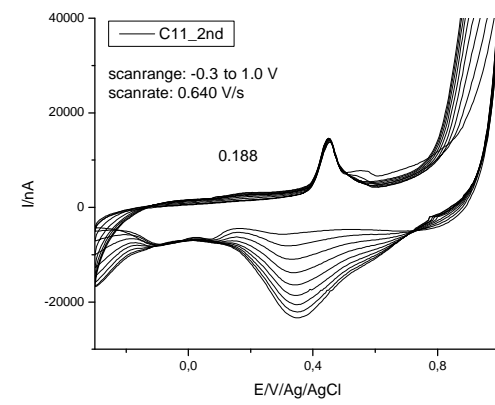
I15_2nd in 0.05 mM Phosphatebuffer, 0.0001 mmol KCl and 10% DMSO



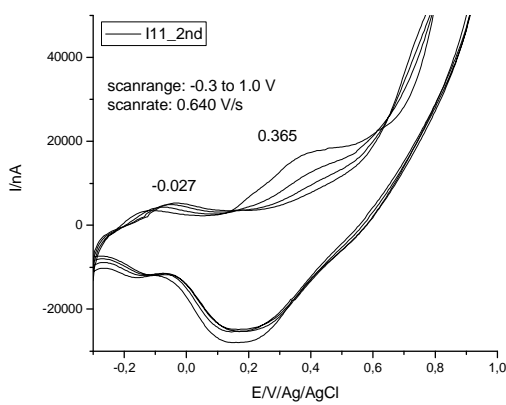
E11_2nd in 0.05 mM Phosphatebuffer, 0.0001 mmol KCl and 10% DMSO



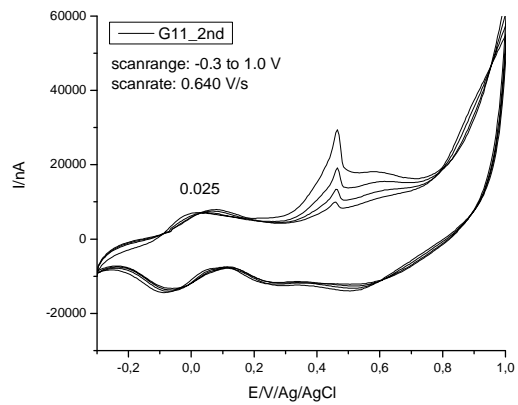
C11_2nd in 0.05 mM Phosphatebuffer, 0.0001 mmol KCl and 10% DMSO



I11_2nd in 0.05 mM Phosphatebuffer, 0.0001mM KCl + DMSO 10%

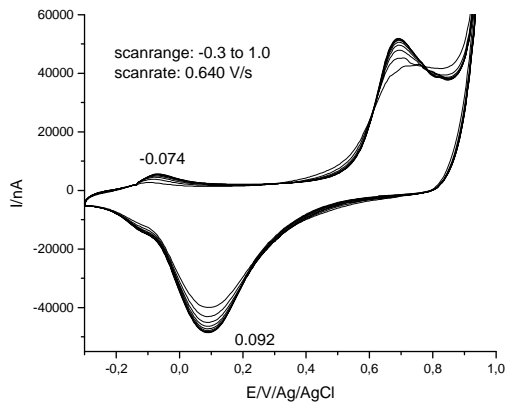


G11_2nd in 0.05 mM Phosphatebuffer, 0.0001mM KCl + DMSO 10%

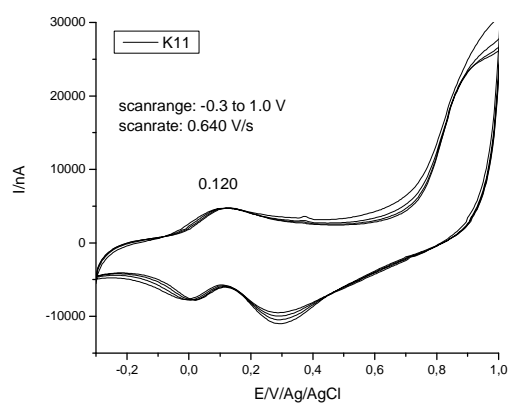


Appendix: Cyclo Voltammograms

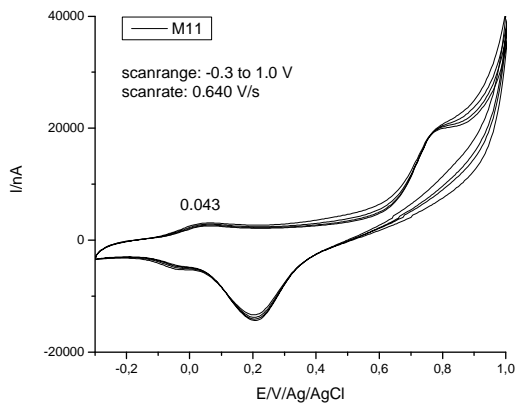
E5_2nd in 0.05mM Phosphatebuffer, 0.0001 mM KCl and 10 % DMSO



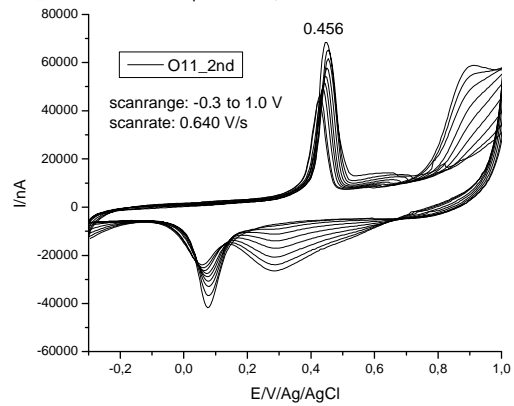
K11_2nd in 0.05 mM Phosphatebuffer, 0.0001mM KCl + DMSO 10%



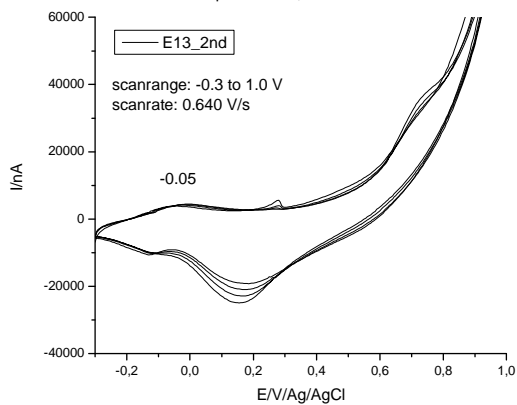
M11_2nd in 0.05 mM Phosphatebuffer, 0.0001mM KCl + DMSO 10%



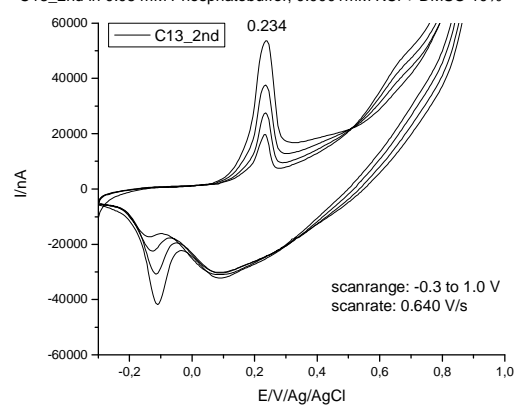
O11_2nd in 0.05mM Phosphatebuffer, 0.0001 mmol KCl and 10% DMSO



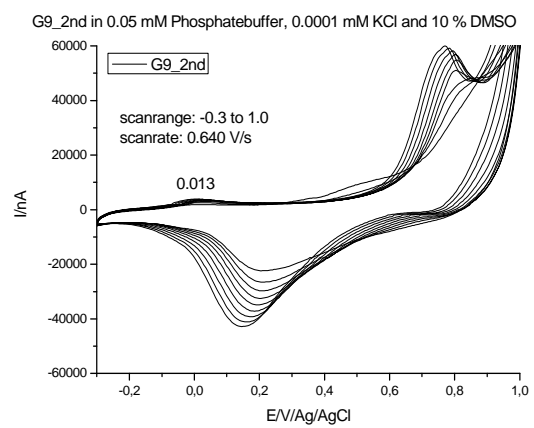
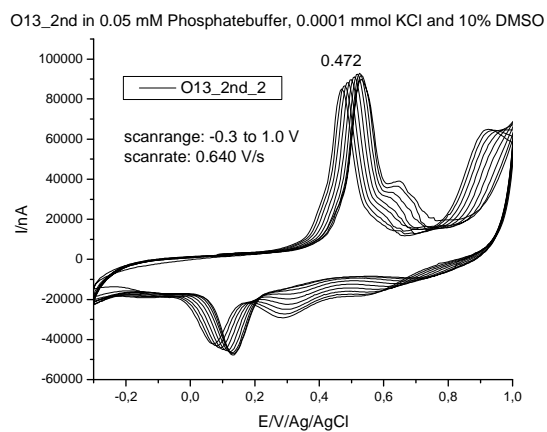
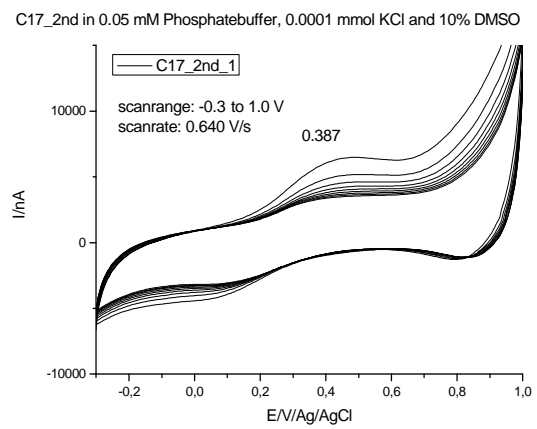
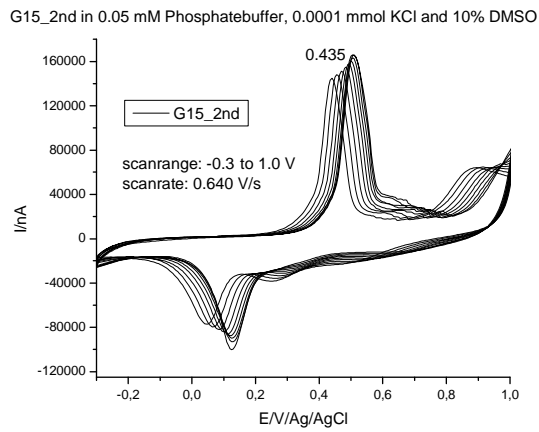
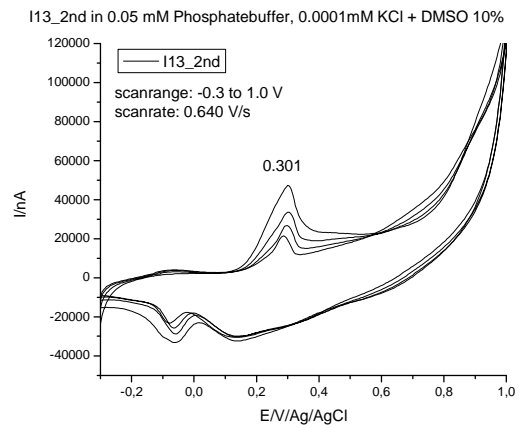
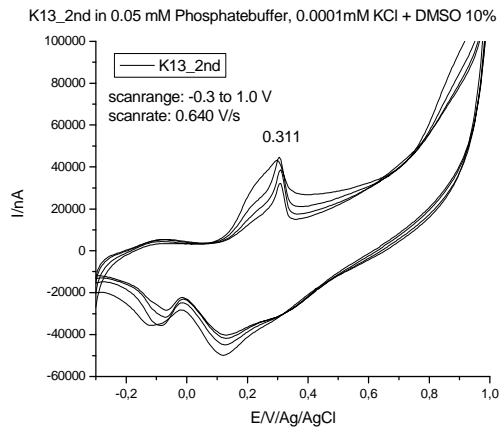
E13_2nd in 0.05 mM Phosphatebuffer, 0.0001mM KCl + DMSO 10%



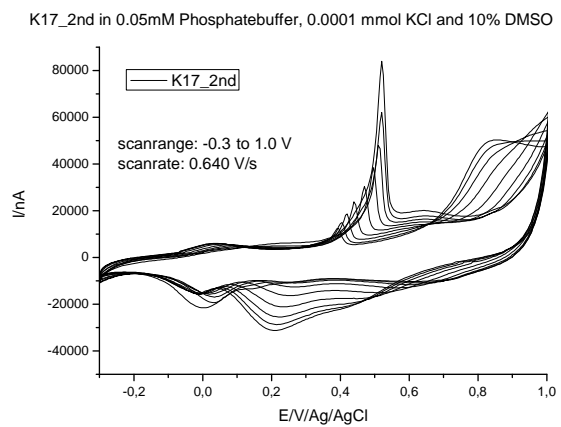
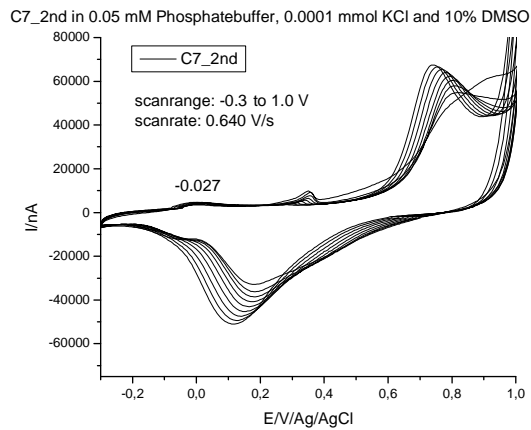
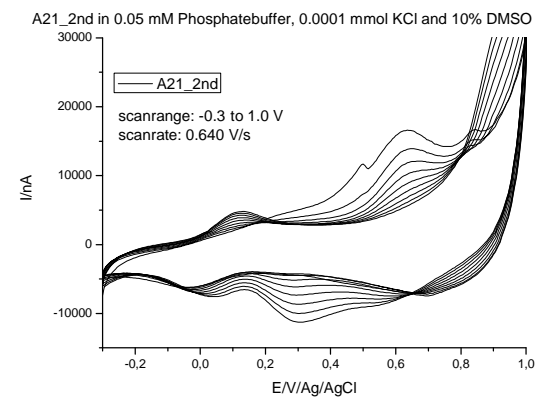
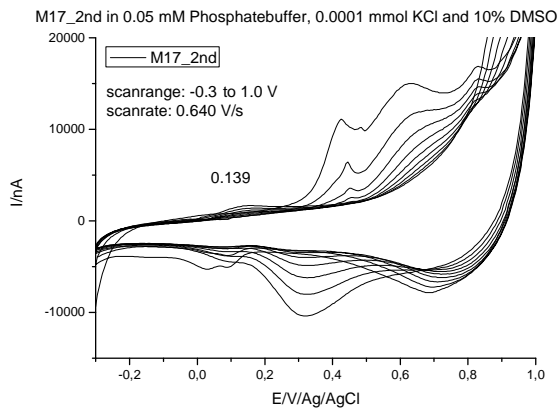
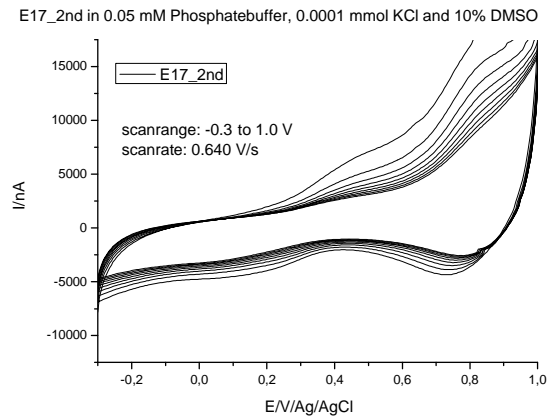
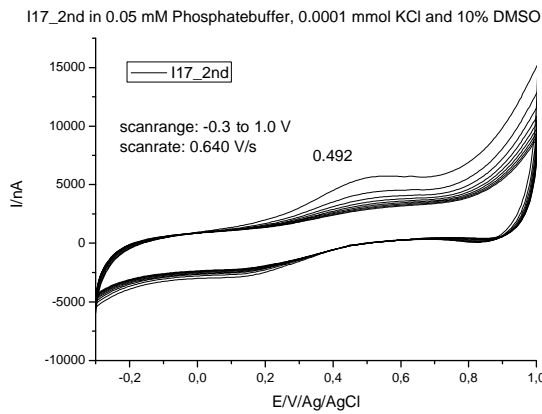
C13_2nd in 0.05 mM Phosphatebuffer, 0.0001mM KCl + DMSO 10%



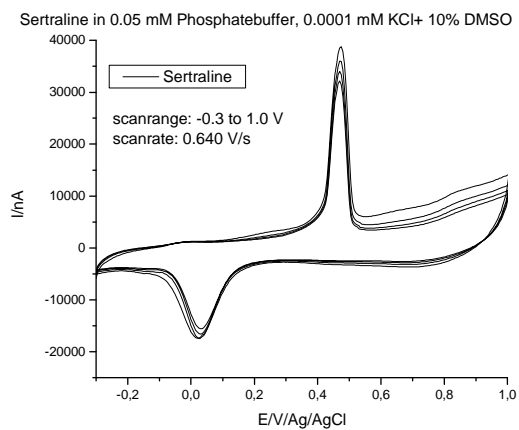
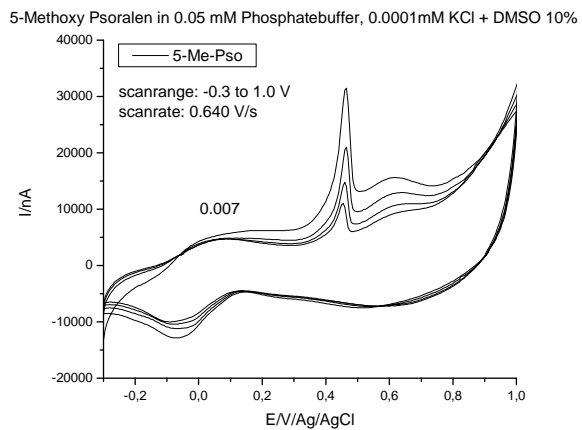
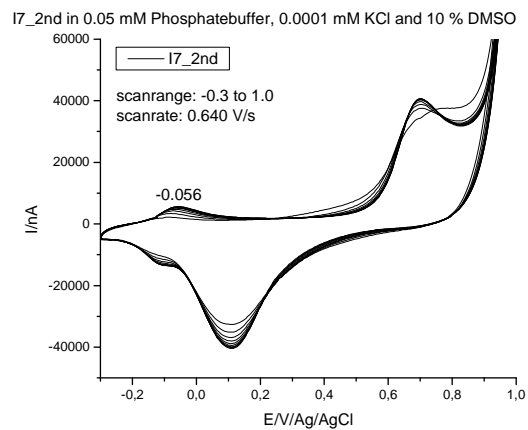
Appendix: Cyclo Voltammograms



Appendix: Cyclo Voltammograms



Appendix: Cyclo Voltammograms



Curriculum Vitae

Personal Information

Name: Anabel Charlotte Felix
Date of Birth: 23rd June 1978
Place of Birth: Basel/CH
Nationality: German

Address: Im Glögglhof 18
CH-4125 Riehen

E-Mail: anabelfelix@yahoo.com

Work Experience

May 2008 – until today

Amavita GaleniCare AG (Zurich Airport, CH)

- team leading pharmacist with management responsibilities
- delegate of the business manager
- dispensing drugs and providing advice for customers in an international environment
- instruction of apprentices

January 2005 – April 2008

University of Basel/F. Hoffmann- La Roche (Basel, CH)

- PhD-thesis: major focus on early ADME and analytical chemistry including LC/MS, UV-spectroscopy, cyclic voltammetry

September 2002 – December 2004

Burgfelder Apotheke, Basel/CH

- part-time Assistant pharmacist with responsibility
- dispensing drugs and providing advice for customers
- team leading experience
- manufacturing pharmaceutical preparations for customers

July-August 2003

Pharmacie Voillot, Paris/F

- three week stage with similar responsibilities as at the Burgfelder Apotheke

Education

January 2005 – April 2008

University Basel (Prof. M. Hamburger)/ F.Hoffmann-La Roche (Dr. M. Kansy) (Basel/CH)

PhD-Thesis: "Redox Potential and Metabolic Stability: Development of High Throughput Assays for Early Compound Profiling"

February - July 2004

University Basel/ University Hospital Basel, Division Clinical Pharmacology and Toxicology, (Prof. S. Krähenbühl)

Diploma thesis: "Characterisation of a novel Testosterone 6 β -Hydroxylase HPLC- Assay to investigate CYP 3A4 activity in Human Liver Microsomes"

- Development of a rapid HPLC-assay
- Working with subcellular hepatic fraction

1999 - 2004

Studies of Pharmacy with the Master of Science degree as diploma, University Basel (Basel/CH)

Language skills

Mother tongue: **German**

Other languages: **English** (excellent, 1999 Certificate in Advanced English (CAE), 1993 and 1997 homestays in England/ UK)

French (fluently, 1999 language course at Berlitz School, Basel/CH, several stays in France)

Hobbies

Dancing (Performances and Teaching in Tapdance, Baden-Württembergischer Meister im Duo 2000)

Languages and foreign cultures

Music (Playing piano and flute, several prizes in "Jugend Musiziert" for piano)

During my studies and PhD studies I have followed the courses of following lecturers:

P. Oelhafen, G.-R. Plattner, W. Schaffner, A. Zuberbühler, P. Strazewski, H.-J. Müller, M. Meyer, A. Hädener, P. Huber, R. Leu Marseiler, U. Spornitz, T.-W. Güntert, G. Imanidis, H. Leuenberger, S. Krähenbühl, M. Hamburger, J. Drewe, K. Hersberger, J. Huwyler, B. Ernst, M. Lampert, G. Folkers, A. Regeniter, K. Berger-Büter, K. Beier, P. Hauser, E. Constable, A. Fahr, A. Vedani, H. Durrer, P. Erb, C. Moroni, J. Meyer, Brian Cutting, O. Potterat, G. Betz,

Basel, 6th May 2008

Anabel Felix